ROLE OF EXTRACELLULAR VESICLES IN NON-ALCOHOLIC FATTY LIVER DISEASE

Linda Anna Ban

A thesis submitted in fulfilment of the requirements for the degree of Doctor of Philosophy.

Faculty of Medicine and Health, University of Sydney

2019

Disclosures

The content of this thesis is the product of original research carried out by the author while enrolled as a candidate for the degree of Doctor of Philosophy in the Sydney Medical School, University of Sydney. All studies were conducted under the supervision of Associate Professor Susan McLennan in the Department of Endocrinology, Central Clinical School of the Sydney Medical School, University of Sydney, Australia.

As the author, I certify that the intellectual content of this thesis is the product of my own work and that any assistance and sources have been acknowledged. Notably, the experimental design of studies presented in Chapter 5 were conceived by collaborators of the author as follows: The breeding of transgenic mice was performed by Miss Christine Yee at Centenary Institute, Sydney, Australia and studies utilising these animals (Chapter 5.2) were conceived by Professor Nicholas Shackel and Associate Professor McLennan. The exercise intervention of mice was performed by Mr Sergio Martinez-Huenchullan (SMH) and Ms Luisa Olaya-Agudo at the Charles Perkins Centre, University of Sydney and studies utilising these animals (Chapter 5.3) were conceived by SMH and Professor Stephen Twigg. The author thanks the individuals above for the opportunity to partake in these studies that contributed in part to this thesis.

This thesis contains material published in the International Journal of Molecular Sciences (see *Manuscripts*). This includes Chapter 1 sections 1.3.2 - 1.3.4. I performed the literature review and wrote this manuscript, produced the figures and tables, as well as edited the manuscript after review by co-authors. This thesis has not been previously submitted for any other degree.

Linda Anna Ban
December 2018

Author Attribution Statement

Author statement

In addition to the statements above (see *Disclosures*), in cases where I am not the corresponding author of a published item, permission to include the published material has been granted by the corresponding author.

Linda Anna Ban
December 2018

Supervisor statement

As supervisor for the candidature upon which this thesis is based, I can confirm that the authorship attribution statements above are correct.

Associate Professor Susan McLennan
December 2018

Acknowledgements

To my mentors…

I would like to express my gratitude foremost to my supervisor and mentor, Associate Professor Susan McLennan. Not only was I encouraged and guided, I was pushed to be better and pushed beyond my comfort zone to succeed. There was no limit to her patience (forgive me for testing!) or her support. Thank you for always having my back. I would also like to extend my gratitude to my associate supervisor, Professor Nicholas Shackel, for his words of wisdom that helped me complete this thesis.

To my family in the Department of Endocrinology…

For your personal and professional advice, and your warm company, I am indebted. Thanks to your smiles, I never felt alone. You were really my family: Danqing, Charmaine and Xiaoyu my role models; Luisa the fairy godmother; Zara my lovely desk buddy with her wonderful desk plants (fungi growing in mugs of tea); Babu with his infinite kindness and patience; my big brother Surya and his cool (not weird) jokes; Christine with her amazing cakes and basically every other skill; and my little sisters – literally, we share the same lab mum – Anh, Carla and Rachael. I'd like to think I was somewhat of a mentor, but it was probably the other way around. Our no holds barred conversations, singing in the lab, and stirring of more than just buffers (that last one was my fault, and you're welcome). A special mention to Sergio, who always made me feel big and important and was there through thick and thin: thank you mijitico. From the doctors of diabetes (Albert and Angela) and the eternal optimist (Kimi) to the magicians behind the scenes (Sharon, Sylvia, Hilary) and the one who saw through my scientist facade into my art soul (Paul): together, we are unstoppable. Never change because the world needs more people like you.

And to my family in the Liver Cell Biology group…

Who formerly called Centenary Institute home, where I began the uphill climb and we grew together through work and life, thank you for the good times. Christine, you are everywhere and I have probably known you forever. My travel buddy Aimei and Thomas the awesome postdoc; I miss you both. Oh and Rob, the doctor with the million-dollar grin (except when the microparticles wipe it off his face).

I would also like to acknowledge everybody beyond the lab who has assisted in any way. The overlords of level 3 west, Macarena Rodriguez and Katherine Barna, thank you for ensuring that my destructive capabilities were not unleashed; Alex Alecu (and his motherland spirit) and Suzanne Pearce from the RPAH animal facility for looking after my fur babies; Sanaz Maleki and Rosie Cheong-Soos from the Histopathology facility for helping with all things histology (and your good company and music); Donna Lai and Sheng Hua from the Bosch Institute for their expertise on NanoSight and my favourite fruit-cross-cytometer, the Guava; all the staff at the Mass Spectrometry facility in the Charles Perkins Centre, and the Sydney Microscopy and Microanalysis unit; and everybody else who has provided me with invaluable advice.

I also gratefully acknowledge the Sydney Medical School for their funding support through a postgraduate scholarship, and Mr Greg Brown for his generous donation to the Department of Endocrinology that had in part supported the studies in this thesis. I also thank the wonderful staff at La Trobe Sydney and the School of Life and Environmental Sciences at the University of Sydney for giving me the opportunity to enforce biology on the next generation. But much more than that, you gave me new mentors and friends. Monica, my twin by birth and level of crazy. And Andy, the soundtrack to my life – you are unique in all the world.

Finally, the greatest thanks goes to my family…

Towards whom my gratitude is boundless and my love unconditional. To everyone at home in Hungary but especially Anyuci, Daddy, and my brother Thomas: for all your support, from your patience to your understanding and love, you deserve the world. I won't let you down.

Abstract

Once thought to be a benign accumulation of hepatic fat, non-alcoholic fatty liver disease (NAFLD) is now recognised as a prevalent complication of obesity with serious consequences if left untreated. This includes liver inflammation and impaired glucose metabolism, and with time may result in cirrhosis and organ failure. While basic diagnostic tools exist, such as ultrasound and serum protein markers, these are often unreliable and warrant the use of more invasive techniques such as tissue biopsy. Given most patients only become symptomatic once the disease is advanced, there is an urgent need to develop a better diagnostic strategy for NAFLD. This project aims to address the issue by exploring a novel biomarker candidate: extracellular vesicles (EVs). These submicron vesicles can be isolated from the circulation and tracked back to their parent cells by nature of their surface markers. EVs are constitutively released by all cell types, however, their abundance and molecular cargo are shown to be changed in various conditions and disease states, which also affects the functions they mediate as "intercellular messengers". Using rodent models of diet-induced NAFLD, we aim to determine whether plasma or liver-derived EVs could be effectively used as a marker for the progression of NAFLD, and whether suitable interventions exist to slow or even reverse the disease. Finally, using *in vitro* models of hepatocyte EV uptake, the project will also investigate how EVs impart signals within the liver, in a paracrine fashion and from extraheptic tissues.

Manuscripts

Published

Ban LA, Shackel NA, McLennan SV. Extracellular Vesicles: A New Frontier in Biomarker Discovery for Non-alcoholic Fatty Liver Disease. *International Journal of Molecular Sciences*. 2016; 17(3):376. doi: 10.3390/ijms17030376.

Unpublished, submitted

Martinez-Huenchullan SF, Ban LA, Olaya-Agudo LF, Maharjan BR, Williams PF, Tam CS, McLennan SV, Twigg SM. Constant-moderate and high-intensity interval training have differential benefits on insulin sensitive tissues in high-fat fed mice. Submitted to *Frontiers in Physiology* (December 2018).

Unpublished, completed draft

Ban LA, Yee C, Tao DA, Maharjan BR, Myanganbayar M, Shackel NA, McLennan SV. Extracellular vesicle profile shows diet and aging trends in a mouse model of non-alcoholic fatty liver disease.

Presentations

International

Ban LA, Sutanto SS, Tao DA, Martinez-Huenchullan SF, Maharjan BR, Twigg SM, Shackel NA, McLennan SV. Circulating extracellular vesicles in the context of non-alcoholic fatty liver disease can modulate the hepatocyte phenotype. *Australasian Diabetes Congress*. 2018. Adelaide, Australia.

Ban LA, Sutanto SS, Tao DA, Martinez-Huenchullan SF, Maharjan BR, Shackel NA, McLennan SV. The changing profile of extracellular vesicles in non-alcoholic fatty liver disease progression and their role in signalling to hepatocytes. *EASL 53rd International Liver Congress.* 2018. Paris, France. ***Selected for Key Opinion Leader guided Poster Tour.***

Ban LA, Yee C, Myanganbayar M, Shackel NA, McLennan SV. Extracellular vesicle changes in a diet induced model of non-alcoholic fatty liver disease progression and the role of TNF alpha. *EASL 52nd International Liver Congress.* 2017. Amsterdam, The Netherlands. ***Young Investigator Registration Bursary.***

Ban LA, Yee C, Maharjan BR, Shackel NA, McLennan SV. Extracellular vesicle modulation with diet and aging in a mouse model of non-alcoholic fatty liver disease. *2nd Australasia Extracellular Vesicles Conference.* 2017. Lorne, Australia.

Ban LA, Yee C, Shackel NA, McLennan SV. Extracellular vesicles: exploring a novel biomarker in nonalcoholic fatty liver disease pathogenesis. *25th Conference of APASL.* 2016. Tokyo, Japan.

Ban LA, Shackel NA, McLennan SV. Microvesicles as novel markers in non-alcoholic fatty liver disease progression. *EASL 50th International Liver Congress*. 2015. Vienna, Austria. ***Young Investigator Registration Bursary.***

Ban LA, Mridha A, Shackel NA, McLennan SV. CD147-mediated hepatocyte injury and stellate cell activity is facilitated by microvesicles in models of steatosis. *Inaugural Australasia Extracellular Vesicles Conference.* 2014. Cairns, Australia.

National

Ban LA, Martinez-Huenchullan SF, Olaya-Agudo LF, Maharjan BR, Yee C, Tam CS, Twigg SM, McLennan SV. Differential benefits of two isocaloric exercise programs on diet-induced non-alcoholic fatty liver disease and circulating extracellular vesicles in mice. *Joint Scientific Meeting of The Australian and New Zealand Obesity Society (ANZOS) and Breakthrough Discoveries in Metabolism, Diabetes and Obesity (MDO)*. 2018. Melbourne, Australia.

Ban LA, Yee C, Myanganbayar M, Shackel NA, McLennan SV. Lifestyle and genetic factors influencing extracellular vesicle changes in a mouse model of non-alcoholic fatty liver disease. *Australian Society for Medical Research 56th National Scientific Conference.* 2017. Sydney, Australia.

Ban LA, Mridha A, Shackel NA, McLennan SV. Microparticles are vectors for CD147-mediated hepatocyte injury and stellate cell activity in non-alcoholic steatohepatitis. *Australian Diabetes Society and Australian Diabetes Educators Association Annual Scientific Meeting.* 2014. Melbourne, Australia. ***ADS Pincus Taft Young Investigator Award finalist.***

University of Sydney

Charles Perkins Centre EMCR Symposium. September 2016.
Bosch Institute Scientific Meeting. July 2016.
Charles Perkins Centre EMCR Symposium. August 2015.
Bosch Young Investigators Symposium. December 2014.

List of Figures

Chapter 1.

Chapter 2.

Chapter 3.

Chapter 4.

Chapter 5.

Chapter 6.

Chapter 7.

Appendix.

List of Tables

Chapter 6.

Appendix.

List of Abbreviations

α-SMA	alpha smooth muscle actin
A2M	alpha 2 macroglobulin
AASLD	American Association for the Study of Liver Diseases
AB	apoptotic bodies
AF	Alexa Fluor™
ALD	alcoholic liver disease
ALP	alkaline phosphatase
ALT	alanine transaminase
AnnxV	annexin A5
APC	allophycocyanin
ApoA1	apolipoprotein A1
ARC	Animal Resources Centre
ASGPR1	asialoglycoprotein receptor 1
AST	aspartate transaminase
AU	arbitrary unit
AUC	area under curve
AUROC	area under the receiver operator curve
BGL	blood glucose level
BMI	body mass index
BSA	bovine serum albumin
BSG	basigin (alias: CD147, EMMPRIN)
CAP	controlled attenuation parameter
CDD	choline deficient diet
cDNA	complementary DNA
CFSE	carboxyfluorescein succinimidyl ester
CK18	cytokeratin 18
CT	computerised tomography
Ct	cycle threshold
CTGF	connective tissue growth factor (alias: CCN2)
CXCL10	chemokine CXC motif ligand 10 (alias: IP-10)
DAG	diacylglycerol

dH_2O	distilled water
DLS	dynamic light scattering
DM	diabetes mellitus (type 2: T2DM)
DMEM	Dulbecco's Modified Eagle's medium
dNTP	deoxy-nucleoside triphosphate
DPX	dibutyl phthalate xylene
DTT	dithiothreitol
EASL	European Association for the Study of the Liver
ECM	extracellular matrix
EDTA	ethylene diamine tetra-acetic acid
ELISA	enzyme-linked immunosorbent assay
END	endurance training
ESCRT	endosomal sorting complexes required for transport
EV	extracellular vesicle
FABP1	fatty acid binding protein 1 (liver-type)
FBS or FCS	foetal bovine serum or foetal calf serum
FC	flow cytometry
FET	Fisher's Exact Test
FFA	free fatty acid
FGF21	fibroblast growth factor 21
FITC	fluorescein isothiocyanate
FLI	fatty liver index
GCK	glucokinase
gDNA	genomic DNA
GGT	gamma glutamyl transferase
H&E	haematoxylin and eosin
HCC	hepatocellular carcinoma
HFD	high-fat diet
HG	haptoglobin
HGF	hepatocyte growth factor
HIIT	high-intensity interval training
H-MRS	proton magnetic resonance spectroscopy
HOMA-IR	homeostatic model assessment of insulin resistance

HSC	hepatic stellate cell (not to be confused with *haematopoietic stem cell*)
HSI	hepatic steatosis index
IFN	interferon
IGF1	insulin-like growth factor 1
IL	interleukin
ION	index of NASH
IR	insulin resistance (not to be confused with *insulin receptor*)
IRS	insulin receptor substrate
ISEV	International Society of Extracellular Vesicles
ITT	insulin tolerance test
KC	Kupffer cell
LAP	lipid accumulation product
LCFA	long-chain fatty acids
LCMS	liquid chromatography with mass spectrometry
LFT	liver function test
MCD	methionine and choline deficient diet
MCP1	monocyte chemotactic protein 1 (alias: CCL2)
MetS	metabolic syndrome
miRNA	micro RNA
MMP	matrix metalloproteinase
MP	microparticle
MRC	maximal running capacity
MRI	magnetic resonance imaging
mRNA	messenger RNA
MV	microvesicle
MVB	multi-vesicular body
NAFLD	non-alcoholic fatty liver disease
NAS	NAFLD activity score
NASH	non-alcoholic steatohepatitis
NK cell	natural killer cell
NTA	nanoparticle tracking analysis
OMV	outer membrane vesicle (bacterial)
ORO	Oil Red O

PBC	primary biliary cirrhosis
PBS	phosphate buffered saline
PCR	polymerase chain reaction
PDGF	platelet-derived growth factor
PE	phycoerythrin
PEG	polyethylene glycol
PerCP	peridinin chlorophyll
PFA	paraformaldehyde
PLIN2	perilipin 2
PPAR	peroxisome proliferator-activated receptor
PS	phosphatidylserine
PSC	primary sclerosing cholangitis
PSR	Picro-Sirius red
RIN	RNA integrity number
RT-qPCR	real-time quantitative polymerase chain reaction
SEC	sinusoidal endothelial cell
SREBP-1c	sterol regulatory element-binding protein 1c
SV40	Simian virus 40
TAG	triacylglycerol (also triglyceride)
TEM	transmission electron microscopy
TGFβ	transforming growth factor beta
TIMP1	tissue inhibitor of metalloproteinase 1
TNF	tumour necrosis factor (alias: TNF alpha)
TRPS	tuneable resistive pulse sensing
UC	ultracentrifugation
US	ultrasound
VAT	visceral adipose tissue
VEGF	vascular endothelial growth factor (receptor: VEGFR)
VLDL	very low density lipoprotein
WB	western blot
WC	waist circumference
WCL or WLL	whole cell lysate or whole liver lysate

Table of Contents

Chapter 1.

Literature Review

Chapter 1. Table of contents

1.1. Liver Overview

The liver is the largest solid organ of the body and is situated in the upper right quadrant of the abdominal cavity. While the microscopic architecture is consistent across the lobes and conserved between species, the liver is involved in a variety of metabolic functions that contribute to systemic homeostasis and health (see section 1.1.2) (VanPutte et al., 2010, Pocock et al., 2013). In this regard, the loss of liver function through acute or chronic disease has a range of extrahepatic consequences, from impaired glycaemia to vascular dyshomeostasis. However, the liver is also highly regenerative, such that a small fraction of healthy tissue (20-30%) is able to compensate for the activity of the whole organ (Guglielmi et al., 2012). This value increases in liver disease, to around 40% in the case of steatosis, for example. Further details of relevant cell populations and their physiological roles are given below.

1.1.1. Normal liver structure

The human liver is divided into four lobes, including the large anterior left and right lobes, and the smaller caudate and quadrate lobes on the posterior (or visceral) surface. These lobes are further divided into functional units called lobules, which have a typically hexagonal structure delineated by portal triads at the vertices (VanPutte et al., 2010, Kmieć, 2001) (Figure 1.1). The triads encompass a portal vein, hepatic artery, and bile duct each, where the two former drain into sinusoids and then subsequently into a central vein at the centre of the lobule. The bile ducts receive bile from canaliculi that run counter-current to the sinusoidal blood, eventually draining into hepatic ducts and the cystic duct of the gallbladder where the bile is stored.

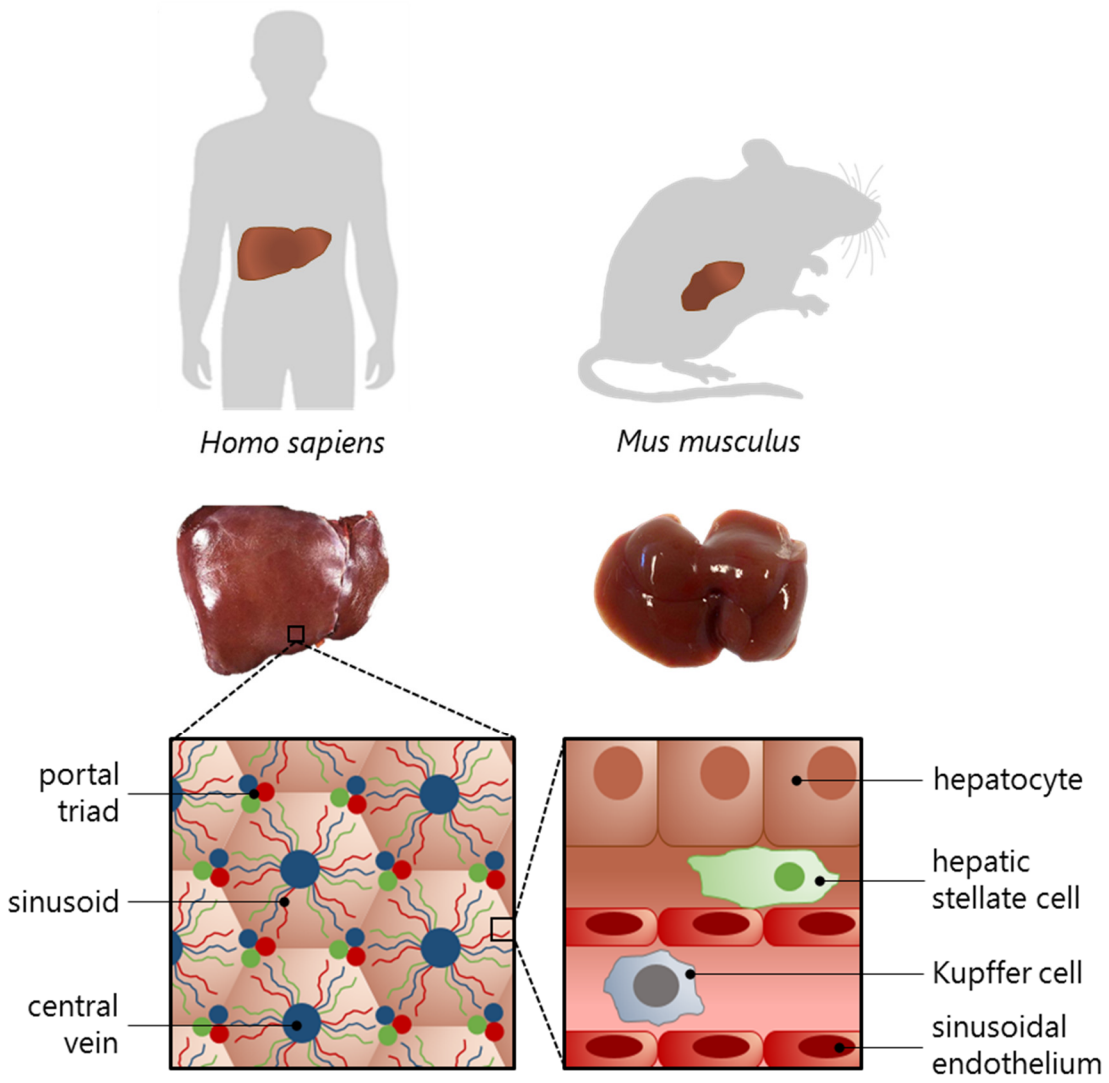

Figure 1.1. Liver structure. The liver is comprised of functional units called lobules, arranged in hexagonal structures where the vertices are defined by a portal triad: the hepatic artery (red) and portal vein (blue) drain into the sinusoid then to the central vein, while the bile duct (green) opens into a larger hepatic duct that delivers bile to the gallbladder. In the lobules, the liver parenchyma is composed mainly of hepatocytes, which perform the metabolic functions of the liver. Between the hepatocytes and sinusoids, which are lined by endothelial cells, is the space of Disse containing quiescent hepatic stellate cells. Within the sinusoids, the Kupffer cells act as the resident macrophages and contribute to the liver's immunotolerance. The location and shape of a mouse liver is shown for comparison (not to scale).

1.1.1.1. Hepatocytes

The vast majority of the liver parenchyma within the lobules is comprised of hepatocytes, the main functional cells of the liver. The role of hepatocytes is diverse, including the processing of nutrients received from the portal circulation, the storage of glucose as inert glycogen as well as glycogenolysis, the detoxification of ammonia and alcohols, and the synthesis of blood proteins such as albumin, to name a few (Kmieć, 2001). Impaired lipid metabolism and storage also results in the accumulation of large fatty vacuoles within these cells, displacing much of the organelles and giving the liver a perforated appearance on histology (*steatosis*).

1.1.1.2. Sinusoidal endothelial cells

The sinusoidal endothelial cells (SECs) line the vessels of the hepatoportal circulation within the lobules. These cells are in immediate contact with the blood draining the mesentery, and act as a nutrient sieve for the hepatocytes (Kmieć, 2001). The endothelium is discontinuous and the SEC membranes are fenestrated with pores that allow the selective passage of macromolecules between the sinusoid and parenchyma. This passage is impaired during liver injury or by aging (see section 1.2.1.3), where *defenestration* leads to metabolic decline of the organ (O'Reilly et al., 2010).

1.1.1.3. Hepatic stellate cells

The hepatic stellate cells (HSCs) are located in the perisinusoidal space of Disse and under normal conditions are metabolically inert, or *quiescent* (Bataller and Brenner, 2005, Kmieć, 2001). The primary function of HSCs in the healthy liver is the storage of retinol (vitamin A) in lipid droplets, for which they were originally termed “lipocytes”. In chronic liver diseases however, a persistent background of inflammation and extrinsic stress will result in HSC activation, whereby the cells adopt a myofibroblastic phenotype and begin producing collagen (Bataller and Brenner, 2005). Excessive collagen deposition into the extracellular matrix, without sufficient turnover or degradation by matrix enzymes, will ultimately result in the accumulation of scar tissue, known as *fibrosis*.

1.1.1.4. Resident immune cells

Under normal conditions, resident macrophages known as Kupffer cells patrol the hepatic sinusoids, preventing incident contamination from gut microflora and dietary toxins or pathogens by antigen presentation to T lymphocytes (Doherty, 2016). They are also responsible for the breakdown of degenerate erythrocyte haemoglobin into bilirubin. However, given the abundance of foreign substances that the liver is exposed to following gastrointestinal digestion, immune cells must also exercise selectivity to allow a small level of tolerance towards our dietary nutrients. During liver disease, resident immune cells will proliferate along with other infiltrating cells, and a sustained inflammatory response will subsequently mediate fibrogenesis in the liver (Bataller and Brenner, 2005).

1.1.1.5. Extracellular matrix

Under normal circumstances, the extracellular matrix (ECM) in the liver is a dynamic micro-environment that facilitates normal cell function. It is composed of various types of structural proteins – collagen, laminin, fibronectin and proteoglycans – as well as matrix enzymes and growth factors, that accommodate the bidirectional diffusion of plasma products across the space of Disse (reviewed in detail elsewhere (Hernandez-Gea and Friedman, 2011)). Ergo, this space is predominantly comprised of the more "soluble" or basement collagen IV, which is regulated by matrix metalloproteinase (MMP) activity during normal ECM turnover. In a fibrogenic environment, the high-density "insoluble" or fibrillar collagen I and III are incorporated into the perisinusoidal region and undergo cross-linking by hydroxyproline. Consequently, regulated turnover by MMPs is replaced by ECM accumulation, such that diffusion becomes less efficient and liver function is impaired.

1.1.2. Normal and abnormal liver function

The liver is arguably the most metabolically versatile organ, capable of performing both exocrine and endocrine functions that contribute to digestion and vascular homeostasis, respectively (VanPutte et al., 2010, Pocock et al., 2013) (Table 1.1). In the context of circulatory maintenance, the liver is involved in the synthesis of plasma proteins, detoxification of portal blood, the degradation of expired red cells, and the production of bile to aid lipid digestion. Finally, the liver is also a storage site for vitamins (in HSCs), and glycogen (in hepatocytes) that is broken down into glucose and released during the post-absorptive state.

Table 1.1. Primary functions of the liver.

Function	*Cells involved*	*Examples*
Digestion		
▪ Nutrient storage	Hepatocyte, HSC	Glycogen, fats, vitamins, trace metals
▪ Nutrient conversion	Hepatocyte	Gluconeogenesis, phospholipid synthesis
▪ Fat digestion	Hepatocyte, cholangiocyte	Produce bile to emulsify fat droplets
Excretion		
▪ Waste clearance	Hepatocyte, KC	Excess cholesterol, bilirubin via bile
▪ Detoxification	Hepatocyte	Ammonia converted to urea
Synthesis		
▪ Blood proteins	Hepatocyte	Albumin, globulin, fibrinogen
▪ Hormones	Hepatocyte, KC	IGF1, angiotensinogen, thrombopoietin, hepcidin

HSC, hepatic stellate cell; KC, Kupffer cell; IGF1, insulin-like growth factor 1.

Given the aforementioned repertoire of functions, diseases of the liver will often have downstream consequences that affect a variety of organ systems, resulting in a decline in general health (Armstrong et al., 2014). As such, there is an urgent push for effective diagnostic tools and therapeutic interventions that limit functional decline of the liver. While successful treatments are becoming available for endemic diseases such as viral hepatitis (World Health Organization, 2017), recent decades have seen a shift in the primary aetiology to a lifestyle-related disorder: fatty liver disease. While part of this burden is attributed to alcoholism, the rise in prevalence can be best explained by an emerging obesity pandemic, especially characteristic of Western countries. Obesity is known to cause a myriad of visceral pathologies, collectively identified by the term "metabolic syndrome" (detailed in section 1.2), whereas non-alcoholic fatty liver disease is the hepatic manifestation of this syndrome. When compared to normal liver function, a fatty liver is characterised by the aberrant regulation of glucose and fatty acid metabolism (reviewed in (Petersen et al., 2017)). This is further elaborated in section 1.2.

1.2. Non-alcoholic Fatty Liver Disease

Non-alcoholic fatty liver disease (NAFLD) is defined by lipid accumulation in at least 5% of hepatocytes, determined by histology, in the absence of secondary causes (European Association for the Study of the Liver (EASL) et al., 2016, Chalasani et al., 2018). In contrast to a similar pathology that develops from chronic alcoholism, NAFLD is instead linked to excessive caloric intake and is often recognised as a complication of metabolic disorders such as obesity and type 2 diabetes. It is unsurprising then, that the increased prevalence of obesity (BMI $\geq$30kg/m^2) in recent decades has seen a parallel increase in NAFLD cases (Loomba and Sanyal, 2013); it is estimated that around 25% of individuals are affected globally (Younossi et al., 2016), with obese populations being at a greater risk (LaBrecque et al., 2014), where NAFLD is almost ubiquitous. In Australia, NAFLD is the leading cause of liver disease by a significant margin, and is second only to hepatitis C in terms of mortality, surpassing primary liver cancer (Deloitte Access Economics, 2013). It is also the fourth-highest indication for liver transplantation (Howell et al., 2016), compared to second-highest in the USA (Cholankeril et al., 2017). Therefore, there is an urgency to understand and manage the progression of this disease in order to stall both its morbidity and mortality.

However, given the significant prevalence of NAFLD and inherent limitations of current diagnostic tools (covered further in section 1.2.2), general screening for the disease is often impractical and not advised. With reference to the Wilson and Jungner screening criteria adopted by the World Health Organization (Andermann et al., 2008), it is difficult to justify the screening for NAFLD in the wider population for a number of reasons, not least due to the expense of "case-finding" since there is no reliable, non-invasive test to predict the disease severity (Chalasani et al., 2018). However, leading hepatology bodies such as the European Association for the Study of the Liver (EASL) and the American Association for the Study of Liver Diseases (AASLD) – as well as the World Gastroenterology Organisation – have proposed guidelines that recommend the screening of individuals that carry known risk factors or comorbidities, including insulin resistance, features of the metabolic syndrome (MetS; Figure 1.2A), or an unexpected elevation of the liver enzyme alanine transaminase (ALT) (European Association for the Study of the Liver (EASL) et al., 2016, Chalasani et al., 2018, LaBrecque et al., 2014).

1.2.1. Pathogenesis of NAFLD

Non-alcoholic fatty liver disease encompasses a spectrum of disorders ranging from simple steatosis (or NAFL) in its early development, to the more severe non-alcoholic steatohepatitis (NASH). The mechanisms involved in the progression from NAFL to NASH are not well understood, however certain anthropometric and clinical parameters have been implicated (LaBrecque et al., 2014) (Figure 1.2A). Whereas NAFLD was once dismissed as a benign accumulation of hepatic fat, its extrahepatic effects are becoming increasingly recognised (Armstrong et al., 2014), such as peripheral insulin resistance and a predisposition to cardiac disease, the leading cause of death in NAFLD patients (Ekstedt et al., 2006). Without due intervention, NAFLD will further develop into the pro-inflammatory phenotype of NASH, which predisposes to more sinister outcomes such as liver cirrhosis (LaBrecque et al., 2014). (Note that cases of *cryptogenic cirrhosis* are often attributed to NASH, as both are determined through exclusion criteria.) This "inflammation driving fibrosis" paradigm is one that is common among liver diseases, although the mechanisms that perpetuate it are unique to each aetiology.

1.2.1.1. Histopathological changes

Changes in liver histology provide the most accurate reflection of the severity of NAFLD (European Association for the Study of the Liver (EASL) et al., 2016, Chalasani et al., 2018, LaBrecque et al., 2014), however classical features may vary between ethnic populations, or between species. In humans, macrovesicular lipid storage in hepatocytes is the hallmark feature of NAFLD and the only anomaly present in simple steatosis. Not to be confused with hepatocellular ballooning, this storage pattern results in the displacement of nuclei by large fatty vacuoles in the cytoplasm (Stern and Castera, 2017) (Figure 1.3B). On the other hand, the additional presence of ballooning (engorged, clarified cytoplasm) and inflammatory foci are distinguishing features of NASH (Lackner, 2011) (Figure 1.3C). These are frequently, but not exclusively, complemented with perisinusoidal fibrosis (Chalasani et al., 2018). As NAFLD progresses further, collagen deposits begin to infiltrate the pericellular regions and may link together, segregating parenchymal "islands" and forming the bridging fibrosis typically seen in pre-cirrhotic and cirrhotic livers. It is now understood that this environment is favourable for the development of hepatocellular carcinoma (HCC) (Michelotti et al., 2013).

A

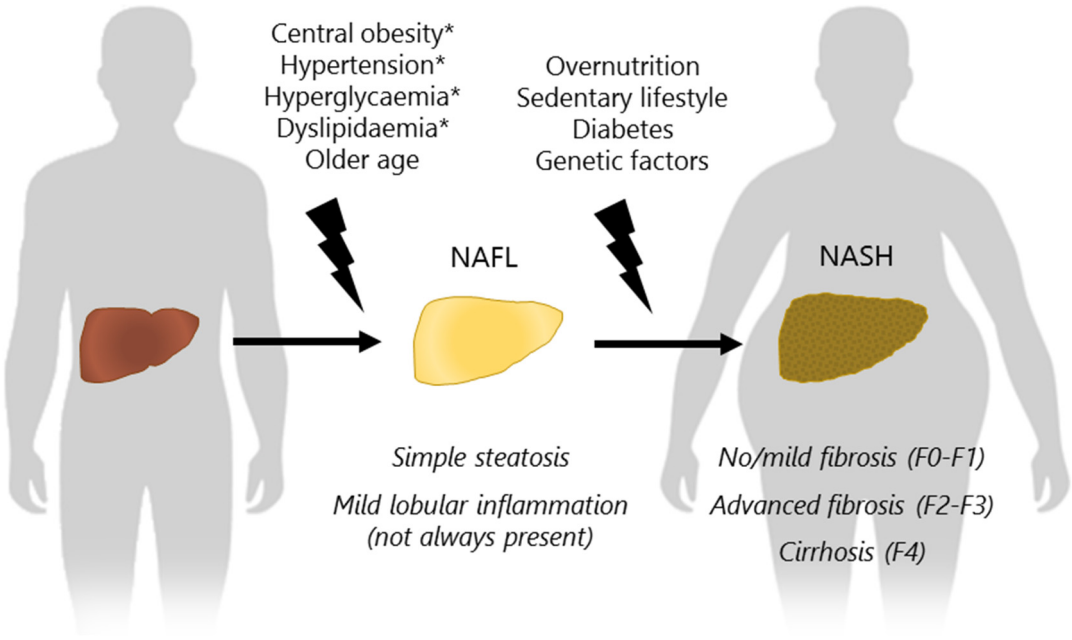
Central obesity*
Hypertension*
Hyperglycaemia*
Dyslipidaemia*
Older age
Overnutrition
Sedentary lifestyle
Diabetes
Genetic factors
NAFL
NASH
Simple steatosis
Mild lobular inflammation
(not always present)
No/mild fibrosis (F0-F1)
Advanced fibrosis (F2-F3)
Cirrhosis (F4)

B

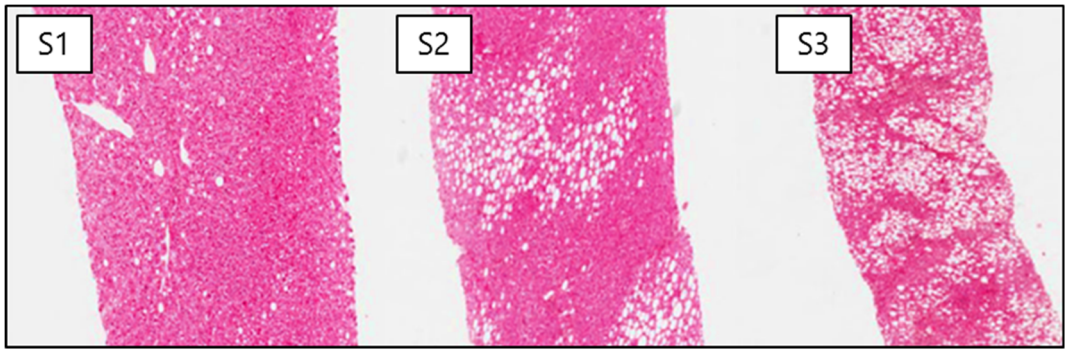
S1
S2
S3

C

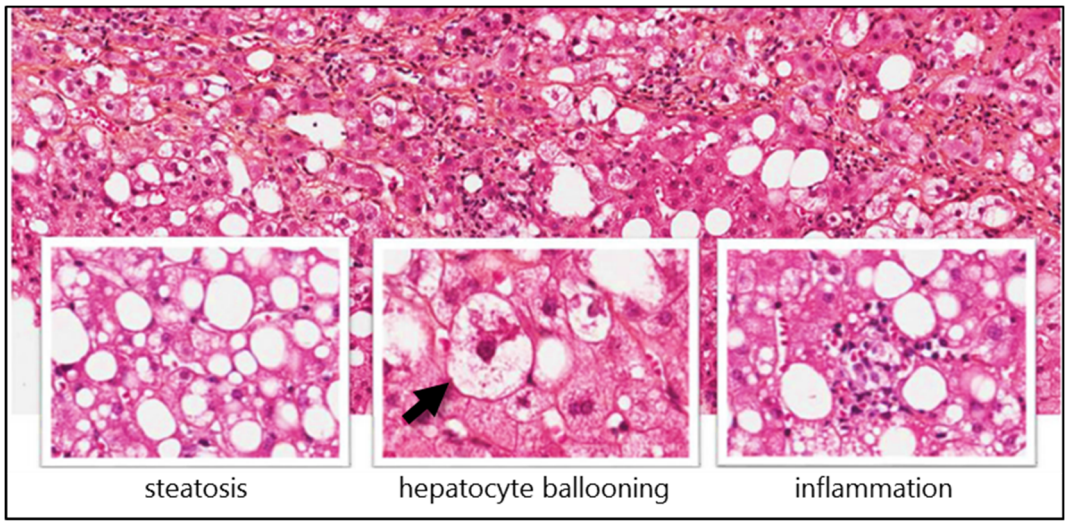
steatosis
hepatocyte ballooning
inflammation

Figure 1.2. Natural history of NAFLD. **A.** Risk factors for progression from simple steatosis (NAFL) to steatohepatitis (NASH) (European Association for the Study of the Liver (EASL) et al., 2016). Components of the metabolic syndrome are denoted by an asterix. Development of NASH usually occurs over decades, with fibrosis severity described according to the Kleiner classification system (F0-F4) (Kleiner et al., 2005). Lipodystrophy and genetic polymorphisms, most notably at the *PNPLA3* locus, are also less frequent modifiers of NAFLD. **B.** NAFLD histology with three independent biopsies representing increasing grades of steatosis: less than 33% (S1), 34-66% (S2), and greater than 66% (S3) of hepatocytes containing lipid droplets. S0 signifies less than 5% steatosis, or absence of NAFLD (not shown). **C.** NASH phenotype with typical characteristics inset. Hepatocyte ballooning and leukocyte infiltrates distinguish NASH from NAFL. Panels B and C adapted from elsewhere (Stern and Castera, 2017).

1.2.1.2. Metabolic and molecular changes

On a background of obesity, NAFLD occurs as a consequence of increased fatty acid flux as a result of adipose tissue expansion and lipolysis (Byrne et al., 2009, Jensen, 2008). When this expansion exceeds the capacity of the adipose extracellular matrix to maintain a stable fat depot, ectopic fat deposition is seen in the visceral organs. This is promoted by the migration of long-chain fatty acids (LCFA) to the liver, for example (Figure 1.3), and together with increased dietary monosaccharides such as glucose and fructose, there is an upregulation of *de novo* lipogenesis (Postic and Girard, 2008). Aside from the formation of hepatocellular lipid droplets containing triacylglycerol (TAG), free fatty acids and intermediates of the lipogenesis pathway – in particular, diacylglycerol (DAG) – are also responsible for hepatic inflammation and insulin resistance (Jornayvaz and Shulman, 2012, Boden et al., 2005). Therefore, an increase in hepatic inflammatory cytokines (TNF and IL6), chemokines (MCP1) and growth factors (TGFβ) are typical features of NAFLD (Braunersreuther et al., 2012, Boden et al., 2005). These are complemented with elevated TAG in both the liver, and in the circulation in the form of chylomicrons or very-low density lipoproteins (VLDL), whereas leukocyte recruitment and hepatocyte injury become evident in NASH.

Some studies have examined the immediacy of NAFLD pathogenesis in rodent models. For instance, Turner and colleagues showed that early events such as increased fasting blood glucose and body weight gain, evident after 5-6 weeks of high-fat feeding in mice, are preceded by acute changes including glucose intolerance, hyperinsulinaemia, and increased fatty acids in the liver (Turner et al., 2013). These changes became present by 1 week, and continued to increase in the case of plasma insulin and hepatic TAG, whereas hepatic DAG remained stable after the initial increase. A similar study in rats confirmed the early onset of hyperinsulinaemia, together with increased liver fatty acids and presence of steatosis (Ciapaite et al., 2011). Interestingly, both parameters were also affected by aging, suggesting that the progression of NAFLD defined by increased liver lipid may also be influenced by (or synergise with) inherent biological factors.

To complement this paradigm, a study of obese humans provided an argument for accelerated epigenetic "aging" of the liver in NAFLD (Horvath et al., 2014). In this cross-sectional analysis, a strong correlation was found between BMI and DNA methylation in the liver specifically, when compared to other tissues. Furthermore, these epigenetic changes were not reversed by acute weight loss, either in the form of exercise or bariatric surgery, which suggests that obesity presence may predispose to more permanent complications.

Systemic changes with obesity are also manifest in the circulation, however the contribution of NAFLD specifically is not always clear. Correlative studies have shown that some biomarkers are elevated and may be useful in aiding diagnosis (see section 1.2.2.2). It is also expected that VLDL, formed during lipogenesis and predominantly comprised of TAG, would be more abundant in obese NAFLD (Figure 1.3). Studies of the hepatic and plasma lipidome have shown that many other lipid species also become dysregulated (Puri et al., 2007, Puri et al., 2009), and are comparable between humans and mice (Gorden et al., 2011), although their utility as biomarkers haven't yet been explored. As in most aetiologies of liver disease, circulating liver transaminases are elevated (LaBrecque et al., 2014), hinting at possible hepatocellular injury. While both alanine (ALT) and aspartate (AST) transaminase are typically present in equal proportion (Botros and Sikaris, 2013), NAFLD tends to favour a De Ritis ratio (AST:ALT) of less than 1, which is useful in its differentiation from alcoholic fatty liver disease that tends to have a ratio >2 (Sorbi et al., 1999, LaBrecque et al., 2014). However, there are some conflicting reports on the utility of circulating liver enzymes for the assessment of NAFLD, particularly ALT. For instance, one study has shown that levels of this enzyme may fluctuate depending on fibrosis severity (Sorbi et al., 1999), whereas levels within the reference range are also commonly observed for NAFLD patients, independently of disease spectrum (LaBrecque et al., 2014, Mofrad et al., 2003).

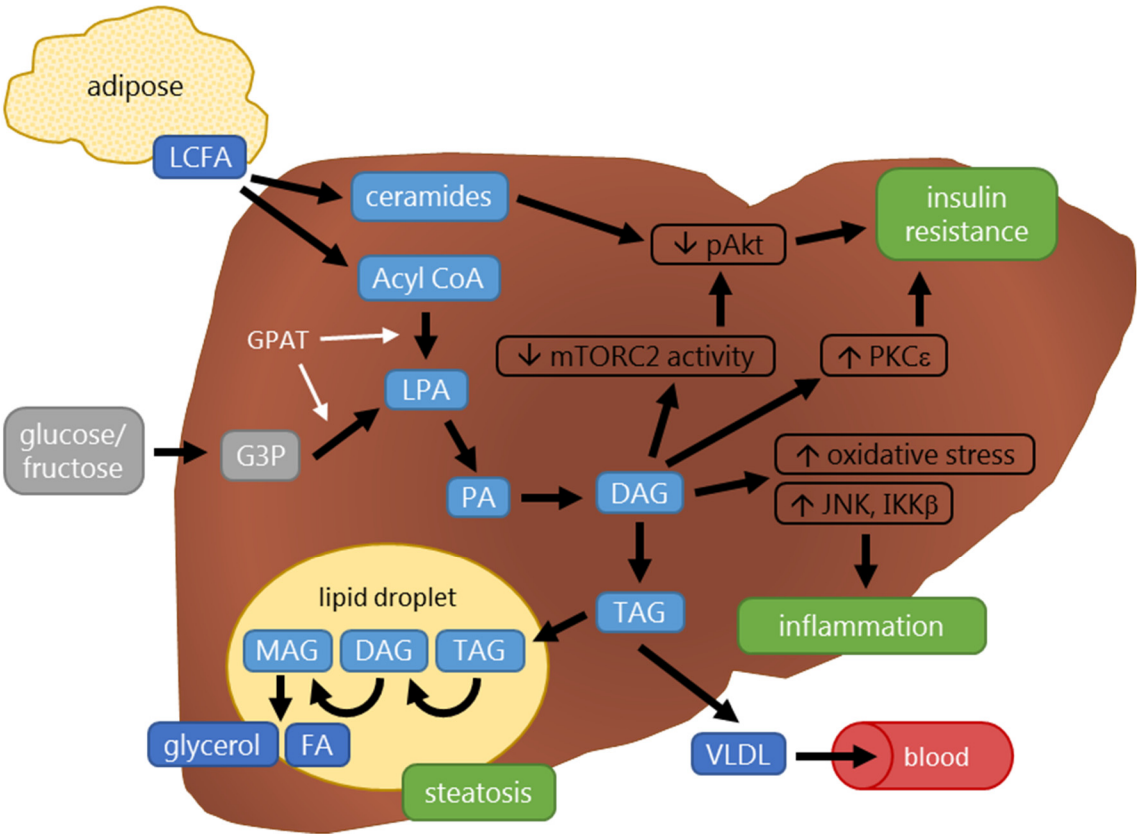

Figure 1.3. Mechanisms of NAFLD development. Both long-chain fatty acids (LCFA) from adipose tissue and glycolytic intermediates are involved in hepatic *de novo* lipogenesis. This process results in the production of triacylglycerol (TAG), which is incorporated into either lipid droplets within hepatocytes, or into very-low-density lipoproteins (VLDL) that are released into the circulation. TAG may be further broken down into its glycerol and fatty acid (FA) components within lipid droplets. Diacylglycerol (DAG), an intermediate of lipogenesis, is also involved in mediating hepatic insulin resistance and increasing the expression of transcription factors that drive inflammation. Schematic developed from (Perry et al., 2014) and (Byrne and Targher, 2015). Abbreviations: G3P, glycerol-3-phosphate; GPAT, G3P acyltransferase; LPA, lysophosphatidic acid; PA, phosphatidic acid; mTORC2, mammalian target of rapamycin complex 2; PKCε, protein kinase C ε; JNK, c-Jun N-terminal kinase; IKKβ, inhibitor of nuclear factor kappa β.

1.2.1.3. Effects of aging

Irrespective of NAFLD, gross changes in liver structure are a recognised feature of aging. The most defining of these are reduced total volume – which translates to reduced cell mass with compensatory cell hypertrophy – and decreased blood flow (Wynne et al., 1989, Wynne and James, 1990). In terms of liver function, there is an impaired capacity to synthesise macromolecules or to clear toxins, and response to stress is also less robust (Wynne and James, 1990). Studies using rodent models have further elucidated the molecular changes that accompany aging, namely those affecting fatty acid oxidation and oxidative stress (Houtkooper et al., 2011), as well as apoptosis pathways (Fontana et al., 2013). These are paralleled by an increase in circulating free fatty acids and a decrease in energy expenditure in older animals (Houtkooper et al., 2011, Xiong et al., 2014). This environment may contribute to increased fatty acid storage in the liver with age.

The intersection between NAFLD and aging has been extensively studied (Bertolotti et al., 2014, Gan et al., 2011). A key mechanism involved in both phenomena is insulin resistance; impaired signalling downstream of the insulin receptor have been linked to insulin resistance in the elderly (Fink et al., 1983, Rowe et al., 1983), which subsequently predisposes to the development of hepatic steatosis. In fact, older patients frequently present with more severe NAFLD and tend to have a worse prognosis than younger sufferers (Frith et al., 2009). This is linked to an increase in risk factors associated with aging, such as hypertension, diabetes, and obesity (Frith et al., 2009), which promote the development of fibrosis (Kichian et al., 2003). A similar trend was also observed in a mouse model of high-fat feeding (Fontana et al., 2013), where aged animals had a (paradoxically) heightened immune response, specifically of a pro-inflammatory nature (M1 macrophage phenotype). Finally, given that estrogen suppressed the rate of NAFLD development and is no longer protective following menopause (Gutierrez-Grobe et al., 2010), it may be inferred that animal studies often favour the use of male subjects to avoid this confounding factor.

1.2.2. Diagnosis of NAFLD

Arguably one of the greatest challenges facing hepatologists in recent decades is the accurate diagnosis of NAFLD. Without effective screening measures (see section 1.2) and in the absence of evidence-based clinical guidelines (LaBrecque et al., 2014), identification of potential cases relies on data from population studies, often with disparate findings due to ethnic variation in anthropometric measurements (Almeda-Valdes et al., 2016). This may in turn lead to systemic under-diagnosis (Alexander et al., 2018). While some indicators are universally accepted (e.g. BMI, waist circumference), an accurate diagnosis requires expensive or sophisticated tools that are not generally accessible (Stern and Castera, 2017). Furthermore, invasive procedures such as tissue biopsy are still considered the gold standard for the staging of disease severity (European Association for the Study of the Liver (EASL) et al., 2016), although the precision of first-line imaging techniques has improved in recent years (Table 1.2). With non-invasive assessment becoming the focus, much effort has been invested in the discovery of biomarkers that are both practical and can provide a reliable snapshot of an individual's NAFLD status.

1.2.2.1. Liver biopsy

Technical limitations and confounding factors of non-invasive tools for diagnosis have meant that direct histological examination is still the preferred option for the assessment of disease grade in NAFLD (reviewed in (Nalbantoglu and Brunt, 2014)). For example, the NAFLD activity score (NAS) is an algorithm derived from biopsy information, and has been validated by the NASH Clinical Research Network (Kleiner et al., 2005). NAS classification addresses steatosis, hepatocellular ballooning, and lobular inflammation to assign a cumulative score depending on the severity of each feature. Not unlike many invasive procedures of a similar nature, liver biopsy suffers from a number of safety limitations, most of which can be controlled given adequate resources. The most common risks include pain and bleeding at the site of biopsy, although these usually resolve within 72 hours, while major complications are rare (Filingeri et al., 2015). Discrepancies in sampling and pathological assessment are another concern, both of which are recognised technical caveats that may further complicate the accurate diagnosis of NAFLD (Ratziu et al., 2005, Vuppalanchi et al., 2009). Nevertheless, pending adherence to clinical guidelines that attempt to standardise the diagnostic workflow, these issues may be circumvented.

1.2.2.2. Non-invasive techniques

Liver biopsy is not a first-line tool for screening patients at a higher risk of NAFLD and is usually reserved for cases where NASH is suspected, due to its invasiveness. For a preliminary diagnosis, imaging techniques are most commonly used in a clinical practice setting (Table 1.2). Ultrasound specifically is the favoured option (LaBrecque et al., 2014, European Association for the Study of the Liver (EASL) et al., 2016), as the technology is both accessible and simple to operate, although it is less sensitive and more error prone when compared to its more expensive counterparts such as magnetic resonance techniques (Reeder et al., 2011).

Since liver imaging is often qualitative, circulating biomarkers are also being used – either in isolation, or in combination with preclinical parameters – as surrogate markers of NAFLD to complement the diagnosis (Table 1.3). While many complex panels have been established, including the popular fatty liver index (FLI), none are universally applied in healthcare. It has been proposed that this may be due to the fact that such panels do not provide any additional information when compared to existing methods, and that their diagnostic superiority is only relative to the standards against which they were validated (Stern and Castera, 2017).

Indeed, the combination of biochemical and/or anthropometric parameters cannot accurately quantify steatosis (Fedchuk et al., 2014) or differentiate NAFL from NASH, which reinforces the necessity for biopsy (European Association for the Study of the Liver (EASL) et al., 2016). Furthermore, both imaging and clinical biomarker alternatives are also susceptible to common confounders, such as visceral adiposity (Castera et al., 2010) and aging (McPherson et al., 2017). Of course, this does not preclude the utility of current and potential biomarkers as important mediators of disease, however, their activity *in vivo* may not be reflective of their circulating abundance. For the reasons above, a novel diagnostic candidate is required to increase the reliability of NAFLD assessment, ergo this thesis will focus on the potential of extracellular vesicles (described in section 1.3) in fulfilment of this role.

Table 1.2. Imaging techniques used for NAFLD diagnosis.

Test	*Advantages*	*Limitations*	*AUROC**	*Population, n*	*References*
Controlled attenuation parameter (CAP)	▪ Simple ▪ Rapid ▪ Accessible	▪ Operator-dependent ▪ Cut-offs vary ▪ FibroScan ™ required	0.67-0.97 0.75-0.97 0.82-0.94 0.88-0.92 0.91-0.95	79 161 65 152 115	(Chan et al., 2017) (Chan et al., 2014) (Karlas et al., 2014) (Shen et al., 2014) (Sasso et al., 2010)
Computerised tomography (CT)	▪ Entire liver	▪ Low sensitivity ▪ Radiation exposure	0.65-0.92 0.99	161 154	(Lee et al., 2010b) (Park et al., 2006)
Magnetic resonance imaging (MRI)	▪ Sensitive ▪ Reproducible ▪ Rapid ▪ Entire liver	▪ Expensive ▪ Less accessible	0.88-0.99	161	(Lee et al., 2010b)
Proton magnetic resonance spectroscopy (^{1}H-MRS)	▪ Sensitive ▪ Reproducible ▪ Entire liver	▪ Expensive ▪ Less accessible ▪ Time consuming ▪ Expertise required	0.85-0.88 0.85-0.91 0.95-0.99	65 161 77	(Karlas et al., 2014) (Lee et al., 2010b) (McPherson et al., 2009)
			Sensitivity, %		
Ultrasound (US)	▪ Simple ▪ Inexpensive ▪ Accessible	▪ Operator-dependent ▪ Low sensitivity ▪ Qualitative	39-49 55-80	187 100	(Mottin et al., 2004) (Ryan et al., 2002)

*AUROC dependent on cut-off values for steatosis grade. Sensitivity ranges determined by steatosis grade or body mass index. Advantages and limitations adapted from elsewhere (Stern and Castera, 2017). Abbreviations: AUROC, area under receiver operator curve.

Table 1.3. Biomarkers and complex panels used for NAFLD diagnosis.

Test	*Parameters*	*AUROC*	*Population, n*	*References*
NAFL (steatosis)				
Cytokeratin 18 (CK18)	Single biomarker, circulating	0.77	424	(Cusi et al., 2014)
Fatty acid binding protein (FABP)	Single biomarker, circulating	0.66	220	(Shen et al., 2012a)
Fibroblast growth factor 21 (FGF21)	Single biomarker, circulating	0.84	220	(Shen et al., 2012a)
Fatty liver index (FLI)	BMI, GGT, TAG, WC	0.84	496	(Bedogni et al., 2006)
Hepatic steatosis index (HSI)	AST/ALT, BMI, DM	0.81	10724	(Lee et al., 2010a)
Lipid accumulation product (LAP)	sex, TAG, WC	0.79	588	(Bedogni et al., 2010)
NAFLD liver fat score	AST/ALT, DM, insulin, MetS	0.87	470	(Kotronen et al., 2009)
SteatoTest ™	A2M, age, ALT, ApoA1, bilirubin, BMI, cholesterol, GGT, glucose, HG, sex, TAG	0.79	744	(Poynard et al., 2005)
NASH				
Index of NASH (ION)	ALT, HOMA-IR, TAG	0.77	4458	(Otgonsuren et al., 2014)
NashTest ™	A2M, age, ALT, AST, ApoA1, BMI, bilirubin, cholesterol, GGT, HG, sex, TAG	0.79	257	(Poynard et al., 2006)

A2M, alpha 2 macroglobulin; ALT, alanine transaminase; AST, aspartate transaminase; ApoA1, apolipoprotein A1; AUROC, area under receiver operator curve; BMI, body mass index; DM, diabetes mellitus; GGT, gamma glutamyl transferase; HG, haptoglobin; HOMA-IR, homeostatic model assessment of insulin resistance; MetS, metabolic syndrome; TAG, triacylglycerol; WC, waist circumference.

1.2.3. Prognosis and monitoring

NAFLD is often classified as a "benign" disease with respect to its evolution (Chalasani et al., 2018). However, this is largely dependent on its severity; being a spectrum of disorders, the prognosis for NAFLD is heterogeneous, where simple steatosis is understood to have a slower progression and better outcomes than NASH (Angulo et al., 2015, Singh et al., 2015). On the other hand, NAFLD is a frequent subclinical complication of obesity and T2DM that relies on incidental diagnosis due to a lack of screening measures (see section 1.2). If detected early, the steatosis may be partially alleviated or stalled from progressing by simple changes to lifestyle habits, including diet and physical activity (Vilar-Gomez et al., 2015, Zelber-Sagi et al., 2011). In fact, such modifications are the preferred prescription in clinical practice (Ratziu et al., 2012). However, in the event of a NASH diagnosis, pharmacological intervention may be necessary; there are several drugs targeting various elements of NAFL to NASH progression, although most are still in the clinical trial phase and are administered off-label (reviewed elsewhere by (Perazzo and Dufour, 2017)). Since a large meta-analysis of clinical data has revealed that NAFLD increases the overall risk of liver-related mortality, as well as the risk of developing T2DM and cardiovascular disease (Musso et al., 2011), monitoring of these patients is recommended at 2-3 year intervals (European Association for the Study of the Liver (EASL) et al., 2016). For NASH and cases at risk of progression, monitoring should take place annually, with a follow-up biopsy at 5 years (at the discretion of the physician). A detailed protocol for NAFLD monitoring is available in the EASL-EASD-EASO clinical guidelines (European Association for the Study of the Liver (EASL) et al., 2016) or in the recent AASLD practice guidance report (Chalasani et al., 2018).

1.2.4. Experimental models

The phenotype of NAFLD has been replicated both *in vivo* and *in vitro* with varying degrees of biological similarity to the human disease (Chavez-Tapia et al., 2011, Machado et al., 2015, Teufel et al., 2016). While certain features of hepatocellular injury in human NAFLD may be absent in mice, hypertrophy due to microvesicular steatosis seems to be more predominant in the latter (Liang et al., 2014). Rodent models that receive liver specific insults are more prone to develop NASH, however, they lack the metabolic features that reflect physiological NAFLD development and therefore they are usually favoured for studies examining liver disease in isolation (Rinella and Green, 2004). The following sections describe some common experimental models of NAFLD, and also outline some genetic and lifestyle interventions that have been used to stall or reverse the disease.

1.2.4.1. Nutritional models

High-fat diet (HFD) is perhaps the most relevant model with respect to the typical aetiology of NAFLD, since obesity, insulin resistance, and other features of the metabolic syndrome are present. Most HFD formulations contain between 30-80% energy (calories) derived from lipid, particularly saturated fats (Hariri and Thibault, 2010). Another key player in obesogenic diets is fructose, which has been shown in rodent models to accelerate NAFLD progression to NASH: a fructose-enriched HFD promotes oxidative stress, as well as increasing leukocyte infiltration and fibrogenesis when compared to HFD alone (Kohli et al., 2010).

Some non-obesogenic diets are also capable of producing steatosis, in the absence of both adiposity and insulin resistance. For example, an atherogenic (high-cholesterol) diet has been shown to result in hepatomegaly with increased hepatic gene expression of molecules involved in fatty acid synthesis and oxidative stress (Matsuzawa et al., 2007). Also commonly used in NASH studies, the methionine and choline deficient diet (MCD) is known to disrupt VLDL secretion and mitochondrial β oxidation, while closely mimicking the histopathology of human NASH but without the metabolic profile (Machado et al., 2015, Rinella and Green, 2004). Due to their liver specificity, elevated serum ALT is observed in both diets, while the typical changes in serum insulin and triglyceride levels seen with obesogenic diets is absent. See Table 1.4 for a summary of outcomes from nutritional models.

1.2.4.2. Genetic models

There are several transgenic rodent strains used as preclinical models of NAFLD (reviewed in (Jacobs et al., 2016)) (Table 1.4). Here, we focus on models that reflect physiological NAFLD progression. Common examples include the leptin mutant (*ob/ob*) or leptin receptor mutant (*db/db*) mouse, where disruption to the signalling pathway of the leptin hormone causes an impaired satiety response and consequent overeating, resulting in obesity and other features of the metabolic syndrome (Trak-Smayra et al., 2011). Spontaneous mutation in the leptin receptor has also been reported in Zucker rats (Phillips et al., 1996), where the autosomal recessive trait (*fa/fa*) results in "inherited obesity" that is metabolically akin to the *ob/ob* and *db/db* phenotypes, whereas early-onset insulin resistance has also been documented in this model (Durham and Truett, 2006). Finally, the dysfunction of neuronal cilia through an *Alms1* gene mutation (*foz/foz*) has also been associated with hyperphagia (Heydet et al., 2013), although the exact mechanisms are unclear. Of interest, the severity of NAFLD in *foz/foz* mice is strain-dependent; while the mutation results in comparable obesity, C57Bl/6 animals are more susceptible to the metabolic and pathological outcomes than their BALB/c counterparts (Farrell et al., 2014).

Table 1.4. Summary of common nutritional and genetic models of NAFLD.

Model	*IR*	*Obese*	*Steatosis*	*NASH*	*Fibrosis*
Nutritional					
▪ High-fat diet (HFD)	yes	yes	yes	yes	yes
▪ High-fat with fructose	yes	yes	yes	yes	yes
▪ Atherogenic (high cholesterol) #	-	-	yes	yes	yes
▪ Methionine-choline deficient #	yes	-	yes	yes	yes
Genetic					
▪ *ob/ob* (leptin$^{-/-}$)	yes	yes	yes	-	- *
▪ *db/db, fa/fa* (leptin receptor$^{-/-}$)	yes	yes	yes	-	-
▪ *foz/foz* (*Alms1* mutation)	yes	yes	yes	yes	yes

*This model is resistant to hepatic fibrosis. # Outcomes may differ for rats. Abbreviations: IR, insulin resistance. Adapted from (Jacobs et al., 2016) and (Kucera and Cervinkova, 2014).

1.2.4.3. Intervention strategies

The most common interventions for treating NAFLD are non-pharmacological, involving either physical activity or a calorie-restricted diet. In animal models, the effect of exercise on steatosis has been extensively documented, typically reporting a decrease in insulin resistance, hepatic lipogenesis, and inflammation with frequent treadmill running (Alex et al., 2015, Cho et al., 2014, Kawanishi et al., 2012). Furthermore, when comparing moderate intensity aerobic exercise to high-intensity interval training, the latter seemed to provide a greater protection against NAFLD pathogenesis, which was linked to increased FFA oxidation and suppression of hypoadiponectinemia (Cho et al., 2015). For information regarding clinical studies using exercise intervention on patients with NAFLD, please refer to Chapter 5.1.

Another approach is to interrupt the molecular pathways that mediate NASH, using genetic ablation of cytokines and their receptors in rodent models (reviewed in (Braunersreuther et al., 2012) and (Tilg and Moschen, 2008)). One example is the global gene deletion of TNF, a cytokine released by stressed parenchymal cells that is known to play a role in insulin resistance by suppressing IRS1 downstream of the insulin receptor (Feinstein et al., 1993, Hotamisligil et al., 1994). However, inconsistent findings are testament to the fact that slight differences in experimental design will often produce heterogeneous results. These thoughts are developed further in Chapter 5.4 – along with details about the biological role of TNF signalling in adipogenesis – where outcomes of our genetic manipulation study are explored in context.

1.3. Extracellular Vesicles

Extracellular vesicles (EVs) are submicron, membrane-bound structures released from cells during activation, physiological stress, or apoptosis. They are present in all biological fluids including blood, urine, bile, semen, milk, amnion, and cerebrospinal fluid and are derived from either local or distant tissues, as well as commensal organisms or pathogens (Yanez-Mo et al., 2015). The rationale for EV-mediated signalling is thought to be increased stability (Kalra et al., 2013, Yanez-Mo et al., 2015); that is, to preserve the integrity of bioactive molecules in a medium where they would otherwise be degraded by soluble enzymes (Valadi et al., 2007). To this end, endogenous EVs increase the efficiency of intercellular communication for their cargo, while artificially manipulated or exogenous EVs have been utilised for efficient drug delivery (Kooijmans et al., 2012).

1.3.1. Extracellular vesicle subtypes

Three main subtypes of extracellular vesicles have been classified in animals, and differ in their biogenesis. The largest in terms of size are apoptotic bodies (ABs), which have similar dimensions to platelets and are often excluded during size-based isolation techniques (Witwer et al., 2013). Strictly speaking, ABs aren't released from cells but rather occur as a product of organelle compartmentalisation during cell apoptosis (Akers et al., 2013). For this reason, they tend to be neglected from most EV-based studies. Other EV subtypes are described below and summarised in Figure 1.4.

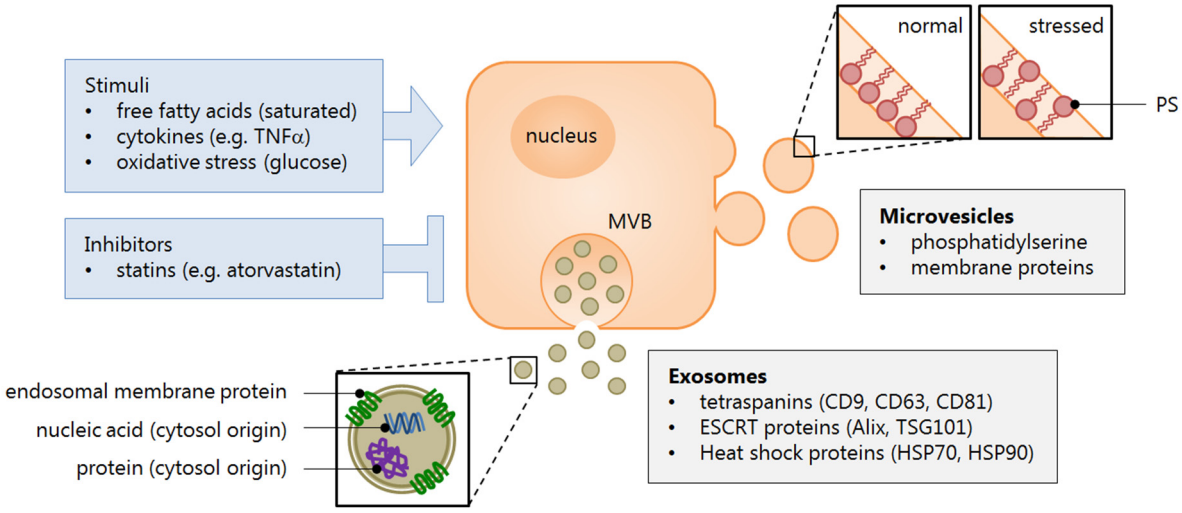

Figure 1.4. Extracellular vesicle subtypes. Cells respond to a variety of stimuli that cause inflammation and metabolic stress, which result in their impaired functioning or apoptosis. This mechanism drives the release of EVs, which signal to paracrine or distal effectors the condition of the cell microenvironment. Effector cells may, in turn, respond by selectively imparting regulatory molecules – small nucleic acids (mRNA and miRNA; blue), lipids, and proteins (purple) – contained within EVs, that are taken up by the recipient cell. The EV subclasses are identified by membrane markers that denote the site of their biogenesis. Exosomes typically express tetraspanins (endosomal membrane protein; green), while microvesicles are understood to contain phosphatidylserine (PS). These lipoproteins are normally oriented towards the cytosol to maintain the cell membrane asymmetry, but during conditions that stimulate EV release, the molecules become everted. The stimuli and inhibitors of EV release described in this figure are in reference to hepatocytes in the context of NAFLD. Abbreviations: ESCRT, endosomal sorting complexes required for transport; MVB, multivesicular body; PS, phosphatidylserine. Image retrieved from a publication by the author and colleagues (Ban et al., 2016).

1.3.1.1. Microvesicles

Microvesicles (MVs) are the larger of the secreted vesicle subtypes (up to 1μm), released from the cell membrane in a *budding* fashion (Hugel et al., 2005) (Figure 1.5). MVs are subsequently taken up by recipient cells by endocytosis (Costa Verdera et al., 2017). Prior to budding, the orientation of membrane phosphatidylserine changes (Hugel et al., 2005); under basal conditions, this phospholipid is largely facing the cytosol (asymmetrical) whereas upon cell stress, it is everted toward the intercellular space. This change is often associated with apoptosis signalling, however in the context of EVs, phosphatidylserine is also a recognised marker of MVs. Since the mammalian protein Annexin A5 binds to phosphatidylserine with high affinity (Rand et al., 2012), this protein is often used for MV targeting in place of antibodies for immunoaffinity assays, such as flow cytometry.

1.3.1.2. Exosomes

Finally, the smallest EV subtype and arguably the most popular for mechanistic studies is the exosome. Often referred to as nanovesicles and measuring under 100nm, these EVs are released by exocytosis from a subset of late endosomes called multivesicular bodies (MVBs) (Simons and Raposo, 2009). Exosomes are formed within MVBs from the endosomal membrane, a process involving the endosomal sorting complexes required for transport (ESCRT). These cytosolic proteins are responsible for MVB biogenesis and the packaging of molecules destined for endo-lysosomal destruction, or release through exosomes (Hessvik and Llorente, 2018). Given their origin, recognised markers of exosomes include endosomal proteins such as tetraspanins (most commonly, CD9 and CD63) as well as accessory proteins of the ESCRT pathway (Alix and TSG101). Exosomes and microvesicles are often difficult to distinguish due to their phenotypic overlap (van der Pol et al., 2012, Yanez-Mo et al., 2015). For instance, size-based comparisons may be erroneous given that smaller MVs are similar in dimension to the upper limit of exosomes. Furthermore, while the expression of membrane proteins is technically unique to each subtype – reflecting their compartment of origin, respectively – there may be considerable overlap in their cytosolic cargo. For this reason, standard techniques for EV isolation and characterisation remain a contested subject among researchers (Gould and Raposo, 2013), which is discussed in more detail in section 1.3.5.

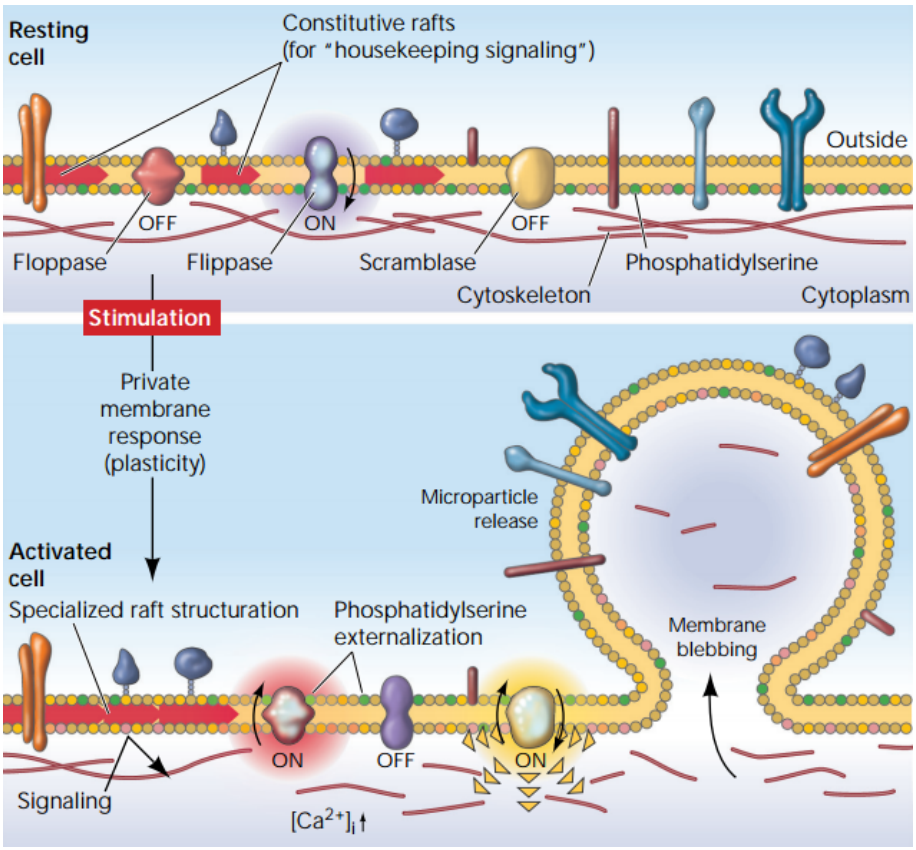

Figure 1.5. Mechanism of microvesicle release. The shedding of vesicles is under the control of a series of membrane protein pumps with antagonistic roles. The stability of resting cells is determined by flippase activity, which maintains the internalisation of phosphatidylserine (PS). During cell stress, a rise in cytosolic Ca^{2+} activates floppase (PS specific) and scramblase (non-specific), which together are responsible for "bidirectional redistribution" of phospholipids. Further to this, calcium-dependent remodelling of cytoskeletal proteins will ultimately result in membrane instability and subsequent MV release. Where necrosis results in the loss of pan-membrane integrity, MV shedding may occur in the absence of regulation by membrane proteins. Image and text modified from elsewhere (Hugel et al., 2005).

1.3.2. Extracellular vesicles in liver disease

Almost all cell types ubiquitously release extracellular vesicles. In normal physiology, most circulating EVs are derived from platelets and endothelial cells, and have been shown to be important in common haemostatic events such as coagulation (Lynch and Ludlam, 2007). While vesicles of the same origin have been implicated in disease complications of a pro-coagulative nature (Ogasawara et al., 2005, Stravitz et al., 2013), there is still a paucity of knowledge regarding the dynamics of EV secretion by different cell types and in particular how the secreted EVs interact to advance the pathogenesis of a given disease.

Controlled *in vitro* experiments have provided the most direct lines of evidence for EV regulation, including how the stimulus for release may affect their phenotype (Bernimoulin et al., 2009). There is a wealth of research using liver injury models to explore EV-mediated fibrosis (Charrier et al., 2014, Chen et al., 2014, Kornek et al., 2011), transcriptomic signalling (Fonsato et al., 2012, Kogure et al., 2011, Kogure et al., 2013, Momen-Heravi et al., 2015, Takahashi et al., 2014), and targeted immunotherapy (Lv et al., 2012, Xiao et al., 2013, Zhang et al., 2014) in artificial cell culture systems. However, *in vivo* studies present an added degree of complexity due to the difficulty of identifying liver specific EVs within the circulating pool. For this reason, most studies have opted to focus on circulating vesicle characterisation and their temporal changes in relation to liver disease development (Brodsky et al., 2008, Freeman et al., 2014, Li et al., 2015, Sugimachi et al., 2015, Sun et al., 2013, Wang et al., 2014), while others have pointed to roles in extrahepatic cancer metastasis to the liver (Costa-Silva et al., 2015, Eldh et al., 2014, Wang et al., 2015), although direct functional relationships have yet to be explored.

Some groups have approached the study of EVs from a more organ-targeted perspective, assessing their role as paracrine mediators. Most of these studies evaluate the effect of EVs in fibrogenesis, for example, the shuttling of pro-fibrogenic connective tissue growth factor (CTGF) between hepatic stellate cells on the one hand (Charrier et al., 2014), or the CTGF inhibiting miRNA-214 between stellate cells and hepatocytes or adjacent stellate cells on the other hand (Chen et al., 2014). Immune-mediated modulation has also been suggested; one study had demonstrated a role for T cell-derived EVs in the induction of stellate cell fibrolytic activity, as defined by an increase in the gene expression of MMPs (Kornek et al., 2011). The findings concluded that this response from the stellate cells was likely mediated by the homodimeric interaction of CD147 at the EV-cell interface. A pro-inflammatory glycoprotein, CD147 had previously been implicated in liver disease pathogenesis by our group (Calabro et al., 2014, Lee et al., 2016) as well as having a well documented role in tumour metastasis, which more recently had been attributed to EV-mediated translocation (Millimaggi et al., 2007, Sidhu et al., 2004, Zhang et al., 2013).

Secreted vesicles have also been linked to paracrine signalling in the tumour micro-environment, whereby miRNAs shuttled from hepatoma cells were able to modulate protein expression in adjacent hepatocytes and to increase their proliferative potential (Kogure et al., 2011, Kogure et al., 2013). Silencing of these miRNAs, in turn, had abrogated the pro-tumorigenic effects, while another study had suggested a role for liver stem cell-derived EVs in miRNA-mediated tumour suppression (Fonsato et al., 2012).

1.3.3. Extracellular vesicles in NAFLD

Liver research involving EVs as disease mediators faces a number of inherent challenges. The most important of these is finding a link between the circulating EV populations and a specific contribution from the liver. From a biomarker perspective, it could be argued that a quantitative or phenotypic change in circulating EVs with disease may validate their diagnostic utility, especially if these changes are intensified with NAFLD progression. Unfortunately, given the complex biological determinants of EV secretion, rather than a linear relationship we are more likely to see dynamic responses from different tissues during the course of pathogenesis. For a start, NAFLD is not an isolated condition and, generally speaking, occurs as a complication of other metabolic disorders where global insulin resistance is also present. Therefore, multiple tissues may be affected by the resulting oxidative stress and fatty acid flux, which in turn promotes the activation of immune cells and their migration to these sites. Consequently, the extrahepatic release of EVs may in fact mask the pathogenesis of NAFLD. For this reason, and the lack of a specifically hepatic molecular marker, ideal studies should examine the circulating EVs against their liver-derived counterparts, where possible.

1.3.3.1. Rodent studies

The fact that such issues remain to be addressed can be explained by the relative infancy of this field of research. To date, there are fewer than a dozen studies to have documented a role for EV signalling in a model of NAFLD, the earliest reported as late as 2009 in mice (Deng et al., 2009a). To better define a role for EVs in the development of hepatic steatosis, researchers have sought to replicate the clinical observations in rodent models of NAFLD, simulated by administering a choline-deficient diet (CDD) or HFD *ad libitum* for several weeks, the latter of which more accurately reflects the development of human metabolic syndrome. It should also be noted, that while CDD animals have comparable liver triglycerides to HFD animals, and a much more rapid progression to hepatic fibrosis, other typical changes such as increased body weight and fat depots, insulin resistance, and elevated fasting glucose and fatty acids are not observed (Raubenheimer et al., 2006). In saying that, contrary to what would be expected, EV studies in rodent models of NAFLD showed similar trends for both diets.

In the original study, Deng and colleagues described a phenomenon in their chronic HFD model whereby circulating EVs that were adoptively transferred to healthy animals were engulfed by myeloid cells that subsequently accumulated in the liver (Deng et al., 2009a). This phenotype was not observed when EVs were transferred from animals on a normal chow diet, which may suggest a selective, EV-driven mechanism for hepatic inflammation as a concomitant to steatosis. While these findings are yet to be reproduced, other groups have instead begun to more comprehensively examine the profile of circulating EVs to better understand their temporal regulation, contents, and possible intervention strategies. Indeed, it was shown that vesicles tend to increase on a background of NAFLD, and do so in a time-dependent manner, according to data obtained from flow cytometry experiments (Ajamieh et al., 2015, Povero et al., 2014, Povero et al., 2013).

To evaluate how the liver contributes to this population, EVs were assessed for their expression of miRNA-122, a molecule that is enriched in mammalian livers and is shown to be involved in early NAFLD progression (Lagos-Quintana et al., 2002, Barad et al., 2004, Yamada et al., 2015). Consistent with previous findings, rodent studies confirmed an increase in circulating EV-associated miRNA-122 accompanied by a decrease in the liver expression of this molecule (Csak et al., 2015, Povero et al., 2014, Povero et al., 2013). Furthermore, one study demonstrated that when miRNA-122 was trafficked in EVs, it was not associated with its protein binding partner AGO2, a phenomenon that is otherwise typically observed in non-disease conditions (Povero et al., 2014). While other miRNAs and proteins were not correlated against disease severity, Povero and colleagues had employed mass spectrometry to identify an EV-specific proteome in NAFLD that was distinct from healthy controls (Povero et al., 2014). These findings complement a previous study done by the group, in which they confirm a role for EV-bound Vanin-1 in hepatocyte vesicle uptake by an endothelial cell line, with subsequent angiogenic behaviour that is only observed when EVs are derived from hepatocytes subjected to lipotoxic stress (Povero et al., 2013).

Taken together, these studies establish a solid foundation for understanding the role of EVs in NAFLD, however, some notable limitations exist. Firstly, changes in EV phenotype were not correlated against histological severity of liver disease, which would otherwise give some insight into their prognostic value. Furthermore, perhaps an emphasis on distinguishing NAFLD from other underlying liver pathologies would give EVs a stronger diagnostic utility, as had been addressed in clinical studies. A summary of the findings are given in Figure 1.6.

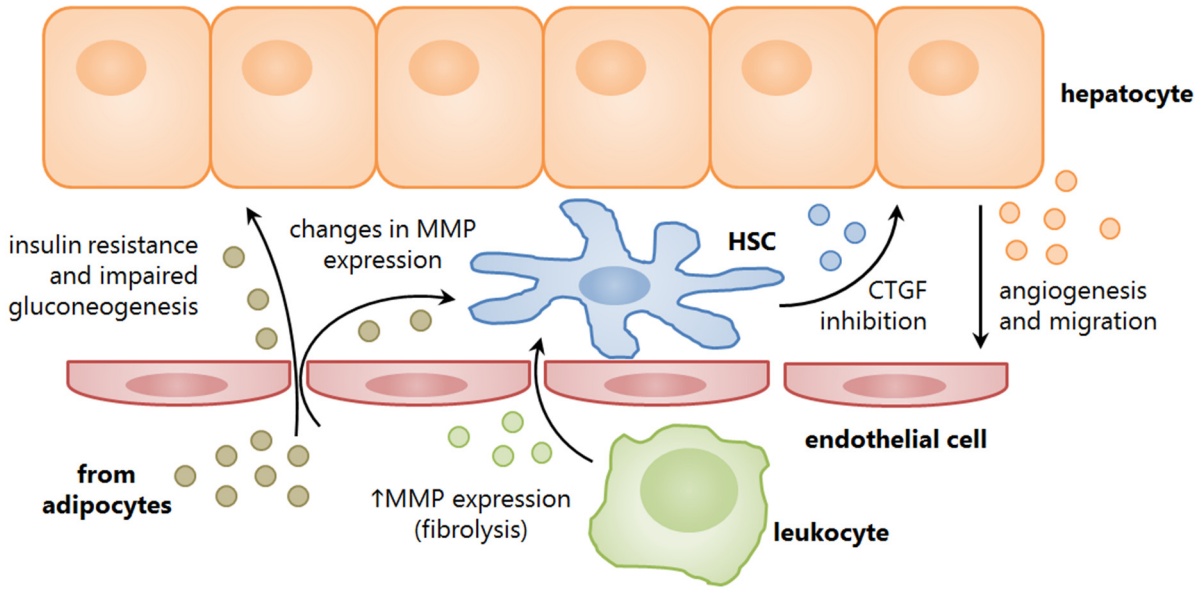

Figure 1.6. Extracellular vesicle roles in NAFLD. EVs are involved in intercellular communication within the liver tissue, as well as other tissues involved in mediating NAFLD pathogenesis, such as adipose and circulating (later resident) leukocytes. Collectively, these EVs are involved in a dynamic response that may exacerbate tissue injury, as well as promoting repair and matrix remodelling. Abbreviations: CTGF, connective tissue growth factor; HSC, hepatic stellate cell; MMP, matrix metalloproteinase. Image retrieved from (Ban et al., 2016).

1.3.3.2. Human studies

The pioneering study to involve human subjects was published three years later by Kornek and colleagues, who for the first time had suggested a correlation between the circulating abundance of leukocyte-derived EVs and disease severity, as determined by liver transaminase levels, biopsy grade, and NAFLD activity score (Kornek et al., 2012). These findings still provide the most compelling evidence in clinical samples for the prognostic value of EVs in NASH development, and have been extensively cited. The authors have additionally noted a distinction between the circulating NAFLD EV profile and that seen in hepatitis C patients. This is further supported by another study where transcriptomic analysis revealed that serum exosome-derived miRNAs are capable of differentiating multiple aetiologies of liver disease, as well as disease from normal liver controls (Murakami et al., 2012). Similar to the first study, it was shown that the expression levels of some miRNAs were regulated either positively or negatively with histological features of disease, such as inflammation and fibrosis. However, these results were limited to the cohort with chronic hepatitis and no such data was available for NAFLD progression to NASH.

More recent studies have described the modulation of hepatocyte and stellate cell activity by EVs isolated from visceral (peritoneal) adipose tissue. While the subjects did not necessarily present with NAFLD, the *ex vivo* experimental designs instead aimed to establish a role for EVs in potentially mediating this disease. As such, Kranendonk and colleagues showed that adipocyte EVs from non-obese patients were capable of interfering with insulin signalling and gluconeogenesis when directly exposed to a hepatocyte cell line (Kranendonk et al., 2014a). Furthermore, the concentration of EVs correlated positively with expression of liver transaminases, which supports the evidence for their role in hepatocyte dysfunction. In another study, albeit on a smaller scale, adipose tissue isolated from obese patients released EVs in culture that subsequently altered the gene expression of a matrix metalloprotease inhibitor, TIMP-1, in both hepatocytes and hepatic stellate cells (Koeck et al., 2014). Collectively, these findings suggest a novel mechanism of NAFLD pathogenesis by EVs through adipocyte-mediated hepatic cell stress and tissue remodelling. A summary of findings from both human and rodent studies is given in Table 1.5.

Table 1.5. Important findings for extracellular vesicles in the context of NAFLD.

Key study findings	*Model*	*Injury*	*EV source*	*Methods*	*References*
Increased circulating total EVs	Rodent	HFD, CDD	plasma	FC	(Ajamieh et al., 2015) (Povero et al., 2013) (Povero et al., 2014)
Increased circulating liver-derived EVs (marker: miR-122)	Rodent	HFD, CDD	plasma, serum	RT-qPCR	(Csak et al., 2015) (Povero et al., 2013) (Povero et al., 2014)
EVs correlate with NAFLD severity	Human	NASH	plasma	FC	(Kornek et al., 2012)
EVs distinguish NAFLD from other liver diseases	Human	NASH	plasma, serum	FC, microarray	(Kornek et al., 2012) (Murakami et al., 2012)
Changes in circulating EV contents	Rodent	CDD	plasma	LCMS, WB	(Povero et al., 2013) (Povero et al., 2014)
Changes in circulating EV interactions with cells	Rodent	HFD	plasma	FC	(Deng et al., 2009a)

CDD, choline deficient diet; EV, extracellular vesicle; FC, flow cytometry; HFD, high-fat diet; LCMS, liquid chromatography with mass spectrometry; NAFLD, non-alcoholic fatty liver disease; NASH, non-alcoholic steatohepatitis; RT-qPCR, real-time quantitative polymerase chain reaction; WB, western blot.

1.3.4. Translational utility

With the urgency to develop a non-invasive biomarker for the diagnosis and staging of NAFLD, research into the biology of extracellular vesicles has provided an opportunity to explore a novel mechanism of disease pathogenesis that can also be harnessed as a clinical tool. However, there is still a long way to go before EV-related assays will have translational utility. Besides the obvious question of disease and tissue specificity, current techniques used in the isolation and characterisation of EVs remain laborious, and suffer from a lack of standardisation as well as high variability (detailed further in section 1.3.5). It will undoubtedly take a few years before the processing of EVs from blood and other bodily fluids as *liquid biopsies* becomes economically viable, reproducible and validated. Until then we are unlikely to see their use in routine clinical practice.

The concept of analysing EVs in the context of NAFLD is still very much a small niche in the literature. One reason could be the limitations mentioned above, or a focus on more accessible biochemistries such as liver transaminases and soluble miRNA-122. But then why look at circulating EVs? Perhaps the answer lies in their active role in disease; they may not only confirm the presence of NAFLD, but also give an insight into which tissues are interacting and how this is driving pathogenesis. It has been shown that adipose tissue EVs taken from obese individuals are capable of signalling to hepatic cells to remodel their extracellular milieu, while these cells in turn may communicate via EVs with the sinusoid to promote angiogenesis (Koeck et al., 2014, Povero et al., 2013). Circulating vesicles have also been implicated in the innate immune response that accompanies steatosis, pointing to a role in the progression from early NAFLD to NASH (Deng et al., 2009a, Kornek et al., 2012). From a physiological perspective, it makes sense to encapsulate certain molecules that are otherwise prone to enzymatic degradation, especially in a complex or unpredictable disease environment. However, if preservation of these molecules within EVs leads to a heightened stimulation of inflammatory cells, as previously suggested, this mechanism may in turn be responsible for the exacerbation of tissue injury.

1.3.4.1. EVs in NAFLD treatment

The multifaceted nature of EVs suggests that these structures may have potential value beyond their use as circulating biomarkers in NAFLD. For instance, cancer studies have explored the transfer of oncogenes and an oncogenic phenotype through EV uptake in cell culture models (Bergsmedh et al., 2001, Redzic et al., 2013, He et al., 2015), which may provide a target for therapeutic intervention. Indeed, it was shown that incubating hepatoma cells with various anti-cancer drugs promoted the secretion of immunogenic EVs that were capable of enhancing natural killer (NK) cell responses (Lv et al., 2012, Xiao et al., 2013). Conversely, exposing macrophages to such drugs may induce the release of EV-derived miRNAs, which suppress cancer growth by epigenetic regulation (Zhang et al., 2014). This concept has been extended to NAFLD models, where it was found that administering cholesterol-lowering drugs to high-fat fed rodents can attenuate the release of EVs, however the exact implication of this was not discussed, except for a potential reduction in liver cell death (Ajamieh et al., 2015, Baron et al., 2011).

Another approach is to use the vesicles themselves as a mode or target of therapy, not simply a marker of injury. This idea has been investigated since the late 1980s, whereby synthetic vesicles were used as a vehicle for drug delivery in both *in vitro* and *in vivo* models of liver injury (Farazuddin et al., 2014, Laakso et al., 1988). It is also possible that in the future, endogenous EVs may be harvested for similar purposes, providing an efficient technique for tissue-specific delivery of molecules. The advantage of this autologous transfer system is that the vesicles are less likely to be rejected by the patient, however still sufficiently immunogenic to elicit a response (Deng et al., 2009a).

1.3.5. EV analysis

Independently of the EV isolation process, there are a number of considerations with regard to sample handling that may affect both the quality and the yield of EVs. For instance, blood samples are particularly sensitive to the presence and activity of platelets. Serum tends to harbour more EVs than plasma, which are produced during clot formation *ex vivo* following blood collection. Therefore, the use of anticoagulants is recommended for EV based studies, however attention must be given to the type of anticoagulant if downstream mechanisms are to be considered (for example, the use of chelators such as EDTA are incompatible with the study of metalloproteases in EV samples). Heparin is typically discouraged as it interferes with EV activity and also acts as a competitive inhibitor during PCR. Finally, diurnal variation and fasting status have also been shown to confound EV analyses, which further emphasises the importance of consistency in sample collection and handling.

Due to the complexity of EV samples, a number of different isolation methods have been developed to accommodate sample type as well as effect on downstream measurements. The most frequently cited are described in Table 1.6. For most EV researchers, ultracentrifugation following differential spins to eliminate debris seems to be the mainstay, as sample yield is maintained and no additional contaminants are introduced. However, this method also suffers from potential contamination by lipoproteins and protein aggregates when compared to some of its more stringent counterparts, and is often referred to as a "crude" sample. For practical purposes and also considering utility for downstream applications, the studies in this thesis have used an amended ultracentrifugation protocol (see section 2.4.1. for details).

There is no single predominating technique for the characterisation of EVs (Table 1.6), with researchers often using multiple complementary analyses to establish the presence of EV subtypes or to enumerate the total population per sample. Traditionally, flow cytometry was used to confirm both outcomes, however given the limitations of conventional cytometers for EV analysis, a combination of western blot and an optical technique (single particle tracking or electron microscopy) may be more robust.

Table 1.6. Popular methods of EV sample processing.

Method	*Freq, %*	*Features*
Isolation:		
Ultracentrifugation	81	Spin 100,000 – 120,000×g after depletion of larger fragments (10,000 – 20,000×g)
Density gradient centrifugation	20	Spin through density gradient to separate EVs (1.1 – 1.2 g/mL) from contaminants, usually overnight
Filtration	18	Pass through membrane with specific pore size, larger fragments trapped on filter
Size-exclusion chromatography	15	Pass through resin column based on hydro-dynamic radius, eluted by decreasing size
Precipitation	14	Polymer-based EV agglutination, usually with polyethylene glycol (PEG)
Immunoaffinity capture	9	Antibody-coated magnetic beads specific to EV surface markers
Characterisation:		
Western blot	74	Protein analysis of typical EV markers
Single particle tracking ▪ NTA ▪ TRPS ▪ DLS	72	Optical methods for intact sample enumeration, particle sizing, and assessment of particle polydispersity
Electron microscopy	60	Visualisation of EV ultrastructure
Flow cytometry ▪ Direct ▪ Immunoaffinity	41	Protein analysis of EV surface markers with quantitation based on particle or bead count (cf. protein concentration)
Protein assay	35	Total or specific protein concentrations
Atomic force microscopy	9	Cantilever probe scans sample surface to determine ultrastructure (nanometre scale)

Popularity (frequency %) determined by a survey of the ISEV community (n=196) reported in *J Extracell Vesicles (2016)* (Gardiner et al., 2016). Additional information sourced from (Witwer et al., 2013) and (Taylor and Shah, 2015). Abbreviations: NTA, nanoparticle tracking analysis; TRPS, tuneable resistive pulse sensing; DLS, dynamic light scattering.

1.4. Study Aims

The work presented in this thesis aims to evaluate the links between NAFLD pathogenesis and the patterns in extracellular vesicle secretion. The studies have been designed to not only address some caveats in the literature – for instance, the lack of tissue-derived EV samples used in analyses – but also to further understand the role that EVs play in NAFLD development *in vivo*, and ultimately whether they are a useful predictor of disease severity.

1.4.1. Changing EV profile with NAFLD progression

The aim of *Chapter 3* is to optimise some conventional techniques used in EV isolation from plasma and conditioned media, and to examine the characteristics of these EVs in the context of our study design. The chapter will introduce the high-fat feeding rodent model of NAFLD, focussing on the two extremes of the disease spectrum: simple steatosis and NASH. These groups will be distinguished by duration of diet, without intervention to accelerate or impede NAFLD development. *Chapter 4* aims to expand on the previous chapter, with the addition of intermediate timepoints to monitor longitudinal changes in the EV profile with NAFLD progression. This study will more comprehensively analyse the liver phenotype and pre-clinical parameters, and characterise in detail the proteome of liver-derived EVs.

Hypothesis 1: Vesicles isolated from plasma and liver-conditioned media by differential centrifugation are expected to express markers that are specific to EV subtypes, and have a size range that is typically reported for EVs (50nm to 1μm).

Hypothesis 2: An obesogenic high-fat diet (HFD) will induce NAFLD, while its chronic consumption will promote development to NASH. Changes in the liver will be reflected in the EV abundance and phenotype: it is expected that circulating and liver EV numbers will increase with NAFLD and be further elevated by NASH, while the EV proteome will reflect the microenvironment of the parent tissue.

1.4.2. Effect of NAFLD intervention on EV profile

Two intervention modalities will be introduced in *Chapter 5*. In the genetic manipulation arm, global deletion of TNF expression will be used to examine how disrupting a key inflammatory pathway that also affects insulin resistance may change the NAFLD phenotype and hence the corresponding EV profile. For the second aim, exercise interventions in the form of endurance or high-intensity training will evaluate not only the optimal program for NAFLD regression, but also whether such a treatment will normalise the EV patterns to that of healthy controls. All intervention studies will be completed using mouse models, in line with previous chapters.

Hypothesis 3: Animals lacking TNF expression will have increased insulin sensitivity. Therefore, the rate of NAFLD development is expected to be reduced and consequently, EV abundance may be decreased.

Hypothesis 4: Animals that consume HFD but undergo exercise training will have improved metabolic parameters and reduced NAFLD burden. Since exercise also liberates EVs, the change in abundance cannot be predicted, however the molecular cargo in EVs of exercised animals is expected to promote NAFLD regression.

1.4.3. Functional studies on the effects of NAFLD-derived EVs

Finally, the effect of EV-cell interactions will be highlighted in *Chapter 6*. Vesicles obtained from either plasma or liver tissue from the aforementioned studies will be co-cultured with a mouse hepatocyte cell line in an aim to determine the specific hepato-modulatory effect of EVs. Whether the dietary background influences EV uptake will also be explored, as well as changes in cellular gene expression after incubation with various EV populations.

Hypothesis 5: Circulating or liver-derived EV populations will be taken up by recipient cells and impart molecular signals that either mediate NAFLD progression (EVs from HFD mice, especially those with NASH) or are hepatoprotective (EVs from exercised mice).

Chapter 2.

Materials & Methods

Chapter 2. Table of contents

2.1. Materials

Table 2.1. Reagents used in this study.

Reagent	*Manufacturer or supplier*
Animal models:	
AIN-76 mineral mix	MP Biomedicals, Santa Ana, CA, USA
AIN-76 vitamin mix	MP Biomedicals, Santa Ana, CA, USA
bovine serum albumin	Sigma-Aldrich, St. Louis, MO, USA
canola oil	Coles Supermarkets, Melbourne, VIC, Australia
cholesterol	Sigma-Aldrich, St. Louis, MO, USA
choline bitartrate	Sigma-Aldrich, St. Louis, MO, USA
DMEM, high glucose	Sigma-Aldrich, St. Louis, MO, USA
formaldehyde	Sigma-Aldrich, St. Louis, MO, USA
gelatine (McKenzie's)	Coles Supermarkets, Melbourne, VIC, Australia
insulin (human, Actrapid)	Novo Nordisk, Bagværd, Denmark
lactic acid casein	Rogers & Co. Foods, Hampton, VIC, Australia
lard (Yorkfoods)	Coles Supermarkets, Melbourne, VIC, Australia
methionine	Sigma-Aldrich, St. Louis, MO, USA
oat bran	Coles Supermarkets, Melbourne, VIC, Australia
starch, from rice	MP Biomedicals, Santa Ana, CA, USA
sucrose	Sigma-Aldrich, St. Louis, MO, USA
Plasma biochemistry:	
glycerol standard solution	Sigma-Aldrich, St. Louis, MO, USA
rat/mouse insulin ELISA kit	Merck, Darmstadt, Germany
serum triglyceride determination kit	Sigma-Aldrich, St. Louis, MO, USA
EV isolation (western blot):	
Clarity™ ECL Western Blotting Substrate	Bio-Rad Laboratories, Hercules, CA, USA
DC™ Protein Assay kit	Bio-Rad Laboratories, Hercules, CA, USA
glacial acetic acid	Thermo Fisher Scientific, Waltham, MA, USA
glycerol	Thermo Fisher Scientific, Waltham, MA, USA
goat anti-rabbit IgG	Sigma-Aldrich, St. Louis, MO, USA
Mini-PROTEAN® TGX™ Precast Gels	Bio-Rad Laboratories, Hercules, CA, USA
Ponceau S powder	Sigma-Aldrich, St. Louis, MO, USA
Precision Plus Protein™ Dual Color Standards	Bio-Rad Laboratories, Hercules, CA, USA
rabbit anti-mouse CD63	Sigma-Aldrich, St. Louis, MO, USA

skim milk powder	Coles Supermarkets, Melbourne, VIC, Australia
sodium chloride	Sigma-Aldrich, St. Louis, MO, USA
sodium deoxycholate	Sigma-Aldrich, St. Louis, MO, USA
sodium dodecyl sulphate	Sigma-Aldrich, St. Louis, MO, USA
Trans-Blot® Turbo™ Mini Nitrocellulose	Bio-Rad Laboratories, Hercules, CA, USA
Tris-HCl	Sigma-Aldrich, St. Louis, MO, USA
Triton X-100	Sigma-Aldrich, St. Louis, MO, USA
Tween 20	Sigma-Aldrich, St. Louis, MO, USA
UltraPure™ Tris base	Invitrogen, Carlsbad, CA, USA

EV isolation (flow cytometry):

AbC™ Antibody Compensation Bead Kit	Thermo Fisher Scientific, Waltham, MA, USA
APC conjugation kit	Abcam, Cambridge, UK
APC-annexin V	BioLegend, San Diego, CA, USA
APC-CD105 antibody	Miltenyi Biotec, Bergisch Gladbach, Germany
APC-CD41 antibody	Miltenyi Biotec, Bergisch Gladbach, Germany
ASGR1/ASGPR1 antibody	R&D Systems, Minneapolis, MN, USA
calcein AM fluorescent dye	Biotium, Fremont, CA, USA
PE-CD63 antibody	BioLegend, San Diego, CA, USA
PerCP/Cy5.5-CD45 antibody	BD Biosciences, San Jose, CA, USA

Liver lipid content:

chloroform	Thermo Fisher Scientific, Waltham, MA, USA
ethanol	Sigma-Aldrich, St. Louis, MO, USA
isopropanol	Sigma-Aldrich, St. Louis, MO, USA
methanol	Thermo Fisher Scientific, Waltham, MA, USA
Oil Red O	BDH Laboratory Supplies, Poole, UK
saline, irrigation 0.9%	Baxter International, Deerfield, IL, USA
TAG reagent	Roche Diagnostics, Basel, Switzerland

Liver gene expression:

First Strand cDNA synthesis kit	Invitrogen, Carlsbad, CA, USA
glycogen (from mussel)	Sigma-Aldrich, St. Louis, MO, USA
primers, SYBR format	Sigma-Aldrich, St. Louis, MO, USA
SensiMix SYBR Hi-ROX	Bioline Reagents, London, UK
SuperScript III reverse transcriptase	Invitrogen, Carlsbad, CA, USA
TRI Reagent	Sigma-Aldrich, St. Louis, MO, USA
trimethylene bromochloride	Sigma-Aldrich, St. Louis, MO, USA

Cell culture:	
CFSE Cell Division Tracker kit	BioLegend, San Diego, CA, USA
foetal bovine serum	AusGeneX, Molendinar, QLD, Australia
Gibco™ DMEM:F12 media	Thermo Fisher Scientific, Waltham, MA, USA

2.2. Animal Models

All animals used in this study were housed in pathogen-free conditions on site, at the animal facilities of Royal Prince Alfred Hospital (RPAH), Centenary Institute, or Charles Perkins Centre (CPC), Sydney, Australia. Experimental protocols were approved by the Animal Ethics Committees of Sydney South West Area Health Services and/or the University of Sydney, Australia (RPAH Protocol No. 2011/004D and 2015/024; CI Protocol No. 2015/005; CPC Protocol No. 2015/816). Male C57Bl/6 mice were purchased at age 5 weeks from the Animal Resources Centre (ARC), Perth, Australia. Studies commenced promptly after a one week acclimation period, or 5 week period for the exercise intervention study.

Genetically modified strains on a C57Bl/6 background were bred on site at the Centenary Institute animal facility by Miss Christine Yee. A global deletion model for tumour necrosis factor ($TNF^{-/-}$) (Korner et al., 1997) was used to investigate the effect of perturbing an inflammation and insulin resistance pathway in the development of obesity-associated NAFLD. Controls for $TNF^{-/-}$ animals were age-matched, C57Bl/6 wild-type mice purchased from ARC. Both groups received dietary intervention only, for 12 weeks.

2.2.1. Dietary Model of NAFLD

A modified high-fat diet (HFD) was used for these studies as it is reflective of clinical NAFLD development associated with obesity and metabolic syndrome (Ito et al., 2007, Lo et al., 2011). The HFD, containing approx. 45% calories from fat and 0.5% cholesterol (non-atherogenic), was prepared in-house and adapted from protocol D12451 provided by Research Diets (New Brunswick, NJ). See Table 2.2 for a complete list of ingredients and their caloric contribution. For all studies, HFD groups were compared against a control group (matched for age, sex and strain) receiving standard laboratory chow (maximum 12% calories from fat). Given the slow development of NAFLD as compared to other liver diseases, or alternatively, the longer time needed to advance to an inflammatory stage (NASH), an extended time course of up to 52 weeks of HFD was used for some experiments. The details of the time course studies are outlined in Figure 2.1 and again in the relevant chapters.

Table 2.2. Modified high-fat diet recipe with added cholesterol.

Ingredient	*Weight (g)*	*Cholesterol (g)*	*Calories (kCal)*	*Calories (%)*
sucrose	224		896	Carbohydrate (32.6)
starch (from rice)	215		860	
casein	261		1044	Protein (20.4)
vitamin mix	15		60	
mineral mix	51			
bran	57			
gelatine	23			
methionine	3.4			
choline bitartrate	4.6			
vegetable oil	32		284	Fats/esters (47.0)
lard (from pork)	250	0.2	2250	
cholesterol	6.0	6.0		
TOTAL	**1142**	**6.2**		

Final concentration of cholesterol per batch is 0.54% w/w. Total weight excludes sweetened condensed milk (approx. 1 Tbsp) added as flavouring, therefore its caloric value is disregarded.

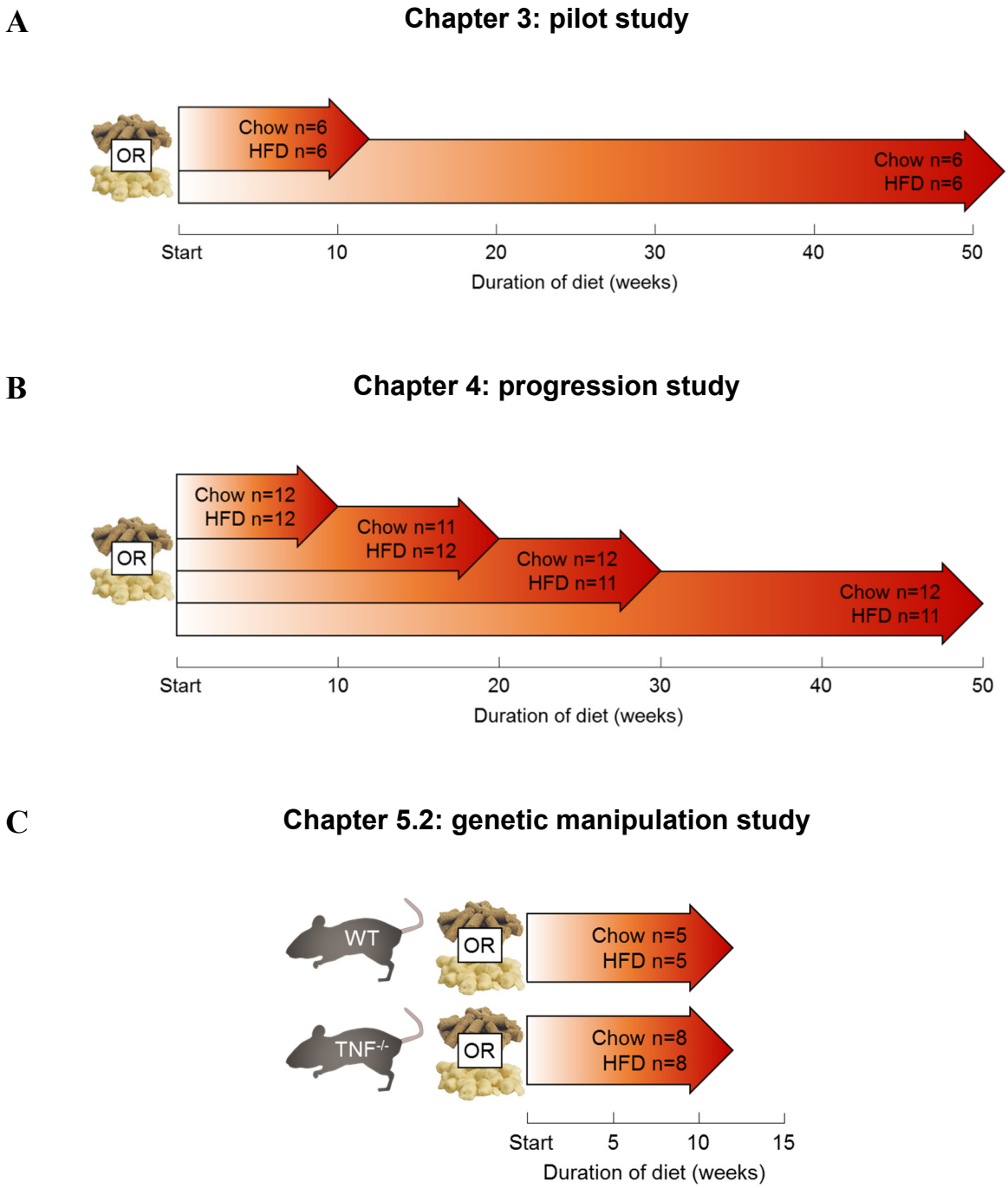

Figure 2.1. Time course and animal numbers for NAFLD models. For all studies, mice were fed either a high-fat diet (HFD) or standard laboratory chow for a specified period. These periods are represented by arrows, drawn to scale, containing the sample size for both treatments at each timepoint. In Chapter 5, the time course was a single duration: 12 weeks for the genetic manipulation study, 20 weeks for the exercise intervention study (the latter detailed in Figure 2.2).

2.2.2. Exercise Intervention

To counteract the impact of obesity development using a clinically relevant model without drug intervention, two isocaloric exercise regimens were administered and compared to an untrained condition (Figure 2.2). After an initial 9 weeks of dietary intervention (as above), mice were acclimatised to a level treadmill over 1 week (6 m/min for 10 min) prior to completing a test for maximal running capacity (MRC). For the test, animals were exercised to exhaustion, where the average MRC was determined for each dietary cohort (chow: 27 m/min, HFD: 21 m/min). For the following 10 weeks, mice were trained three times per week on alternating days while maintaining their original diet. Each session lasted a total of 40 min with varying degrees of aerobic intensity: animals from each diet group were randomly assigned to either an endurance training (END) regimen where they were subjected to a constant 70% MRC, or high-intensity interval training (HIIT) with alternating 85-90% and 50% MRC in 5 min cycles. Untrained groups for each diet acted as controls and were not subjected to further exercise. For ethical reasons, animals that failed to perform the MRC test were withdrawn from the study.

The animals described here were part of another study investigating the impact of exercise intervention on muscle function. The exercise protocols for this study were developed and performed by Sergio Martinez-Huenchullan. Blood and liver samples from these animals were obtained by the author of this thesis and were processed for isolation of EVs and analysis of NAFLD according to the methods described herein. Results of the liver changes have contributed to the publication.

A

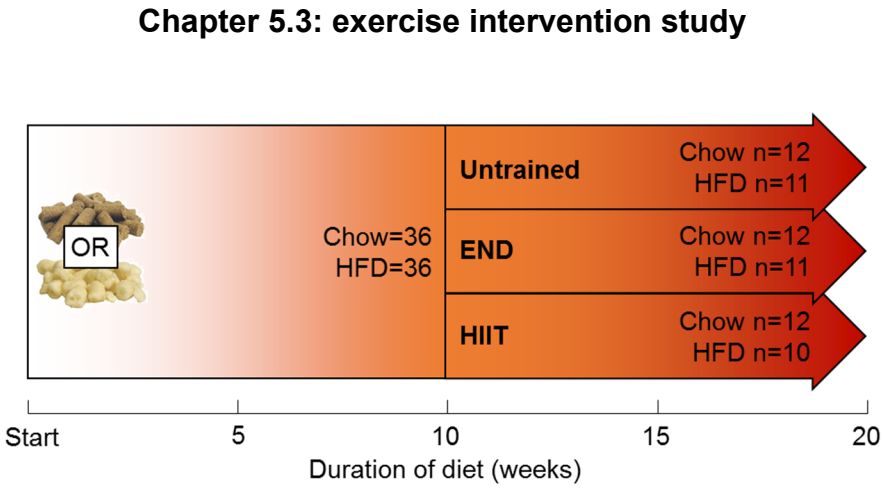

B

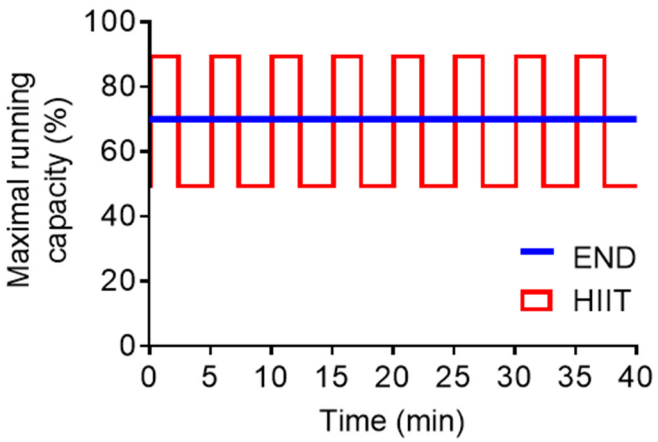

Figure 2.2. Exercise intervention study design. (**A**) Time course for the study, including a diet duration of 20 weeks with the exercise program (END, endurance training; HIIT, high-intensity interval training) commencing at the halfway point, after 10 weeks. Animals were maintained on the same diet for the duration of the study. Discrepancies in sample size from week 10 to 20 are due to animals being withdrawn from the study if they failed to complete the maximal running capacity (MRC) test. (**B**) Graphical representation of exercise intensity for END and HIIT groups during the training sessions. Percentage MRC is relative to the average MRC determined for each dietary group (chow: 27 m/min, HFD: 21 m/min). *NB: The study design represented here was developed by Sergio Martinez-Huenchullan.*

(

2.2.3. Insulin tolerance test (ITT)

To monitor the effect of HFD on whole-body insulin sensitivity, all animals in the progression study (Chapter 4) and exercise intervention study (Chapter 5.3; see below for further details) were subjected to an insulin tolerance test in the penultimate week of the respective study. Mice were fasted minimum 4 hours prior to an intraperitoneal injection of human insulin (Actrapid, Novo Nordisk, Bagværd, Denmark) at a dose of 0.65IU/kg. Blood glucose levels were monitored at baseline, then at 5, 15, 30, 60 and 90 min post-injection by collecting blood from the tail vein using a blood glucose monitoring system (FreeStyle Lite, Abbott Diabetes Care, Alameda, CA). Hypoglycaemic animals were rescued with a 100μL intra-peritoneal injection of 50% w/v glucose. Insulin sensitivity represented by blood glucose excursion was calculated as area under the curve (AUC), and excluded rescued animals (maximum n=2).

2.2.4. Tissue collection

All animals were weighed at the beginning of the experiment and weekly until termination, where they were anaesthetized by inhaled isoflurane prior to exsanguination by cardiac puncture. Blood was collected into blood tubes containing 3.2% w/v sodium citrate (Greiner Bio-One, Kremsmünster, Austria), which typically recovered approximately 0.5mL plasma volume following a 3000×g spin for 15 min. Livers were excised and weighed, then portions of tissue were either i) snap-frozen in liquid nitrogen and stored at -80ºC until further use, ii) fixed in 10% neutral buffered formalin for 24 hr and then 70% ethanol prior to paraffin embedding, or iii) sections from the right lobe were isolated into phosphate buffered saline (PBS) for study of liver-derived EVs. For experiments pertaining to the latter, the right lobe (chow: 453±131mg, HFD: 726±225mg in progression study) was diced into approx. 10-20mm^3 segments and immersed in 1.5mL filtered Dulbecco's Modified Eagle's Medium (DMEM) supplemented with 0.1% bovine serum albumin (BSA), as exemplified in Figure 2.3. Diced livers were incubated overnight at 37ºC in 5% CO_2 before collection of conditioned medium for isolation of EVs. Liver slices were weighed for normalisation of EV numbers. (Note that incubating whole-tissue for EV collection has been performed previously on adipose tissue (Koeck et al., 2014, Kranendonk et al., 2014b) but not liver, whereas the validity of incubating liver tissue slices has been reviewed (Li et al., 2010)).

A

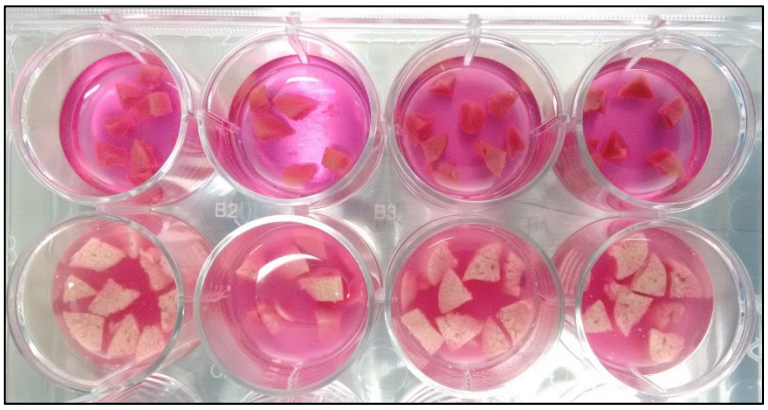

B

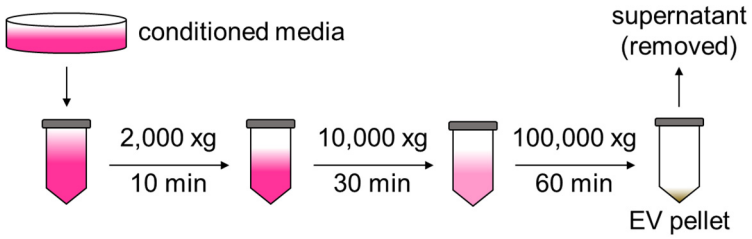

Figure 2.3. Tissue culture of liver slices and EV isolation. (**A**) Representative liver slices from animals fed standard chow (top row) or high-fat diet (bottom row) immersed in DMEM media prior to overnight incubation. (**B**) Conditioned media was collected for extracellular vesicle (EV) isolation by a series of differential centrifugation steps (see section 2.4.1).

2.3. Plasma Biochemistry

Whole blood collected at termination was centrifuged at 800×g for 15 min to obtain the plasma fraction, which was used for biochemical analysis and EV isolation (see section 2.4). Plasma insulin was measured with an enzyme-linked immunosorbent assay (ELISA) kit (Merck, Darmstadt, Germany) while total triglycerides were quantified using an enzymatic assay (Sigma-Aldrich, St. Louis, MO), both according to manufacturers' instructions. To obtain the standard liver function test (LFT) panel, samples were submitted to the Chemical Pathology Laboratory of the NSW Health Pathology Facility at Royal Prince Alfred Hospital for processing using a Roche Cobas IT-3000 auto-analyser.

2.3.1. Circulating insulin

All reagents necessary to perform the ELISA were provided in the kit (see Table 2.1) and prepared following the manufacturer instructions. Rat insulin standards were used to generate a dilution curve (0-10ng/mL), and were compared against two quality controls (QC). The assay was sandwich format; 10μL of either standard, QC or plasma sample (diluted 2-fold) was added to the insulin antibody-coated well, followed by 80μL detection antibody (biotinylated anti-insulin). After 2 hr incubation, unbound substances were washed off and bound antibody was conjugated with an enzyme (horseradish peroxidase) for a further 30 min. Assays were washed again, before addition of substrate (3,3',5,5'-tetramethylbenzidine), which reacted rapidly with immobilised antibody-enzyme conjugates. Finally, the reaction was stopped by acidification and absorbance of the coloured product was determined spectrophotometrically at wavelength 450nm, corrected to 590nm. The dilution curve was then used to determine the QC and sample insulin concentrations.

2.3.2. Circulating triglycerides

Components of the working solution (free glycerol and triglyceride reagents) were provided in the kit (see Table 2.1), while the 2.5mg/mL glycerol standard solution was purchased separately (Sigma-Aldrich, St. Louis, MO). The assay was performed following the protocol for determination of total triglycerides (B1) supplied by the manufacturer, with modification. Briefly, free glycerol reagent and triglyceride reagent were combined in a 4:1 ratio to prepare the working solution, then incubated with blank (water), glycerol standard, or neat plasma samples using a 1:100 dilution. For instance, 2.5µL sample was diluted in 250µL working solution in a 96-well plate format. Following a 15 min incubation at room temperature, during which time triglycerides were enzymatically converted to a quinoneimine dye (triolein), the absorbance of coloured product was determined at wavelength 540nm. Total triglyceride concentration was then calculated using the formula given below, where TAG represents triglycerides and ABS is absorbance.

$$TAG = [standard] * \frac{ABS_{sample} - ABS_{blank}}{ABS_{standard} - ABS_{blank}}$$

2.3.3. Liver function tests

Reports for LFT panels were generated for standard clinical biomarkers using assays validated for human samples. The plasma biomarkers included bilirubin, albumin, protein, gamma-glutamyl transferase (GGT), alkaline phosphatase (ALP), alanine transaminase (ALT) and aspartate transaminase (AST). However, our study focused on the latter two parameters as these are the predominantly assessed markers of hepatocellular injury in the clinic, and were most affected by our dietary intervention.

2.4. Extracellular Vesicle Isolation

There is no consensus in the literature regarding the isolation of extracellular vesicles, and oftentimes the technique depends on the downstream application. A lack of standard protocols for the isolation and characterisation of EVs is a caveat that is recognised by the EV research community, with guidelines published by the International Society of Extracellular Vesicles (Witwer et al., 2013) which have aimed to address this problem. The original and most frequently cited technique is still differential centrifugation (see Chapter 1 section 1.3.5). Here, the EV fraction is retrieved by a final ultracentrigation step of 100,000 – 200,000×g and may be further purified by centrifugation through a density gradient, such as with sucrose. This study used a basic protocol of "crude" EV isolation modified from a previously described protocol (Thery et al., 2006).

2.4.1. Differential centrifugation

EVs were collected as described earlier (see section 2.2.4). Conditioned media from tissue-derived vesicles were first cleared of larger cell debris with a 10 min spin at 2,000×g. The supernatants from these spins, as well as the plasma samples (recovered as per section 2.2.4), were then centrifuged at 4^{o}C for 30 min at 10,000×g to clear platelets and apoptotic bodies. Finally, supernatants were transferred to a hard-walled polypropylene microfuge tube (Beckman Coulter, Brea, CA) and EVs were pelleted by ultracentrifugation at 4^{o}C for 1 hr at 100,000×g before resuspending in equal volume filtered PBS (50μL for plasma, 100μL for conditioned media). To maintain stability of their ultrastructure and cargo, EVs were stored at -80^{o}C either after the final spin (pilot study) or after the 10,000×g spin. For the latter, samples were thawed, followed by ultracentrifugation and same-day characterisation.

2.4.2. Transmission electron microscopy

To confirm the presence of EVs, and to determine whether their ultrastructure is changed with diet, transmission electron microscopy (TEM) was performed on EV suspensions. Briefly, samples were diluted 10-fold and 20μL drops were placed on 400-mesh formvar-coated copper grids (ProSciTech, Kirwan, QLD, Australia). After drying overnight at room temperature, adhered samples were stained with a 2% w/v uranyl acetate solution for 2 min then dabbed dry from the edges, before visualising on a JEOL 1400 TEM instrument at the Sydney Microscopy and Microanalysis facility, Australian Centre for Microscopy and Microanalysis, University of Sydney. Setup and visualisation were performed according to the instrument operation manual, with power set to 120kV. Sample magnifications are given with images in the Results section (see Chapter 3).

2.4.3. Validation by western blot

To confirm that samples were enriched with EVs and void of other contaminants, plasma and liver-derived EVs were compared against their corresponding liver lysate for positive staining of the exosomal marker CD63. Representative samples were diluted in RIPA solubilisation buffer (modified from Bio-Rad Buffer Formulations, bulletin 6199; with 10% glycerol) before protein quantification using the DC™ Protein Assay kit (Bio-Rad Laboratories, Hercules, CA) following the manufacturer instructions. Equal concentration protein (40μg) was diluted in 4X loading buffer prepared in-house, and loaded into a precast polyacrylamide gel (4-15% Mini-PROTEAN® TGX™ Precast Protein Gels; Bio-Rad Laboratories) with a molecular weight ladder (Precision Plus Protein™ Dual Color Standards; Bio-Rad Laboratories) and run at 120V until adequate separation. Protein was transferred at 25V for 7 min to a membrane (Trans-Blot® Turbo™ Mini Nitrocellulose; Bio-Rad Laboratories) before staining with Ponceau S solution (0.5% w/v in 5% glacial acetic acid) to determine transfer efficiency. Given the lack of a universal loading control between EVs and tissue lysates, total protein staining with Ponceau S was instead used for normalisation.

Following SDS-PAGE and sample transfer, the membrane was blocked in 5% w/v skim milk power dissolved in TBST buffer (Tris-buffered saline with 0.5% v/v Tween-20) for 1 hr, then washed 3 times for 10 min each in TBST buffer. Primary antibody (rabbit anti-mouse CD63; Sigma-Aldrich, St. Louis, MO) was diluted 1:500 in TBST with 0.5% w/v skim milk powder and incubated with the membrane overnight at 4^{o}C. After washing as above, the membrane was incubated with secondary antibody (goat anti-rabbit IgG, peroxidase conjugated; Sigma-Aldrich) for 2 hr. Following a final wash, the membrane was immersed in chemiluminescent substrate (Clarity™ ECL Western Blotting Substrate; Bio-Rad Laboratories) to resolve bands on a ChemiDoc™ Imaging System with ImageLab™ software (Bio-Rad Laboratories) for sample analysis. The CD63 protein band was expected to resolve at 26kDa (native) or 40-60kDa (glycosylated). BSA alone was used as a negative control.

2.4.4. Nanoparticle tracking analysis

Routine enumeration and size distribution of EVs was measured using a NanoSight™ LM10 instrument (Malvern Panalytical, Malvern, UK) with Nanoparticle Tracking Analysis (NTA) software version 2.4 provided by the Molecular Biology Facility of Bosch Institute, University of Sydney. The technology utilises the Brownian motion of particles in solution to determine size, and thus allows concentrations with respect to size to be calculated by the software. Since the machine uses a laser to illuminate particles, all experiments were recorded in the dark. Samples in PBS were further diluted to reach an optimal recording concentration of 50-100 particles per frame, as recommended by the manufacturer. The use of inconsistent dilutions was validated by performing dilution curves with either polystyrene beads of known diameter, or with EV samples (see Chapter 3). Optimal resolution of particles was achieved by adjusting the camera level to 13 during recording (most optimal shutter speed and gain), while a detection threshold of 5 was determined to be most sensitive for particle enumeration.

2.4.5. Characterisation by flow cytometry

To examine the utility of flow cytometry for the characterisation of EVs isolated in our study, samples were stained with typical markers for cell origin (Ban et al., 2016) and analysed by standard cytometry with modified staining protocols.

Using bead-based sample precipitation modified from (Thery et al., 2006) and (Inglis et al., 2015), polystyrene beads (AbC™ Total Antibody Compensation Bead Kit, Thermo Fisher Scientific, Waltham, MA) were used to adsorb 10μL EVs overnight at 4ºC, prior to blocking with 5% w/v BSA or 100mM glycine (1 hr on shaker) and staining with a single antibody of interest, together with calcein AM dye (Biotium, Fremont, CA), for 30 min with shaking. Finally, stained bead-EV samples were collected by centrifugation at 250×g for 5 min. In a parallel experiment, individual EVs (no beads) were diluted 1:10 and blocked as above, then stained overnight at 4ºC before precipitation with polyethylene glycol (final concentration 10% v/v) for 2 hr on ice. Precipitated stained EVs were then collected by centrifugation at 3,000×g for 10 min (Weng et al., 2016). Both methods allowed for the removal of residual antibody that may contribute to background fluorescent signals. Finally, samples were resuspended in 200μL PBS before reading on a Guava® easyCyte flow cytometer with Guavasoft InCyte software (Merck, Darmstadt, Germany) at the Bosch Institute, University of Sydney.

Antibodies used in this study were diluted as per Table 2.3 in filtered PBS with 0.5% w/v BSA prior to staining. They were specific for either platelets (CD41), endothelial cells (CD105), leukocytes (CD45), or hepatocytes (ASGPR1). The latter antibody was conjugated in-house using an APC conjugation kit (Abcam, Cambridge, UK). To discern the EV subtypes, reagents specific to microvesicles (annexin A5) or exosomes (anti-CD63 antibody) were co-incubated per sample. Compensation was performed using EVs stained with a single antibody or dye (individual method), or beads adhered to a single antibody as per the manufacturer instructions (bead-based method). For troubleshooting and gating strategies, see Chapter 3.

Table 2.3. Anti-mouse antibodies used for EV characterisation by flow cytometry.

Target	*Antibody clone*	*Conjugate*	*Source*	*Dilution: bead method*	*Dilution: individual method*
PS	annexin A5*	APC	BioLegend	-	1:5,000
CD63	NVG-2	PE	BioLegend	-	1:5,000
CD41	MWReg30	APC	Miltenyi Biotec	1:10	1:5,000
CD105	MJ7/18	APC	Miltenyi Biotec	1:10	1:5,000
CD45	30-F11	PerCP/Cy5.5	BD Biosciences	1:50	1:5,000
ASGPR1	polyclonal	APC	R&D Systems	1:50	1:5,000

*Not antibody format. Abbreviations: APC, allophycocyanin; ASGPR1, asialoglycoprotein receptor 1; PE, phycoerythrin; PerCP, peridinin chlorophyll; PS, phosphatidylserine.

2.4.6. Characterisation by mass spectrometry

Liver-derived EVs from 10 and 50 weeks of either diet (n=3 per group) were used for the study. Samples were chosen at random from the progression study (Chapter 4). Conditioned media (0.5mL) was ultracentrifuged as previously described, and the frozen EV pellet was submitted to the Sydney Mass Spectrometry facility in the Charles Perkins Centre, University of Sydney for 1D liquid chromatography-mass spectrometry. The following work-flow was performed by Angela Connolly, prior to data acquisition on a Q Exactive™ Plus mass spectrometer (Thermo Fisher Scientific, Waltham, MA).

EV pellets were thawed and resuspended in a 6M urea/2M thiourea solution before sonicating for 1 min, followed by centrifugation for 5 min at 16,000×g. The supernatant (100μL) was collected for clean-up in a chloroform-methanol (4:1) solution at a final concentration of 80% v/v before further centrifugation for 5 min at 9,000×g. The sample was washed in methanol, spun as before, and the pellet was air-dried. The final protein sample was again resuspended in 6M urea/2M thiourea solution, sonicated, and quantified using a Qubit fluorometer (Invitrogen, Carlsbad, CA). Total protein concentrations for EV samples were in the range of 15-62μg, with an average of 31μg. For protein digestion, samples were reduced in DTT (30 min), alkylated in iodoacetamide (30 min) and quenched in DTT, then diluted 10-fold in 100mM HEPES buffer before incubating in trypsin (1:50) overnight at 30ºC. Prior to spectrometry, samples were diluted in trifluoroacetic acid (1% v/v) and spun for 5 min at 6,000×g, before hydrophilic-lipophilic balanced clean-up. Finally, the resulting sample was eluted in a 50% v/v acetonitrile/ 0.1% v/v trifluoroacetic acid solution, dried, and resuspended to 1μg/3μL protein.

Following mass spectrometry, the output data was analysed by the author with the assistance of Dr Ben Crossett from the Sydney Mass Spectrometry facility. Data was first retrieved from the MASCOT® server (Matrix Science, London, UK) then analysed using Scaffold 4 software (Proteome Software, Portland, OR). Statistical differences between treatment groups were determined by Fisher's Exact Test. Protein terms in UniProt format were imported into the online gene ontology software DAVID Bioinformatics (Huang da et al., 2009) and hierarchical clustering of enriched pathways was performed using the online matrix visualisation tool Morpheus (https://software.broadinstitute.org/morpheus/).

2.5. Liver Lipid Content

2.5.1. Intrahepatic lipid staining

Intrahepatic neutral lipids (fatty acid glycerols) were visualised using a semi-quantitative *in vitro* staining method with Oil Red O (ORO), modified from Lillie and Ashburn (Lillie and Ashburn, 1943). A 3mg/mL stock solution of ORO in isopropanol was prepared in advance. Prior to the experiment, an ORO working solution (3:2 in dH_2O) was prepared and passed through a 0.1μm syringe filter. Homogenised livers (20-100mg) were incubated in 500μL working solution for 1 hr in darkness, then pelleted by centrifugation at 3000rpm for 10 min. Samples were washed in 60% v/v isopropanol, then resuspended in 1mL of 100% v/v isopropanol for 1 hr in darkness, to allow lipid-bound ORO to elute back into solution. Finally, samples were again pelleted at 5000rpm for 5 min, then 50μL supernatant was collected for spectrophotometric reading of absorbance at 490nm. Concentrations were determined against a 5-fold serial dilution standard curve of ORO stock solution.

2.5.2. Intrahepatic triglyceride extraction

Tissue triglycerides were quantified using a chloroform-methanol extraction method. Briefly, homogenised livers (5-20mg) were vortexed in 2mL chloroform-methanol solution (2:1 v/v) before a minimum 2 hr incubation on a rocker. A further 2mL of saline (0.9% w/v solution) was then added to samples, followed again by vortexing. To allow phase separation, samples were centrifuged at 1580×g for 3 min after which 100μL infranatant was collected into a glass tube. (NB: Air was released from the pipette tip after submerging into infranatant to avoid contamination from the supernatant.) The infranatant containing triglycerides was concentrated with a nitrogen evaporator for approx. 30 min, or until the sample was dried. Triglyceride samples were dissolved in 100μL ethanol, where 10μL was resuspended in 300μL TAG reagent (Roche Diagnostics, Basel, Switzerland) and incubated for 15 min before taking absorbance readings at 492nm. Sample concentrations were determined against a 2-fold dilution standard curve using glycerol standard solution (Sigma-Aldrich, St. Louis, MO) as in section 2.3.2. The standards were prepared as per Table 2.4 below.

Table 2.4. Standard curve preparation for liver triglyceride extraction.

TAG concentration (mg/mL)	*Glycerol standard (μL)*	*dH_2O (μL)*	*Serial dilution, from previous (μL)*	*Final volume in TAG reagent (μL)*
5.00	20			20
2.50	10			10
1.25	15	15		10
0.62		15	15	10
0.31		15	15	10
0.00		10		10

Abbreviations: TAG, triacylglycerol (aka triglyceride).

2.6. Liver Gene Expression

To validate the NAFLD profile, changes in mRNA expression of inflammation and tissue remodelling associated molecules were assessed in mouse liver, and in hepatocyte cell lines stimulated with EVs from the mouse models.

2.6.1. RNA extraction

All extraction reagents were acquired from Sigma-Aldrich, St. Louis, MO. Samples were homogenised and immersed in 0.5mL TRI Reagent with 0.1mL trimethylene bromochloride, vortexed, and allowed to separate into phases for 5-10 min. They were then centrifuged at 14,000×g for 15 min at 4ºC, and the aqueous supernatant was collected into equal volume (approx. 0.2mL) isopropanol before overnight precipitation at -30ºC. Samples were again centrifuged under the same conditions, then the RNA pellets were washed twice with cold 70% w/v ethanol at 14,000rpm for 10 min at 4ºC. Finally, after clearing the ethanol and air-drying to avoid contamination, pellets were resuspended in 50µL nuclease-free water and assessed for yield and purity using a NanoDrop spectrophotometer. Acceptable quality was deemed to be >100ng/µL RNA with both $A_{260:280}$ and $A_{260:230}$ ratios in the range 1.8-2.2.

2.6.2. RNA integrity

RNA integrity was determined using an Agilent Bioanalyzer which uses a capillary gel electrophoresis format for resolving RNA degradation and gDNA contamination. Briefly, randomly selected samples were loaded onto a RNA 6000 Nano Chip and handled as per the manufacturer's protocol. After running the chip, the RNA integrity number (RIN) was used to validate the extraction quality. Values above 7.0 are considered acceptable for whole liver tissue, which was consistently achieved in our samples. For more information about RNA integrity, including absorbance ratios from NanoDrop, please see Figure A9 in the appendix.

2.6.3. Reverse transcription

RNA samples were diluted to 100ng/μL, of which 10μL (1μg) was used as synthesis template per 20μL assay. Oligo-dT, random hexamers, and water were first added to the RNA template and placed in a PCR thermocycler for 10 min at 70ºC to allow denaturation. Once the temperature lowered to 4ºC, samples were retrieved and supplemented with deoxy-nucleoside triphosphates (dNTPs), dithiothreitol (DTT), reverse transcriptase, and commercial assay buffer. Samples were then returned to the machine to complete the annealing (25ºC for 10 min) and extension steps (42ºC for 60 min followed by 70ºC for 15 min) of reverse transcription. Once cDNA was synthesised, the temperature returned to 4ºC until the run was terminated. Final concentration for all assay reagents is given in Table 2.5. All reagents used for reverse transcription were purchased from Invitrogen, Carlsbad, CA.

2.6.4. Real-time quantitative PCR

Following reverse transcription, cDNA samples were diluted 5-fold in nuclease free water, of which 5μL (1μL equivalent) was used per 15μL assay. The remaining volume consisted of sense and anti-sense primers, water, and a commercial master mix (SensiMix SYBR Hi-ROX; Bioline Reagents, London, UK), as detailed in Table 2.5. Samples were then amplified on a Qiagen Roto-Gene™ real-time PCR machine under standard conditions for 40 cycles, including a final melt step to assess primer specificity. Run data was collected on the Roto-Gene™ 6000 software (version 1.7) available from Corbett Research. Dilution curves were generated for each primer set (sequences given in Table 2.6) and used to determine mRNA expression for each sample, corrected to an endogenous reference gene (Table 2.6) and control group using the delta-delta method. Please see appendix for more details about the reference gene consistency during the RT-qPCR studies in Chapter 3 through 6. Where genes of interest were compared across multiple runs within an experiment, samples were also corrected to an internal control sample.

Table 2.5. Working concentrations for PCR reagents.

Reagent	*Stock concentration*	*Volume (μL)*	*Final concentration*
Reverse transcription:			
Oligo(dT)$_{12-18}$	0.5μg/μL	0.5	250ng
Random hexamers	2μM	0.5	50nM
dH_2O		1.5	
5X First Strand buffer	5X	4.0	1X
DTT	100mM	2.0	10mM
dNTPs	10mM	1.0	0.5mM
SuperScript III *	200U/μL	0.5	100U
Real-time qPCR:			
primer (sense)	10μM	0.5	333nM
primer (anti-sense)	10μM	0.5	333nM
SensiMix SYBR Hi-ROX	2X	7.5	1X
dH_2O		1.5	

*SuperScript III used as reverse transcriptase enzyme for cDNA synthesis. Abbreviations: DTT, dithiothreitol; dNTPs, deoxy-nucleoside triphosphate cocktail including adenosine (dATP), guanosine (dGTP), cytidine (dCTP) and thymidine (dTTP) nucleosides.

Table 2.6. SYBR primer sequences used in this study.

Marker	*Forward (sense) sequence*	*Reverse (anti-sense) sequence*
Inflammation:		
F4/80	CTTTGGCTATGGGCTTCCAGTC	GCAAGGAGGACAGAGTTTATCGTG
MCP1	AGCCAACTCTCACTGAAGCC	GCGTTAACTGCATCTGGCTG
TNF alpha	GTCCCCAAAGGGATGAGAAGT	TGAGTGTGAGGGTCTGGG
ECM remodelling:		
alpha SMA	AGAGCAAGAGAGGGATCCTGA	GTCGTCCCAGTTGGTGATGAT
collagen I	CCCTCGACTCCTACATCTTCTGA	GATGACGTGCAATGCAATGAA
collagen IV	AGCGAGATGTTCAAGAAG	TGGACAGTGAGGTACACA
CTGF	GCATCTCCACCCGAGTTA	TTGACAGGCTTGGCGATT
MMP9	GCCGACTTTTGTGGTCTTCC	AGCGGTACAAGTATGCCTCTG
TGF beta	TGACGTCACTGGAGTTGTAC	GGTTCATGTCATGGATGGTG
TIMP1	CACAAGTCCCAGAACCGC	GGATTCCGTGGCAGGC
Lipid metabolism:		
FABP1	AAGTCAAGGCAGTCGTCAAGCT	TGAGTTCAGTCACGGACTTTATGC
glucokinase	AGGAGGCCAGTGTAAAGATGT	CTCCCAGGTCTAAGGAGAGAAA
perilipin 2	CTTGTGTCCTCCGCTTATGTC	GCAGAGGTCACGGTCTTCAC
PPAR alpha	CATGTGAAGGCTGTAAGGGCTT	TCTTGCAGCTCCGATCACACT
PPAR gamma	CTGCTCAAGTATGGTGTCCATGA	TGAGATGAGGACTCCATCTTTATTCA
SREBP-1c	TGGATTGCACATTTGAAGACATG	TGTCTCACCCCCAGCATAGG
Endogenous reference:		
18S	GCAATTATTCCCCATGAACG	GGCCTCACTAAACCATCCAA
36B4	GGCCCTGCACTCTCGCTTT	TGCCAGGACGCGCTTGT

All sequences are given 5'-3' and are specific for *Mus musculus* cDNA. Abbreviations: MCP1, monocyte chemotactic protein 1; TNF alpha, tumour necrosis factor alpha; ECM, extracellular matrix; alpha SMA, alpha smooth muscle actin; CTGF, connective tissue growth factor; MMP9, matrix metalloproteinase 9; TGF beta, transforming growth factor beta; TIMP1, tissue inhibitor of metalloproteases 1; FABP1, fatty acid binding protein 1 (liver type); PPAR, peroxisome proliferator-activated receptor; SREBP-1c, sterol regulatory element-binding protein 1c.

2.6.5. cDNA array analysis

cDNA was prepared as per section 2.6.3 with a starting RNA concentration of 100ng/μL. All reagents and instruments described in this section were purchased from Thermo Fisher Scientific, Waltham, MA. The Accufill™ and QuantStudio™ 12K Flex real-time PCR systems were supplied by the Molecular Biology Facility of the Bosch Institute, University of Sydney. Immediately prior to array analysis, samples were prepared as follows: in a 384-well plate, cDNA was diluted in equal volume OpenArray™ PCR master mix up to 6μL and centrifuged at 1000-1500rpm for 1 min with the plate covered. The OpenArray™ chip was equilibrated at room temperature for 10-15 min, then placed in the Accufill™ machine with the plate of samples and a box of Accufill™ tips. The machine was operated according to standard protocols. Upon completion of sample loading, the chip was removed and prepared for analysis using the QuantStudio™ system.

Briefly, the top two of three layers of tape were removed from the chip before sealing with the lid. Using the provided syringe with immersion fluid, the cap was removed and replaced with a tip, and any bubbles were evacuated. The immersion fluid was slowly injected through the opening at one end of the chip until completely filled, then the opening was sealed using a screw plug. Finally, the assembled chip was placed under a compressor for 20 sec to ensure the lid was tightly adhered, then stored in the dark before analysis.

Before initiating the QuantStudio™ program, a USB containing a chip-specific .tsp file was inserted into the machine (the file was obtained from https://www.thermofisher.com/au/en/home/products-and-services/product-types/download-openarray-tpf-and-spf-plate-files.html). After launching, the chip identification number was entered into the program and the .tsp file opened, before being prompted to insert the chip into the machine. The analysis was finally configured by following instructions within the program to confirm and run the chip. Once the run was completed, data was obtained from and processed using the same program.

Table 2.7. Taqman primers used on custom designed OpenArray™ panel.

Target	*Format*	*Reference*	*Format*
alpha SMA	Mm00725412_s1	36B4	Mm00725448_s1
basigin	Mm01144228_g1	aldolase B	Mm00523293_m1
collagen I	Mm00801666_g1	HPRT	Mm01545399_m1
collagen IV	Mm01210125_m1	ubiquitin C	Mm02525934_g1
CTGF	Mm01192932_g1		
CXCL10	Mm00445235_m1		
HGF	Mm01135193_m1		
IFN gamma	Mm01168134_m1		
IL2	Mm00434256_m1		
IL10	Mm00439614_m1		
MCP1	Mm00441242_m1		
MMP2	Mm00439498_m1		
MMP3	Mm00440295_m1		
MMP9	Mm00442991_m1		
MMP10	Mm01168399_m1		
MMP13	Mm00439491_m1		
MMP14	Mm00485054_m1		
PDGF-B	Mm00440677_m1		
TGF beta	Mm01178820_m1		
TIMP1	Mm00441818_m1		
TIMP2	Mm00441825_m1		
TNF alpha	Mm00443258_m1		
VEGF-A	Mm01281449_m1		
VEGF receptor 2	Mm01222421_m1		

Abbreviations: alpha SMA, alpha smooth muscle actin; CTGF, connective tissue growth factor; CXCL10, chemokine CXC motif ligand 10; HGF, hepatocyte growth factor; IFN gamma, interferon gamma; IL, interleukin; MCP1, monocyte chemotactic protein 1; MMP, matrix metalloprotease; PDGF-B, platelet-derived growth factor subunit B; TGF beta, transforming growth factor beta; TIMP, tissue inhibitor of metalloprotease; TNF alpha, tumour necrosis factor alpha; VEGF-A, vascular endothelial growth factor A.

2.7. Liver Histology

Embedding of formalin-fixed liver samples was performed with assistance from Sanaz Maleki and Rosie Cheong-Soos at the Histopathology Laboratory, Charles Perkins Centre, University of Sydney. Embedded samples were cut into 5µm sections. To remove the paraffin wax from sections, slides were placed in a 60ºC oven for 30 min then passed through two changes of xylene for 10 min each. Sections were then rehydrated through two changes of 100% and 95% w/v ethanol, then 70% w/v ethanol followed by running water, each for 2 min duration. Dewaxed sections were stained as described below. Sections were imaged using an Olympus BX53 microscope with cellSens microimaging software (Olympus, Tokyo, Japan).

2.7.1. Haematoxylin and eosin staining

Haematoxylin and eosin (H&E) staining was used to visualise general morphology, whereby nuclei appear blue and cytoplasmic structures are stained pink with acidic eosin. Nuclei were first stained with Harris' haematoxylin for 2 min, then differentiated in acid alcohol (1% HCl in 70% ethanol) for 10 sec, and blued in Scott's bluing solution for 20 sec. After each step, sections were washed in running water until excess staining was cleared. Sections were then dehydrated through the graded ethanol washes in reverse order, with two 40 sec changes of eosin counterstaining after the 70% ethanol wash. Excess ethanol was removed from slides by placing in the 60ºC oven for 15 min and then in histolene for at least 5 min, before mounting with dibutylphthalate xylene (DPX). See Figure 2.4 for an example H&E stain.

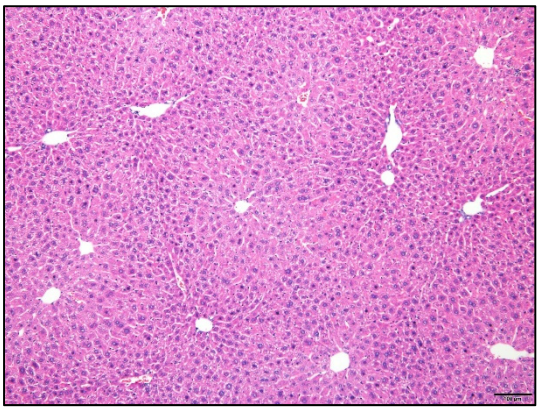

Figure 2.4. Haematoxylin and eosin staining of normal mouse liver (100× magnification).

2.7.2. Picro-Sirius red staining

Picro-Sirius red (PSR) staining of connective tissue was used to assess the severity of fibrosis in NASH models. When visualising stained sections, collagen fibres appeared red (Sirius red) while cellular structures had yellow hues (picric acid). Deparaffinised and rehydrated liver sections were stained with haematoxylin for 10 min. After washing excess stain in water, samples were incubated in PSR solution (0.1% w/v Sirius red F3B in aqueous picric acid) for 1 hr, then drained on filter paper, submerged in acidified water (0.1% HCl) for 3 slow dips, drained again then washed in 100% ethanol. (NB: Any items containing residual PSR stain were washed thoroughly, as dried picric acid is highly volatile and flammable.) Finally, removal of excess ethanol and mounting were performed as in 2.7.1. See Figure 2.5 for an example of PSR staining in normal and fibrotic livers.

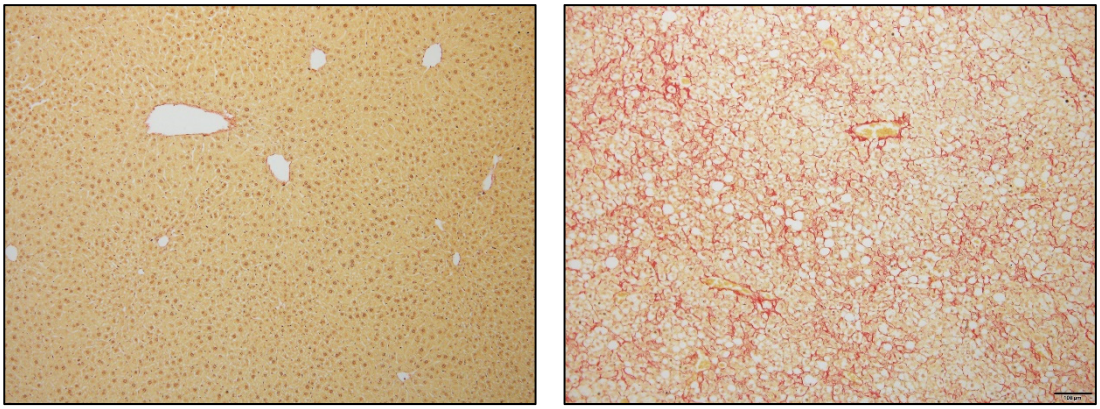

Figure 2.5. Picro-Sirius red staining of normal mouse liver (left) and liver with NASH fibrosis (100× magnification).

For a complete set of the histological images that contributed to the studies in this thesis, please refer to Figures A1 to A8 in the appendix.

2.8. Cell Culture

For studies investigating the mechanism of EV action (Chapter 6), EV samples obtained from mouse liver or plasma were co-cultured with the *Mus musculus* hepatocyte cell line AML12, kindly donated by Dr Andrew Hoy from the Lipid Metabolism Laboratory at the Charles Perkins Centre. The cell line has an adherent epithelial phenotype and is non-tumorigenic. Cells were maintained at 37ºC with 5% CO_2 in DMEM: F12 medium, supplemented with 10% foetal bovine serum (FBS) and antibiotics (100 U/ml penicillin and 100 μg/ml streptomycin). These studies were performed over cell passage numbers 38-40.

2.8.1. EV uptake by hepatocytes

To investigate the uptake of EVs by AML12 cells using fluorescent tracking, the EVs were labelled with 5μM carboxyfluorescein succinimidyl ester (CFSE; BioLegend, San Diego, CA) in PBS supplemented with 0.5% BSA, for 30 min at 37ºC. The reaction was quenched with 10-fold volume of serum-enriched medium before incubating with cells at 60-80% confluence. EV uptake was then monitored at 24 and 48 hours. At the conclusion of each timepoint, media was aspirated and cells were washed in PBS to remove peripheral EVs. To quantify uptake by flow cytometry, cells were detached into 500uL PBS with a pipette tip then aspirated into a 1.5mL tube. EV uptake was assessed using the Guava® easyCyte flow cytometer to determine the proportion of CFSE-positive cells (Ex 488, Em 525/30).

2.8.2. Hepatocyte phenotype

The impact on AML12 hepatocyte phenotype after EV uptake was assessed by real-time PCR as follows. Briefly, cells were incubated with EVs (1,000/sample) in a 12-well plate for 24 hr after which time media was removed, cells were washed with PBS, then covered in 400μL TRI Reagent (Sigma-Aldrich, St. Louis, MO) before storing at -80ºC overnight to aid freeze-thaw mediated cell lysis. Cell samples were then scraped to resuspend in the TRI Reagent, aspirated from the wells, and processed according to section 2.6. To aid nucleic acid precipitation, glycogen (from mussel; Sigma-Aldrich, St. Louis, MO) was added at 1μL per sample during the isopropanol overnight precipitation step.

2.9. Statistical Analysis

Results are expressed as mean ± standard deviation (SD) for animal characterisation and mean ± standard error of the mean (SEM) for liver and EV characterisation, unless otherwise stated. Where applicable, outliers were removed using the ROUT method, with false discovery rate set to 5.0% (Q=5.0). Values were $\log_{10}$-transformed if failing the Shapiro-Wilk normality test. Data with two related independent variables were analysed using two-way ANOVA, corrected for multiple comparisons using Bonferroni's post-hoc test (for 2 pairs), Tukey's test (for >2 pairs), or Dunnet's test (comparing multiple groups to a control group). When using two-way ANOVA preceding the multiple comparisons, overall effects of a given variable are stated in terms of "source of variation" as a percentage of total variation within the analysed data. Data with a single variable or two unrelated independent variables were analysed using a Student's t test for isolated pairs, or one-way ANOVA when comparing to a control group. Statistical significance was accepted at $p<0.05$. Linear correlations were analysed using Spearman nonparametric analysis to obtain a correlation coefficient (r value) with significance (p value). All analyses were performed using GraphPad Prism version 7 (GraphPad Software, San Diego, CA).

Chapter 3.

Technique optimisation and application in a pilot study of extracellular vesicles in NAFLD progression

Chapter 3. Table of contents

3.1. Introduction

The study of extracellular vesicles (EVs) in the context of animal models of NAFLD are to our knowledge lacking. To date, most studies have examined *in vitro* models using fatty acid stimulation of hepatic cells, or simple rodent models which distinguish the normal and steatotic phenotypes (Ban et al., 2016). While both models contribute knowledge, their caveats are typically arising from the "missing link" to human disease progression: is the stimulus physiologically relevant, or the time course representative of NAFLD development from simple steatosis to advanced NASH? The popular choline-deficient diets, for example, artificially accelerate the development to NASH without the corresponding metabolic disturbances (Machado et al., 2015), whereas *in vitro* studies provide information regarding single cell types with no information about the microenvironment.

Another approach is the use of flow cytometric techniques with "positive controls" (such as Annexin A5) to analyse larger vesicles that are theoretically at the threshold of detection for most flow cytometric equipment (Arraud et al., 2015, Kornek et al., 2012). However, despite this limitation, flow cytometry will likely remain the mainstay for EV characterisation until a robust, standardised alternative is developed. Researchers have also started to use other technologies such as nanoparticle tracking analysis (NTA), laser diffraction, and tuneable resistive pulse sensing (TRPS) for EV enumeration (Gardiner et al., 2016). In other studies designed to assess molecular targets, or determine the tissue of origin, antibody labelling is often performed in addition to staining with generic cytosolic or membrane (lipophilic) dyes to resolve intact EVs (Pospichalova et al., 2015). In this Chapter, we labelled EVs with calcein AM dye which reacts with cytosolic esterases, then co-incubated with fluorophore-conjugated antibodies against markers of cell of origin (e.g. to platelets, endothelial cells or leukocytes). This was used in an attempt to determine absolute population counts, while bead-adsorbed samples were used to determine relative changes between treatment groups. These tissue of origin studies were complemented with qualitative techniques for EV characterisation, such as western blot to examine EV biomarker enrichment within our samples, and electron microscopy to visualise the sample itself.

Following technique optimisation, particularly for the enumeration of EVs, the Chapter continued with a proof of concept study in mice fed a high fat diet for up to 52 weeks to validate our approach. The aim of the current work was to model the physiological progression of NAFLD in a high-fat fed mouse model for a relatively short time course (12 weeks) as well as a long duration of continuous feeding (52 weeks). These two different durations of feeding are characterised in the liver by simple lipid accumulation (Lo et al., 2011, Machado et al., 2015) and the latter by the NASH phenotype of inflammation and fibrosis (Fontana et al., 2013, Ito et al., 2007), which reflects the progression of NAFLD across the human lifespan (Frith et al., 2009). For a comparison of mouse age with the human equivalent, refer to Figure 3.1 below. In this study, the chronological and diet related change in the physical and metabolic phenotype of the animals were compared with plasma EV abundance. The impact of these variables on liver-derived EVs was also considered; to the best of our knowledge, this is a sample that has not yet been explored in any NAFLD study.

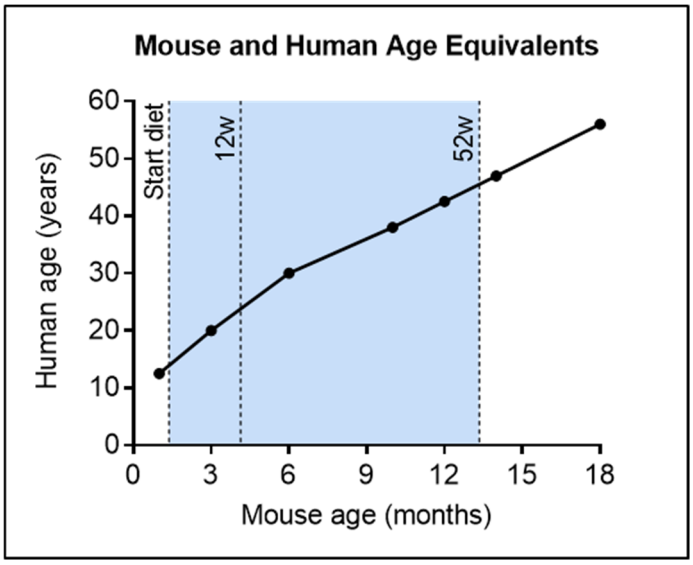

Figure 3.1. Mouse and human age equivalents. Animals were 6 weeks old (human adolescent) at the commencement of the study. The diet duration of 12 and 52 weeks corresponded to final mouse ages of 18 weeks (human mature adult) and 58 weeks (human middle age), respectively. This in turn relates to the typical progression period from NAFL to NASH seen in humans. Figure values were adapted from The Jackson Laboratory website (Hagan, 2017).

3.2. Technique Optimisation

Due to the variety of techniques available for EV isolation, purification and characterisation, as well as the diversity of sample type studied, a consistent standard protocol was developed for the sample analyses described in this work. The simple isolation procedure described in section 2.4.1 was employed without further purification. This procedure yielded small EVs without significant lipoprotein contamination, as shown by transmission electron microscopy (TEM). Optimal conditions for EV enumeration and phenotyping of origin were established using the NanoSight™ system (see section 2.4.4) and the Guava™ easyCyte flow cytometer (section 2.4.5), respectively. These conditions were then applied to plasma and liver-derived EVs obtained from mice fed either a normal laboratory chow diet or a HFD as mentioned above and further described in section 3.3.

3.2.1. Sample purity and ultrastructure

Electron microscopy was performed to confirm that the isolation and purification technique resulted in presence of EVs in the samples obtained by the method described in section 2.4.1. Shown in Figure 3.2A, the predominant structures in plasma isolates were vesicles that were uniformly round and electron dense, with the characteristic bilayer membrane also visible (Figure 3.2A, inset). These structures were also seen in isolates of conditioned media from an untreated hepatocyte cell line (Figure 3.2B). At this scale, it was also possible to determine the EV diameter; most structures tended to be under 200nm (typical of exosomes or small microvesicles), which was further confirmed by enumeration of size using NanoSight™ (see section 3.2.2). Further evidence that these structures can be called EVs was shown by western blot analysis, whereby the exosome marker CD63 was enriched in the ultracentrifuged pellet, compared to pre-ultracentrifugation and whole tissue lysate fractions (Figure 3.3). Together these observations suggest that the isolation technique enabled purification of vesicles that were predominantly EVs. Furthermore, these structures were shown to take up dyes that are subsequently catalysed by cytosolic esterase to produce a fluorescent signal (see section 3.2.3). This data further confirmed that the isolated structures were not protein contaminants, or lipoproteins with no esterase activity.

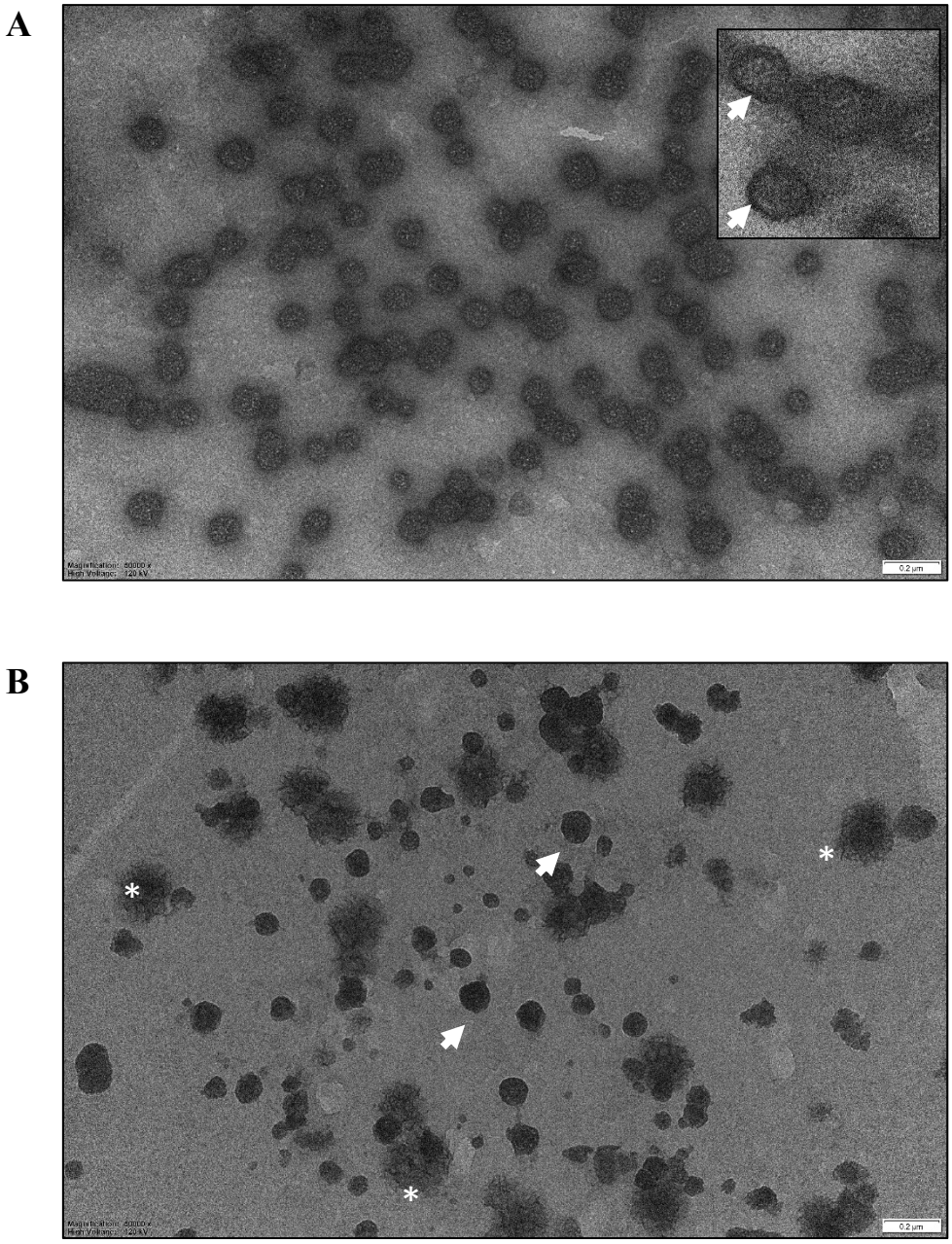

Figure 3.2. Electron micrograph of extracellular vesicles. **A.** Sample is of plasma origin from animals on a standard chow diet. Inset: Arrows highlight vesicle membrane. **B.** Sample from HepG2 cell line conditioned media. Arrows indicate EVs. Splintered halos around vesicles (*) indicate aggregation of uranyl acetate counterstain on EVs, due to insufficient washing. Magnifications are 50,000× and scale bars represent 0.2μm.

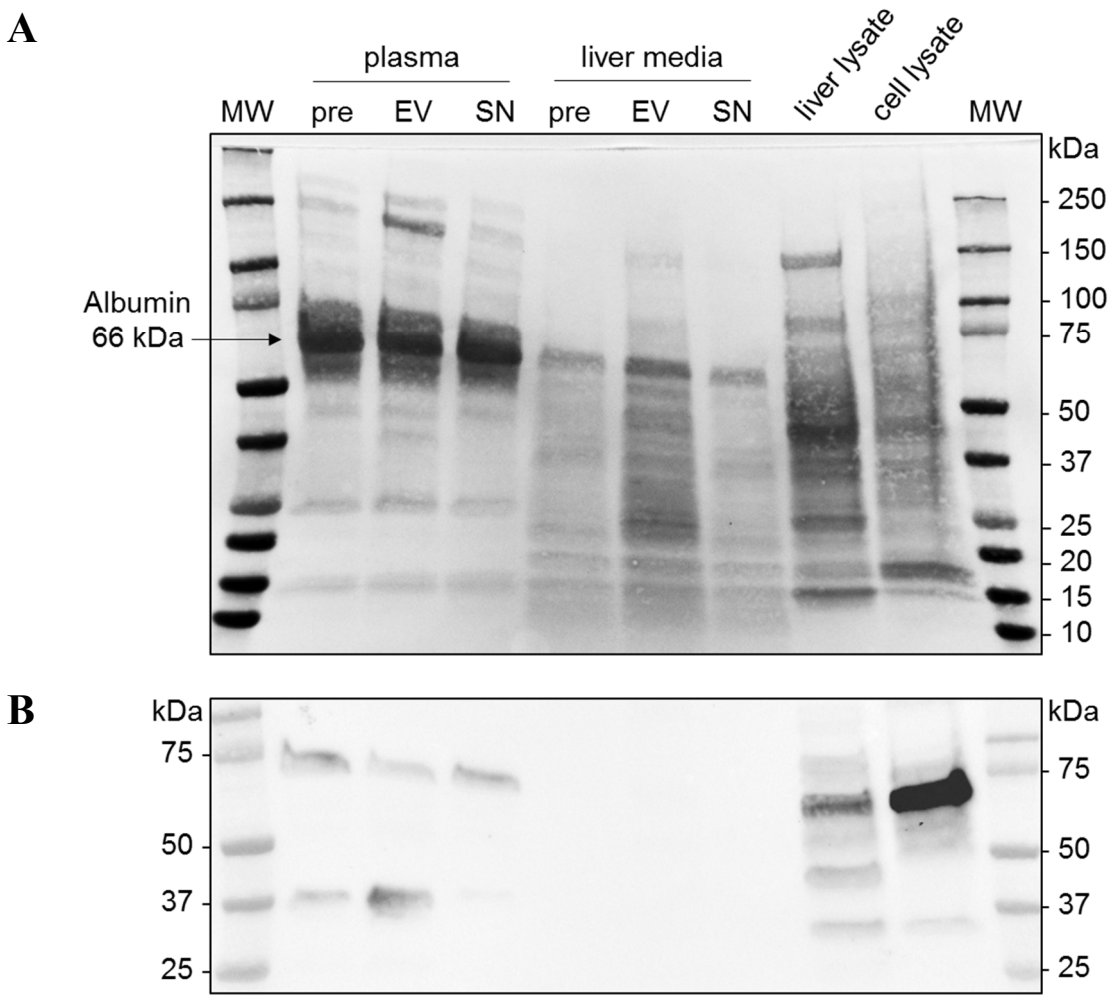

Figure 3.3. Confirmation of extracellular vesicle presence by western blot. **A.** Total protein staining by Ponceau S for plasma and liver-conditioned media, either prior to ultra-centrifugation (pre), or the EV pellet (EV) and supernatant (SN) following ultracentrifugation. Whole liver lysate and cell lysate of AML12 hepatocytes were used as a positive control. All samples except cell lysate were obtained from the same animal on a standard chow diet. **B.** Staining of CD63 exosomal/late endosomal marker in our samples. The native protein (expected 26kDa) was not present, while a small glycoform (approx. 40kDa) was enriched in plasma EV samples relative to whole plasma or liver and cell lysates. A larger glycoform or complex (approx. 70kDa) had the opposite expression pattern, while CD63 was absent from liver-conditioned media altogether. A pre-stained molecular weight (MW) ladder was used as a reference.

3.2.2. Extracellular vesicle enumeration by NanoSight™

Prior to study sample analysis, the sensitivity of the NanoSight™ was calibrated using the polystyrene beads supplied by the manufacturer (Malvern Panalytical, Malvern, UK). To perform this, the three sizes of spherical beads (100, 200 and 400nm) were added in equal concentration (one drop) to the same diluent used for sample analysis (PBS) and were then enumerated by the Nanoparticle Tracking Analysis (NTA) software. Three parameters were assessed for optimisation: the dilution of beads (sample based), the duration of recording (instrument based), and the particle detection threshold (software based). With the exception of the dilution curve, the graphs in figure 3.4 display sample concentration as a function of the particle diameter. Each graph relates dilution and recording time, while different detection thresholds were assessed independently. All measurements of EV samples were recorded in duplicate for each condition and no statistical analyses were performed.

For smaller beads, neither dilution (1000 to 5000-fold) nor recording duration (60 versus 90 sec) affected the analysis, that is, the relative number of particles recovered (Figure 3.4A-B). However, sensitivity decreased with increasing particle size, and with a higher concentration of beads. Reducing the detection threshold – or the visual acuity of image processing – did not have an appreciable effect for beads (Figure 3.4B). This and the lack of large peaks at particle sizes of 200 and 400nm suggests that the software was most sensitive to the motion of particles around 100nm, which is ideal for the analysis of EVs isolated by the technique used in the work described in this thesis (see Figure 3.2 for reference).

When analysing the more heterogenous plasma EV samples, peaks had a higher standard deviation and were skewed to the right, with most particles smaller than 200nm (Figure 3.4C-D). The effect of the detection threshold was more relevant for polydispersed samples such as the EVs analysed in this work. A threshold of 5 was found to be optimally sensitive, with more particles being detected than at the default threshold of 10 for dilutions up to 100-fold (Figure 3.4E), while more background noise was excluded when compared to lower thresholds. On the other hand, higher dilutions were more affected by recording duration, whereby 90 seconds gave the most consistent readings.

Liver-derived EVs were also assessed in a similar manner for comparison. These vesicles were slightly larger than plasma EVs, especially at the higher concentrations (Figure 3.4F). Low concentrations of EVs (less than 10×10^6 particles/mL) in both plasma and liver-derived samples showed greater polydispersity, which may imply that the software is less sensitive to polydispersity in more concentrated samples due to the particle swarming effect. Following the aforementioned calibrations, the optimal settings for NanoSight™ enumeration of EVs was standardised across experiments. These can be viewed in Table 3.1.

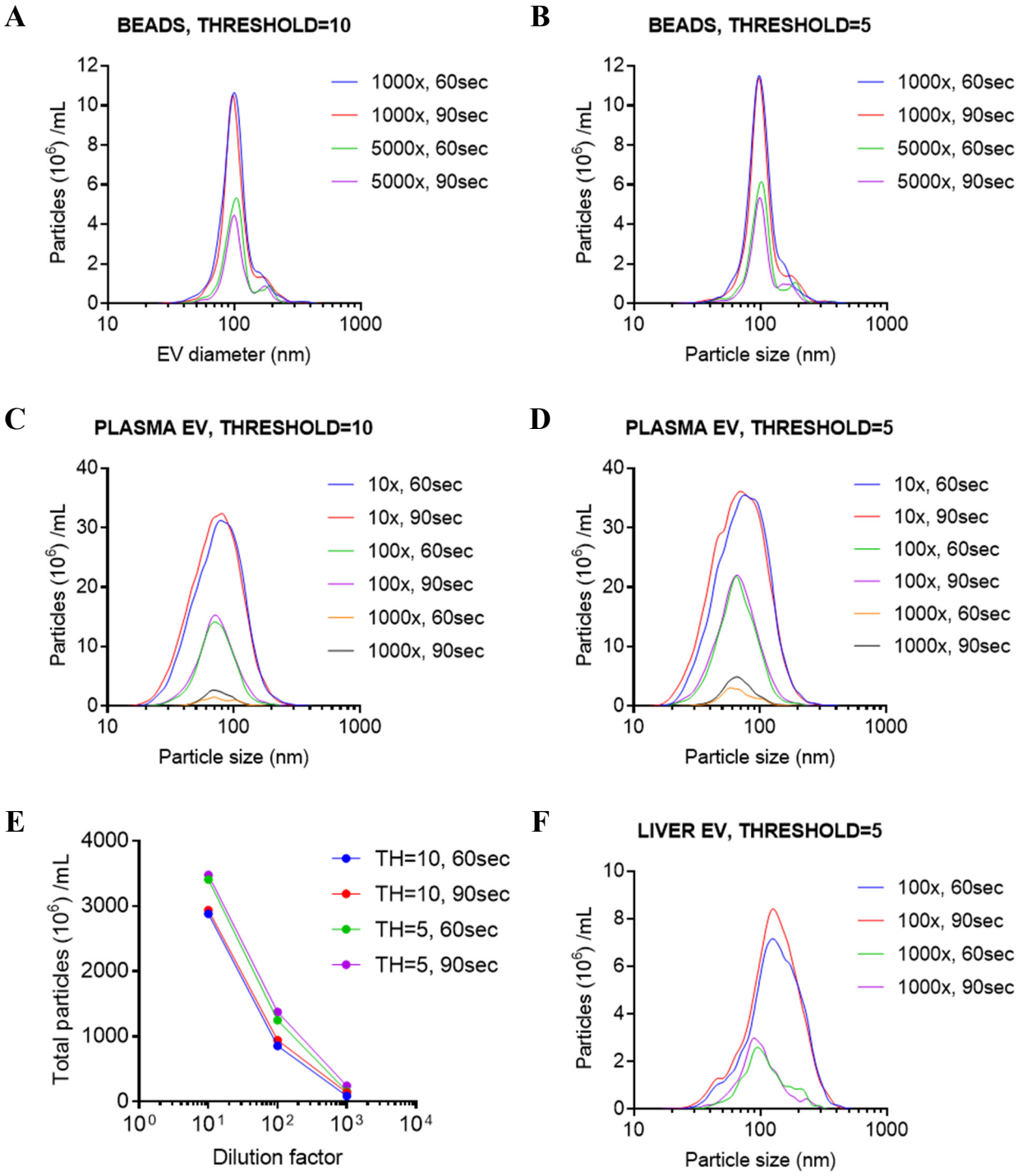

Figure 3.4. Optimisation of extracellular vesicle enumeration. The technique was calibrated using polystyrene beads with the software detection threshold set to default 10 (**A**) or optimal 5 (**B**). Similar plots for plasma EV samples across three dilutions (**C-D**) with the effect of all parameters on total particle concentration (**E**). Liver-derived EVs are shown for comparison (**F**). Detection threshold (TH) refers to sensitivity, time (60 or 90 sec) refers to recording length of particle motion.

Table 3.1. Standardisation of NanoSight™ settings.

Calibrated settings		*Optimal setting*
Sample parameter:	Particle concentration	100 particles/frame *
Instrument parameter:	Recording duration	90 seconds **
Software parameter:	Detection threshold	Level 5

*Manufacturers' recommendation is 40-100 particles/frame. Samples were diluted to 100 particles/frame to minimise the swarming effect seen at higher concentrations. Dilution depended on sample concentration and was corrected for during data analysis. **Some studies used 60 sec recordings, however, recording duration was consistent across samples within each study. All sample recordings were performed in at least duplicate to minimise technical error.

3.2.3. EV characterisation by flow cytometry

Following the gold standard for characterising the composition of intact EVs, we employed a conventional cytometric technique using an instrument that was optimised for the detection of subthreshold particles (0.2μm compared to 0.4-0.5μm for traditional cytometers). Despite the biophysical limitations of exosome assessment by this method (Thery et al., 2006, Witwer et al., 2013), we attempted to optimise a protocol for the staining of EVs coupled to latex beads versus individual EVs to determine the cell origin of plasma and liver-derived samples using a designated cytometer (Guava easyCyte™; Merck, Darmstadt, Germany).

For individual EV characterisation, troubleshooting was performed for a number of parameters to compensate for ultracentrifugal washing, which results in sample loss: titration of antibody, incubation time and temperature, blocking sample with BSA, and precipitation of stained sample with polyethylene glycol (PEG). Findings for blocked, PEG-precipitated samples following overnight incubation at 4^{o}C (see section 2.4.5) are shown in Figure 3.5. Sizing beads (1.33μm) were used to determine the upper limit for forward and side scatter of individual EVs (Figure 3.5A). In most samples analysed, the EVs were near the limit of detection for forward scatter, or size (Figure 3.5B), while the diluent (filtered PBS) did not contribute to background signal (Figure 3.5C). To determine whether the samples were intact, they were stained with calcein AM and again analysed by flow cytometry. Almost all detected events were positive when compared to unstained sample (Figure 3.5D), confirming that the samples were unlikely to be contaminating lipoproteins or aggregates that lack esterase activity. Additionally, events were almost ubiquitously staining double-positive for discrete populations, which included exosome (CD63) and microvesicle (Annexin-bound phosphatidylserine) markers (Figure 3.5E), or markers of cellular origin for endothelial cells (CD105) and leukocytes (CD45) (Figure 3.5F). The precipitation of the sample with PEG prior to analysis did reduce background "noise", but it was difficult to accurately delineate the EV origins as there was an unexpected overlap between mutually exclusive markers, which may suggest the presence of immune complexes. Using the individual EV staining technique, it was not possible to discern these complexes from true single-EV staining, given their proximity to the limit of detection.

To circumvent this issue, an alternative approach for the analysis of smaller particles is immunoprecipitation (see section 2.4.5). In our study, filter gains were first calibrated with beads coated directly in our antibodies of interest (positive controls; red), while BSA- or glycine-adsorbed beads were used as a negative control (white). Once again, samples were gated on bead size (Figure 3.5G), where adsorbed samples were expected to resolve within this gate. However, sample recovery was reduced for EV-adsorbed beads (Figure 3.5H) compared to beads alone. Following antibody labelling, we concluded that EV sample readings (blue) consistently failed to produce a fluorescence intensity greater than that of the respective negative controls (Figure 3.5I-K), and therefore, flow cytometry as a means of EV characterisation was not pursued in further studies.

A Sizing beads

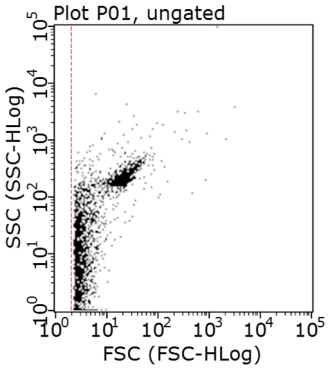

B EV unstained

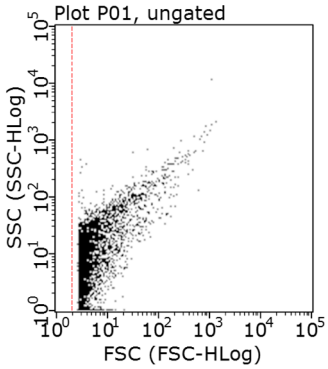

C Diluent

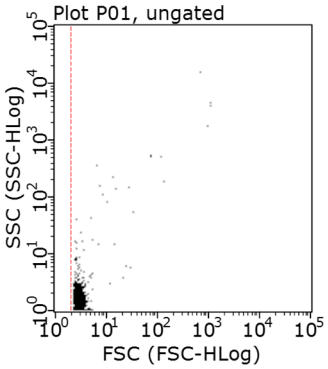

D EV positive stain

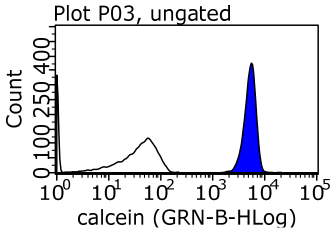

E CD63 + Annexin A5

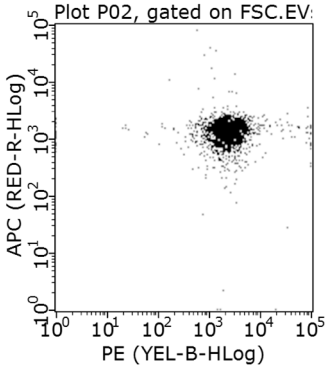

F CD45 + CD105

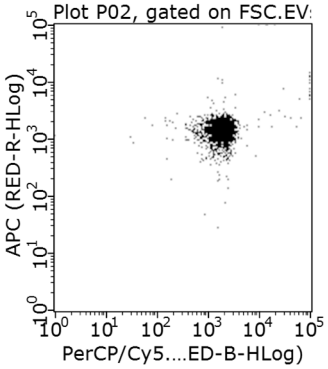

G Beads only

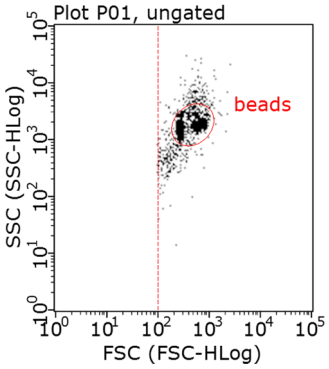

H Beads + EV

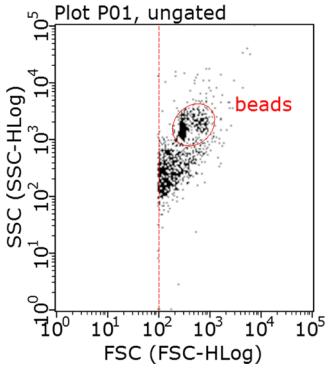

I CD45

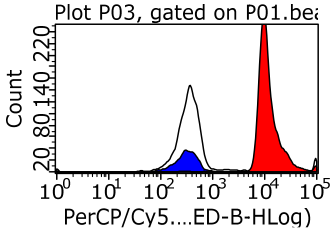

J CD105

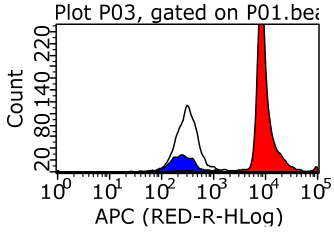

K CD41

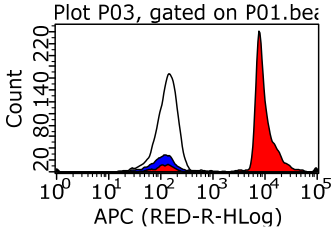

Figure 3.5. Optimisation of flow cytometric analysis of extracellular vesicles. Panels A-F show readings for individual EV detection: 1.33μm sizing beads (**A**); unstained EV sample in diluent (**B**) and diluent only (**C**); sample stained with calcein alone to show EV-positive events (**D**), EV double-labelled with PE-anti-CD63 (exosome) and APC-Annexin A5 (microvesicle) to demonstrate subtype overlap (**E**) or PerCP/Cy5.5-anti-CD45 (leukocyte) and APC-anti-CD105 (endothelium) to demonstrate false population overlap (**F**). Panels G-K show readings for the bead-based detection technique: polystyrene beads alone (**G**) or with EVs adsorbed onto the surface (**H**); polystyrene beads alone as a negative control (white), with antibody adsorbed as a positive control (red), or with EV adsorbed prior to antibody labelling (blue) against CD45 (**I**), CD105 (**J**), or the platelet marker CD41 (**K**).

3.3. Effect of High-Fat Diet on Extracellular Vesicles

Our group has previously shown that mice fed a high-fat diet (HFD) have an increase in body weight by up to 30% with elevated liver triglycerides after 15 weeks (Lo et al., 2011). We hypothesise from the literature that HFD can alter circulating EVs, but it is not known whether they are altered in association with the development of NAFLD. Therefore, the aim of this study was to use the developed methodology to examine the impact of HFD on number and type of circulating and liver-derived EVs. Whether these changes occur in association with the development of NAFLD was also studied.

3.3.1. Animal characteristics

As described in section 2.2.1, mice were fed either HFD or standard chow for 12 and 52 weeks. After 12 weeks of HFD, animals were significantly heavier (43% increase) with hepatomegaly (64% increase) compared to their counterparts receiving the standard chow diet (both $p<0.01$; Table 3.2). This pattern was amplified at 52 weeks (body weight: 2-fold increase, liver weight: 3-fold increase; both $p<0.001$). Hyperinsulinaemia associated with HFD-induced obesity was also present, however, since this parameter was prone to biological variation, significance was only reached at 52 weeks (12 weeks: $p=0.072$, 52 weeks: $p=0.002$ versus chow). Elevated liver enzymes, a typical hallmark of NASH, only became apparent at 52 weeks in HFD mice (ALT: 17-fold, AST: 5-fold versus 12 week HFD; both $p<0.001$), although biological variation was high for both enzymes. There were no significant changes in these parameters for animals on standard chow diet for 52 weeks, when compared to 12 weeks on the same diet.

Table 3.2. Animal characteristics in pilot study.

	Chow		*HFD*	
	12 weeks	*52 weeks*	*12 weeks*	*52 weeks*
Weights:				
body (g)	29.1±1.82	30.8±1.23	41.5±1.97 *	60.4±1.65 *#
liver (g)	1.45±0.15	1.30±0.24	2.38±0.15 *	5.53±0.71 *#
liver (% body)	4.97±0.22	4.20±0.62	5.75±0.28	9.15±1.00 *#
Plasma chemistry:				
ALT (U/L)	25.0±9.03	23.4±7.47	38.4±37.6	396±72.1 *#
AST (U/L)	55.0±31.4	62.0±18.2	85.0±65.7	333±53.6 *#
ALT/AST ratio	0.49±0.09	0.40±0.11	0.57±0.30	1.19±0.10 *#
triglycerides (mg/dL)	51.6±14.5	29.7±23.8	43.4±10.5	49.1±9.29
insulin (pg/mL)	128±17.5	141±39.7	383±306	877±723 *

Data are mean ± SD for n=6 animals per group, excluding outliers determined by the ROUT method (Q=5%). Significantly different from age-matched chow control (*) or 12 weeks of respective diet (#) accepted at $p<0.05$ as determined by 2-way ANOVA with Tukey's test for multiple comparisons. Abbreviations: ALT, alanine transaminase; AST; aspartate transaminase.

3.3.1.1. Hepatic steatosis

Steatosis was quantified in two ways: one approach used *ex vivo* staining of neutral lipids in whole liver tissue with Oil Red O (ORO), while hepatic TAG was extracted prior to colorimetric quantification (detailed in section 2.5). The latter revealed a significant increase in TAG content in the HFD groups at both timepoints when compared to age-matched chow fed animals ($p<0.001$), which remained stable across time-points (Figure 3.6A). A trend toward increased TAG was observed in the older chow group, however this did not reach significance. Like TAG levels, the intrahepatic lipid determined by ORO was increased by HFD at both timepoints when compared to chow diet (both $p<0.001$; Figure 3.6B). Interestingly, an aging effect was also noted with significantly increased ($p<0.001$) neutral lipid in the 52 week chow fed group. This finding was supported by the liver histology analyses in section 3.3.2.

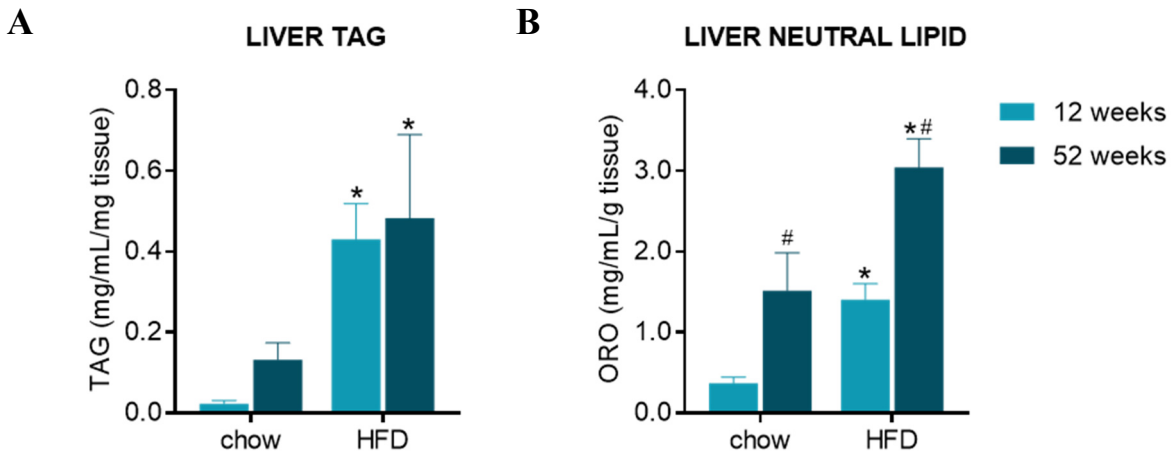

Figure 3.6. Liver lipid quantitation. **A.** Triacylglycerol (TAG) extracted from homogenised liver. **B.** Neutral lipids (fatty acid glycerols) were stained with Oil Red O (ORO) in homogenised liver prior to elution. Data are mean ± SD given per unit tissue, for n=6 animals per group. Significantly different from age-matched chow control (*) or 12 weeks of respective diet ($^{\#}$) accepted at $p<0.05$ as determined by 2-way ANOVA with Tukey's test for multiple comparisons.

3.3.2. NAFLD phenotype

To evaluate the histological severity of NAFLD with short-term and long-term HFD leading to obesity, liver sections were assessed for general morphology by H&E staining (section 2.7.1) or for collagen accumulation (basement and fibrillar) by PSR staining (section 2.7.2). This was further complemented with the evaluation of molecular changes – including inflammation and ECM remodelling – by using gene expression as a surrogate marker (section 2.6.4). The findings herein aimed to demonstrate the typical features of NAFL development to NASH over time with HFD consumption, whereas comprehensive histological and molecular profiling was beyond the scope of this study.

3.3.2.1. Liver histology

Histological examination of livers revealed changing patterns of steatosis with progressive high-fat feeding, and also with age. When compared with standard diet at 12 weeks (Figure 3.7A), livers of HFD mice had abundant microvesicular steatosis and some hepatocyte ballooning, while sparse macrovesiculation was also evident in adjacent regions (Figure 3.7C). In contrast, after HFD consumption for 52 weeks, macrovesicular steatosis dominated and much of the liver architecture was lost (Figure 3.7G). In this context, the interspersed tissue appears highly nucleated, suggesting the increased presence of infiltrating leukocytes that have formed multiple inflammatory foci. Pan-collagen staining also showed evidence of periportal and pericellular fibrotic bands (Figure 3.7H). In contrast, mice on a standard diet for 52 weeks showed no fibrosis or disrupted architecture (Figure 3.7E-F), although mild steatosis and ballooning was present.

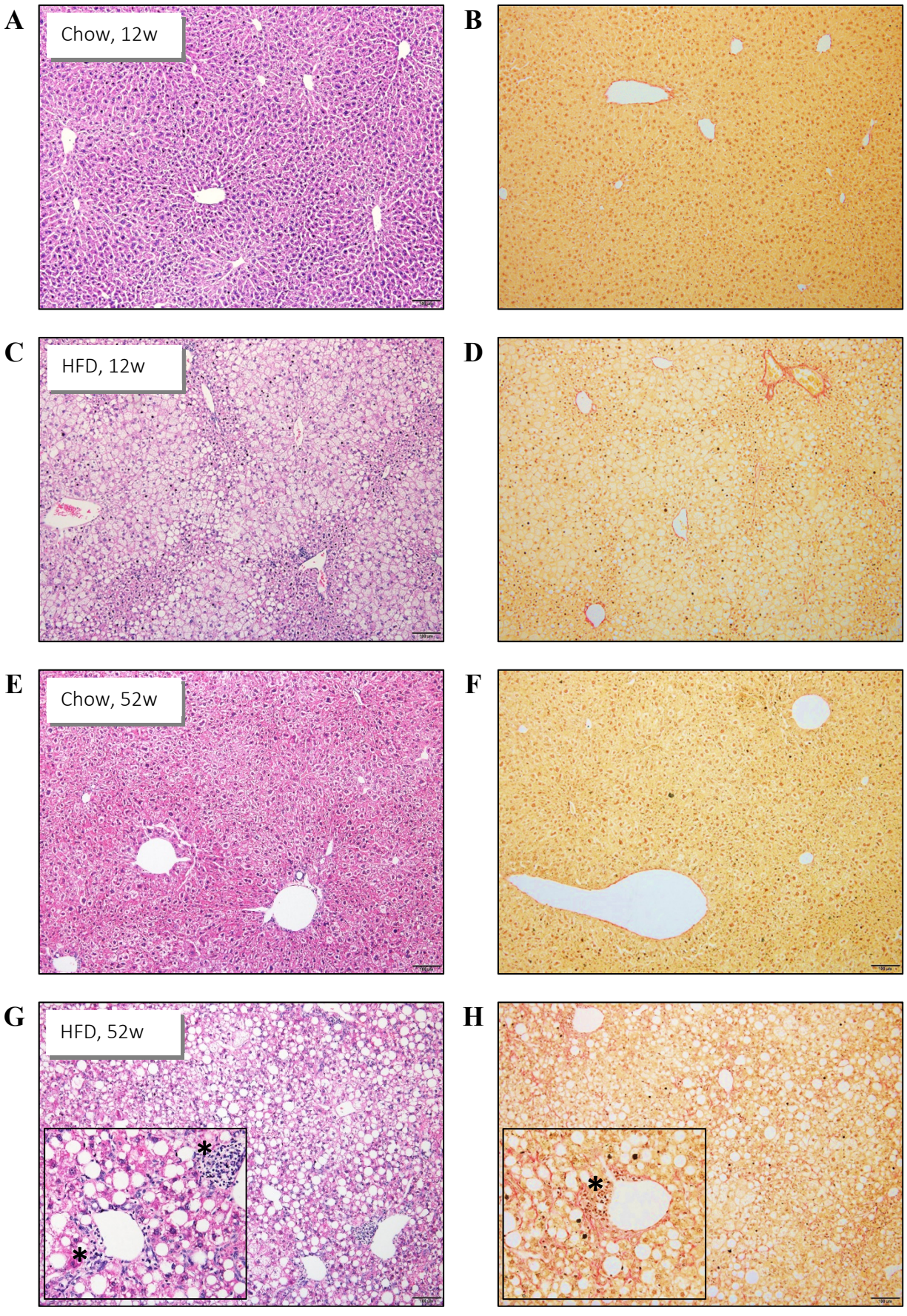
A
Chow, 12w
B
C
HFD, 12w
D
E
Chow, 52w
F
G
HFD, 52w
H

Figure 3.7. Liver histology. Left panels show general morphology using H&E staining, right panels show collagen accumulation (red) by PSR staining for respective samples. Animals on 12 week standard chow diet have normal liver architecture (**A-B**) while high-fat fed mice show the early presence of NAFLD with steatosis but no major scarring (**C-D**). At 52 weeks, mild steatosis is visible in chow fed mice (**E-F**) while their obese counterparts have demonstrable NASH with increased nuclei dense areas by H&E stain and diffuse, non-bridging fibrosis by PSR (**G-H**). Asterix denotes immune infiltrates. Representative images at 100× magnification (scale bar = 100μm), inset 200× magnification.

3.3.2.2. Liver gene expression

To further validate the phenotype of NAFLD and its progression to NASH, changes in the liver transcripts of key inflammatory and ECM remodelling markers were assessed by qPCR (see section 2.6 for detailed methods). The mRNA levels of genes associated with inflammation (TNF and MCP1) peaked early with HFD (6.7 and 10-fold respectively, both $p<0.01$), with no further increase observed at 52 weeks (Figure 3.8A-B). The expression of the macrophage marker (F4/80) tended to increase with 12 weeks of HFD, and reached significance compared to age matched control (approx. 4-fold, $p<0.001$) at 52 weeks (Figure 3.8C). On the contrary, the presence of activated hepatic stellate cells (αSMA) was not altered by HFD at either time-point (Figure 3.8D), despite an upregulation of collagen transcripts (collagen I by 8-fold and collagen IV by 2.4-fold, both $p<0.001$) at 52 weeks (Figure 3.8E-F). TGFβ showed a similar pattern in gene expression changes when compared to collagens (Figure 3.8G). Interestingly, when examining TIMP1 – a key regulator of ECM turnover – there was a 9-fold increase with HFD at 52 weeks ($p=0.002$ versus chow diet) but no change at 12 weeks (Figure 3.8H). This finding was likely due to a 5-fold decrease in TIMP1 expression with aging alone, although the difference was not significant ($p=0.280$ versus 12 weeks) and no such pattern existed between the HFD groups at different timepoints.

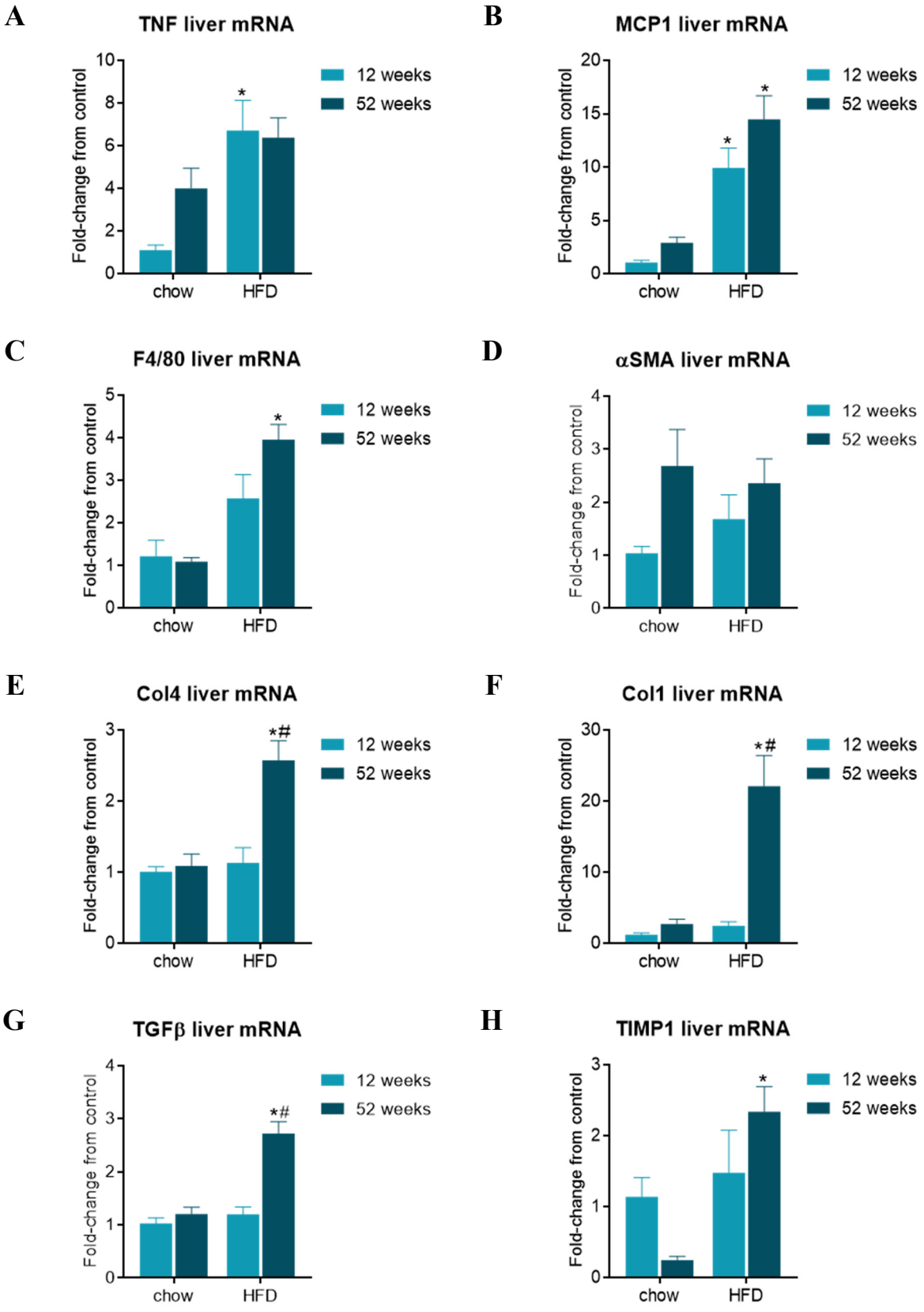
A
TNF liver mRNA
Fold-change from control
12 weeks
52 weeks
chow
HFD
B
MCP1 liver mRNA
C
F4/80 liver mRNA
D
αSMA liver mRNA
E
Col4 liver mRNA
F
Col1 liver mRNA
G
TGFβ liver mRNA
H
TIMP1 liver mRNA

Figure 3.8. Liver gene expression. Graphs represent transcripts of inflammatory genes (**A-C**) and genes involved in ECM remodelling or fibrosis (**D-H**). Data is expressed as mean ± SEM of fold-change from 12 weeks chow diet (control group), for n=6 mice excluding outliers. Significant difference from chow (*) or 12 weeks of diet ($^{\#}$) accepted at $p<0.05$ as determined by 2-way ANOVA with Tukey's test for multiple comparisons. Abbreviations: TNF, tumour necrosis factor; MCP1, monocyte chemotactic protein 1; αSMA, alpha smooth muscle actin; Col, collagen; TGFβ, transforming growth factor beta; TIMP1, tissue inhibitor of metallo-proteinase 1.

3.3.3. Extracellular vesicle enumeration

Extracellular vesicles isolated from the ultracentrifuged pellet of plasma and respective liver-conditioned media samples were enumerated by NanoSight™ using Nanoparticle Tracking Analysis (NTA) software, in accordance with the optimised parameters from Table 3.1. The isolation process of EVs is detailed in Chapter 2 (see section 2.4.1 and 2.4.4).

3.3.3.1. EV abundance in plasma and liver conditioned media

Enumeration of vesicles showed an increase with HFD in the circulation, consistent with the literature, however these changes were not significant (Figure 3.9A). Although biological variation was large at 52 weeks, aging showed a more convincing effect for both diets, with significantly elevated EV abundance at 52 weeks when compared to 12 weeks (chow: 9-fold, HFD: 6-fold; both $p<0.001$). Interestingly, the opposite pattern was seen in the EVs derived from the liver-conditioned media, where abundance was decreased by aging (chow: 7-fold, HFD: 26-fold; both $p<0.001$). As with the plasma studies, the number of EVs isolated from liver-conditioned media were unaffected by diet at 12 weeks (Figure 3.9B). In contrast, liver EVs showed a diet effect at 52 weeks, with a significant decrease in abundance in the HFD group (3-fold, $p<0.001$). This data was corrected for the weight of cultured liver tissue (0.6-1.2g). However, when the data was adjusted for total liver weight, these significant changes were completely abrogated (data not shown).

In addition to the counting of EVs, the NTA technology also enables an estimate of particle size. The overall size distribution of EVs was unaffected by either diet or aging, and did not differ markedly between the two sampling sites (Figure 3.9C-D). Liver-derived EVs tended to be slightly larger (100nm on average compared to 80nm for plasma EVs), while the abundance of plasma EVs was inversely correlated with liver-derived EV samples ($r=-0.881$, $p<0.001$) with a small 95% CI (-0.949 to -0.735) using Spearman correlation (Figure 3.9E).

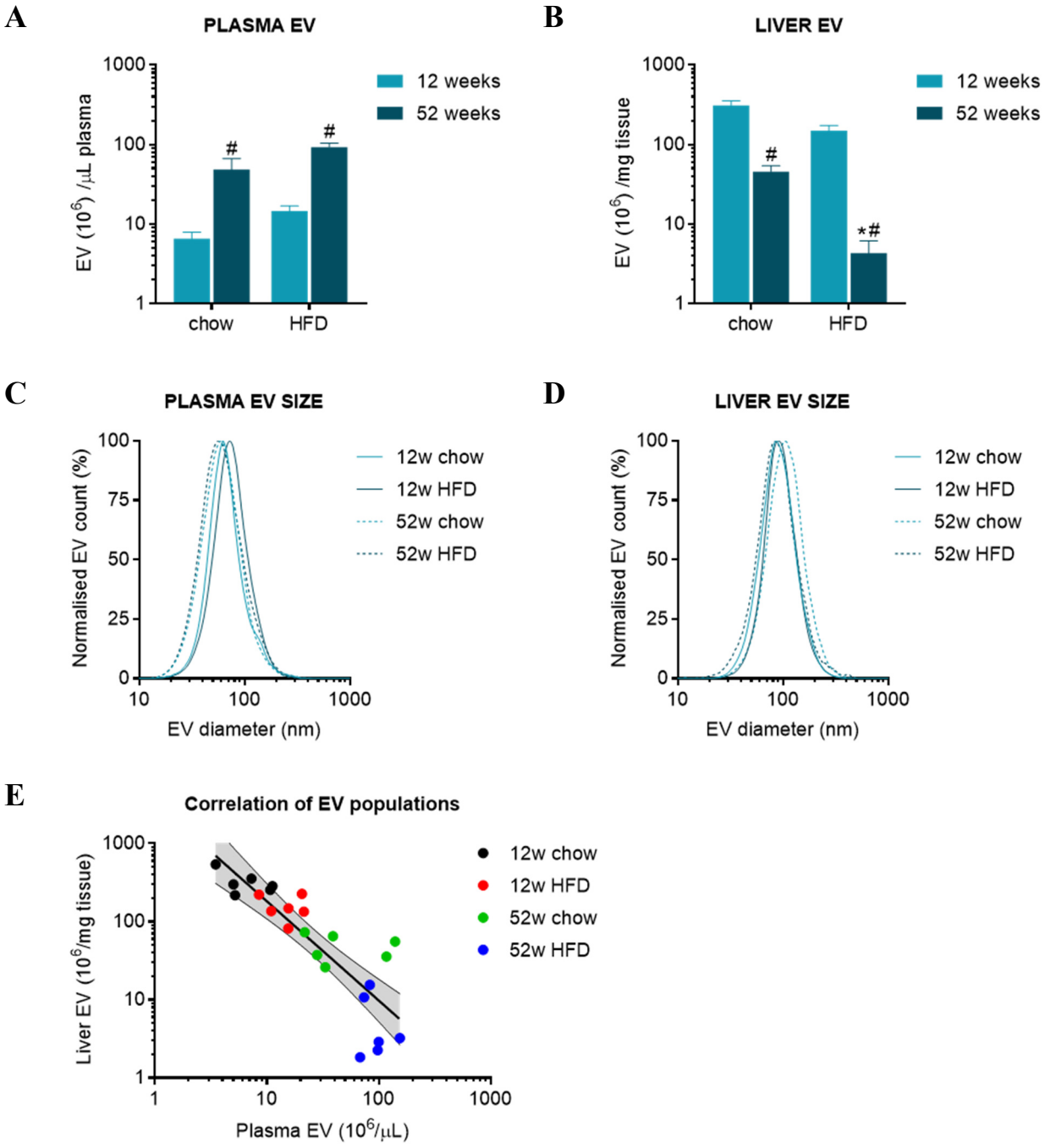

Figure 3.9. Extracellular vesicle quantitation. Total particles calculated for plasma (**A**) and liver-derived samples (**B**), with respective size distribution (**C-D**), using Nanoparticle Tracking Analysis. Plasma and liver-derived EVs correlated negatively (**E**). Panels A-B show mean ± SEM for n=6 animals per group. Significantly different from chow (*) or 12 weeks of diet ($^{\#}$) accepted at $p<0.05$ as determined by 2-way ANOVA with Tukey's test for multiple comparisons. Panel E shows linear regression with 95% confidence interval.

3.3.3.2. EV correlations with liver changes

Given the aging-predominant changes in the abundance of EVs, most trends that were observed in the plasma biochemistry or other animal characteristics – significant or otherwise – were largely influenced by diet and therefore, did not relate directly to either circulating or liver EV numbers.

Interestingly, when either EV population was correlated against liver gene expression in the format delta-delta Ct (log transformed fold-change), most differences were significant by the Spearman test; that is, all markers with the exception of αSMA were correlated with EV abundance, albeit in different directions: positively for plasma and negatively for liver-derived samples, respectively (data not shown). However, 95% CI tended to be quite large: for example, correlations ranged from slightly significant ($p<0.05$) against TIMP1 for both plasma ($r=0.487$, CI 0.091 to 0.750) and liver EVs ($r=-0.478$, CI -0.744 to -0.079), to highly significant ($p<0.001$) against MCP1, again for both plasma ($r=0.819$, CI 0.606 to 0.923) and liver EV samples ($r=-0.829$, CI -0.927 to -0.625).

Finally, the most convincing relationships were evident between EV number and hepatic lipid load. Although the correlations with TAG (Figure 3.10A-B) were not as strong (plasma EV: $r=0.485$, $p=0.016$; liver EV: $r=-0.567$, $p=0.004$) due to divergent clustering of treatment groups, this effect was less prominent for neutral lipid measurement by ORO (Figure 3.10C-D) where the correlations were highly significant ($p<0.001$) for both EV populations (plasma EV: $r=0.846$; liver EV: $r=-0.898$). As expected, plasma EVs correlated positively while liver-derived EVs correlated negatively with the respective lipid measurements. These findings suggest that circulating (or liver) EV abundance may be a reliable predictor of hepatic lipid accumulation and may be a potential biomarker for this parameter.

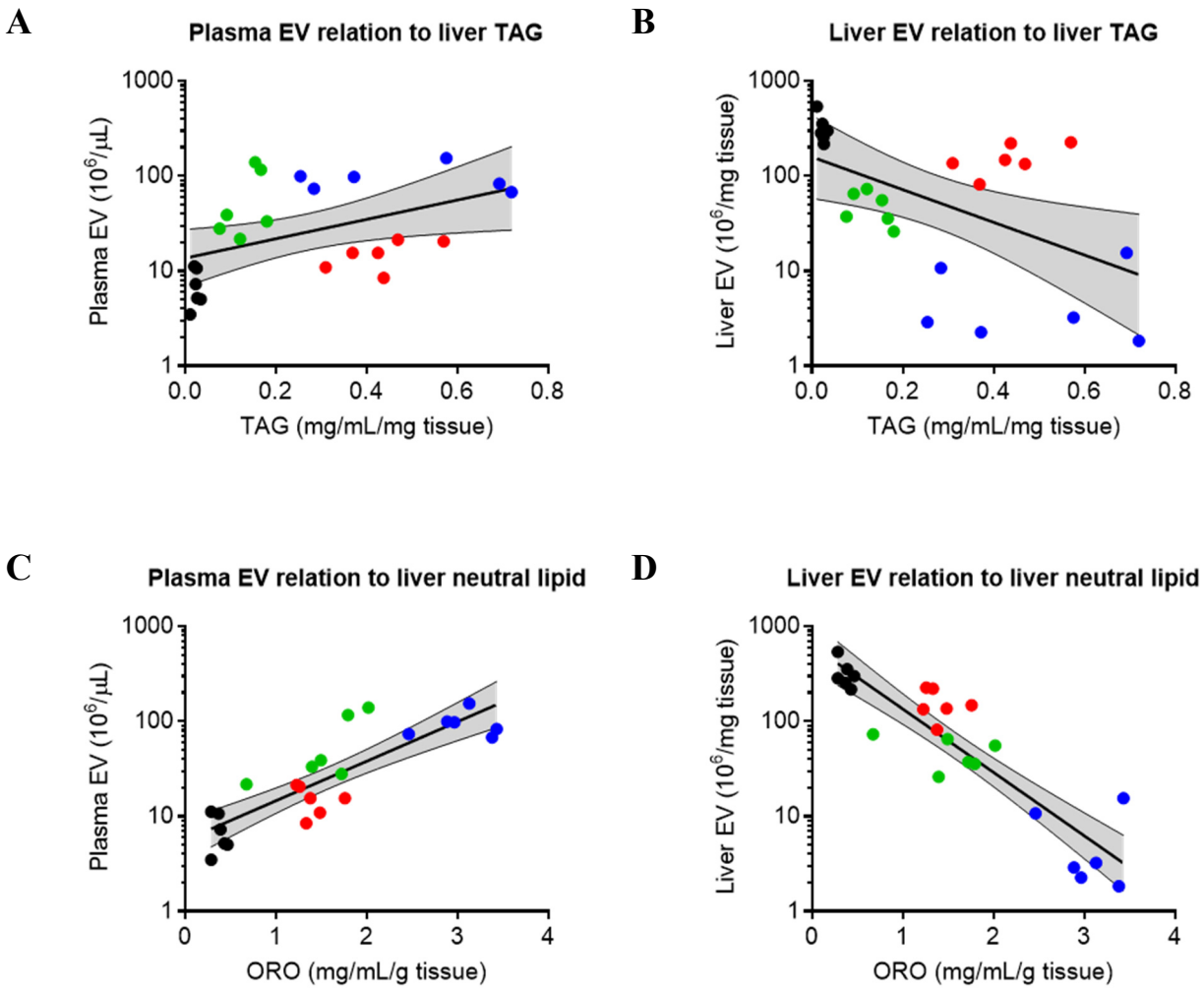

Figure 3.10. Extracellular vesicle correlations with liver lipids. Relationship between liver triacylglycerol (TAG) and (**A**) plasma EVs (r=0.485) or (**B**) liver-derived EVs (r=-0.567). Oil Red O (ORO) staining of neutral lipids – representing hepatic lipid droplets – and correlation with (**C**) plasma EVs (r=0.846) or (**D**) liver EVs (r=-0.898). Treatment groups include 12 weeks chow (black) or high-fat diet (red), and 52 weeks chow (green) or high-fat diet (blue). Linear regression with 95% confidence interval as determined by Spearman test. All correlations were significant ($p<0.05$).

3.4. Interpretation

The findings from this Chapter highlight the utility of EV enumeration and physical profiling by optical methods (NanoSight™) and reiterate the current limitations of EV characterisation by flow cytometry. They then continue to explore the relationship between EVs (from plasma or liver) and other clinical or molecular parameters associated with NAFLD development, in a pilot study of diet-induced obesity in rodents (summarised in 3.4.2). Briefly, it was shown that circulating EVs may predict the extent of hepatic steatosis and possibly indicate the level of inflammation in the liver (through gene expression of MCP1, for example). Similar patterns were also observed for liver-derived EVs, albeit in the inverse direction. To confirm these findings, a larger study with more timepoints was addressed in Chapter 4.

3.4.1. Technique optimisation and validating EV presence

Using a combination of transmission EM, western blot analysis, and intracellular esterase staining for flow cytometry, we initially determined the presence of EVs in ultracentrifuged plasma and liver-conditioned media. Structures shown under electron microscopy were relatively uniform in size and shape, consistent with exosomes, which was further confirmed during EV enumeration by NTA. While the bilayer membranes were visible with increased contrast, the electron density was unusual for EVs when compared to images in the literature. This could be explained by over-staining with counterstain, however, similar findings were also documented by some other groups (Jenjaroenpun et al., 2013, Ko et al., 2015).

Probing for CD63 by western blot analysis confirmed the presence of exosomes, as this late-endosomal protein was enriched in the plasma EV fractions when compared to whole plasma or liver lysates. Interestingly, liver-derived EVs more closely resembled whole liver in their protein profile and did not show the CD63 enrichment typical of plasma EVs. Given the comparable methods of isolation, it is possible that liver vesicles are instead predominantly MV subtype as opposed to exosomes.

The uptake of calcein dye by particles examined by flow cytometry further confirmed the presence of EVs rather than lipoproteins (which lack esterase activity) or contaminating protein aggregates. To aid in the phenotypic analysis of smaller EVs using this technique, adsorption of sample to larger beads (around 5μm) is required to allow for adequate washing following the antibody detection step (Inglis et al., 2015). Polystyrene (i.e. latex) beads are particularly useful, due to their high-affinity hydrophobic surface which indiscriminately attracts most proteins, such as those on the surface of EVs. The limitation of this technique is that it cannot predict the proportion of EVs derived from a given population; that is, readings between samples (and treatments) are relative. However, as evidenced in this study, even adsorption was insufficient to provide a conclusive answer about EV surface markers, as discrete populations (such as unrelated cell type origins) were unable to be delineated. One explanation could be the formation of immune complexes, which may be circumvented by blocking the Fc portion of staining antibodies or alternatively, using Fab fragments conjugated to fluorophores. While there is no direct comparison of this method and the protocols used in our study in the literature, future studies expanding on the concepts in this thesis may benefit from trialling these techniques during cytometric EV analysis.

While ultracentrifugation without a density gradient is considered to be a "crude" technique for EV isolation, we were confident that our samples represented EVs of interest. Given the known differences in density between EVs and lipoproteins of the same size (Figure 3.11), there is a possibility of co-isolation at higher centrifugal speeds (Sodar et al., 2016, Witwer et al., 2013); however, the structures would appear as discrete populations under TEM, albeit liposomes in the VLDL-chylomicron range (comparable in size to EVs) are largely absent from HepG2 cell conditioned media (Thrift et al., 1986). This implies that the electron dense vesicles in our HepG2 preparation are in fact EVs, which in turn substantiates the presence of EVs in the plasma sample preparation. Were the cytometric techniques successful, antibody labelling of EVs would have provided additional information about their tissue origin. This limitation is addressed in Chapter 4, where mass spectrometry analysis of liver EVs provided further insight into the content of these vesicles, in both NAFL and NASH, as well as their otherwise healthy counterparts.

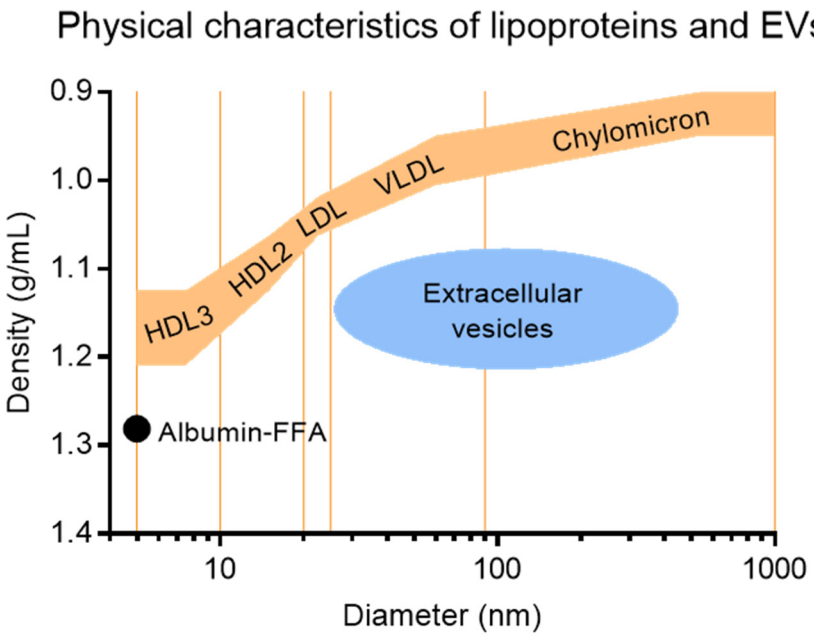

Figure 3.11. Physical characteristics of vesicles. Lipoprotein densities generated from (Jairam et al., 2012, Memon and Gilani, 1995), EV densities from (Witwer et al., 2013). Orange vertical lines represent boundaries between lipoprotein sizes. Abbreviations: HDL, high-density lipoprotein (types 2 and 3); LDL, low-density lipoprotein; VLDL, very low-density lipoprotein; FFA, free fatty acid (albumin conjugated).

3.4.2. Establishing a NAFLD model for the study of EVs

In the pilot study described, C57Bl/6 mice (n=24) were fed HFD or standard chow for 12 or 52 weeks to observe NAFL progression to NASH. This model reflects features of NAFLD development in humans, as the hepatic phenotype is comparable and systemic metabolic disturbances are preserved. Indeed, animals in our study were overweight with enlarged fatty livers by 12 weeks of HFD, however, their NAFLD was subclinical as determined by the liver function test (circulating ALT and AST). There were some perturbations in plasma insulin, although intragroup variability was high and hyperinsulinaemia was not recorded at this timepoint. By 52 weeks, the HFD group were morbidly obese and the severity of their NAFLD was reflected in their grossly elevated liver enzymes. While the group was hyperinsulinaemic on average, again the variability was high, which suggests that plasma insulin is not a reliable predictor of NAFLD progression.

Examining the liver phenotype – in terms of histology and lipid content – showed that hepatic TAG and neutral lipids (all fatty acid glycerols, including TAG) were elevated in the HFD group at either timepoint, whereas aging had a compounding effect on the latter. NAFLD progression did not affect TAG content relative to tissue weight, however, differences in lipid storage pattern were observed by histology. As expected, mice at 12 weeks had pronounced steatosis but lacked other features of NASH, while 52 weeks of HFD produced widespread punctate (or macrovesicular) steatosis with immune infiltrates and pericellular fibrosis. These findings were reinforced by the gene expression data, which showed elevations in both fibrillar (type I) and basement (type IV) collagens, with a corresponding increase in TGFβ. This growth factor plays a known role in tissue fibrosis (Biernacka et al., 2011), and has been shown to promote NASH (Yang et al., 2014). Markers of inflammation, on the other hand, were increased by 12 weeks and remained stable; this suggests an early response to lipotoxic stress by the liver parenchyma. Ergo, the limitations of current technologies to detect these subclinical changes warranted the use of EVs as a potential biomarker.

Interestingly, in our study, aging had the most profound effect on both circulating and liver-derived EVs, irrespective of diet. That is, enumeration by NanoSight™ showed that progression of NAFLD specifically (or even obesity) may not be detectable by changes in the plasma EV number when other biological confounders are involved. This pilot data suggests a case for the re-evaluation of guidelines that aim to standardise the diagnostic practices for NAFLD; while older age is a known risk factor for progression to NASH, it is seldom accounted for when developing reference values, although some groups have argued that it should be considered (McPherson et al., 2017). Another interesting observation was the inverse trend between plasma and liver EVs, whereby aging caused a decrease in the liver-derived population. This was magnified at 52 weeks, such that total EVs were further decreased by HFD. Despite the lack of observable changes in EVs at 12 weeks, when all samples were correlated against hepatic neutral lipid (ORO staining), there was a significant positive and negative trend with plasma and liver origin, respectively. The study data suggests that absolute EV numbers may not be a strong predictor for NAFLD presence or progression, however they could be used as an indicator for liver lipid accumulation. Whether this is applicable longitudinally – that is, throughout the development of NAFLD – is examined in detail in the following Chapter.

Chapter 4.

Extracellular vesicles in a diet-induced rodent model of NAFLD progression

Chapter 4. Table of contents

4.1. Introduction

As described in Chapter 1, NAFLD is an almost ubiquitous complication of obesity, where a proportion of sufferers (up to 30%) will advance to NASH (Chalasani et al., 2018). Whether the EV number and profile changes in association with the development of NAFLD is not known, as most studies in this context have typically been cross-sectional (Ban et al., 2016). In the present study, animals were maintained on an obesogenic HFD or standard chow for up to 50 weeks, to assess NAFLD progression (see Figure 4.1). The effects of both diet and aging were examined to compare the effects of extrinsic and intrinsic changes respectively, as well as their intersection (defined as NAFLD progression).

In a similar study design by Ito and colleagues, animals were fed a HFD (60%kcal fat) or standard chow for up to 50 weeks, with metabolic parameters and liver phenotype recorded (Ito et al., 2007). Significant increases in plasma insulin and cholesterol were observed at the earliest timepoint (10 weeks), whereas liver enzymes were unchanged up to 19 weeks. While liver TAG was increased at all timepoints, evidence of NASH was not present up to 19 weeks and fibrosis was only present by 50 weeks, consistent with our findings in Chapter 3. Our group has also described previously in a diabetic mouse model that by 20 weeks of HFD, animals show early signs of fibrotic changes as well as an increase in liver macrophages (Lo et al., 2011). Whether the EV signature of these animals can be used to track pathological changes has yet to be explored, although shorter-term studies on mice (Povero et al., 2014) and cross-sectional studies on humans (Kornek et al., 2012) have shown that the circulating EV abundance – either total or specific populations – may indeed be a predictor of NAFLD severity. Whereas the former mouse study by Povero and colleagues (2014) utilised mass spectrometry to characterise plasma EV content, the present Chapter will analyse the protein cargo of liver EVs and how these are changed from 10 to 50 weeks of HFD.

While the previous chapter identified trends that could be associated with either diet or aging in a small sample cohort, the progression study outlined here will focus on temporal changes in the liver and EV populations in a larger group of animals and compare this back to the findings in Chapter 3. By following the development of NAFLD over one year, fluctuations in EVs coinciding with otherwise subclinical events can be further dissected, while changes in the EV cargo may hint at their functional role as intercellular messengers. The latter will then be explored through functional studies in Chapter 6.

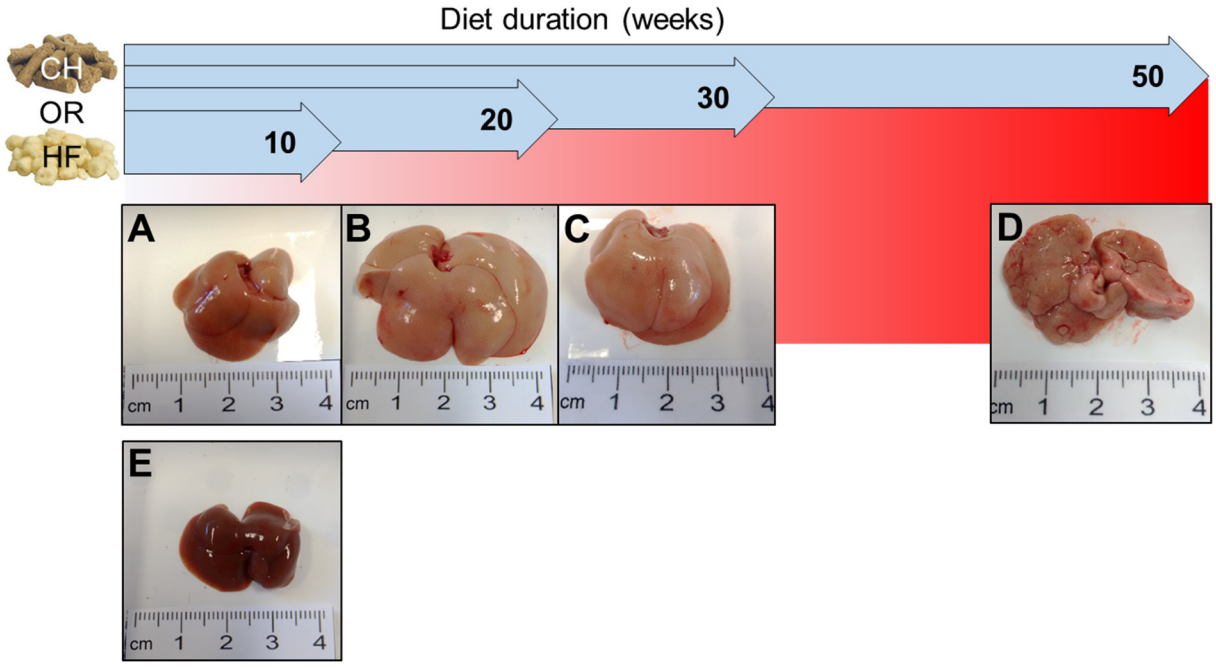

Figure 4.1. Time course for NAFLD progression study. Arrows represent diet durations for either standard chow (CH) or high-fat (HF) diet. Images show representative mouse livers following 10 weeks (**A**), 20 weeks (**B**), 30 weeks (**C**) and 50 weeks (**D**) of HF diet, the latter showing evidence of NASH fibrosis. A liver from CH diet (**E**) is shown for comparison. Images were taken immediately following excision (not perfused) at termination.

4.2. Animal Characteristics

Average body weight was increased by HFD at all timepoints ($p<0.001$) and continued to rise with the duration of feeding (Table 4.1). The same trend was observed for subcutaneous fat depots. Epididymal fat seemed to expand to capacity by 10 weeks, increasing by over 9-fold relative to the chow diet ($p=0.001$) and remaining stable in weight across the later timepoints ($p>0.05$ versus 10 weeks HFD), although intragroup variation was substantial. HFD did not significantly alter liver weight until 20 weeks ($p<0.001$), however, there was very little change in weight between 20 and 30 weeks of HFD (4% decrease) in contrast to other intervals. Finally, tissue weights remained stable over time in groups receiving standard chow diet, while body weight increased in a manner consistent with the normal growth of rodents: 22% increase from 10 to 50 weeks, versus 46% increase within the HFD cohort.

4.2.1. Insulin and insulin tolerance

In HFD animals, increased blood glucose was seen only after 10 weeks ($p<0.001$) of the diet, whereas there was no statistical significance thereafter (Table 4.1). Interestingly, from 30 weeks, this value dropped in HFD animals compared to the same diet at 10 weeks ($p<0.001$). These trends, in turn, affected the glucose curve after a single dose of insulin; the area under the curve was higher with HFD compared to standard chow diet at all timepoints – implying a tendency towards insulin resistance – however, these differences were only significant at 10 weeks ($p=0.011$) and 20 weeks ($p=0.037$) with the gap closing thereafter. Plasma insulin levels showed a different profile, more comparable to the findings in Chapter 3. Animals on HFD had consistently elevated insulin ($p<0.001$ at all timepoints), which was significantly increased by 50 weeks compared to 10 weeks HFD ($p=0.012$), despite the high intra-group variations (Table 4.1). By comparison, insulin levels remained low in chow-fed animals and were unaffected by aging.

4.2.2. Plasma biochemistry

Plasma TAG levels were also similar to previous results in Chapter 3, where HFD tended to decrease TAG (between 33% and 53%), although these did not generally reach statistical significance, with the exception of a transient decrease at 20 weeks ($p=0.002$). Liver disease severity was reflected in the plasma transaminase levels (Table 4.1), where both ALT and AST were elevated by HFD ($p<0.001$) from 20 weeks onwards and continued to increase before plateauing at 50 weeks. Consequently, the values at these later timepoints were higher than at 10 weeks ($p<0.001$), where HFD had comparable values to standard chow (ALT: 40% increase, AST: 7.5% decrease; both $p>0.05$). Furthermore, the ALT/AST ratio was increased around 2-fold by 20 weeks ($p<0.001$) and up to 3-fold from 30 weeks onwards ($p<0.001$) in HFD animals compared to their chow counterparts, suggesting a proportionally greater increase of plasma ALT (representing liver-specific injury). When compared to 10 weeks of HFD, the ALT/AST ratio was 2-fold greater for HFD animals at all other timepoints (each $p<0.001$). No changes were observed with age in animals receiving standard chow.

Table 4.1. Animal characteristics for NAFLD progression study.

	Chow				*HFD*			
	10 weeks	*20 weeks*	*30 weeks*	*50 weeks*	*10 weeks*	*20 weeks*	*30 weeks*	*50 weeks*
Weights (g):								
body	28.8±1.93	31.7±1.39	33.3±2.12 #	35.1±2.95 #	39.0±3.56 *	48.0±4.31 *#	51.9±4.19 *#	57.3±5.24 *#
liver	1.23±0.18	1.51±0.10	1.45±0.15	1.60±0.22	1.83±0.34	3.55±0.99 *#	3.84±0.85 *#	5.07±1.24 *#
epididymal fat	0.32±0.08	0.31±0.07	0.56±0.27	0.80±0.43	2.34±0.58 *	1.93±0.28 *	2.08±0.39 *	2.13±0.42 *
subcutaneous fat	0.20±0.07	0.25±0.07	0.33±0.09	0.34±0.12	1.06±0.27 *	1.70±0.40 *#	2.28±0.36 *#	2.63±0.35 *#
Plasma chemistry:								
ALT (U/L)	25.0±6.71	33.0±7.10	24.5±4.58	23.5±3.53	35.1±12.4	189±103 *#	230±95.6 *#	254±97.8 *#
AST (U/L)	73.6±18.2	65.3±5.50	97.4±48.2	87.2±20.7	68.1±12.5	190±99.4 *#	260±116 *#	278±93.6 *#
ALT/AST ratio	0.44±0.14	0.46±0.12	0.27±0.09	0.30±0.08	0.53±0.24	1.00±0.28 *#	0.91±0.3 *#	0.90±0.19 *#
TAG (mg/dL)	51.7±18.2	75.6±27.7	67.1±30.3	53.3±32.4	40.7±19.3	44.3±16.9 *	39.6±12.0	22.5±2.18
insulin (pg/mL)	212±68.4	159±24.3	170±46.3	217±116	567±255 *	610±228 *	736±460 *	1118±552 *#
Insulin tolerance:								
fasting glucose (mM)	7.22±0.80	8.22±1.26	6.78±1.12	7.73±1.35	9.23±1.61 *	8.15±0.90	7.44±0.94 #	7.28±1.09 #
ITT (AUC)	263±34.9	314±97.2	328±38.8 #	314±51.1	344±54.5 *	383±85.1 *	365±45.9	323±51.5

Data are mean ± SD for n=11-12 animals per group, excluding outliers determined by the ROUT method (Q=5%). Significant difference from age-matched chow (*) or 10 weeks of HFD (#) accepted at $p<0.05$ as determined by 2-way ANOVA with Bonferroni's (diet) or Dunnett's (timepoint) post hoc test for multiple comparisons. Abbreviations: ALT, alanine transaminase; AST; aspartate transaminase; TAG, triacylglycerol; AUC, area under the curve in arbitrary units.

4.2.3. Hepatic steatosis

Consistent with the findings in Chapter 3, liver TAG was increased by HFD independently of diet duration ($p<0.001$ all timepoints), with a peak at 20 weeks ($p<0.001$ versus 10 weeks HFD), after which time it tended to decline (Figure 4.2A). At 50 weeks of HFD, the hepatic TAG level was significantly decreased relative to 10 weeks on the same diet ($p=0.001$). Mice on standard chow had consistently lower hepatic TAG than their HFD counterparts, which was unaffected by aging. In contrast, ORO staining of total neutral lipids – generally found in the lipid droplets – tended to decline with aging, independently of diet (Figure 4.2B). This decrease became significant after 50 weeks of diet within the chow cohort ($p=0.010$ versus 10 weeks). Irrespective of the variability within HFD groups, lipid content was significantly higher than the normal chow fed mice at the same timepoints ($p=0.008$ at 10 weeks, $p<0.001$ for longer duration), except at 20 weeks where there was no difference (cf. peak in TAG level for same group).

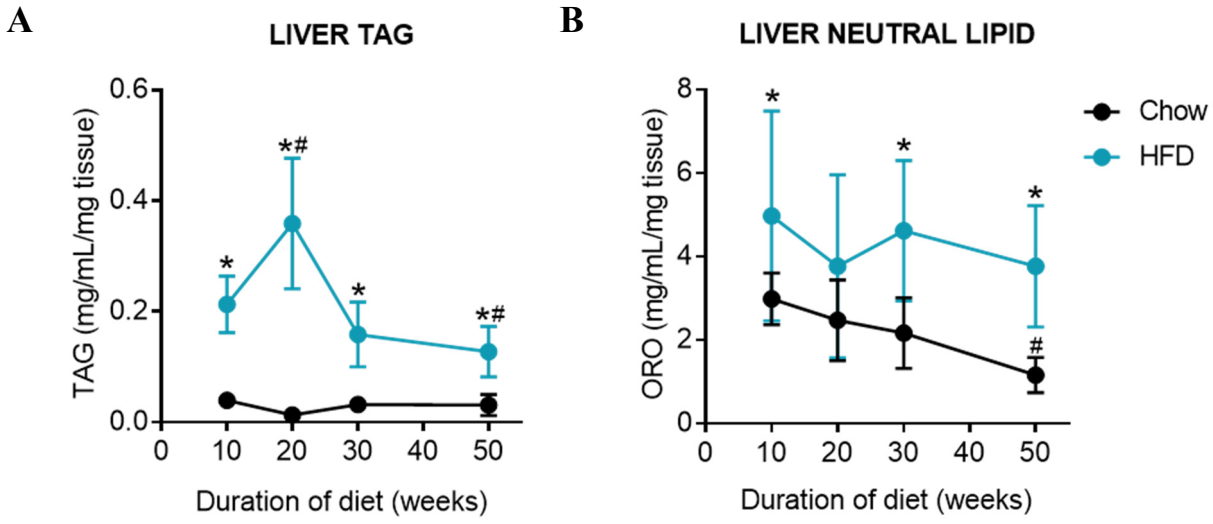

Figure 4.2. Liver lipid quantification. Liver triacylglycerol (TAG) (**A**) and total neutral lipids (**B**) per unit tissue mass were both increased with HFD. Data are mean ± SD for n=11-12 animals per group, excluding outliers determined by the ROUT method (Q=5%). Significant difference from chow (*) or 10 weeks of diet ($^{\#}$) accepted at $p<0.05$ as determined by 2-way ANOVA with Bonferroni's (diet pairs) or Dunnett's (timepoint) post hoc test for multiple comparisons. Abbreviations: HFD, high-fat diet; ORO, Oil Red O.

4.3. NAFLD Phenotype

4.3.1. Liver histology

4.3.1.1. General morphology

Using standard H&E staining, the characteristic evolution of NAFLD could be observed. At 10 weeks of HFD, the majority of livers (4/6 samples) had developed microvesicular steatosis predominantly in the centrilobular regions (Figure 4.3B). By 20 weeks, macrovesicular steatosis had also become present (Figure 4.3D). Animals receiving HFD for 30 weeks had ubiquitous steatotic bands; these were generally defined by a microvesicular pattern, with macrovesicular steatosis becoming more abundant in the adjacent periportal regions (Figure 4.3F). Finally, after 50 weeks of high-fat feeding, there was a loss of normal liver architecture with a macrovesicular pattern of lipid accumulation throughout (Figure 4.3H). Inflammatory foci had also become obvious, and pale nuclear staining in the perisinusoidal region suggested the presence of hepatic stellate cells. Interesting to note was the fact that "slow progressors" – that is, animals with only sparse or diffuse microvesicular steatosis up to 20 weeks – showed greater evidence of leukocyte aggregates throughout the liver sections (Figure 4.3I-J). Livers of mice on standard chow appeared normal at all timepoints.

4.3.1.2. Liver fibrosis

To delineate the transition between NAFL and advanced NASH, collagen fibres were stained red using PSR. As expected, 10 weeks of HFD was insufficient to progress to NASH, with collagen staining limited to the basement membrane around vessels (Figure 4.4A). Quite surprisingly, pericellular collagen staining was observed in approximately half of the livers from HFD mice by 20 weeks (Figure 4.4B) with a similar proportion at 30 weeks (Figure 4.4C). Of interest, the collagen bands seen at 20 weeks were often more pronounced when compared to 30 weeks of HFD. By 50 weeks, all livers in high-fat fed animals had diffuse but substantial collagen staining (Figure 4.4D), with bridging fibrosis evident in half the samples. No fibrosis was present in livers of standard chow animals (data not shown).

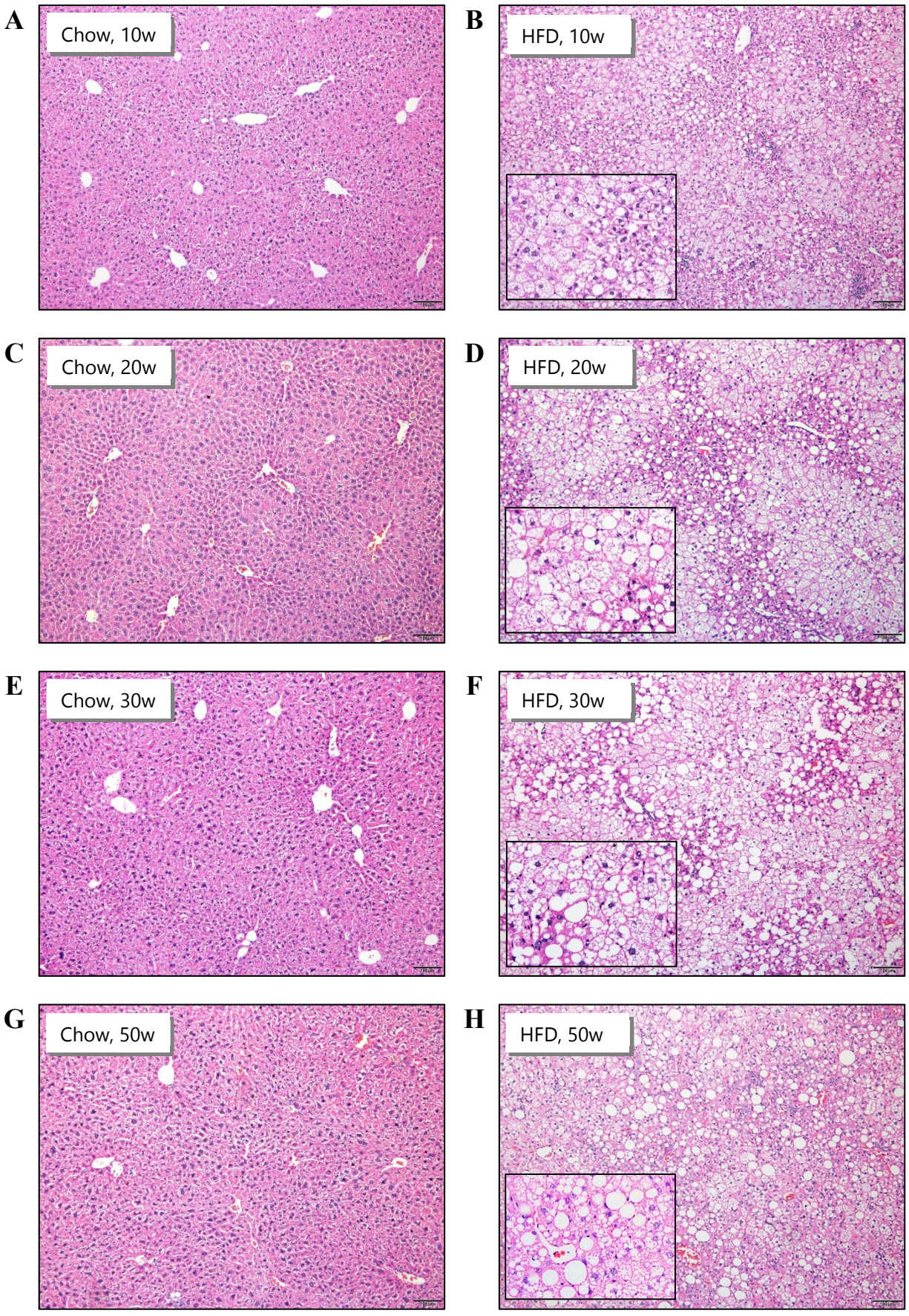
A
Chow, 10w
B
HFD, 10w
C
Chow, 20w
D
HFD, 20w
E
Chow, 30w
F
HFD, 30w
G
Chow, 50w
H
HFD, 50w

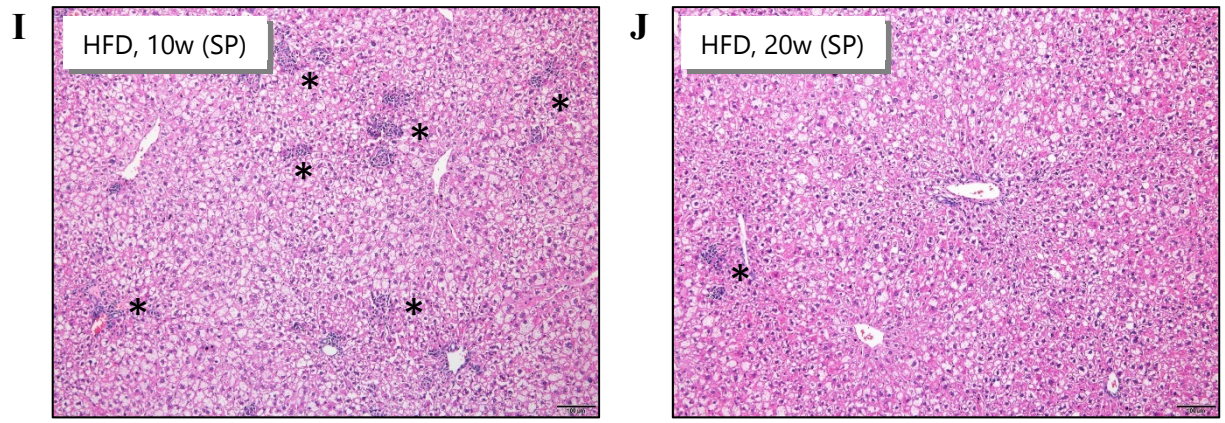

Figure 4.3. Liver morphology by H&E staining. Left panels (excluding I and J) show livers from mice on standard chow diet, and right panels are representative livers from mice fed HFD showing NAFLD progression, with a predominantly microvesicular to macrovesicular transition over time. Animals with delayed steatosis development (slow progressors, SP) at 10 weeks (**I**) and 20 weeks (**J**) HFD have more leukocyte aggregates, denoted by (*) on each. Representative images at 100× magnification (scale bar = 100μm), inset 200× magnification.

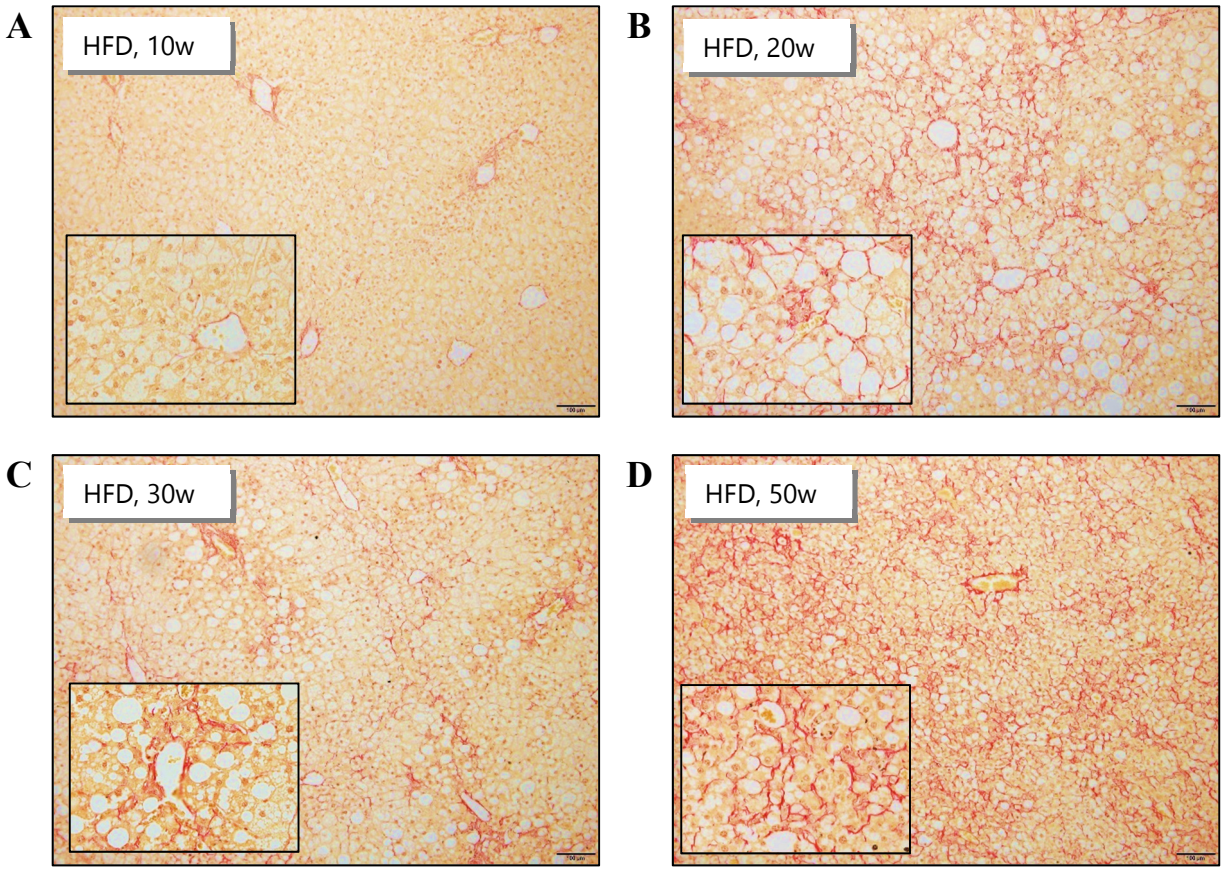

Figure 4.4. Liver fibrosis staining by Picro-Sirius red (PSR). No collagen accumulation is seen after 10 weeks of HFD (**A**), with pericellular collagen staining becoming evident from 20 weeks (**B**). No increase in staining from 20 to 30 weeks (**C**), with abundant PSR-positive staining at 50 weeks (**D**) showing evidence of bridging fibrosis. Representative images with PSR staining at 100× magnification (scale bar = 100μm), inset 200× magnification.

4.3.2. Liver gene expression

4.3.2.1. Inflammation

In accordance with the classical model of liver disease progression, inflammatory changes are expected to precede and drive fibrogenesis, as observed in Chapter 3. In the current study, gene expression of TNF was significantly higher in HFD animals at all timepoints (minimum 3-fold, $p=0.002$) and did not fluctuate from the initial increase seen after 10 weeks (Figure 4.5A). Gene expression of molecules involved in monocyte recruitment (MCP1; Figure 4.5B) and macrophage presence (F4/80; Figure 4.5C) only became substantially elevated in HFD mice at 20 weeks (MCP1: 9-fold, $p<0.001$; F4/80: 3-fold, $p=0.006$), reaching a peak at 30 weeks before declining towards (or surpassing) the baseline by 50 weeks (MCP1: $p>0.05$, F4/80: $p=0.001$ versus 10 weeks HFD). No notable changes were observed in the chow-fed animals at any of the studied timepoints, which was also true for ECM remodelling markers.

4.3.2.2. ECM remodelling

The transcriptomic response to fibrogenesis was much more dynamic. The gene expression of α-SMA, a surrogate marker of stellate cell activity, did not deviate more than 2-fold from the baseline across HFD groups, and tended to decline with age irrespective of diet (Figure 4.5D). However, a statistically significant elevation at 20 weeks ($p=0.013$ versus 10 weeks) also coincided with a peak in the expression of collagen I ($p<0.001$; Figure 4.5E), possibly linking stellate cell activity with the production of fibrillar collagen. The mRNA expression pattern of collagen I – with another sharp increase at 50 weeks ($p=0.013$) – also seemed to correlate with the increased collagen staining seen by liver histology (refer to Figure 4.4). In contrast, while collagen IV became initially elevated at 20 weeks in HFD ($p<0.001$ versus chow), its gene expression plateaued after this time (Figure 4.5F). Irrespective of these varied trends, transcription levels for both collagens were significantly higher with HFD compared to chow from 20 weeks onwards (collagen I: >6-fold, collagen IV: >2-fold; both $p<0.05$). Other regulators of collagen turnover, TGFβ (Figure 4.5G) and TIMP1 (Figure 4.5H), were both increased up to 30 weeks in HFD mice ($p<0.01$ versus 10 weeks), before stabilising (TIMP1) or returning to baseline (TGFβ; $p>0.05$ versus 10 weeks HFD) at 50 weeks.

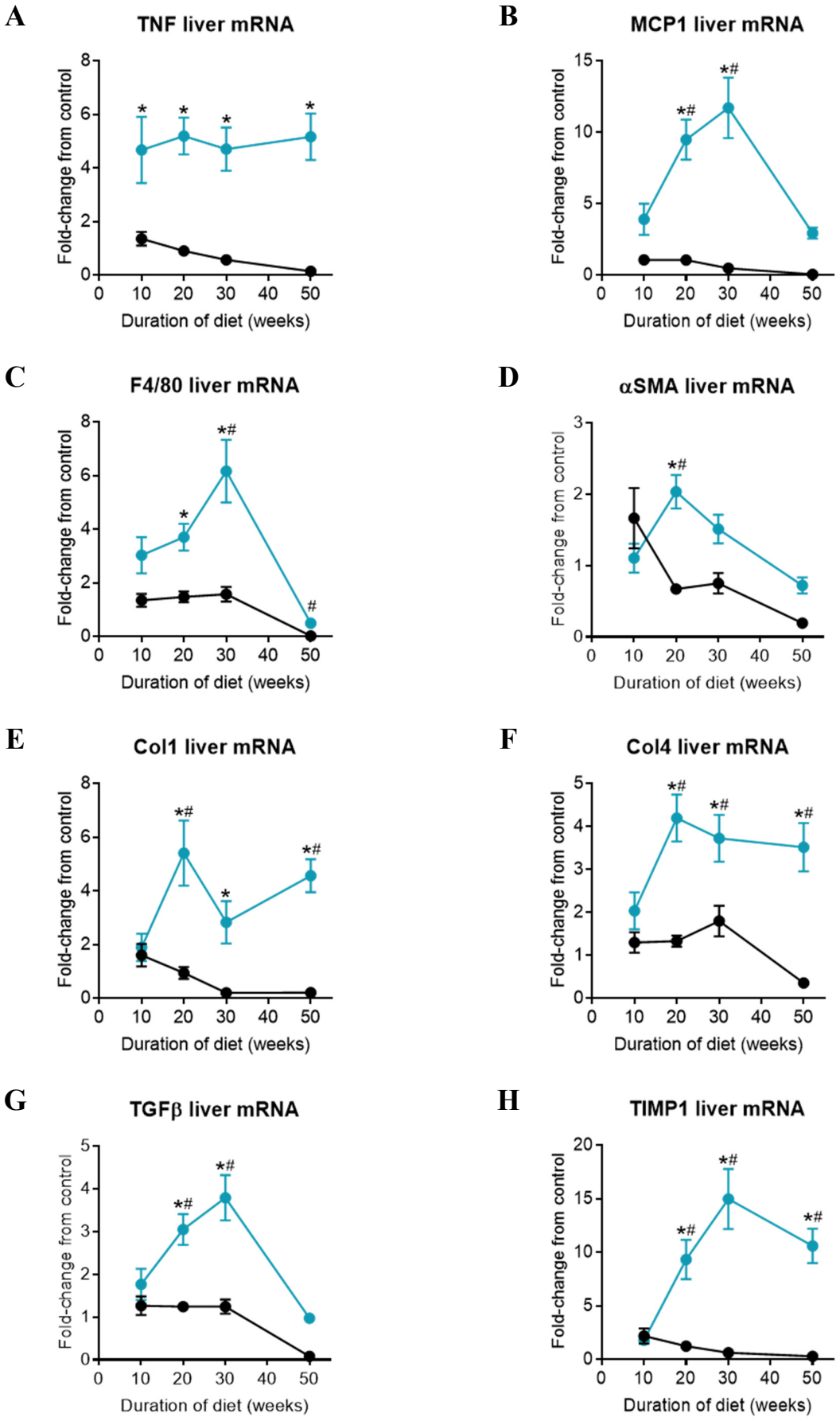
A
TNF liver mRNA
Fold-change from control
Duration of diet (weeks)
B
MCP1 liver mRNA
Fold-change from control
Duration of diet (weeks)
C
F4/80 liver mRNA
Fold-change from control
Duration of diet (weeks)
D
αSMA liver mRNA
Fold-change from control
Duration of diet (weeks)
E
Col1 liver mRNA
Fold-change from control
Duration of diet (weeks)
F
Col4 liver mRNA
Fold-change from control
Duration of diet (weeks)
G
TGFβ liver mRNA
Fold-change from control
Duration of diet (weeks)
H
TIMP1 liver mRNA
Fold-change from control
Duration of diet (weeks)

Figure 4.5. Changes in liver gene expression with NAFLD progression. Graphs represent transcripts of pro-inflammatory genes (**A-C**) and genes involved in ECM remodelling or fibrosis (**D-H**) for chow (black) and HFD (blue) animals, calculated as fold-change versus the control (10 week chow). Data are mean ± SEM for n=10-12 animals per group, excluding outliers determined by the ROUT method (Q=5%). Significant difference from chow (*) or 10 week HFD ($^{\#}$) accepted at $p<0.05$ as determined by 2-way ANOVA with Bonferroni's test (diet pairs) or Dunnett's test (timepoint) for multiple comparisons. Abbreviations: TNF, tumour necrosis factor; MCP1, monocyte chemotactic protein 1; αSMA, alpha smooth muscle actin; Col, collagen; TGFβ, transforming growth factor beta; TIMP1, tissue inhibitor of metalloproteinase 1.

With the exception of TGFβ, the mRNA expression of ECM remodelling genes seemed to reflect the findings in Chapter 3. Consistent with this, HFD at 10 weeks did not significantly increase any gene of interest above the level of the chow diet. This was not the case for collagen IV when using one-sample t testing for HFD fold-change with respect to the corresponding age-matched chow group (Figure 4.6).

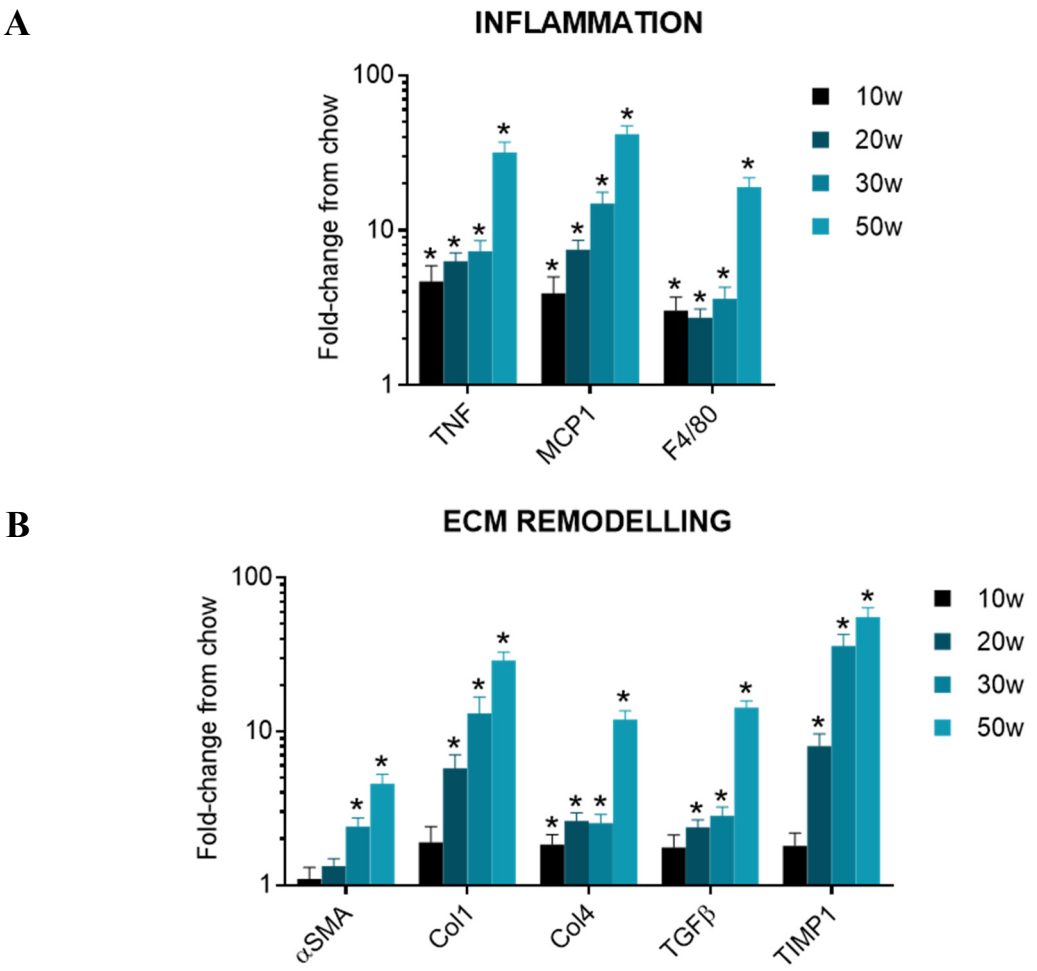

Figure 4.6. Age-adjusted changes in liver gene expression for HFD groups. Data are fold-change from the chow group at the corresponding timepoint, represented as mean ± SEM for n=10-12 animals, excluding outliers. Significant difference from chow (*) accepted at $p<0.05$ as determined by a one-sample t test against a hypothetical value of 1 (correcting for the respective chow group as the baseline). Changes are relative to timepoint, thus statistical differences across timepoints cannot be inferred. Abbreviations: see Figure 4.4.

4.4. Extracellular Vesicle Phenotype

Having established the physical profile of obese animals and the molecular changes in their liver at varying stages of NAFLD progression, we next sought to determine whether the EV abundance in the plasma or derived from the liver may reflect these subclinical changes and hence indicate the severity of disease. To further elaborate on the potential role of liver EVs in paracrine signalling, we assessed their protein cargo for changes between simple steatosis and NASH, which may be indicative of the phenotype they impart to recipient cells.

4.4.1. EV enumeration

Interestingly, trends in the total EV number – from both plasma and liver – differed markedly from the findings in Chapter 3. (This may be explained by an adjustment in the protocol, whereby in the present Chapter, samples were stored frozen prior to the ultracentrifugation step, which was performed after thawing and immediately prior to analysis. EVs in Chapter 3 were stored following ultracentrifugation and thawed prior to analysis.)

4.4.1.1. Patterns in EV abundance

Consistent with our previous findings, the size distribution of both plasma and liver-derived EVs showed a lognormal trend (Figure 4.7A). Plasma EVs again had a smaller diameter on average when compared to the liver vesicles (83nm versus 106nm, respectively), while the variation or standard error across time (10 weeks versus 50 weeks) and between diets was small, which implies that EVs within a sampling population are likely to be biophysically similar. In terms of sample abundance, plasma EVs from HFD mice were consistently – although not significantly – lower than those from their chow counterparts (Figure 4.7B). The exception was at 20 weeks, where a peak in the HFD EVs marginally surpassed the chow values, before normalising for the remaining timepoints. This peak was also significantly elevated ($p<0.001$) compared to the 10 weeks HFD group. Values for the chow groups, on the other hand, remained consistent over time.

Unlike the trends observed in Chapter 3, liver-derived EVs in the longitudinal study failed to show the same decline with aging or diet. In fact, the abundance increased with time across the HFD groups, whereby the values at 50 weeks were significantly higher ($p=0.002$) than those at 10 weeks (Figure 4.7C). A similar pattern was also seen for the chow groups, with the exception of a sharp elevation at 10 weeks. There were otherwise no differences reported between the two diets. When the EV numbers were adjusted for whole liver weight, on the other hand, the HFD groups became elevated (though not significantly) over their chow counterparts at 20 and 30 weeks of diet (Figure 4.7D). Consequently, the EV trend across time in the HFD cohort was more linear – both 30 and 50 week groups were significantly greater than 10 weeks ($p=0.038$ and $p<0.001$, respectively) – although the discrepancy between the two diets at 10 weeks was still evident.

Among the HFD cohort, there was a statistically significant inverse correlation between plasma and liver EVs ($r=-0.382$, $p=0.012$), however the 95% CI was high (Figure 4.7E). In an attempt to compare the findings of the present study to Chapter 3 (Figure 3.9E), the two EV populations were also correlated for the 10 and 50 weeks timepoints for both diets (Figure 4.7F). However, this data failed to show any relationships ($r=0.088$, $p=0.577$), although this cannot be attributed to treatment clustering as intragroup variability was high.

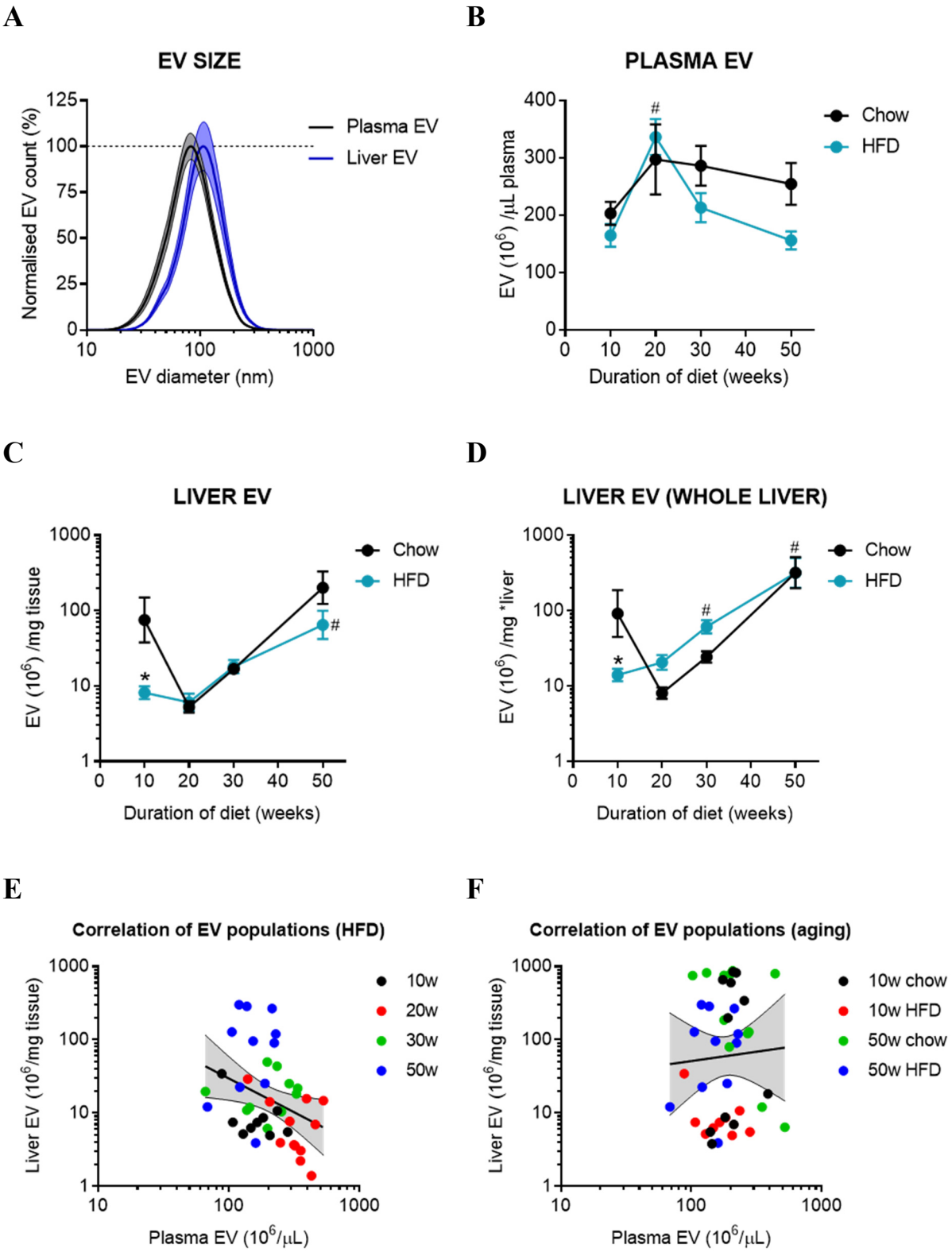
A
EV SIZE
Normalised EV count (%)
125
100
75
50
25
0
10
100
1000
EV diameter (nm)
Plasma EV
Liver EV
B
PLASMA EV
EV (10^6) /µL plasma
400
300
200
100
0
#
0
10
20
30
40
50
Duration of diet (weeks)
Chow
HFD
C
LIVER EV
EV (10^6) /mg tissue
1000
100
10
1
*
#
Duration of diet (weeks)
Chow
HFD
D
LIVER EV (WHOLE LIVER)
EV (10^6) /mg *liver
1000
100
10
1
*
#
#
Duration of diet (weeks)
Chow
HFD
E
Correlation of EV populations (HFD)
Liver EV (10^6/mg tissue)
1000
100
10
1
10
100
1000
Plasma EV (10^6/µL)
10w
20w
30w
50w
F
Correlation of EV populations (aging)
Liver EV (10^6/mg tissue)
1000
100
10
1
10
100
1000
Plasma EV (10^6/µL)
10w chow
10w HFD
50w chow
50w HFD

Figure 4.7. Plasma and liver EV enumeration and correlations. EV size distributions (**A**) for plasma EVs (peak at 83nm) or liver EVs (peak at 106nm) were similarly lognormal and monophasic. Abundance per diameter is normalised and shows mean ± SEM for both curves; data for each curve includes EV samples from HFD and standard chow at the 10 and 50 week timepoints (n=47). Total plasma EVs (**B**), liver-derived EVs not adjusted (**C**) and adjusted (**D**) for total liver weight. Data are mean ± SEM for n=11-12 animals per group, excluding outliers. Significant difference from chow (*) or 10 weeks of HFD ($^{\#}$) accepted at $p<0.05$ as determined by 2-way ANOVA with Bonferroni's test (diet pairs) or Dunnett's test (timepoint) for multiple comparisons. Correlation of the two EV populations (plasma versus liver) showed a significant inverse trend ($r=-0.382$, $p=0.012$) by the Spearman test when HFD samples from all timepoints (n=46) were considered (**E**). There was no significant trend ($r=0.088$, $p=0.577$) when both diets from the extreme timepoints (n=47) were considered (**F**).

4.4.1.2. EV correlations with other parameters

When the EVs from HFD animals were correlated against physical and metabolic parameters, the strong relationship to hepatic lipids observed in Chapter 3 was no longer present (Table 4.2). However, other trends became apparent for plasma and liver EVs, respectively. In terms of the former, there was a significant positive correlation with plasma TAG (Figure 4.8A; values in Table 4.2). Irrespective of a coincident trend with α-SMA gene expression, this correlation did not reach significance (r=0.262, p=0.098). In the context of liver EVs, there was a significant negative correlation when compared against liver TAG (Figure 4.8B; values in Table 4.2). There was also a weaker yet significant decline when compared to fasting glucose levels, and a positive correlation with plasma AST, body weight, and subcutaneous fat weight (Table 4.2), although the latter often suffers from sampling bias.

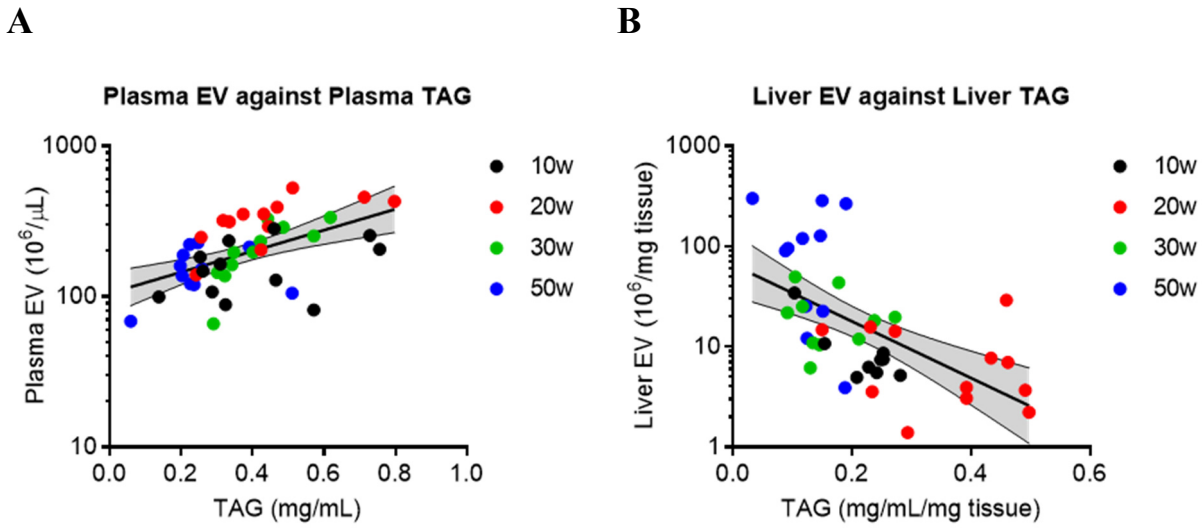

Figure 4.8. Extracellular vesicle correlations with TAG. Linear regression shows a positive correlation (r=0.548, p<0.001) between plasma EVs and circulating TAG (**A**) and an inverse correlation (r=-0.658, p<0.001) between liver-derived EVs and liver TAG (**B**). Data represent HFD groups (10-50 weeks, w) taken collectively with n=46 per correlation, with significant correlations determined by the Spearman test. Abbreviations: TAG, triacylglycerol.

Table 4.2. Extracellular vesicle correlations with physical and metabolic parameters.

Parameter	*Plasma EVs*		*Liver EVs*	
	r value	*p value*	*r value*	*p value*
Physical parameters:				
Body weight (g)	-0.096	0.526	**0.339**	**0.028**
Fat, epididymal (g)	-0.172	0.254	0.016	0.919
Fat, subcutaneous (g)	-0.142	0.346	**0.501**	**0.001**
Liver weight (g)	-0.005	0.972	0.270	0.083
Liver TAG (/mg tissue)	0.263	0.078	**-0.658**	**0.000**
Liver neutral lipids (/mg tissue)	-0.088	0.565	-0.199	0.212
Metabolic parameters:				
ALT (U/L)	-0.002	0.990	0.246	0.121
AST (U/L)	-0.084	0.585	**0.383**	**0.013**
Plasma TAG (mg/dL)	**0.548**	**0.000**	-0.274	0.079
Plasma insulin (pg/mL)	-0.077	0.609	-0.264	0.092
Fasting glucose (mM)	0.166	0.277	**-0.432**	**0.005**
Insulin tolerance, AUC	0.195	0.199	-0.158	0.324

Data represent HFD groups (10-50 weeks) with n=46 per correlation, excluding previously determined outliers. Columns show Spearman regression (r value) with significance (p value), where significant correlations ($p<0.05$) are in bold. Both liver TAG and neutral lipids are represented as mg/mL/mg liver tissue. Abbreviations: TAG, triacylglycerol; ALT, alanine transaminase; AST, aspartate transaminase; AUC, area under the curve in arbitrary units.

4.4.2. EV protein content

To characterise the protein cargo of liver-derived EVs, ultracentrifuged pellets were submitted to the Sydney Mass Spectrometry facility, University of Sydney for 1D liquid chromatography mass spectrometry (LCMS). Three samples each across four groups were considered (10-week HFD and chow, 50-week HFD and chow; total n=12) to highlight differences between early steatosis and NASH, as well as changes with aging. The proteomes were first imported and analysed for intergroup differences using Scaffold 4 software, while lists of interest in UniProt format were entered into an online gene ontology server for functional analysis.

4.4.2.1. Preliminary analysis of unique proteins

When considering all proteins that were present in liver-derived EVs across treatment groups, an overwhelming majority were shared between groups upon comparison. For instance, only 3.8% of proteins on average were uniquely expressed in any given group (intragroup range 1.1-8.5%) with higher values reported in the younger animals (Figure 4.9A). In this dataset, 744 of the total 4,592 proteins (16.2%) were common to all samples. These shared proteins were subsequently compared against reference datasets of mouse proteins known to be expressed in EVs (see section 4.4.2.2).

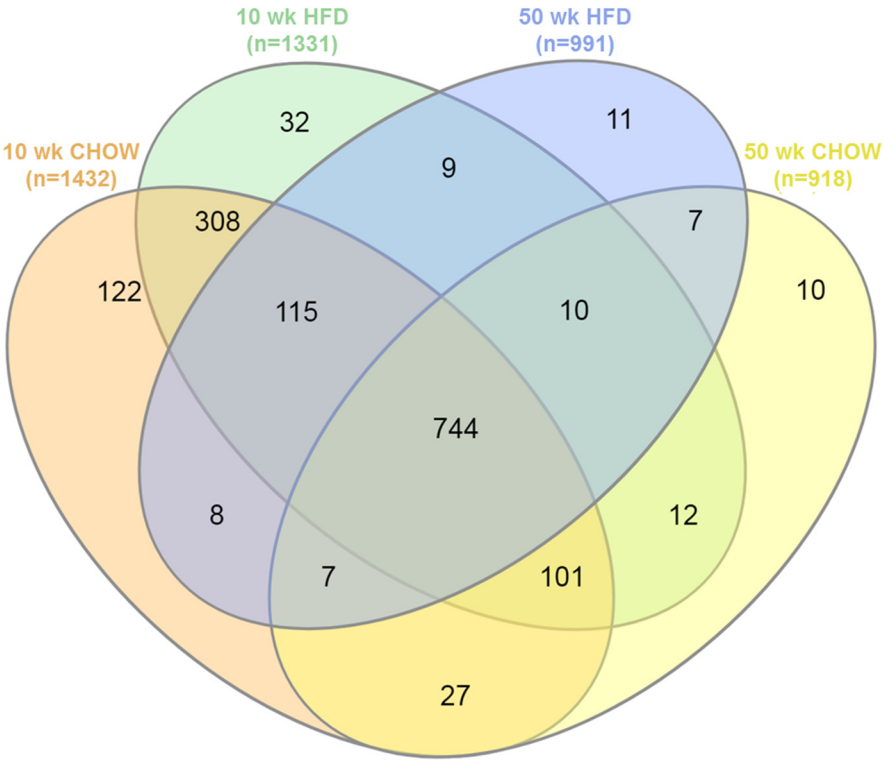

Figure 4.9. Proteomic analysis of liver-derived extracellular vesicles. Absolute count of total proteins within treatment groups (n=3 each), retrieved from Scaffold 4 software, where overlap shows proteins common to two or more groups. The number of uniquely expressed proteins were: 122/1432 in 10 weeks chow and 10/918 in 50 weeks chow, with 27 proteins overlapping between these groups; 32/1331 in 10 weeks HFD and 11/991 in 50 weeks HFD, with 9 proteins overlapping. EV proteins that were shared amongst all treatments constituted the largest group, with 744 proteins. Values within the Venn diagram were derived from UniProt_ID lists entered into the online server InteractiVenn (Heberle et al., 2015). Numbers in brackets represent total proteins per group.

4.4.2.2. Comparison with reference datasets

The proteome of *Mus musculus* is well documented and can be accessed from various online gene ontology servers, like QuickGo (Binns et al., 2009). Most proteins can be attributed to a particular gene ontology identifier, including extracellular vesicles (GO:1903561), which is itself a parent term and also an element of multiple hierarchies (Figure 4.10A). The predominant daughter term is "extracellular exosome" (GO:0070062), which makes up some 91% of the 143 recognised EV proteins in this database, including CD63. (Note that the sample sources that define this reference set are not explicitly reported.) To determine whether our liver-derived EV samples overlap with this set, or alternatively, whether they provide unique contributions to EV proteins, the 744 shared proteins (Figure 4.9) were compared against the reference set (Figure 4.10B). Interestingly, a vast majority of shared EV proteins were unique to our study and excluded the typical exosomal markers. (This was consistent with our western blot findings in Chapter 3 (Figure 3.3) where the exosomal marker CD63 was more typical of plasma EVs and absent in liver EVs). Proteins of interest included FGGY (carbohydrate kinase), FABPL (liver-type fatty acid binding protein), and PLIN2 (perilipin 2), all of which are involved in hepatic lipid metabolism and were therefore examined further in Chapter 6.

A more comprehensive database of EV-associated proteins (as well as RNA subtypes and lipids) can be found on servers dedicated to EV research, including Exocarta (Keerthikumar et al., 2016) and Vesiclepedia (Kalra et al., 2012). These reference datasets provide a pooled sample size of 1012 proteins (26 studies) and 4845 proteins (77 studies) from *Mus musculus* tissues, respectively (correct as of August 2018). However, despite their majority concordance (89.7% from Exocarta represented in Vesiclepedia), only 196 of 744 shared proteins from our sample data (26.3%) were recognised in one or both reference datasets (Figure 4.10C and Table A1 in Appendix). In fact, there was no concordance between our samples and the Exocarta set, so only Vesiclepedia was used for further comparisons (see Appendix). To this end, 548 proteins identified in our liver EVs were unique to this study (Figure 4.10C and Table A2).

A

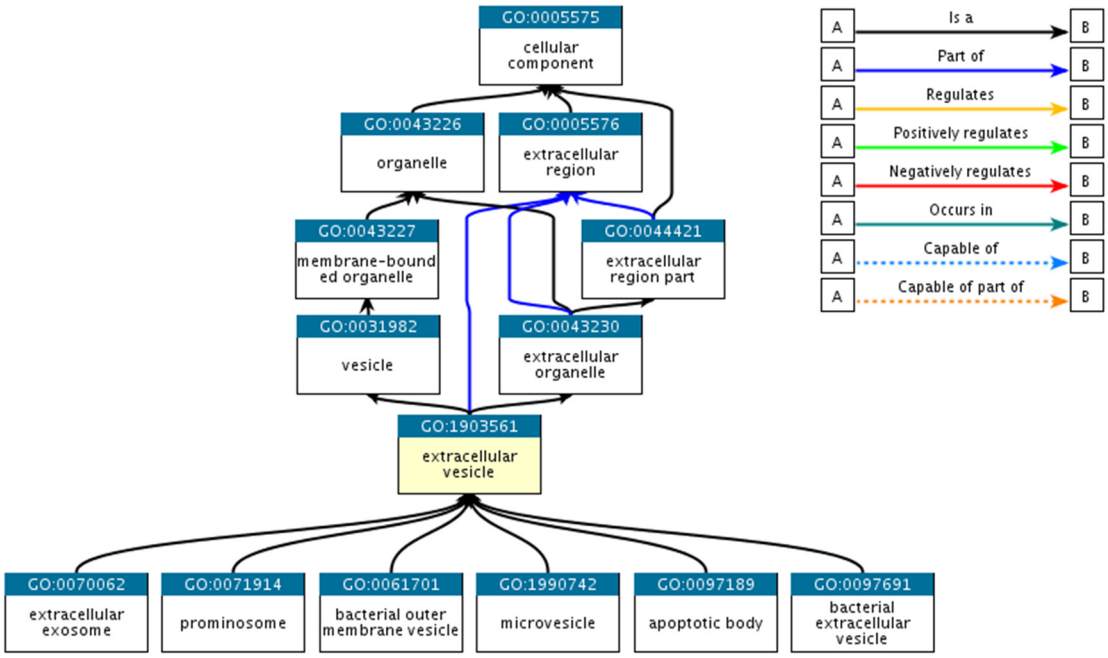
GO:0005575
cellular component
GO:0043226
organelle
GO:0005576
extracellular region
GO:0043227
membrane-bounded organelle
GO:0044421
extracellular region part
GO:0031982
vesicle
GO:0043230
extracellular organelle
GO:1903561
extracellular vesicle
GO:0070062
extracellular exosome
GO:0071914
prominosome
GO:0061701
bacterial outer membrane vesicle
GO:1990742
microvesicle
GO:0097189
apoptotic body
GO:0097691
bacterial extracellular vesicle
Is a
Part of
Regulates
Positively regulates
Negatively regulates
Occurs in
Capable of
Capable of part of

B

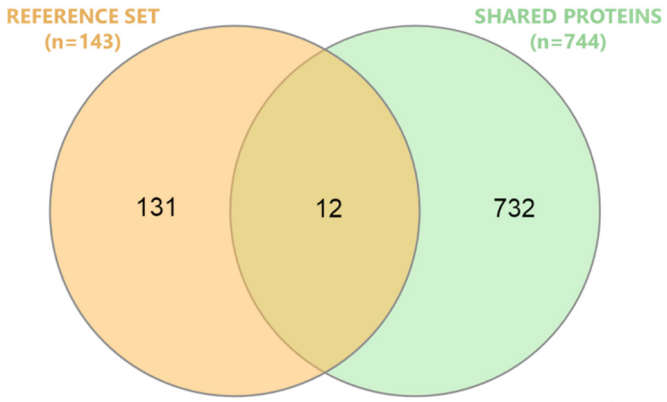
REFERENCE SET
(n=143)
SHARED PROTEINS
(n=744)
131
12
732

C

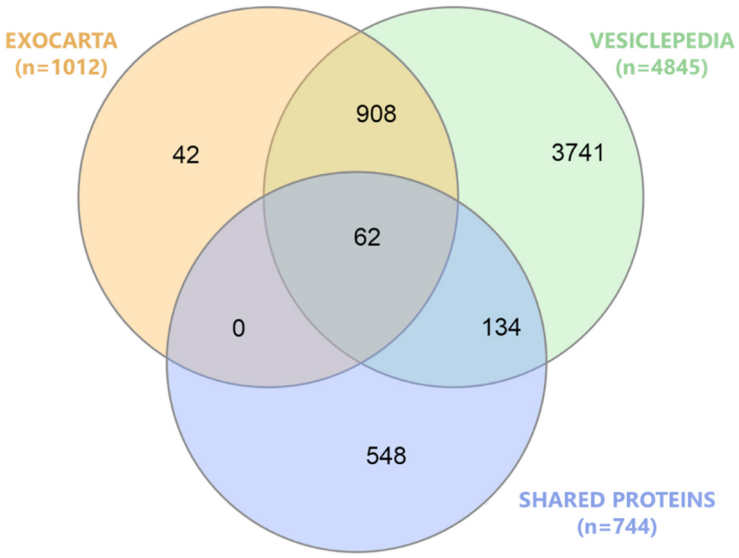
EXOCARTA
(n=1012)
VESICLEPEDIA
(n=4845)
908
42
3741
62
0
134
548
SHARED PROTEINS
(n=744)

Figure 4.10. Comparison of liver EV proteome with *Mus musculus* reference datasets. (**A**) Family tree of gene ontology (GO) terms related to extracellular vesicles (image retrieved from QuickGo (Binns et al., 2009)). Hierarchy of least specific (top) to most specific terms (bottom row); arrows show relationship where more specific terms feed into the more general terms, as defined by the legend on the right. (**B**) A comparison of reference proteins from QuickGo with the 744 shared liver EV proteins in our study. (**C**) These shared proteins were compared against a pool of EV proteins from the Exocarta (Keerthikumar et al., 2016) and Vesiclepedia (Kalra et al., 2012) large study databases. Values within the Venn diagram were derived from UniProt_ID lists entered into the online server InteractiVenn (Heberle et al., 2015). Numbers in brackets represent total proteins per group.

4.4.2.3. Enrichment analysis 1: qualitative approach

To perform enrichment analysis, our study dataset was compared against the total recognised *Mus musculus* proteome as a reference for fold-enrichment of molecular pathways. Briefly, protein symbols were imported into the online gene ontology software DAVID Bioinformatics (Huang da et al., 2009) whereupon enriched molecular pathways – that is, KEGG pathways (Kyoto Encyclopedia of Genes and Genomes) – were retrieved. Enrichment values were obtained for unique proteins that were shared amongst all EVs (n=744), using total proteins per treatment group, as per Figure 4.9A. For the comparison of treatment groups, we employed hierarchical clustering of enriched pathways using the online matrix visualisation tool Morpheus (https://software.broadinstitute.org/morpheus). Pathways for unrelated diseases of either a communicable or non-communicable nature were excluded.

When applying the KEGG analysis to the shared EV proteins in our study, 52 pathways were reflected in our data after filtering unrelated associations as per above (Figure 4.11). Of these, 16 (30.8%) were involved in protein metabolism – the largest combined representation – while at least 7 (13.5%) were known to be associated with NAFLD pathogenesis. These latter pathways included proteins involved in the synthesis (n=8), elongation (n=6) and metabolism (n=13) of FFAs, as well as their degradation (n=19) and beta oxidation by PPAR signalling (n=15) and peroxisomal activity (n=28). The glycolysis/gluconeogenesis pathway involved in energy homeostasis was also highly represented (n=28), and subsequently enriched by over 6-fold ($p<0.001$) when compared to the reference proteome. This was unsurprising given that the liver is the primary site of this biochemical process.

The enrichment of seemingly antagonistic pathways can be explained by the variations between treatment groups. Indeed, when the four treatments were compared for enriched pathways, the relative changes between groups were not consistent across many biologically related pathways (Figure 4.12). Trends between samples within treatment groups were not consistent either; in fact, hierarchical clustering showed that similarities in the sample proteomes were often independent of the treatment. Consequently, the fold-change between any two treatment groups (on average) was less than 2-fold and therefore unlikely to have large biological significance. Whether this is also reflected in functional studies will be investigated further in Chapter 6.

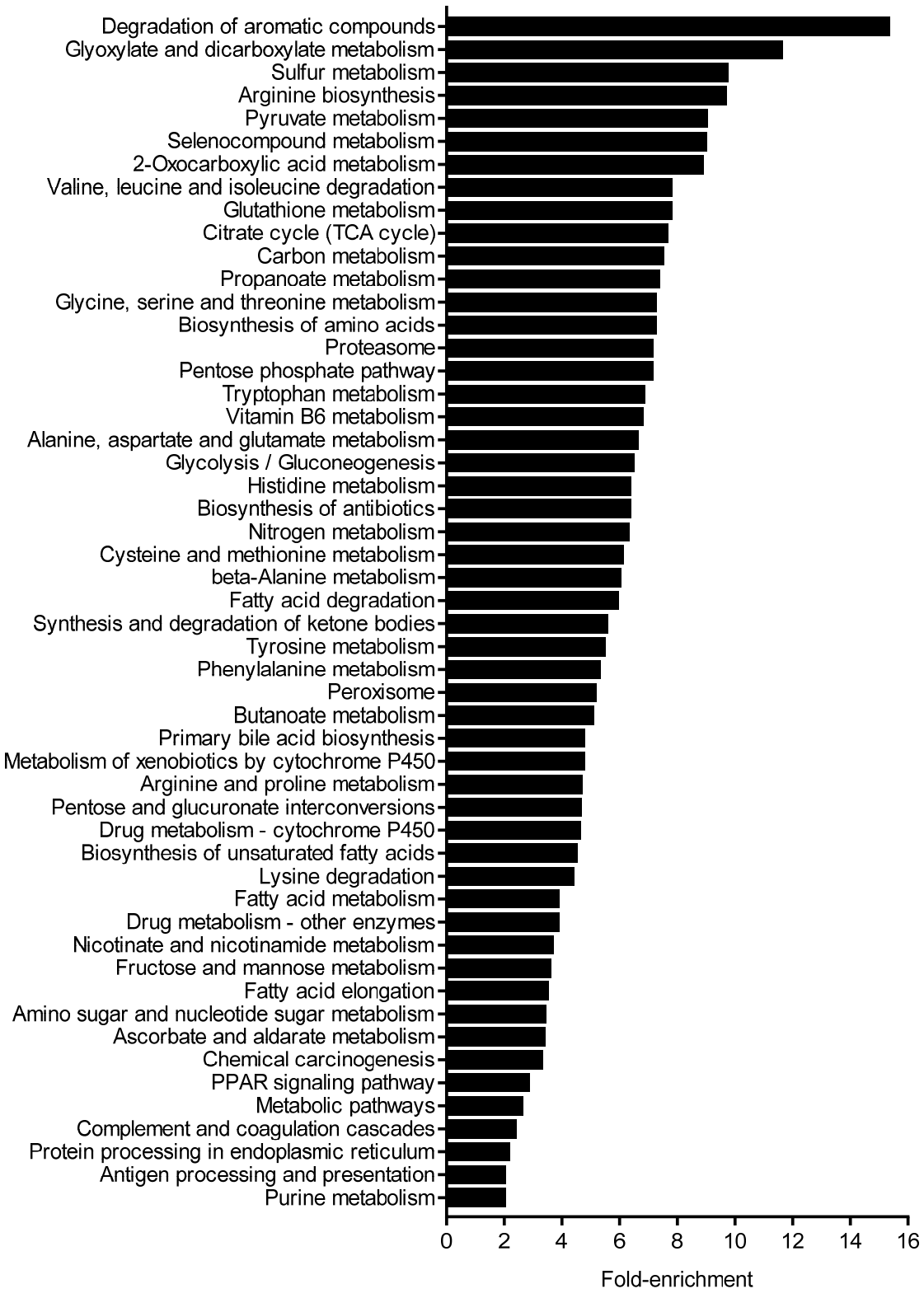

Figure 4.11. Enriched KEGG pathways for shared liver EVs. Data shows enriched pathways within shared unique proteins (n=744) relative to *Mus musculus* proteomic expression.

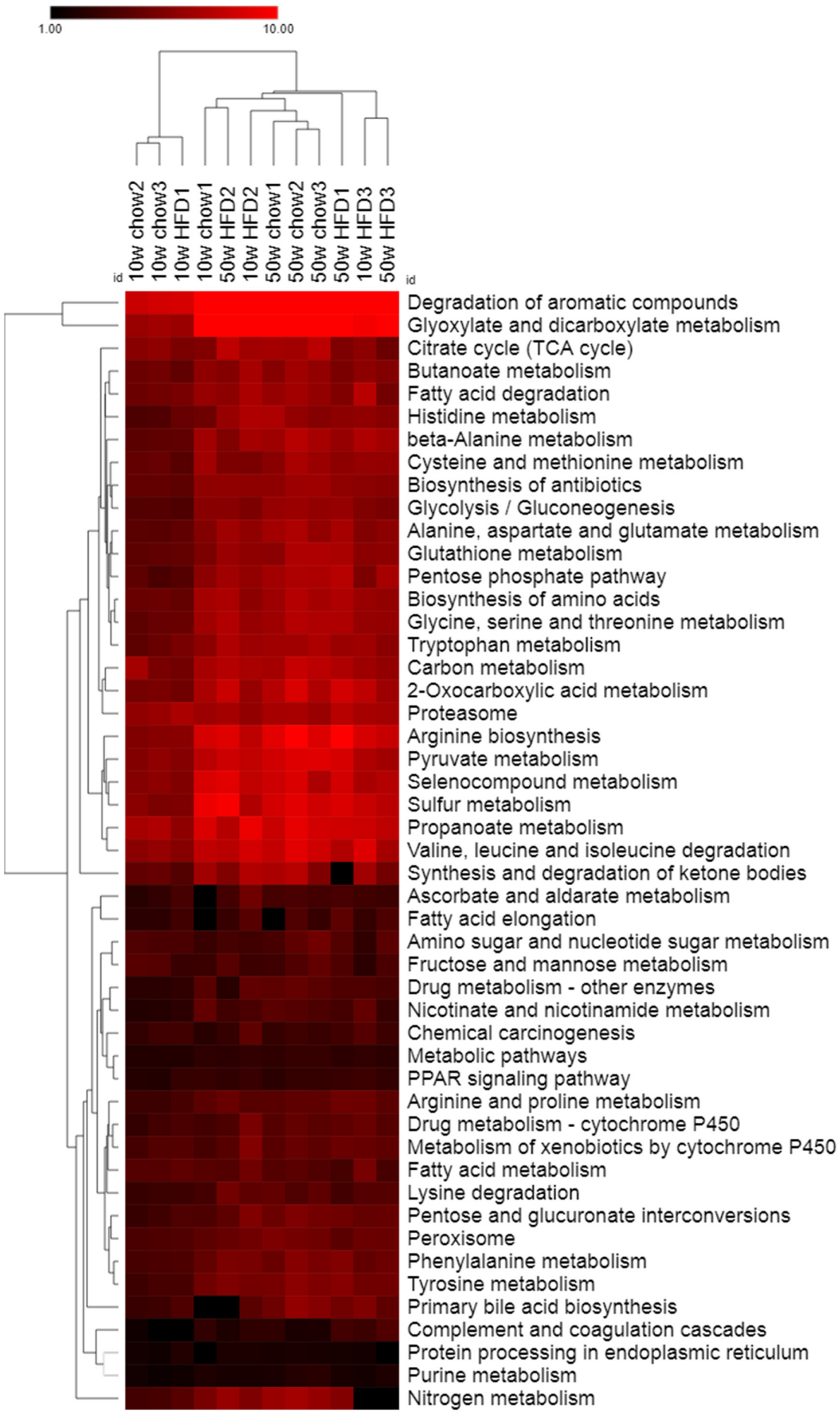
1.00
10.00
id
10w chow2
10w chow3
10w HFD1
10w chow1
50w HFD2
10w HFD2
50w chow1
50w chow2
50w chow3
50w HFD1
10w HFD3
50w HFD3
id
Degradation of aromatic compounds
Glyoxylate and dicarboxylate metabolism
Citrate cycle (TCA cycle)
Butanoate metabolism
Fatty acid degradation
Histidine metabolism
beta-Alanine metabolism
Cysteine and methionine metabolism
Biosynthesis of antibiotics
Glycolysis / Gluconeogenesis
Alanine, aspartate and glutamate metabolism
Glutathione metabolism
Pentose phosphate pathway
Biosynthesis of amino acids
Glycine, serine and threonine metabolism
Tryptophan metabolism
Carbon metabolism
2-Oxocarboxylic acid metabolism
Proteasome
Arginine biosynthesis
Pyruvate metabolism
Selenocompound metabolism
Sulfur metabolism
Propanoate metabolism
Valine, leucine and isoleucine degradation
Synthesis and degradation of ketone bodies
Ascorbate and aldarate metabolism
Fatty acid elongation
Amino sugar and nucleotide sugar metabolism
Fructose and mannose metabolism
Drug metabolism - other enzymes
Nicotinate and nicotinamide metabolism
Chemical carcinogenesis
Metabolic pathways
PPAR signaling pathway
Arginine and proline metabolism
Drug metabolism - cytochrome P450
Metabolism of xenobiotics by cytochrome P450
Fatty acid metabolism
Lysine degradation
Pentose and glucuronate interconversions
Peroxisome
Phenylalanine metabolism
Tyrosine metabolism
Primary bile acid biosynthesis
Complement and coagulation cascades
Protein processing in endoplasmic reticulum
Purine metabolism
Nitrogen metabolism

Figure 4.12. Enriched KEGG pathways across liver EV samples. Unique proteins per sample were entered into the DAVID gene ontology software (Huang da et al., 2009) to identify enriched pathways. The output data was consolidated for the n=12 samples and pruned to exclude pathways where more than three values were not reported. Finally, the dataset was entered into the Morpheus online tool (https://software.broadinstitute.org/morpheus) for hierarchical clustering of pathways, arranged by Euclidean distance and expressed as fold-enrichment (range 1 to 10-fold) in a heatmap format.

4.4.2.4. Enrichment analysis 2: quantitative approach

A limitation of the LCMS methodology used in this study is that output from the sample data is theoretically qualitative; that is, absolute changes in protein abundance are less reliable and ought to be expressed as relative changes. Using Scaffold 4 software for paired analyses with Fisher's Exact Test (FET), proteins that were significantly different between treatment groups were recorded and subsequently entered into the DAVID gene ontology software (Huang da et al., 2009) to identify enriched pathways. Our study focused on three treatment comparisons: the effect of diet (10 weeks chow versus 10 week HFD), the effect of aging (10 weeks versus 50 weeks chow), and changes with NAFL progression to NASH (10 weeks versus 50 weeks HFD). The findings for these comparisons are presented in Figure 4.13.

For proteins that were significantly increased in their expression in NASH, enriched pathways included those associated with lipid metabolism as well as glycolysis and gluconeogenesis (Figure 4.13A). Interestingly, both fatty acid elongation and degradation featured in the 25 most enriched pathways, which highlights the pleiotropic role of many proteins. As expected, just under one third of the pathways involved protein synthesis and metabolism, consistent with previous data examining the general proteome across all liver EV samples (Figure 4.11). This trend was also reflected in the effect of diet analysis (Figure 4.13B), whereas lipid metabolism was similarly overrepresented. As a comparison, the fold-enrichment of pathways involved in protein metabolism tended to be greater in the NAFLD progression analysis (Figure 4.13A), while those related to lipid metabolism were similar between the two analyses. One notable difference in the effect of diet analysis was the presence of a fatty acid biosynthetic pathway (Figure 4.13B). Finally, when the effect of aging alone was considered (that is, proteins that were significantly increased in 50 weeks versus 10 weeks chow), a majority of the most enriched pathways were dedicated to protein synthesis and metabolism (Figure 4.13C), while lipid metabolism was no longer present. Examples of pathways that were enriched across all three analyses (excluding specific amino acid related) included glyoxylate and dicarboxylate metabolism (6-fold to 23-fold) and the pentose phosphate pathway (8-fold to 14-fold), both of which are anabolic.

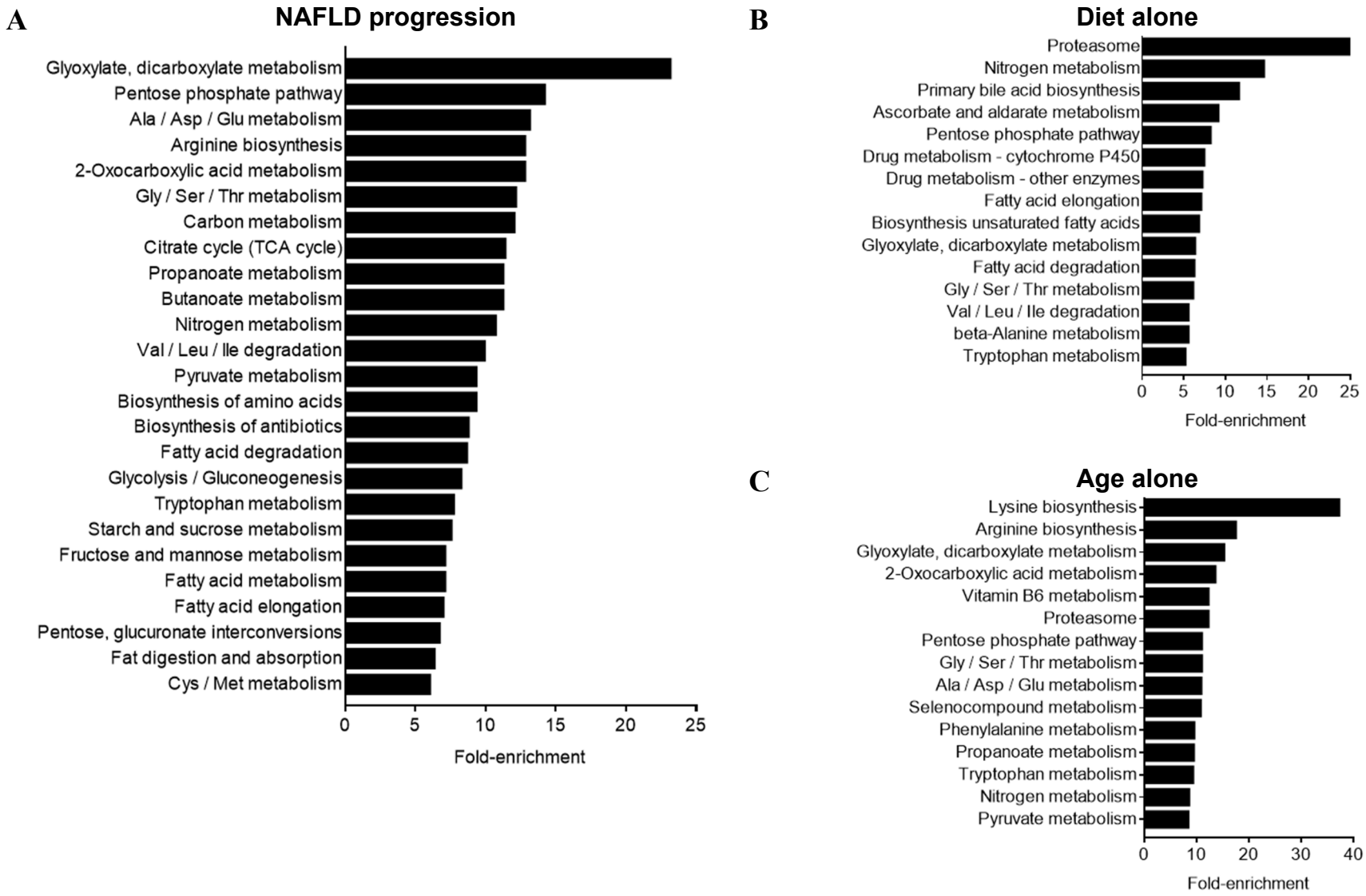
A
NAFLD progression
Glyoxylate, dicarboxylate metabolism
Pentose phosphate pathway
Ala / Asp / Glu metabolism
Arginine biosynthesis
2-Oxocarboxylic acid metabolism
Gly / Ser / Thr metabolism
Carbon metabolism
Citrate cycle (TCA cycle)
Propanoate metabolism
Butanoate metabolism
Nitrogen metabolism
Val / Leu / Ile degradation
Pyruvate metabolism
Biosynthesis of amino acids
Biosynthesis of antibiotics
Fatty acid degradation
Glycolysis / Gluconeogenesis
Tryptophan metabolism
Starch and sucrose metabolism
Fructose and mannose metabolism
Fatty acid metabolism
Fatty acid elongation
Pentose, glucuronate interconversions
Fat digestion and absorption
Cys / Met metabolism
0 5 10 15 20 25
Fold-enrichment
B
Diet alone
Proteasome
Nitrogen metabolism
Primary bile acid biosynthesis
Ascorbate and aldarate metabolism
Pentose phosphate pathway
Drug metabolism - cytochrome P450
Drug metabolism - other enzymes
Fatty acid elongation
Biosynthesis unsaturated fatty acids
Glyoxylate, dicarboxylate metabolism
Fatty acid degradation
Gly / Ser / Thr metabolism
Val / Leu / Ile degradation
beta-Alanine metabolism
Tryptophan metabolism
0 5 10 15 20 25
Fold-enrichment
C
Age alone
Lysine biosynthesis
Arginine biosynthesis
Glyoxylate, dicarboxylate metabolism
2-Oxocarboxylic acid metabolism
Vitamin B6 metabolism
Proteasome
Pentose phosphate pathway
Gly / Ser / Thr metabolism
Ala / Asp / Glu metabolism
Selenocompound metabolism
Phenylalanine metabolism
Propanoate metabolism
Tryptophan metabolism
Nitrogen metabolism
Pyruvate metabolism
0 10 20 30 40
Fold-enrichment

Figure 4.13. Enriched KEGG pathways for significantly elevated proteins in liver EVs. (**A**) Top 25 most enriched pathways for proteins that were elevated in NAFLD progression, that is, EVs from 50 weeks versus 10 weeks of HFD. (**B**) Top 15 pathways for proteins that were elevated in 10 weeks HFD versus chow diet, and (**C**) elevated in 50 weeks chow diet versus 10 weeks chow. Statistically elevated proteins were determined by Fisher's Exact Test (FET). Data shows enriched pathways relative to *Mus musculus* proteomic expression. Amino acid abbreviations: Ala, alanine; Asp, aspartate; Glu, glutamate; Gly, glycine; Ser, serine; Thr, threonine; Val, valine; Leu, leucine; Ile, isoleucine; Cys, cysteine; Met, methionine.

4.5. Interpretation

The findings from this Chapter highlight the general metabolic and physical profile of animals with HFD-induced NAFLD, including the progression from simple steatosis in the liver at 10 weeks to NASH at 50 weeks. Intermittent timepoints demonstrate the temporal milestones in the development of NAFLD and emphasise the fact that disease progression does not tend to be linear. In this study, fibrotic changes were completely absent in the earliest stage (10 weeks of HFD) whereas collagen staining on histology and gene expression of related markers were increased by 20 weeks, but plateaued at 30 weeks before accelerating to widespread fibrosis after 50 weeks of HFD. These patterns were also reflected in other parameters – including liver TAG and EV abundance – which will be detailed further below.

4.5.1. Non-linear evolution of NAFLD

While the findings from Chapter 3 were effective in comparing the differences between two discrete stages on the NAFLD spectrum – that is, simple steatosis and NASH – this study provided a more comprehensive "longitudinal" profile of NAFLD development. For rodents commencing on a HFD at an early age (6 weeks, equivalent to adolescent humans; see Figure 3.1), 10 weeks of diet was sufficient to increase body weight and fat mass in both epididymal and subcutaneous depots, as well as plasma insulin levels. This is in line with a previous study that investigated the onset of metabolic features in high-fat fed mice (Turner et al., 2013). In contrast, preclinical blood glucose and insulin tolerance were inconsistent with the classical patterns of insulin resistance expected in progressive obesity (see prediabetes phase in (Ramlo-Halsted and Edelman, 1999)), although the findings in our study were similar to other rodent studies modelling HFD-induced obesity (Ito et al., 2007, Turner et al., 2013). In parallel with the increase in NAFLD severity by 20 weeks, the circulating liver enzymes ALT and AST were increased above the control (age-matched standard chow diet) as well as the baseline (10 weeks HFD). In contrast, plasma TAG in the HFD cohort was consistently below the control groups – significantly or otherwise – which is supported by other mouse studies (Gao et al., 2010, Kirk et al., 1995) and thought to be a product of decreased hepatic VLDL secretion (Gao et al., 2010), contrary to humans where plasma TAG is increased in obesity concomitant with insulin resistance (Adeli et al., 2001, Lewis and Steiner, 1996).

In the context of the liver, 10 weeks of HFD was insufficient to significantly increase the organ weight above the control chow group, whereas mild steatosis was already present. Intriguingly, the 20 week feeding timepoint was a milestone for dramatic changes in NAFLD pathogenesis; these were accompanied by an increase in liver enzymes and a spike in hepatic TAG content, as well as significant changes in the gene expression of ECM remodelling markers and MCP1, a chemokine responsible for leukocyte recruitment to sites of inflammation (Deshmane et al., 2009). MCP1 is also known to be sensitive to insulin and is thus increased in obesity and T2DM (Rull et al., 2010, Sartipy and Loskutoff, 2003). Most striking, however, were the patterns in hepatic lipid accumulation and fibrogenesis as determined by liver histology. When observing the HFD cohort across all timepoints, both hepatic TAG and total neutral lipids (all fatty acid glycerols, typically in lipid droplets) were consistently elevated above the respective chow group, with the exception of the 20 week timepoint: here, TAG was significantly increased and neutral lipids decreased when compared to 10 weeks of HFD, and consequently there was no difference between the two diets for the latter. Furthermore, while the general morphology in terms of steatosis did progress typically from microvesicular to a predominantly macrovesicular phenotype, diffuse collagen staining was apparent as early as 20 weeks in some animals. Although unusual, this phenomenon had been observed previously (Lo et al., 2011). Perhaps unexpectedly, there was no increase in collagen staining at 30 weeks, whereas bridging fibrosis was ubiquitous by 50 weeks on HFD; these patterns were in turn reflected in the gene expression of collagen I.

4.5.2. EV abundance reflects TAG levels

When compared to the findings in the previous Chapter, there were several dissimilarities in both the plasma and liver-derived EV populations in terms of their abundance. This raises the question of sample handling and the need to account for logistical issues; for instance, since ultracentrifugation is a low-throughput technique, it was not feasible to complete each step of the differential centrifugation series prior to storage at -80^{o}C for the samples in the present Chapter. Such variations in the workflow may in turn alter the final EV yield (Jeyaram and Jay, 2017, Yuana et al., 2015), however, there are currently no universally accepted standards for the isolation of EVs according to ISEV guidelines (Witwer et al., 2013, Witwer et al., 2017). Due to the random effect on EV yield in our findings (see Figure 4.14), it was important to maintain consistency in the isolation method across the remaining studies.

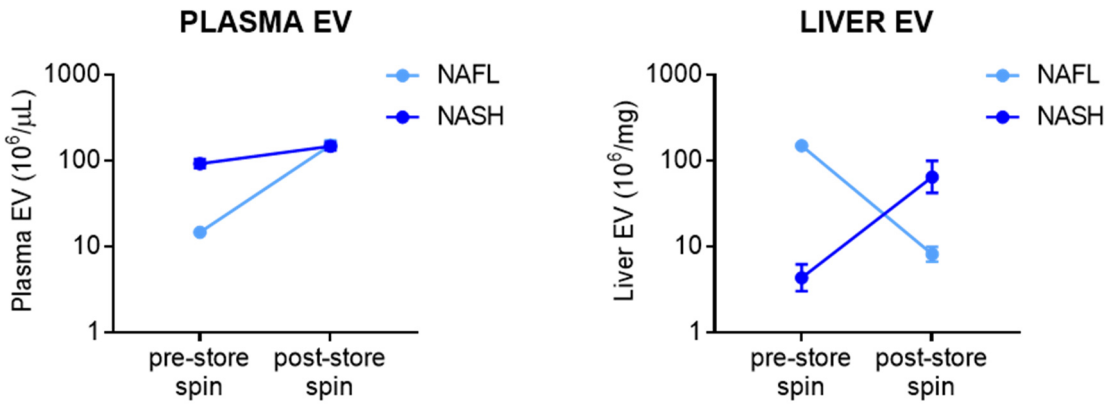

Figure 4.14. Effect of storage timing on EV abundance. In Chapter 3, the ultracentrifugation step was performed before storage at -80ºC (pre-store spin), while in Chapter 4 the EVs were stored prior to ultracentrifugation (post-store spin) following the 10,000×g spin step. Data show mean ± SEM for n=6-12 animals per group.

Despite these variations, there was a statistically significant inverse correlation between plasma and liver-derived EVs when only HFD samples were considered, a trend that is consistent with the findings in Chapter 3. However, the same outcome was not achieved when matching the treatment conditions to the Chapter 3 data. It is worth noting that the discrepancy also coincides with a different trend in hepatic lipid accumulation as measured by ORO staining; this suggests that the relationship between absolute hepatic lipid (irrespective of diet) and EV number that was seen in Chapter 3 may not be representative of the general population. Therefore, the remainder of the analyses in this Chapter considered HFD groups only, over all timepoints. Interestingly, when EV abundance by NTA was correlated against other physical and metabolic parameters, liver-derived EVs were significantly related to more clinical outcomes than plasma EVs. Furthermore, the abundance from each sampling site was reflected in the TAG content from the respective site: that is, there was a significant positive correlation between plasma EV and plasma TAG concentration, whereas there was a negative correlation between liver EV and hepatic TAG. These findings were not only intriguing but also novel, given that *in vivo* studies tend to either correlate EV abundance to NASH fibrosis severity (Kornek et al., 2012, Povero et al., 2014, Welsh et al., 2018), or measure EVs as an independent parameter that is changed in the treatment group (Baron et al., 2011, Kornek et al., 2011, Kakazu et al., 2016).

4.5.3. Liver EV proteome is heterogeneous

Characterisation of our EV samples was performed using a discovery method (spectrometry) rather than a targeted approach (flow cytometry) in the first instance. For the purpose of this study, the liver-derived EV proteome was examined to complement previous studies in the literature that have analysed the plasma EV proteome in the context of NAFLD (Povero et al., 2014) or the hepatocyte lipidome following palmitate treatment to promote a NAFLD-like lipotoxic environment (Kakazu et al., 2016). The latter reported an increase in C16:0 ceramide within the EV cargo of lipotoxic hepatocytes, which was subsequently confirmed *in vivo* by sampling plasma EVs from various models of NASH (Kakazu et al., 2016). Of interest, HFD is known to enrich hepatic C16:0 ceramide, which in turn promotes insulin resistance and blocks fatty acid beta oxidation (reviewed in (Hla and Kolesnick, 2014)).

In our study, we identified 744 proteins that were expressed across all liver EV samples within the confines of the experimental parameters; for example, using a protein threshold of 99% and a peptide threshold of 95% (accepting a minimum of 2 peptides). In general, very few proteins were unique to any given treatment group, with the majority expressed across all treatments. When these shared proteins were considered for gene ontology analysis and mapped to KEGG pathways, it was shown that liver EV proteins were predominantly involved in protein and lipid metabolism, as well as glycolysis and gluconeogenesis. This suggests that EVs likely play an important role in hepatocellular homeostasis, and also highlights their paracrine influence on the whole lipid life cycle, from synthesis to oxidation and degradation. The catabolic pathway of aromatic compounds was also overrepresented, although the exact implication of this is unclear given that many biological molecules – including nucleotides, some amino acids, and the haeme portion of haemoglobin – have an aromatic structure, which are chemically more stable than their non-aromatic counterparts, such as lipids for example. By comparison, an *in vitro* study using primary or immortalised rodent hepatocytes confirmed the enrichment of fatty acid metabolic pathways in the exosomal proteome, whereas pathways related to cell cycle and protein synthesis were downregulated (Conde-Vancells et al., 2008). This was the first study of its kind to comprehensively examine the EV protein cargo of untreated hepatic cells, and has been succeeded by many studies that employ a more targeted profiling and functional analysis of hepatocyte EVs in culture (discussed in further detail in Chapter 6).

When the liver EV samples from the four treatment groups (10 and 50 weeks HFD and chow) were independently analysed for enriched pathways and subjected to hierarchical clustering, it was found that their proteomes were heterogeneous. That is, with the exception of 50 weeks chow, EV samples that clustered together were not necessarily from the same treatment group. Therefore, it was difficult to determine by qualitative analysis which biological pathways are affected by aging, diet, or a combination of the two. It is worth noting, however, that these inconsistencies may be explained by limitations in the methodology: for instance, a batch effect can be observed whereby two samples from different treatment groups that were used for calibration (10w HFD3 and 50w HFD3) clustered together across the enriched pathways. The small sample size (n=3 per group) is another factor that may have impacted the consistency of findings, although a previous study with a similar experimental design did not report on such issues (Povero et al., 2014). In contrast to the present study, the authors showed that select protein groups tended to cluster samples based on their dietary treatment (Povero et al., 2014), whereas age was a stronger predictor of proteomic signature in this study.

On the other hand, quantitative analysis of the liver EV proteome between pairs of treatment groups showed that significantly elevated proteins could be mapped to biological pathways, which in turn could be assessed for enrichment relative to the species proteome. From here, we compared the effect of age (elevated in 50 weeks versus 10 weeks chow), HFD (elevated in 10 weeks HFD versus chow), and NAFLD progression (elevated in 50 weeks versus 10 weeks HFD) on the expression of EV proteins. Interestingly, the two pathways that were enriched across all analyses (glyoxylate/dicarboxylate metabolism and the pentose phosphate pathway) are both anabolic, in contrast to the homeostatic pathways that were shared across all EVs, which were primarily catabolic. The glyoxylate cycle has a similar function to the Krebs (TCA) cycle and is involved in gluconeogenesis (Kornberg, 2000), while the pentose phosphate shunt occurs in parallel to glycolysis and produces $NADPH^{+}$ which subsequently protects against oxidative stress (Stincone et al., 2015, Wood, 1986). These two pathways were also the most enriched in NAFLD progression, in complement to the TCA cycle, glycolysis and gluconeogenesis, as well as fatty acid metabolism. Collectively, these enriched pathways seemed to imply a protective role for liver EVs in NAFLD, whereas in the study by Povero and colleagues, proteins involved in cell stress were elevated in plasma EVs from animals with diet-induced steatohepatitis (Povero et al., 2014).

The biosynthesis and metabolism of various amino acids were also ubiquitously enriched in liver EVs that were subjected to extrinsic (HFD) or intrinsic changes (aging), or the interaction of both. In fact, these pathways accounted for the majority of the 15 most enriched pathways in terms of EV proteins that were elevated in aging. Again, it is difficult to ascertain the exact implications of these findings, although they further highlight the important role of (liver) EVs in paracrine homeostasis. In the context of aging, the role of circulating EVs in cell senescence has been documented previously (Kadota et al., 2018, Robbins, 2017). However, studies examining the EV cargo have tended to focus on a targeted approach, such as western blot or protein array (Baek et al., 2016, Takasugi et al., 2017). In the latter, sample clustering based on protein co-expression resolved that, much like in our findings, neither aging nor the other demographic parameters showed proteomic consistency (Baek et al., 2016). Furthermore, none of the studies to date have reported on enriched pathways related to amino acid metabolism in either circulating or tissue-derived EVs. The effect of HFD, on the other hand, was comparable to the NAFLD progression analysis with a few exceptions, namely the enrichment of fatty acid biosynthesis and (perhaps in contradiction) the synthesis of bile acid, which acts to emulsify dietary lipids.

4.5.4. Consolidation

The findings in the present Chapter reinforce the effect of both the intrinsic and extrinsic factors that contribute to the development of NAFLD. Subclinical changes in the liver are summarised and their relationship to the circulating and liver-derived EV profile are highlighted, whereby both EV populations are strongly correlated with TAG levels. Further to their potential role as biomarkers of hepatic steatosis, liver EVs were characterised in terms of their proteome, where it was determined that while intragroup heterogeneity was present, specific biological pathways were enriched in the context of HFD or aging, or their combination (NAFLD progression). The cell localisation of proteins that were shared across all liver EV samples in our study are illustrated in Figure 4.15. To link the characterisation here with a functional analysis, the continuation of this study will investigate the changes in hepatocyte gene expression upon exposure to plasma and liver-derived EVs obtained from the current study, which will be detailed in Chapter 6.

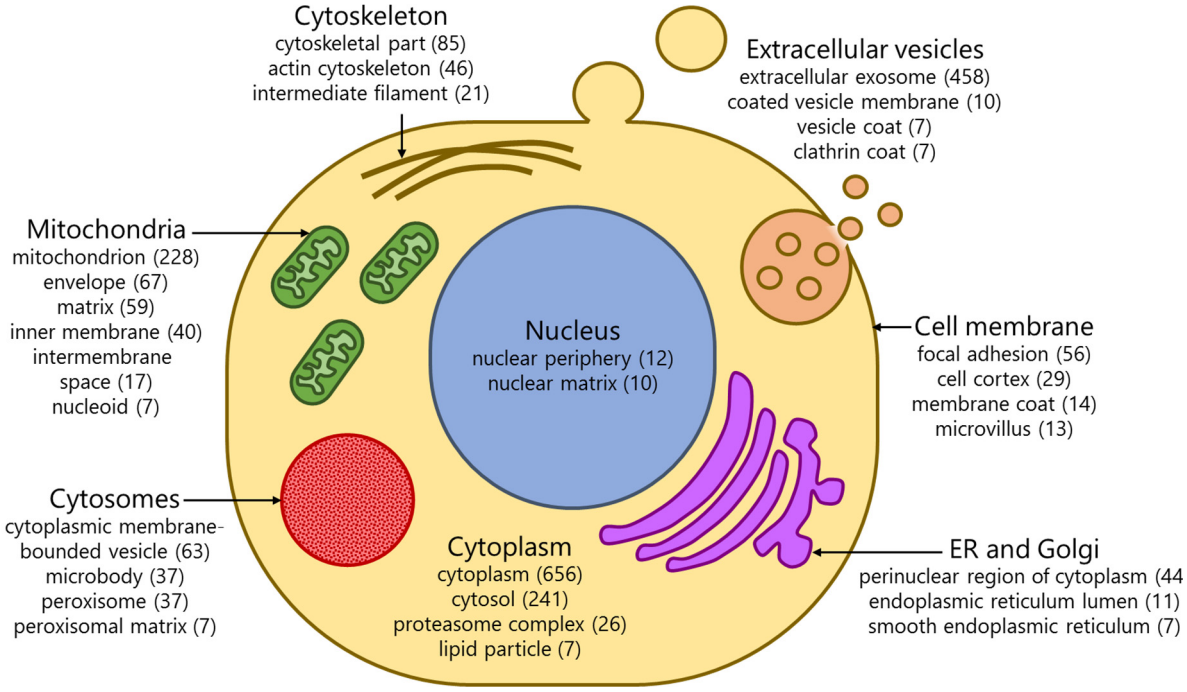

Figure 4.15. Cellular localisation of proteins derived from mouse liver EVs. Numbers indicate the protein counts (from n=744 unique liver EV proteins) that were attributed to the given sub-cellular categories, as determined by gene ontology analysis (Huang da et al., 2009).

Chapter 5.

Impact of genetic manipulation and lifestyle intervention for NAFLD on extracellular vesicles

Chapter 5. Table of contents

5.1. Introduction

While the pathogenesis of NAFLD is complex, much is known about the lifestyle factors that exacerbate the disease. Consequently, the impact of physical interventions are well documented (Hashida et al., 2017, Keating et al., 2012) and manipulation of the cytokines that drive inflammatory tissue injury have also been explored (Chen et al., 2016). The study of EVs in either context with respect to NAFLD has not been reported, and thus underpins the investigations described in this Chapter (see Figure 5.1 for animal models).

Lifestyle changes are a commonly prescribed therapeutic intervention in NAFLD patients, and provide a drug-free alternative to improving liver outcomes in the absence of fibrotic NASH. Although there is no consensus on an ideal training program (Keating et al., 2012), aerobic exercises seem to provide greater health benefits in terms of decreasing hepatic fat (Ismail et al., 2012), irrespective of exercise dose or significant weight loss (Johnson et al., 2009, Keating et al., 2015). While most studies have explored moderate-intensity *endurance* training (END), a few have reported on *high-intensity interval training* (HIIT), a program that is delivered in bouts of high intensity exercise interspersed with low intensity recovery periods. Improvements to NAFLD burden have been documented in both humans (Hallsworth et al., 2015) and rodents (Marcinko et al., 2015) undergoing HIIT. However, the differential effect of END and HIIT programs in normalising EV profiles towards a healthy liver baseline is not known.

Similarly, the genetic deletion of pro-inflammatory cytokines such as TNF have been shown to affect the development of NAFLD (Salles et al., 2012, Uysal et al., 1997). An upstream regulator of NFκB signalling in inflammation, TNF is also known to intersect with the insulin signalling pathway (Feinstein et al., 1993, Hotamisligil et al., 1994). However, there is a paucity in knowledge surrounding the interplay of EVs and the genetic manipulation of NAFLD models. The studies described in this Chapter will investigate the impact of HFD on EV number in TNF-ablated ($TNF^{-/-}$) mice bred onsite, using a single 12-week timepoint that captures the early stages of NAFLD development and has previously been used for metabolic studies on $TNF^{-/-}$ animals (Chen et al., 2016, Turner et al., 2013). The study commenced at around 8 weeks of age, similar to the models presented in the previous Chapters.

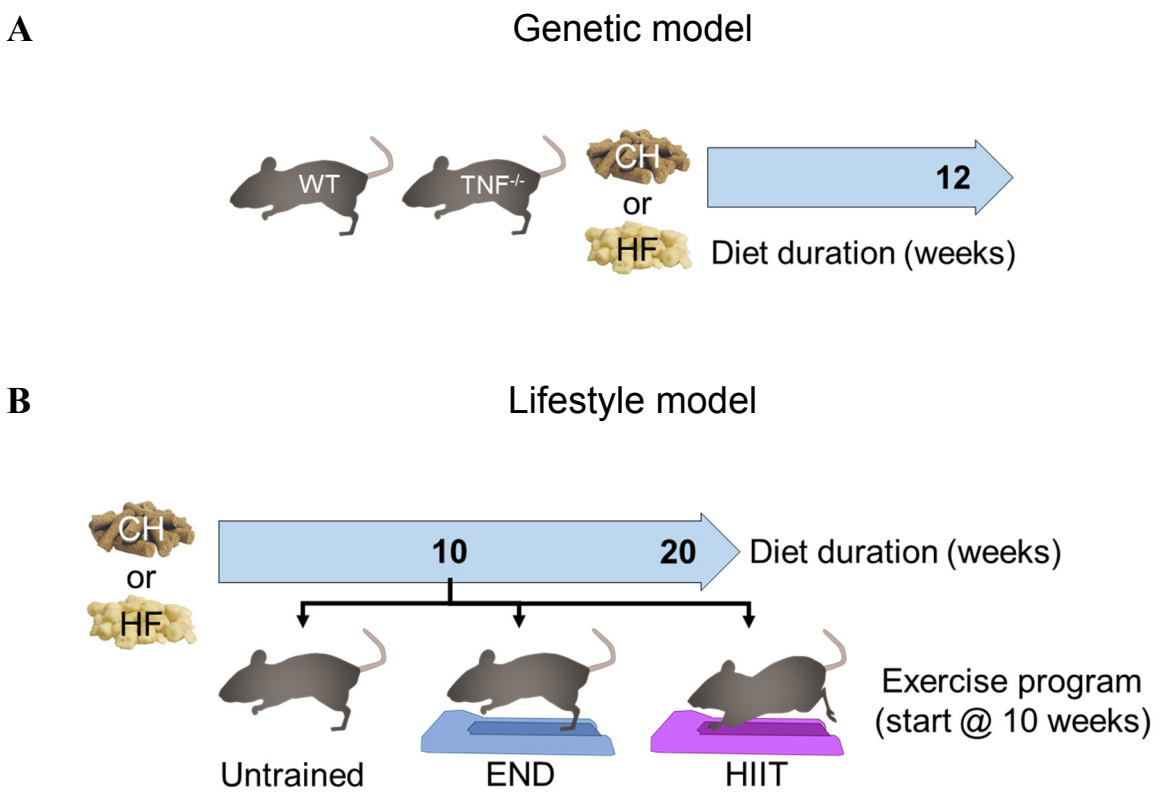

Figure 5.1. Schematics for the genetic manipulation or exercise intervention in diet-induced NAFLD. **(A)** Genetic model: transgenic animals lacking expression of TNF ligand ($TNF^{-/-}$) and wild-type C57Bl/6 mice matched for age, gender and strain were administered either a standard chow (CH) or high-fat diet (HF; 45%kcal fat) for 12 weeks, commencing at 8 weeks of age. **(B)** Lifestyle model: male C57Bl/6 mice were administered either CH or HF diet for 20 weeks, commencing at 10 weeks of age. During the second half of dietary intervention, animals were randomly allocated to one of two exercise programs: endurance training (END) or high-intensity interval training (HIIT), with untrained animals in each diet cohort acting as controls for dietary effects. For further details on the methodology of exercise programs, see Chapter 2 (section 2.2.2).

5.2. Genetic Manipulation: TNF$^{-/-}$

This study sought to examine the effects of TNF gene inactivation on NAFLD development and the release of EVs in this context. The TNF$^{-/-}$ mice were generated by the insertion of a modified neomycin resistance cassette into an excised region of exon IV, thereby inhibiting the production of functional TNF molecules (Korner et al., 1997). No structural abnormalities were detected by histology across the multiple organs examined, including the liver (see previous reference). Animal breeding and phenotyping was managed on-site in the animal facility of the Centenary Institute by Ms Christine Yee. Mice were commenced on the diet at 8 weeks of age; male TNF$^{-/-}$ mice were fed a HFD or standard chow for a further 12 weeks, and results were compared with commercially acquired, gender- and age-matched C57Bl/6 wild-type (WT) mice as a control.

5.2.1. Animal characteristics

While the metabolic profile for the TNF$^{-/-}$ and WT animals maintained on a chow diet were comparable, the knockout group had a significantly increased average body weight (by 11%), with a negligible increase also seen in the liver weight (Table 5.1). Genetic manipulation and HFD seemed to have a synergistic effect, with a much worse metabolic profile seen in TNF$^{-/-}$ mice. In the absence of TNF, mice on HFD were obese after 12 weeks (50% heavier than WT) with grossly enlarged livers, double the weight of WT controls on the same diet. Liver enzymes were also significantly elevated in the knockout group, especially circulating ALT which experienced a greater than 6-fold change ($p=0.046$ versus WT). Despite the biological variation, hyperinsulinaemia was also present (greater than 4-fold change, $p=0.015$), while plasma TAG was statistically elevated in TNF$^{-/-}$ mice on HFD compared to their chow counterparts ($p=0.007$).

Table 5.1. Animal characteristics in TNF$^{-/-}$ genetic study.

	Chow		*HFD*	
	Wild-type	*TNF $^{-/-}$*	*Wild-type*	*TNF $^{-/-}$*
Weights:				
body (g)	29.3±1.65	32.8±1.09 $^{\#}$	32.5±2.34 *	48.8±0.75 *$^{\#}$
liver (g)	1.22±0.18	1.39±0.17	1.36±0.09	3.25±0.84 *$^{\#}$
liver as % body	4.16±0.64	4.25±0.59	4.21±0.28	6.63±1.66 *$^{\#}$
Plasma chemistry:				
ALT (U/L)	22.2±5.02	30.0±7.17	26.3±4.50	173±125 *$^{\#}$
AST (U/L)	50.4±14.4	49.1±12.6	48.8±13.7	124±54.3 *$^{\#}$
ALT/AST ratio	0.45±0.06	0.64±0.19	0.61±0.21	1.30±0.44 *$^{\#}$
TAG (mg/mL)	0.70±0.03	0.60±0.14	0.66±0.19	0.89±0.22 *
insulin (pg/mL)	137±22.2	276±202	347±141	1623±974 *$^{\#}$

Data are mean ± SD for n=5-8 mice per group, excluding outliers determined by the ROUT method (Q=5%). Significant difference from chow (*) or wild-type ($^{\#}$) accepted at $p<0.05$ as determined multiple Student's t test, per diet or genotype pairs, respectively. Abbreviations: ALT, alanine transaminase; AST; aspartate transaminase; TAG, triacylglycerol.

5.2.1.1. Hepatic steatosis

Unsurprisingly, liver triglycerides and total neutral lipids – both associated with lipid droplets – were ubiquitously elevated by HFD in TNF$^{-/-}$ mice (Figure 5.2). Like previous findings in this thesis, TAG extraction seemed to more accurately reflect the liver histology (see Figure 5.3), whereby the transgenic animals had a significantly increased hepatic TAG content when compared to their WT counterparts on HFD (Figure 5.2A), with no changes seen between the two genotypes in the chow-fed groups. In contrast, these patterns were not observed when examining liver neutral lipid content (Figure 5.2B), although this could be explained by the high intragroup variations. An additional increase in ORO staining in the TNF$^{-/-}$ group was seen for the chow diet, suggesting that the presence of TNF may regulate the storage of fatty acids in the liver as lipid droplets.

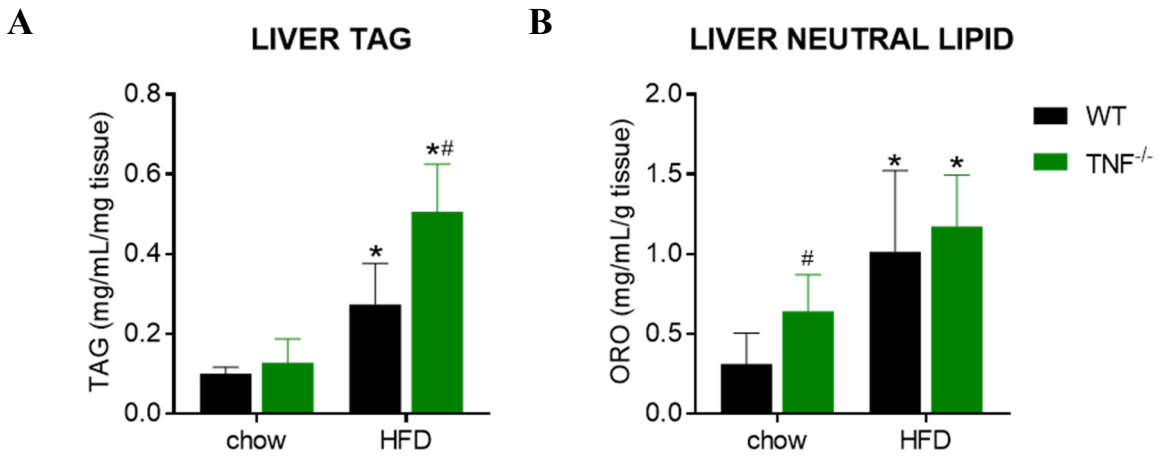

Figure 5.2. Impact of TNF knockout on liver lipid. **A.** Triacylglycerol (TAG) extracted from homogenised liver. **B.** Neutral lipids (fatty acid glycerols) were stained with Oil Red O (ORO) in homogenised liver prior to elution. Data are mean ± SD given per unit tissue for n=5-8 animals per group, excluding one chow outlier. Significantly different from chow (*) or wild-type ($^{\#}$) accepted at $p<0.05$ as determined by multiple Student's t test, per diet or genotype pairs, respectively.

5.2.2. NAFLD phenotype in TNF$^{-/-}$ mice

5.2.2.1. Liver histology

Liver histology showed a unique pattern of early NAFLD development in TNF$^{-/-}$ mice when compared to their WT counterparts. Macrovesicular steatosis was observed in the livers of WT animals on HFD (Figure 5.3E), with diffuse pericellular collagen deposits evident in some samples (Figure 5.3F). This latter phenomenon was unusual considering the short duration of the diet, however, it seemed to indicate a possible protective role of TNF deletion against fibrosis development (Figure 5.3H); that is, TNF may promote fibrogenic changes. In contrast, knockout mice receiving HFD had diffuse macrovesicular steatosis with large distinct islands of microvesiculated hepatocytes, often in periportal regions, giving the liver a histologically "foamy" appearance (Figure 5.3G). Enlarged pale staining hepatocyte nuclei were evident in HFD animals of both genetic backgrounds (Figure 5.3E and G, inset), although these changes were more prominent in the WT group, suggesting heightened levels of cell activity (typically protein synthesis). Finally, animals receiving a standard chow diet had seemingly normal livers, irrespective of genotype, with basal collagen staining in the perivascular connective tissue (Figure 5.3A-B and C-D, respectively).

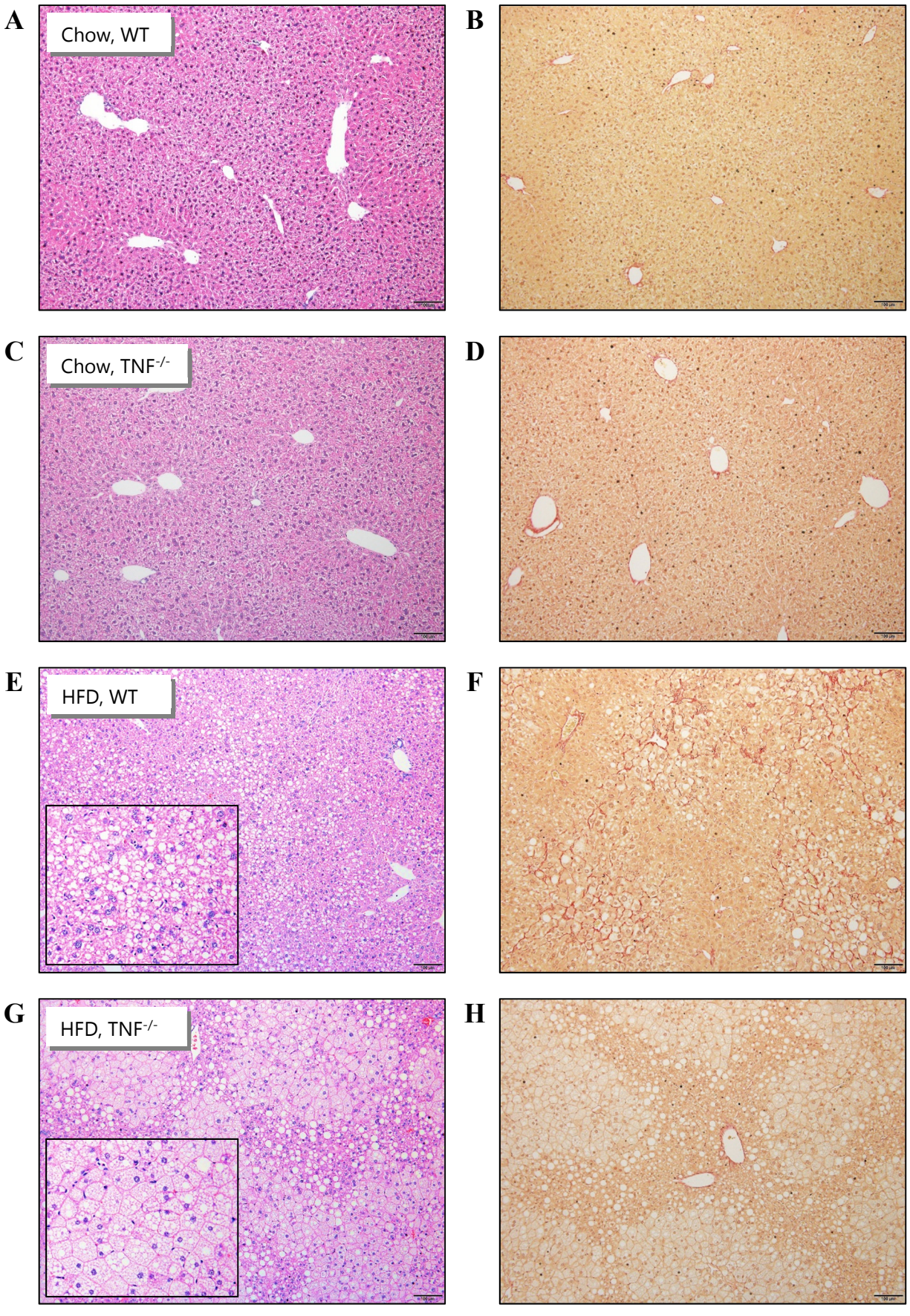
A
Chow, WT
B
C
Chow, TNF-/-
D
E
HFD, WT
F
G
HFD, TNF-/-
H

Figure 5.3. Impact of TNF knockout on liver histology. Left panels show general morphology by H&E staining, right panels show collagen accumulation (red) by PSR staining for respective treatment group. Livers of mice fed chow diet appear normal for both wild-type (WT; **A-B**) and $TNF^{-/-}$ background (**C-D**), whereas high-fat diet (HFD) livers showed different patterns of steatosis in WT (**E-F**) compared to $TNF^{-/-}$ (**G-H**), with mild fibrosis in some WT livers (**F**). Representative images at 100× magnification (scale bar = 100μm), inset 200×.

5.2.2.2. Liver gene expression

To confirm the absence of TNF from the genome of knockout mice, we examined the levels of transcript in these animals in relation to their wild-type counterparts (Figure 5.4A). As expected, TNF was undetectable in $TNF^{-/-}$ animals on either diet, whereas in WT mice on HFD there was a trend toward increased TNF expression, although this was not significant ($p=0.211$). For the remaining genes of interest, no difference was observed between HFD and chow groups for WT animals. This was also the case for $TNF^{-/-}$ animals, with the exception of the macrophage marker F4/80 which was decreased 3-fold by HFD ($p=0.011$) in the knockout group (Figure 5.4C).

Interestingly, other notable trends (significant or otherwise) tended to occur between $TNF^{-/-}$ and corresponding WT groups irrespective of diet. Aside from TNF, the cytokine MCP1 was also decreased in knockout animals, although the change only reached significance for the chow diet ($p=0.009$; Figure 5.4B). On the other hand, TNF deletion increased the expression of F4/80 (Figure 5.4C) as well as ECM remodelling genes (Figure 5.4D-F), although in most cases – as in for MCP1 – the difference was only significant between the chow groups (F4/80: $p=0.015$; collagen IV: $p=0.008$; TIMP1: $p=0.033$). The exception was collagen I, where the elevation failed to reach statistical significance (Figure 5.4D; $p<0.10$ both diets). These discrepancies could be explained by high biological variability within HFD groups, primarily for $TNF^{-/-}$ animals. Furthermore, a defined batch effect was also seen in TIMP1 expression (Figure 5.4F) for $TNF^{-/-}$ mice on HFD, where staggering the experiment (n=4+4) had resulted in disparate fold-change ranges of approximately 1-5 ($p=0.04$ versus WT) and 40-140 ($p=0.01$), respectively (overall $p=0.14$). Therefore, it was difficult to interpret the data related to this particular finding.

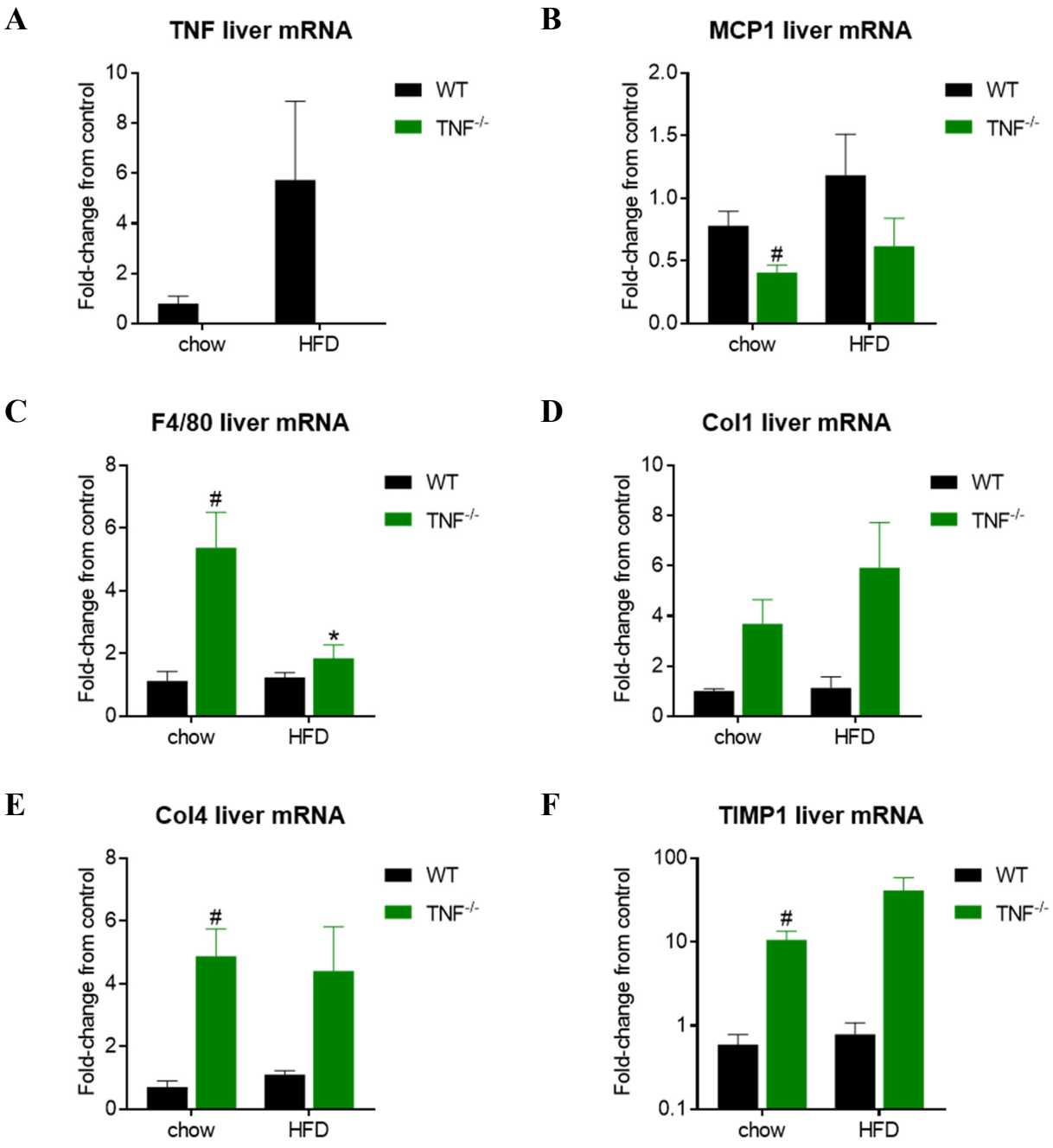

Figure 5.4. Liver gene expression for the genetic study. Graphs represent transcripts of pro-inflammatory genes (**A-C**) and genes involved in ECM remodelling or fibrosis (**D-F**). Data is expressed as mean ± SEM of fold-change from control (wild-type (WT) mice on chow diet) for n=5-8 mice excluding outliers. Significant difference from chow (*) or WT ($^{\#}$) accepted at $p<0.05$ as determined by multiple Student's t test, per diet or genotype pairs, respectively. Abbreviations: TNF, tumour necrosis factor; MCP1, monocyte chemotactic protein 1; Col, collagen; TIMP1, tissue inhibitor of metalloproteinase 1.

5.2.3. Extracellular vesicle enumeration

Following 12 weeks of HFD, neither diet nor genotype had an effect on EV enumeration. For both EV abundance and normalised size distribution, no trends were observed in our data when either plasma (Figure 5.5A-B) or liver EVs (Figure 5.5C-D) were considered. This was intriguing, given the obvious changes noted previously in metabolic parameters (Table 5.1), as well as the liver phenotype in terms of lipid content (Figure 5.2), histology (Figure 5.3), and gene expression (Figure 5.4). With a predominantly genotype effect shown in the latter, it was expected that this parameter may contribute to potential EV fluctuations. When liver EV abundance was adjusted for total liver weight, there was a 9-fold increase in EVs ($p=0.009$) for high-fat fed knockout mice relative to their WT counterparts (Figure 5.5E). Since the unadjusted values were similar between these groups ($p=0.732$ versus 'per mg tissue'), this change can likely be explained by the accelerated steatosis seen in $TNF^{-/-}$ animals on HFD. Finally, while the size distributions were unchanged between treatment groups, the trends were consistent with previous findings in this thesis whereby the diameter of plasma EVs tended to be around 70nm (Figure 5.5B), while liver EVs were slightly larger at 100nm (Figure 5.5D). Together, this data suggests that TNF expression does not affect the EV profile in NAFLD, or alternatively, only affects the abundance of liver-derived EVs insofar as the estimated total vesicles released from the whole liver, which in turn can be attributed to an increase in liver size.

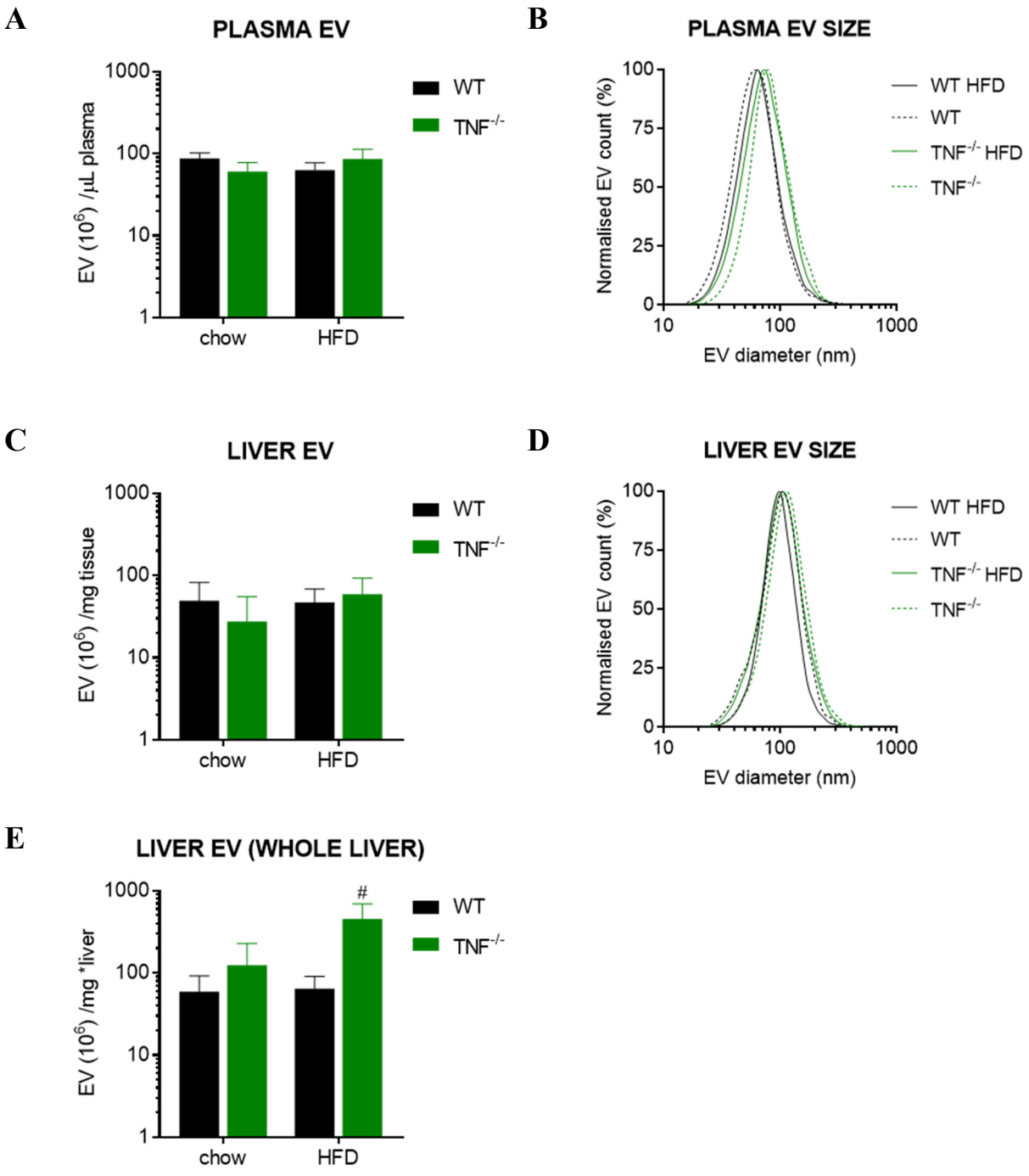

Figure 5.5. Extracellular vesicle enumeration for the genetic study. Data for total EVs (left panes) shows mean ± SEM for n=5-8 mice per group, excluding outliers. Size distribution graphs (right panes) show group normalised mean values for EV diameter. Significant difference from respective diet ($^{\#}$) accepted at $p<0.05$ determined by Student's t test. No change was seen between diets for either genotype.

5.3. Lifestyle Intervention: Exercise

In a study designed to explore how different exercise modalities can impact on obesity and its complications (including NAFLD), mice receiving HFD or standard chow were randomly assigned to one of three groups: endurance training (END), high-intensity interval training (HIIT), or untrained. Following 9 weeks of diet without further intervention, animals were acclimated to the treadmill for one week, then continued on one of the three programs above for a further 10 weeks while maintaining their original diet. Metabolic parameters were recorded, and an ITT performed, in the final week before conclusion of the experiment. For the purpose of this study, only the plasma and liver were considered, with the aim of identifying changes in their respective EV populations in association with liver changes following HFD with or without the exercise intervention.

5.3.1. Animal characteristics

While it was expected that the burden of most physical and metabolic changes that occur with high-fat feeding would be reversed by exercise, this was not seen in our study. The increased body weight with HFD was unperturbed by either exercise program (Table 5.2), although this is consistent with clinical studies in the literature (Johnson et al., 2009, Keating et al., 2015). In contrast, increased liver weight in HFD was decreased by both END and HIIT but did not normalise to chow-fed levels, while only HIIT affected the weight of adipose depots; these were differentially regulated, with a decrease in the subcutaneous fat mass, and conversely, an increase in epididymal fat mass.

5.3.1.1. Plasma biochemistry

The findings above were supported by the biochemical profile of the exercised HFD groups. Circulating liver enzymes were consistently lower in exercised animals compared to their untrained counterpart (Table 5.2). Interestingly, END also increased AST levels outside the HFD context ($p=0.001$ versus untrained chow), a trend that was not seen for ALT and was therefore unlikely to be related to changes in the liver. Plasma TAG was normalised by END in HFD mice ($p=0.010$ versus untrained) and was indistinct from the chow group undergoing END ($p=0.992$). In contrast, the hyperinsulinaemia in the END-trained HFD group ($p=0.001$ versus untrained) points to a synergy of the combined interventions ($p=0.004$ interaction of sources of variation by two-way ANOVA). Finally, exercise had no impact on the ITT, while untrained HFD animals had an elevated AUC ($p=0.011$ versus chow), suggesting decreased insulin sensitivity.

5.3.1.2. Hepatic steatosis

When examining changes in the liver lipid, disparate results were observed between the two methodologies used for these measurements. The TAG extraction technique, which is more sensitive, showed no effect of exercise on TAG levels in livers of animals fed a standard chow diet. However, liver TAG was increased across all HFD groups ($p<0.001$ for all diet pairs) and was further elevated by both END and HIIT (Figure 5.6A; both $p<0.001$ versus untrained HFD). In contrast, the diet effect was much weaker for ORO-stained neutral lipids due to intragroup variability, whereas no difference was observed between diets in the HIIT program ($p=0.314$; Figure 5.6B). While ORO staining in the HFD livers was only increased relative to chow in the untrained ($p=0.014$) and END ($p<0.001$) groups, the HIIT program was capable of normalising this parameter ($p=0.011$ versus untrained HFD).

Table 5.2. Animal characteristics for the exercise intervention study.

	Chow			*HFD*		
	Untrained	*Endurance*	*HIIT*	*Untrained*	*Endurance*	*HIIT*
Weights (g):						
whole body	33.3±2.35	32.2±1.74	32.9±1.19	47.7±2.63 *	47.5±4.14 *	45.4±4.70 *
liver	1.52±0.14	1.46±0.15	1.43±0.18	3.69±0.52 *	2.98±0.93 *#	2.61±0.61 *#
epididymal fat	0.70±0.22	0.52±0.11	0.54±0.16	1.76±0.32 *	1.96±0.35 *	2.14±0.30 *#
subcutaneous fat	0.35±0.09	0.29±0.05	0.29±0.06	1.81±0.27 *	1.70±0.45 *	1.38±0.44 *#
Plasma chemistry:						
ALT (U/L)	19.0±3.46	36.5±19.2	20.5±4.41	208±116 *	91.5±47.5 *#	41.6±24.3 *#
AST (U/L)	57.8±12.5	120±59.3 #	67.3±28.3	160±65.3 *	114±41.0 #	76.9±16.7 #
ALT/AST ratio	0.31±0.05	0.34±0.12	0.36±0.11	1.10±0.23 *	0.89±0.36 *	0.61±0.31 *#
TAG (mg/mL)	1.83±0.61	1.80±0.57	1.33±0.39 #	1.12±0.30 *	1.77±0.71 #	1.14±0.23
insulin (pg/mL)	157±80.4	141±50.0	163±78.4	1193±636 *	4284±1882 *#	1737±937 *
Insulin tolerance test:						
fasting glucose (mM)	7.98±1.14	7.47±0.85	8.11±1.61	8.35±1.54	8.37±1.17 *	8.33±1.42
area under curve (AU)	275±52.5	333±127	310±60.8	336±53.6 *	336±31.2	311±52.5

Data are mean ± SD for n=10-12 animals per group, excluding outliers determined by the ROUT method (Q=5%). Significantly different from chow (*) or untrained animals on the same diet (#), accepted at $p<0.05$ as determined by Student's t test (diet pairs), or 2-way ANOVA (training) with Dunnett's test for multiple comparisons. Abbreviations: ALT, alanine transaminase; AST; aspartate transaminase; TAG, triacylglycerol; AU, arbitrary units.

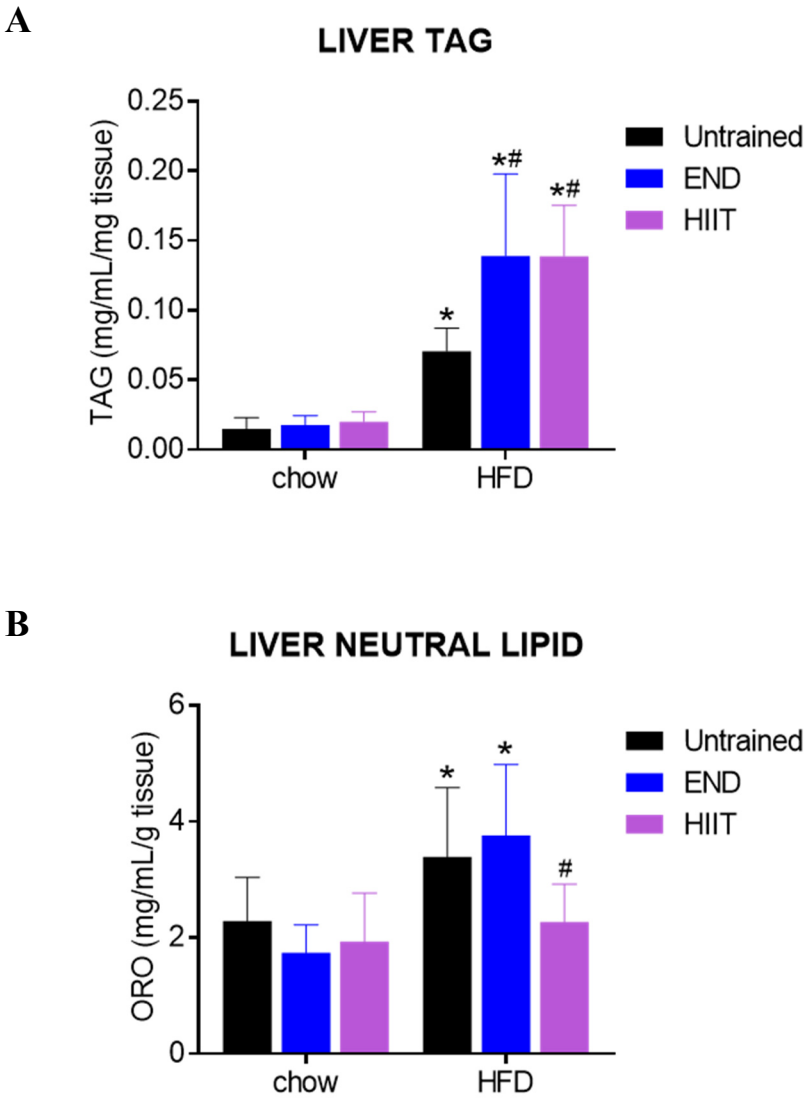

Figure 5.6. Impact of exercise on liver lipid. **A.** Triacylglycerol (TAG) extracted from homogenised liver. **B.** Neutral lipids stained with Oil Red O (ORO) in homogenised liver. Data are mean ± SD per unit weight of tissue for n=10-12 animals per group, excluding outliers. Significant difference from chow (*) or untrained animals on the same diet ($^{\#}$) accepted at $p<0.05$ as determined by Student's t test (diet pairs), or 2-way ANOVA (training) with Dunnett's test for multiple comparisons.

5.3.2. NAFLD phenotype in exercised mice

Both structurally and on a molecular level, the livers of animals on a standard chow diet were invariably normal, irrespective of exercise intervention. For simplicity of interpretation, controls in this section will be represented by the untrained chow group.

5.3.2.1. Liver histology

The livers of mice receiving a standard chow diet appeared unremarkable in either general structure (Figure 5.7A) or collagen staining by PSR (data not show), irrespective of exercise. In contrast, 20 weeks of HFD without exercise intervention resulted in profound architectural changes, including both microvesicular and abundant macrovesicular steatosis (Figure 5.7B), although fibrotic changes were mild (Figure 5.7C). The progression of NAFLD appeared to be impeded by both END (Figure 5.7D-E) and HIIT (Figure 5.7F-G), however, bands of microvesicular steatosis were still present. There was a differential impact of the two exercise programs in the HFD mice. In END-trained animals, steatosis tended to be periportal (Figure 5.7D) and fibrosis was absent (Figure 5.7E); conversely, mild peri-cellular collagen staining was evident in the livers of mice undergoing HIIT (Figure 5.7G), although not to the same extent as seen in the untrained NAFLD livers. Interestingly, whilst HIIT did not seem to afford any benefit over END in terms of visible steatosis, there appeared to be a greater impairment of the liver architecture in these animals (Figure 5.7F), such that the lobules were less defined.

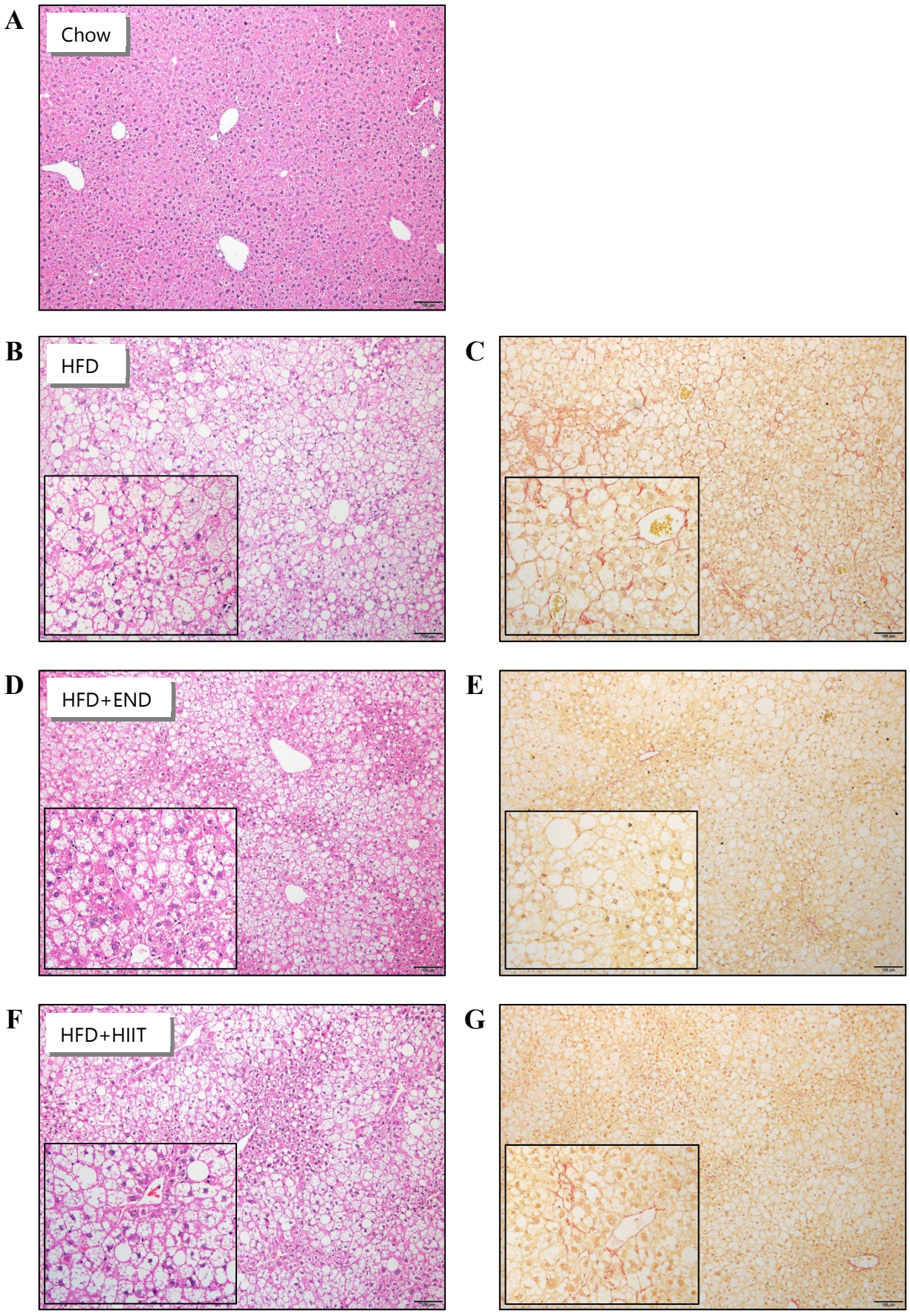
A
Chow
B
HFD
C
D
HFD+END
E
F
HFD+HIIT
G

Figure 5.7. Impact of the exercise programs on liver histology. Left panels are representative general morphology by H&E staining, right panels show collagen accumulation (red) by PSR staining for respective treatment group. Livers of mice fed chow diet appeared normal (**A**) whereas high-fat diet (HFD) livers showed considerable steatotic changes with some loss of architecture and mild fibrosis (**B-C**). Steatosis was milder following END (**D-E**) and HIIT (**F-G**) in HFD groups, with no or limited fibrotic changes with either exercise. Images given at 100× magnification (scale bar = 100μm), inset 200×.

5.3.2.2. Liver gene expression

Changes in the liver transcript levels of inflammatory markers, growth factors, and regulators of ECM remodelling were determined using a custom-designed OpenArray™ chip for real-time qPCR. This included 24 genes of interest and 4 reference genes (see Table 2.7). Of the reference genes, aldolase B was most consistently amplified and for this reason was used for normalisation. A total of 50 samples were assessed (n=6-10 per group), following exclusion of reference gene outliers and samples that failed to express any gene. In addition, some genes were undetectable in many of the control animals. Consequently, only genes that were expressed in at least three control (untrained chow) animals were reported in this work. A heatmap of genes in mice reaching these criteria is shown in Figure 5.8. below. A total of 14 genes were included in the final analysis. Of these, sufficient data was only available for 7 genes in the HFD+HIIT group. Analysis of the remaining 7 genes focused only on the effects of END on HFD.

Compared to the control group, the expression of 8 of 14 genes was increased in untrained HFD animals, whereas END reversed this change in all instances (Figure 5.9). This included collagen I and IV, as well as ECM regulators (TGFβ, TIMP2, and basigin) and chemokines (MCP1 and CXCL10). For collagen I, this finding was also reflected in the liver protein expression (performed by S. Martinez-Huenchullan, unpublished manuscript). Interestingly, the response from the HFD+HIIT group was less consistent: decreasing similar to HFD+END (MCP1 and TIMP2), or comparable to HFD alone (CXCL10, TGFβ, and basigin). These findings suggest that the END program may exert a broader effect in terms of normalising gene expression in HFD animals. In fact, even where changes with HFD were not observed or trended towards a decrease (CTGF, VEGF, and α-SMA), the expression levels of these genes tended to be further decreased by END training.

Unfortunately, due to the high intragroup variability in untrained animals across multiple genes, statistical analyses often failed to show a significant change. Furthermore, given the inconsistent fluctuations across functionally related genes, it was difficult to identify specific outcomes of exercise intervention in the context of HFD, at least in terms of molecular regulation in the liver.

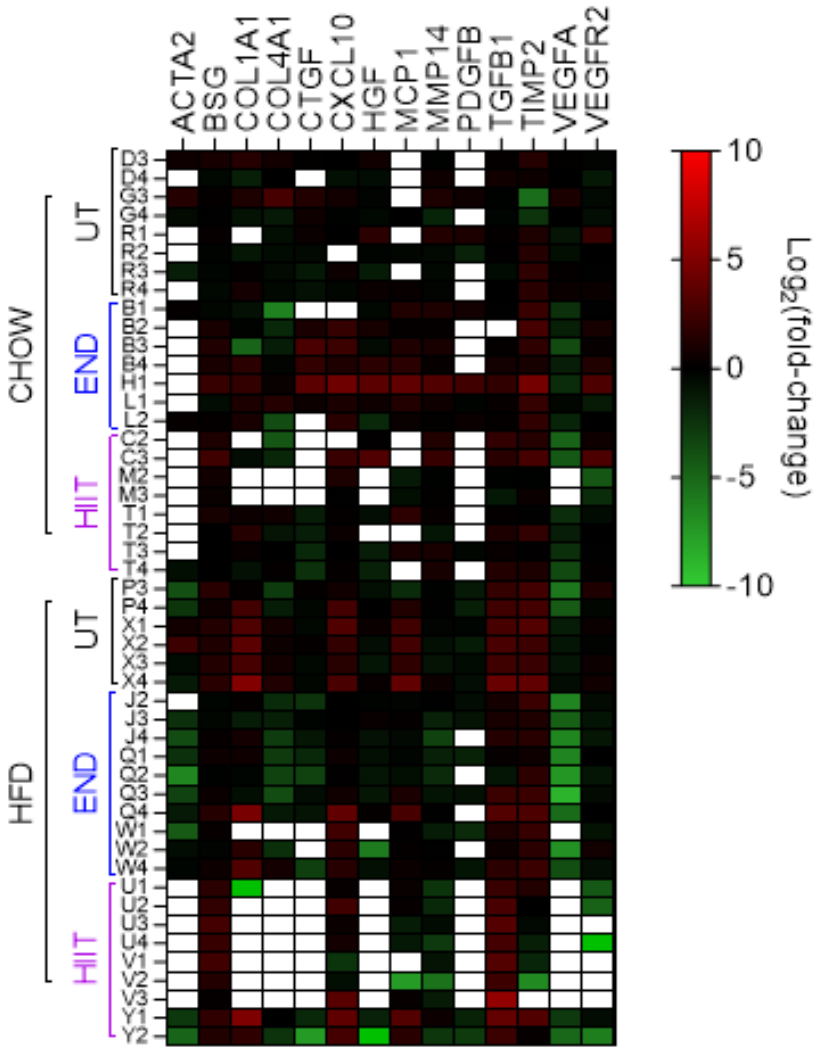

Figure 5.8. Heatmap of gene array for exercise intervention study. Non-hierarchical display of genes of interest (columns) across respective samples (rows) divided into untrained, endurance (END) and high-intensity interval training (HIIT) per diet. Legend represents negative delta-delta cycle threshold, given as $\log_2$(fold-change) versus control group (untrained chow). Empty squares where no cycle threshold values were recorded. Gene symbol abbreviations: ACTA, alpha smooth muscle actin (also αSMA); BSG, basigin; COL1A1 and 4A1, collagen I and IV subunit A1; CTGF, connective tissue growth factor; CXCL10, C-X-C motif chemokine 10; HGF, hepatocyte growth factor; MCP1, monocyte chemotactic protein 1; MMP14, matrix metalloprotease 14; PDGFB, platelet-derived growth factor subunit B; TGFB1, transforming growth factor beta subunit 1 (also TGFβ); TIMP2, tissue inhibitor of metalloprotease 2; VEGFA and R2, vascular endothelial growth factor subunit A and receptor 2.

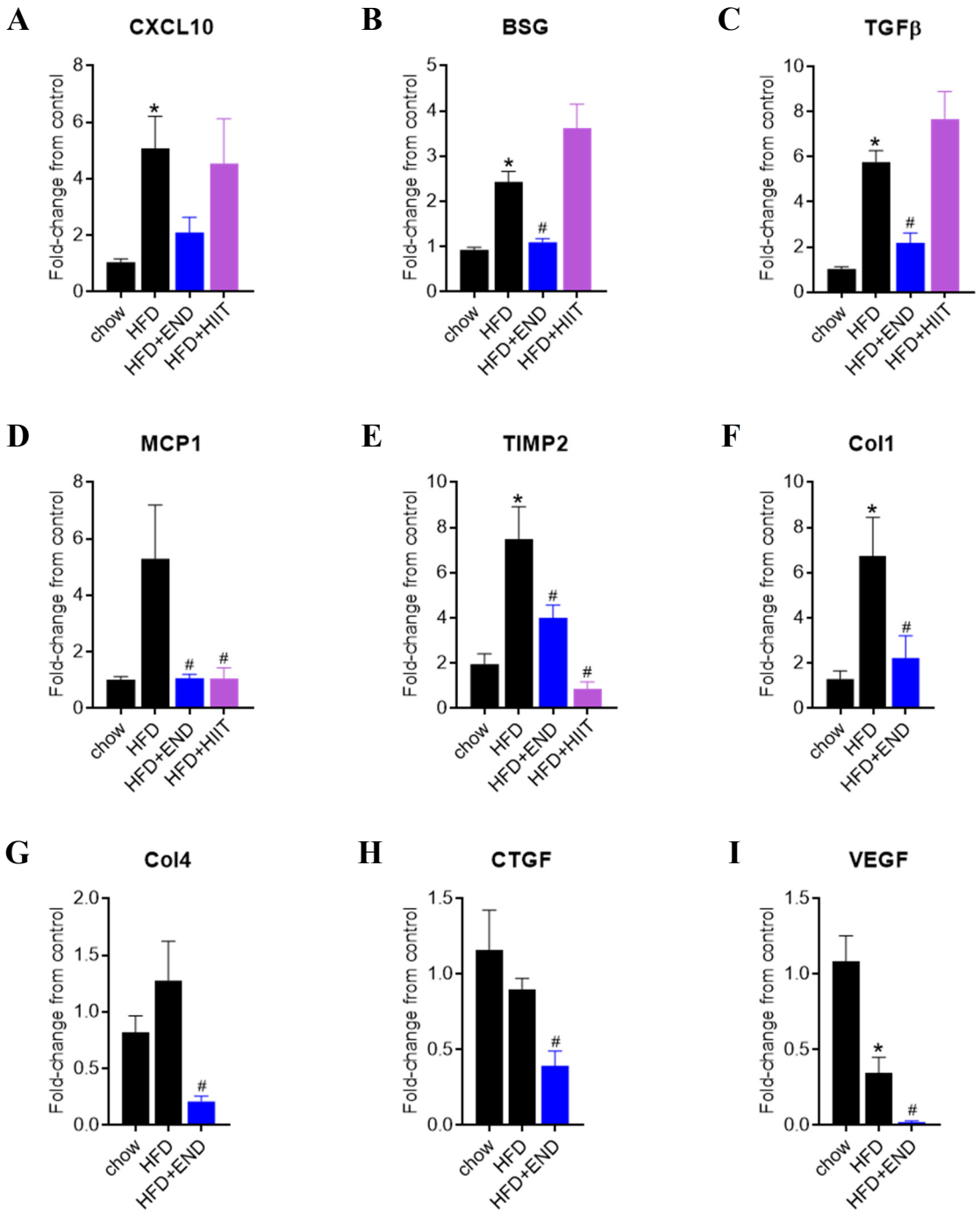

Figure 5.9. Liver gene expression for exercise intervention study. Genes where END was more effective than HIIT at normalising HFD changes (**A-C**), END and HIIT were equally as effective (**D-E**), END was effective and HIIT was unknown (**F-I**). Data show mean ± SEM for n=3-10 per group excluding outliers. Significant difference from control, untrained chow (*), or HFD ($^{\#}$) as determined by Student's t test, or where HIIT data was available, 2-way ANOVA (vs HFD) with Dunnett's test for multiple comparisons. See Figure 5.8 for gene abbreviations.

5.3.3. Extracellular vesicle enumeration

Consistent with previous findings in this thesis, dietary intervention (up to 20 weeks) failed to change the profile of either circulating or liver-derived EVs in mice. While EV abundance has been shown to fluctuate over time irrespective of diet (see Figures 3.8 and 4.7), the present data offers a snapshot of the effect of 10 weeks of exercise on these parameters.

At termination, there was no difference between untrained HFD and chow group for either plasma ($p=0.742$) or liver-derived ($p=0.931$) EV abundance, whereas the effects of the two training programs could be seen in both EV populations. Plasma EV number was increased by around 2-fold by END independently of diet (chow: $p=0.003$; HFD: $p=0.022$), while HIIT failed to show any changes (Figure 5.10A). In contrast, both programs similarly decreased liver-derived EVs (Figure 5.10B), by at least 15-fold in the chow cohort (END: $p=0.019$; HIIT: $p=0.015$ versus untrained) and at least 11-fold in the HFD cohort (both $p=0.011$ versus untrained HFD).

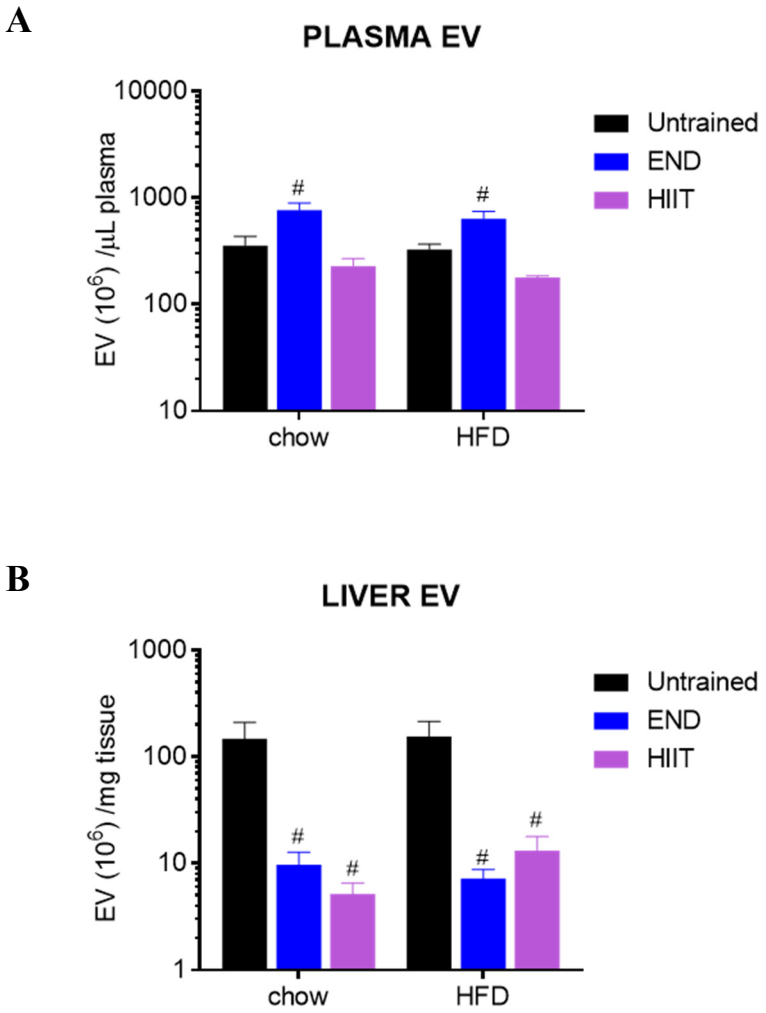

Figure 5.10. EV enumeration for exercise intervention study. Graphs represent plasma (**A**) and liver-derived EVs (**B**) corrected for volume and incubated tissue weight, respectively. Data are mean ± SEM for n=10-12 animals per group, excluding outliers. Significant difference from chow (*) or untrained ($^{\#}$) accepted at $p<0.05$ as determined by Student's t test (diet pairs), or 2-way ANOVA (training) with Dunnett's test for multiple comparisons

5.4. Interpretation

The outcomes of diet-induced obesity and its metabolic complications, including NAFLD, are a well recognised concept in modern healthcare systems. Given the plethora of guidelines that address NAFLD specifically (European Association for the Study of the Liver et al., 2016, Chalasani et al., 2018, LaBrecque et al., 2014) – from its socioeconomic burden to critique of screening efforts and importantly, a lack of reliable tools to assess disease progression – it is unsurprising that exploratory research to develop novel biomarkers has become so popular (see Table 1.3 in Chapter 1). EVs have also been considered as a desirable candidate (Ban et al., 2016), however, their translational utility is limited by the current technologies used for their isolation and characterisation. Furthermore, it can be expected that comorbidities or physical interventions may alter the EV profile, which hence can be used for monitoring disease progression. This Chapter aimed to dissect the interaction between HFD and a second variable in two models: one examining the role of an immune mediator in NAFLD development (TNF) through genetic manipulation of its expression (Chapter 5.2), and another comparing the effect of different exercise programs as a lifestyle intervention (Chapter 5.3).

5.4.1. Diet, TNF expression, and their combined effect on EVs

As described previously in Chapter 1, inflammatory molecules such as TNF are central to driving the progression of NAFL to NASH (Braunersreuther et al., 2012), which follows the paradigm of liver disease evolution from inflammation through fibrosis. Depending on the context, TNF will employ different signalling pathways via its receptors (TNFR1 and TNFR2) resulting in disparate outcomes for hepatocyte viability (Cosgrove et al., 2008, Xu et al., 1998). Previous studies have shown that steatotic hepatocytes stimulated with TNF *in vitro* are more prone to apoptosis (Zhang et al., 2010), which suggests that the TNFR1 pathway is likely to predominate. While viability was not investigated in this thesis, two other widely documented phenomena may be considered: TNF-mediated regulation of insulin signalling (leading to insulin resistance), and control of adipose tissue development and function.

It had been demonstrated in adipocytes that enzymes downstream of TNFR are capable of intercepting the insulin signalling pathway (Feinstein et al., 1993, Hotamisligil et al., 1994). Subsequent studies in obesity have supported this theory, with a majority of rodent high-fat feeding models noting that in the absence of TNF ligand or its receptors, animals fail to develop insulin resistance and their NAFLD severity is reduced when compared to WT mice on the same diet (Salles et al., 2012, Tomita et al., 2006, Uysal et al., 1997). Similar findings were also shown in genetic models of obesity (Kakino et al., 2018, Uysal et al., 1998). However, others have reported conflicting findings whereby TNF or TNFR deletion resulted in poorer insulin sensitivity and increased liver TAG (Chen et al., 2016, Pamir et al., 2009). One study also pointed to an increased propensity for weight gain in $TNF^{-/-}$ mice on HFD for 12 weeks when compared to WT (Chen et al., 2016), a phenotype that is consistent with the changes observed in our study using a comparable model (see Figure 5.11). In fact, even at baseline the transgenic cohort of our study was around 20% heavier, despite matching for age and diet. This could be explained by the cytokine's role in the regulation of adipocyte biology (Cawthorn and Sethi, 2008, Warne, 2003); that is, in the absence of TNF, both lipolysis and the associated suppression of lipogenesis are likely to be impaired. This in turn leads to an increase in the lipid storage/retention within adipose depots.

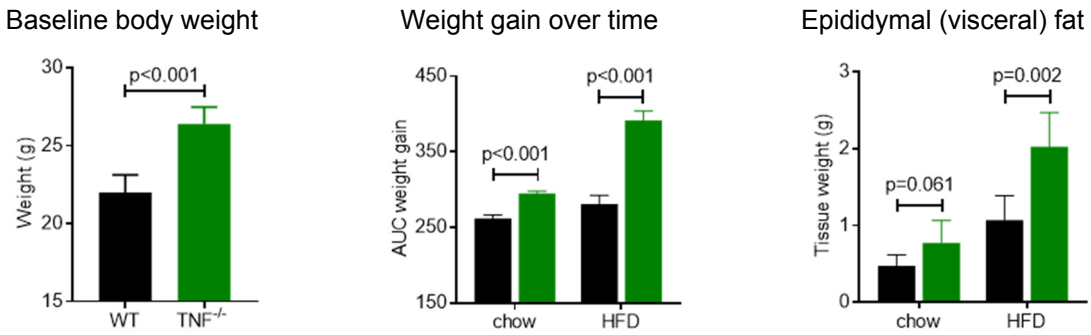

Figure 5.11. $TNF^{-/-}$ affects adipose tissue mass and weight gain. Body weight at baseline, weight gain during the experimental period (area under curve; AUC), and terminal adipose mass (epididymal) were all increased in transgenic mice (green) compared to wild-type (black), irrespective of diet. Data for n=4-8 animals per group; statistical analysis by Student's t tests ($p<0.05$ significant).

Therefore, we can assume that the accelerated liver steatosis during high-fat feeding relies on a mechanism other than FFA influx due to its liberation from adipose tissue. It is possible that 1) insulin resistance in transgenic mice (evidenced by hyperinsulinaemia) gives rise to excess lipid substrates in the liver through gluconeogenesis, or 2) since TNF is known to suppress fatty acid transporters (Memon et al., 1999, Memon et al., 1998), perhaps the increased expression of these proteins in TNF deficient animals act in synergy with dietary lipids to promote the formation of lipid droplets. Indeed, this was confirmed by a 2-fold elevation in hepatic TAG compared to WT mice on a HFD. Hepatic ORO staining was elevated in transgenic mice on a standard chow diet, suggesting that TNF alone may be involved in the regulation of other neutral lipids (including DAG, a precursor in TAG synthesis).

The gene expressions of fibrogenic markers (both fibrillar and network collagens, as well as TIMP1) were also substantially elevated in $TNF^{-/-}$ animals independently of diet, which was unusual given that TNF has been reported to promote the survival of hepatic stellate cells in the liver (Pradere et al., 2013), although findings on stellate cell activation are mixed (Knittel et al., 1999, Saile et al., 1999). In contrast to liver lipid, our histological findings showed an increase in collagen staining in WT livers after high-fat feeding, but not in the livers of transgenic animals. This pattern is more consistent with the aforementioned "inflammation driving fibrosis" paradigm, and therefore, it could be that the gene expression profile doesn't necessarily reflect protein expression or activity. However, this data was not investigated in our studies.

With respect to EVs, our data shows that TNF expression does not affect the EV profiles *per se*, however the increased liver size in $TNF^{-/-}$ animals may contribute to a higher abundance of liver-derived EVs in the circulation (or biliary system or lymphatics). Furthermore, it was shown that genotype does not influence the physical characteristics of EVs, at least in terms of their diameter, and together with our previous findings it may be assumed that EV biogenesis follows a tissue-specific pattern in mice. On the other hand, while it is possible that the EV molecular cargo was varied between treatment groups and may affect the hepatocyte phenotype, this was not investigated in our work.

5.4.2. Diet, exercise, and their combined effect on EVs

Lifestyle interventions are the current gold standard for the treatment of non-fibrotic NAFLD. These are usually delivered as a hypocaloric diet or aerobic training regimen, the latter of which is known to alleviate NAFLD burden, even in the absence of body weight changes (Johnson et al., 2009). This phenomenon was also reflected in our study, where a stagnation of weight gain was apparent only during the first five weeks of training, before eventually compensating for the caloric deficit and again matching the untrained group (see Figure 5.12). By termination, only HIIT had affected the fat depot weights (although interestingly, it seems that beige-like (Zhang et al., 2018) subcutaneous adipose tissue may have potentially been redistributed to the epididymal site, given the inverse changes in their weights).

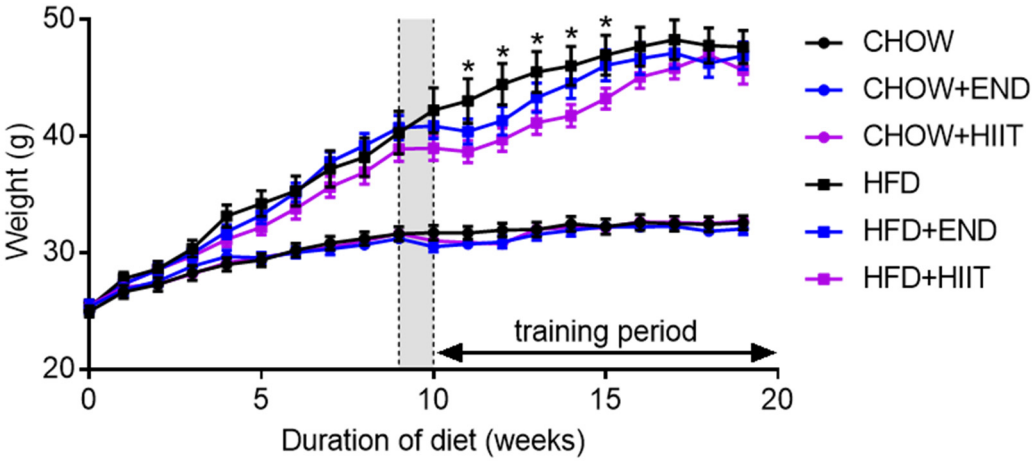

Figure 5.12. Weight gain chart for exercise intervention study. Grey band shows acclimation period. Data for n=10-12 animals per group; statistical analysis by 2-way ANOVA with Dunnett's test for multiple comparisons (*p<0.05 HFD+HIIT vs HFD).

In terms of the liver, both END and HIIT were effective in reducing the tissue weight as well as stabilising the HFD-mediated increase in liver enzymes (ALT and AST). On the other hand, these changes did not correlate with a quantitative decrease in hepatic lipids; the modest yet statistically significant increase in neutral lipids due to HFD (equivalent to lipid droplet formation and its precursors) was only reversed by HIIT, whereas the substantial HFD-induced increase in TAG was further elevated (around two-fold) by both training programs. This is unsurprising, as exercise is a known inducer of lipolysis in adipose tissue, thereby increasing the circulating FFA and compounding the effect of HFD.

The elevated hepatic TAG may also result from a combination of increased FFA influx and decreased efflux in VLDL lipoproteins, a phenomenon that has previously been reported in clinical exercise studies (Shojaee-Moradie et al., 2016, Sullivan et al., 2012) and in rodent models (Gorski et al., 1988, Horton et al., 1999). In this work, we showed an effect of both diet and exercise on plasma TAG (usually associated with VLDL), where HFD significantly decreased TAG in the absence of exercise, as noted in previous studies (Biddinger et al., 2005, Guo et al., 2009). END training prevented this change, which may imply that NAFLD-related derangements to VLDL secretion were normalised, liberating more TAG into the circulation. In contrast, HIIT showed a reduction in TAG with standard diet and an inability to normalise the HFD-induced decrease. In comparison to the quantitative changes in liver lipids, histological analysis showed a decrease in hepatocellular lipid droplets and fibrotic staining with exercise for mice on HFD. This result confirms the hepatoprotective effect of exercise, as most END and HIIT samples had only microvesicular steatosis which is evident in the earlier stages of NAFLD.

Analysis of gene expression was more specific in differentiating the exercise-related benefits on the liver. Using a gene array panel with predominantly inflammation and matrix turnover markers that are key to liver disease progression, we noted an intriguing pattern in the liver gene expressions relative to the control group (untrained standard chow): these tended to occur in two distinct profiles, independently of known molecular links, such that 1) where HFD increased gene expression, either exercise normalised these changes; or 2) only END training was capable of normalising the change with HFD whereas HIIT had no effect (or gene expression was undetectable for a majority of samples). Therefore, it appeared that END was more protective against the molecular changes associated with NAFLD progression (c.f. steatosis quantitation with ORO where HIIT showed greater efficacy). An example was collagen I, a fibrillar collagen subtype linked to hepatic fibrogenesis, which was regulated by END at both the mRNA (Figure 5.9) and protein level (Martinez-Huenchullan et al., unpublished manuscript).

Finally, the differential effects of exercise were once again reflected in the circulating and liver-derived EV profiles. Consistent with the trends seen throughout this thesis, there was no change concomitant with dietary intervention at this timepoint (20 weeks cross-section), for either of the studied EV populations. However, there was a substantial decline (over 10-fold) in vesicles released from the liver following either exercise program, with no statistical variation between END and HIIT within (and even across) respective dietary cohorts. While the mechanism for this is not entirely clear, it is interesting that these differences were maintained for the week preceding euthanasia when no exercise was performed. From a global perspective on the role of EVs in intercellular communication, it may be that incoming signals to the liver are more relevant than outgoing ones, a theory that may in fact be supported by a recent seminal study on the biodistribution of EVs following acute exercise (Whitham et al., 2018). Using intravital imaging of mice injected with fluorescently labelled EVs from exercised or sedentary donors, the authors showed that exercised EVs specifically will home to the liver (Whitham et al., 2018).

On the other hand, the abundance of plasma EVs in our study depended on the type of training: while EV numbers were doubled by END training, surprisingly, HIIT had no observable effect over untrained conditions for the respective diets. This raises two very interesting points. Firstly, the increased secretion of EVs into the circulation during moderate intensity exercise has been reported previously (Safdar et al., 2016). Characterisation and functional studies of these vesicles further show a link to haematological events (Durrer et al., 2015, Sossdorf et al., 2011, Wahl et al., 2014, Wilhelm et al., 2016), although their molecular cargo is unsurprisingly complex, involved in a diverse range of biological processes (Whitham et al., 2018). Secondly, the exercise protocol may impact the EV number, with a majority of studies (including all the aforementioned) examining the impact of an acute trial; either a single session, typically on a cycle ergometer, or multiple sessions across one week. Despite these limitations, there is potential for future studies to explore the correlation between EVs in exercise and other relevant clinical parameters such as cardiac output or quantitative muscle injury.

5.4.3. Functional relevance

Since there were no remarkable changes in the EV profile for transgenic animals on either diet (Figure 5.5), they were not investigated for their functional effects in this thesis, although the characterisation of these EVs and their physiological role would be of interest in future studies. On the other hand, EV samples obtained from exercised humans and mice have been shown to be involved in intercellular communication (Whitham et al., 2018). In our study, exercise-related changes in the EV profile suggest that interventions against diet-induced NAFLD (and obesity as a whole) may have a more significant impact on EV signalling than the metabolic condition itself. This is especially relevant for the END program, however, the trends in either EV profile do not tend to reflect the changes observed in other measured parameters; that is, they cannot be correlated with markers of NAFLD development unless the chow cohort is excluded from consideration. Given that liver-derived EVs for both END and HIIT groups were significantly reduced in abundance, it can be inferred that their collective effect *in vivo* is probably also limited. For this reason, only the highly abundant plasma EVs were considered for further mechanistic studies *in vitro* (Chapter 6).

Chapter 6.

Investigating the mechanism of action of extracellular vesicles in NAFLD

Chapter 6. Table of contents

6.1. Introduction

Previous studies in this thesis have explored the patterns of EV release *in vivo* in a dietary model of NAFLD, characterising both the circulating and liver-derived population of vesicles, and whether these were affected by lifestyle and genetic interventions. The two populations were found to be dissimilar in both their biogenesis (CD63 protein expression; see Figure 3.2) and abundance, with changes reported between treatment groups as well as over time and with exercise. However, a linear relationship was not observed between the temporal fluctuation of EVs and NAFLD severity defined by fibrosis or gene expression of ECM remodelling and inflammatory markers. This result would suggest that simply counting the number of EVs is not a useful marker of NAFLD progression. They are, however, useful in predicting steatosis level.

Another important point to consider is the link between EV abundance and their downstream effect on tissues; is abundance the limiting factor, or is the complex molecular cargo of EVs responsible for eliciting the changes seen in receptive cells? Such phenotypic changes have not yet been explored in the context of NAFLD, beyond controlled *in vitro* studies using hepatocyte models of lipotoxic stress where EVs from conditioned media were shown to affect hepatic stellate cell activation (Lee et al., 2017, Povero et al., 2015), macrophage activation (Cannito et al., 2017, Hirsova et al., 2016) and chemotaxis (Ibrahim et al., 2016, Kakazu et al., 2016), and angiogenic behaviour in endothelial cells (Povero et al., 2013). Similar studies in models of obesity have found that adipocyte-derived EVs may activate ECM remodelling in hepatic cells (Koeck et al., 2014) and macrophage-induced insulin resistance (Deng et al., 2009b), whereas in contrast, EVs from adipocyte stem cells promote the non-classical M2 polarisation of macrophages, in turn leading to increased insulin sensitivity (Zhao et al., 2018).

To address the "marker versus mediator" paradigm described in the literature, this Chapter aimed to combine *ex vivo* and *in vitro* systems to assess the mechanism of action of NAFLD-derived EVs on hepatocytes. These studies used a mouse hepatocyte cell line (AML12) stimulated with either liver-derived or plasma vesicles from animals described in the longitudinal study (Chapter 4) and the lifestyle intervention study (Chapter 5.3). Outcomes included the quantification of EV uptake by flow cytometry and the effect of this uptake on hepatocyte gene expression. Aside from co-culture with EVs, the hepatocyte cell line was otherwise untreated.

The gene expression studies assessed typical markers of hepatocyte inflammatory stress (TNF), growth factors (CTGF, TGFβ), tissue remodelling (MMP9, TIMP1) and fibrogenesis (collagen I), as in previous Chapters. To elaborate on the functional effect of EVs in an obesity context, some key players in hepatic lipid metabolism (Kohjima et al., 2007) were also characterised. Perilipin 2 (PLIN2) and liver-type fatty acid binding protein (L-FABP or FABP1) are both transporter proteins, however, they have different roles in lipid metabolism. While PLIN2 facilitates the uptake of neutral lipids into lipid droplets (Okumura, 2011), FABP1 is involved in the cellular import of long-chain fatty acids and their subsequent delivery to the peroxisome for beta oxidation (Atshaves et al., 2010, Binas and Erol, 2007). This catabolism of fatty acids is primarily mediated by the transcription factor peroxisome proliferator-activated receptor (PPAR) alpha, which is typically relevant during the post-absorptive state (Kersten et al., 1999, Leone et al., 1999), however, there is also a compensatory upregulation during NAFLD to handle the excess presence of fatty acids (Patsouris et al., 2006, Redonnet et al., 2001). On the other hand, sterol regulatory element-binding protein 1c (SREBP-1c) is a master transcriptional regulator for key enzymes that mediate *de novo* lipogenesis (Shimano et al., 1999) and is most abundant during the absorptive state, given its sensitivity to insulin (Foretz et al., 1999). While excess fatty acids would normally suppress the activity of SREBP-1c (Xu et al., 2001), both human and rodent studies have confirmed its elevation in the context of NAFLD (Kohjima et al., 2007, Yahagi et al., 2002).

Finally, when considering mass spectroscopic data, there was a significant fold-enrichment of carbohydrate kinases (also known as hexokinases) in liver EVs derived from HFD animals when compared to chow controls (see Chapter 4, section 4.4.2). Therefore, we also assessed the hepatocyte gene expression of the most abundant isoform of hexokinase in the liver, known as glucokinase (GCK), following EV stimulation. GCK is a low-affinity glucose sensor that phosphorylates its substrate to glucose-6-phosphate (Postic et al., 2001), the first step of carbohydrate metabolism and an upstream event of lipogenesis. In accordance with this, the bioavailability of GCK is regulated by plasma insulin levels via SREBP-1c in the absorptive state (Foretz et al., 1999), whereas an increase in the mRNA levels of GCK (Peter et al., 2011) and gene polymorphism of its regulator protein (Petit et al., 2016) are both associated with NAFLD development.

The anticipated outcome from this *ex vivo* study was to establish the possible mechanisms by which EVs communicate as "intercellular messengers" *in vivo*. Specifically, by stimulating AML12 hepatocytes with complex plasma and liver EV populations derived from our animal models – diluted to an equal concentration (as determined by NanoSight™) – we were able to resolve whether EVs have a pathogenic or compensatory role in NAFLD development, and whether this role is context dependent. The experimental workflow for the studies in this Chapter is shown in Figure 6.1 below.

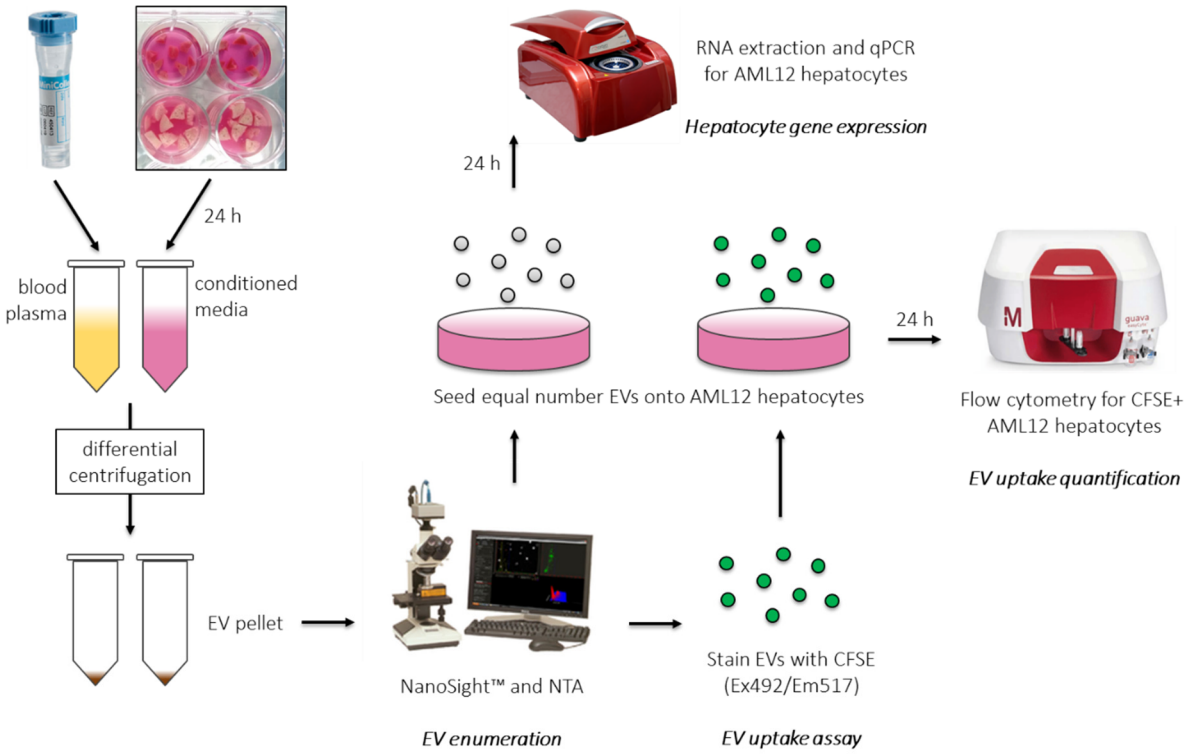

Figure 6.1. Experimental workflow for the functional analysis of EVs. For a more detailed explanation of the methodology, refer to Chapter 2 (section 2.8).

6.2. Extracellular Vesicle Uptake

Size is an inherent limitation for visually detecting EV uptake into cells. However, staining of EVs with fluorescent dye (lipophilic or cytosolic) allows for the co-localisation of vesicles and cell membrane or cytoplasm to be visualised, akin to protein immunofluorescence. Previous studies have performed this over an arbitrarily defined period (Koeck et al., 2014, Povero et al., 2013, Povero et al., 2015), although image resolution has been a persistent issue in the absence of confocal or three-dimensional techniques; that is, to accurately assess the cellular localisation of EVs (membrane adherence versus internalised).

Here, we used a quantitative approach to estimate EV uptake over a period of 24 hours. Uptake into hepatocytes was determined by quantifying CFSE-positive cells following exposure to EVs labelled with the fluorescent dye. Cells not exposed to EVs ("unstimulated") acted as controls; the positive control was CFSE-labelled hepatocytes, while negative controls were unlabelled. EV uptake into the cell samples was assessed using flow cytometry, whereby 5,000 events were recorded and the proportion of fluorescent events (versus unstained cells as the baseline) were considered positive for EV uptake. The cytometric gating strategy is outlined in Figure 6.2 and below.

6.2.1. Gating strategy for flow cytometry

Cells were first delineated from electrical noise by gating the population most distal from the forward scatter (FSC) threshold, on a forward-side scatter axis (FSC-SSC). This population typically represented at least 50% of events (Figure 6.2A). When considering CFSE-positive events on a forward scatter-green fluorescence axis, events were delineated by exclusion of the negative control population (defined in Figure 6.2B), while the positive control acted as a reference only (Figure 6.2C). A representative sample gated on cells, as defined in Figure 6.2A, shows the typical low-intensity CFSE staining following EV uptake (Figure 6.2D), whereas a green fluorescence histogram (Figure 6.3E) overlays the sample population (blue) with the negative control given in Figure 6.2B (white) and the positive control from Figure 6.2C (red). Gating with quadrants was also analysed, however, this strategy excluded many CFSE-positive events due to the obliqueness of the control populations.

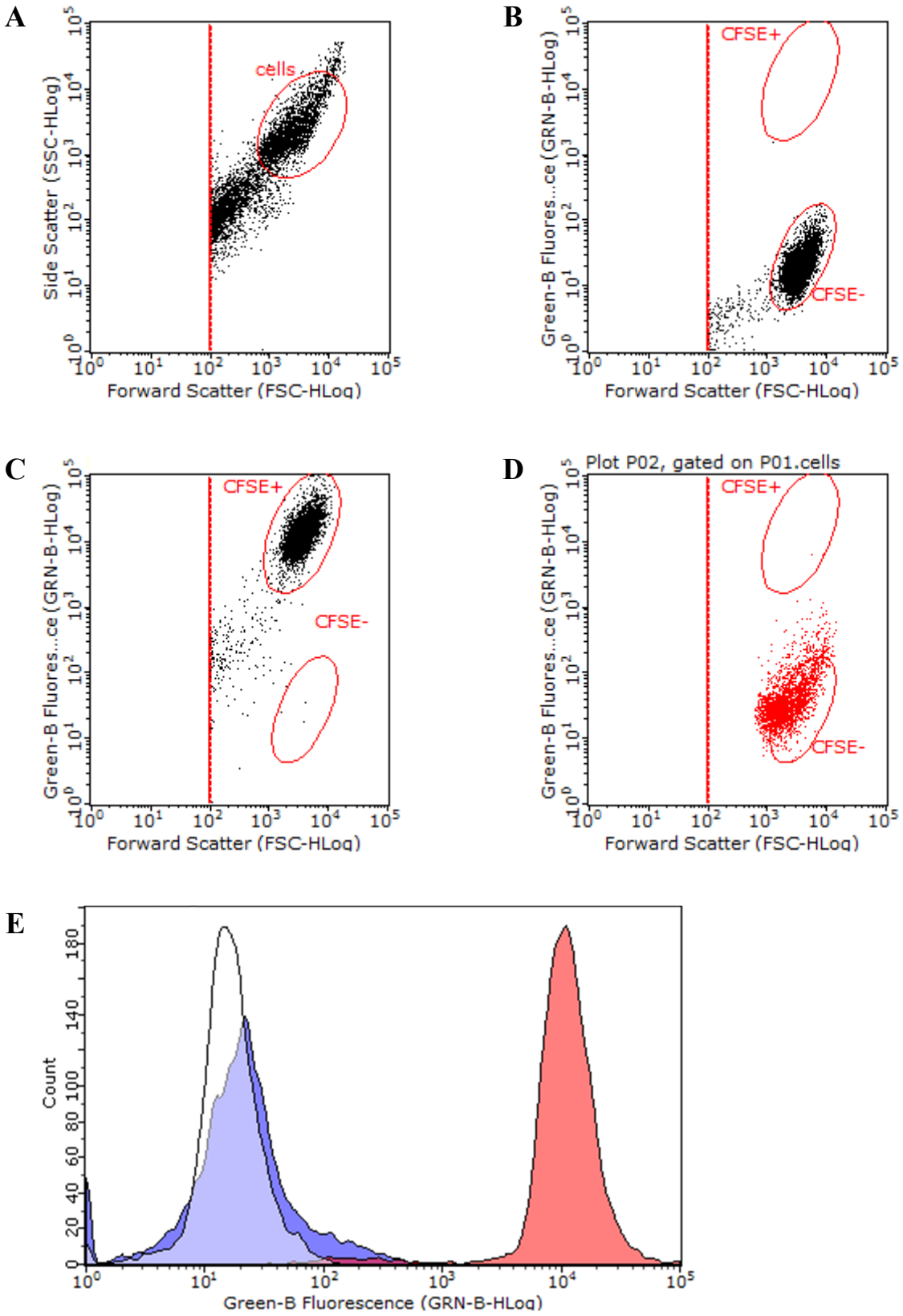
A
cells
Side Scatter (SSC-HLog)
Forward Scatter (FSC-HLog)
B
CFSE+
CFSE-
Green-B Fluores...ce (GRN-B-HLog)
Forward Scatter (FSC-HLog)
C
CFSE+
CFSE-
Green-B Fluores...ce (GRN-B-HLog)
Forward Scatter (FSC-HLog)
D
Plot P02, gated on P01.cells
CFSE+
CFSE-
Green-B Fluores...ce (GRN-B-HLog)
Forward Scatter (FSC-HLog)
E
Count
Green-B Fluorescence (GRN-B-HLog)

Figure 6.2. Gating strategy for hepatocellular EV uptake. A representative sample shows the *cell gate* on the forward-side scatter plot as defined by the unstimulated control populations (**A**). The forward scatter-green fluorescence plot was used to display CFSE negative (**B**) and positive (**C**) events, which included unstimulated unstained and unstimulated CFSE-stained hepatocytes, respectively. The same representative sample from panel A was gated on the *cell gate* (included events red, excluded events not visible) and compared against the *negative control (CFSE-) gate* as the baseline to determine the proportion of CFSE-positive cells (**D**). Finally, a histogram representing the sample (blue) with both controls overlayed (negative: white, positive: red) is shown to demonstrate the typical sample fluorescence profile (**E**).

6.2.2. Quantification of EV uptake by hepatocytes

Applying the gating strategies described above, uptake of fluorescently labelled EVs was quantified at 24 or 48 hr for samples isolated from animals in the NAFLD progression study (Chapter 4) and lifestyle intervention study (Chapter 5.3). Note that hepatocyte fluorescence following EV uptake was quite weak, and that uptake was not present in a majority of cells, with the sample population often overlapping the negative control (refer to Figure 6.2E).

6.2.2.1. EV uptake for NAFLD progression study

For hepatocytes exposed to plasma-derived EVs for 24 hr, there was no difference in uptake between diets up to 30 weeks, however CFSE-positive cells decreased from approx. 30% to 20% over time (Figure 6.3A). In contrast, a significant increase in the uptake of HFD-derived EVs became apparent at 50 weeks ($p=0.009$), which suggests a heightened responsiveness of hepatocytes to EVs from this context. By 48 hr, EV uptake was confined to less than 20% of cells and no differences were seen with either diet or treatment duration (data not shown). Furthermore, given that samples were matched across incubation time-points, it was possible to describe a significant overall decrease in uptake from 24 to 48 hr ($p<0.0001$; Wilcoxon matched-pairs signed rank test). For this reason, 24 hr was chosen as the desired time-point for further investigations on changes in hepatocyte phenotype (section 6.3).

Experiments using the same conditions were performed with liver-derived EVs at 24 hr only (Figure 6.3B), as widespread cell death was observed after 48 hr. Even at this time-point, under 25% of cells were CFSE-positive for all treatment groups. There were no differences between diets, with the exception of 20 weeks, where a peak in the uptake of EVs from chow fed animals coincided with a transient decrease in the HFD group ($p=0.020$). The decline in absolute EV uptake (as a proportion of cells) can be attributed to discrepancies in EV concentrations: EVs from liver were incubated at 50/μL while those from plasma were incubated at 1,000/μL, owing to sample availability.

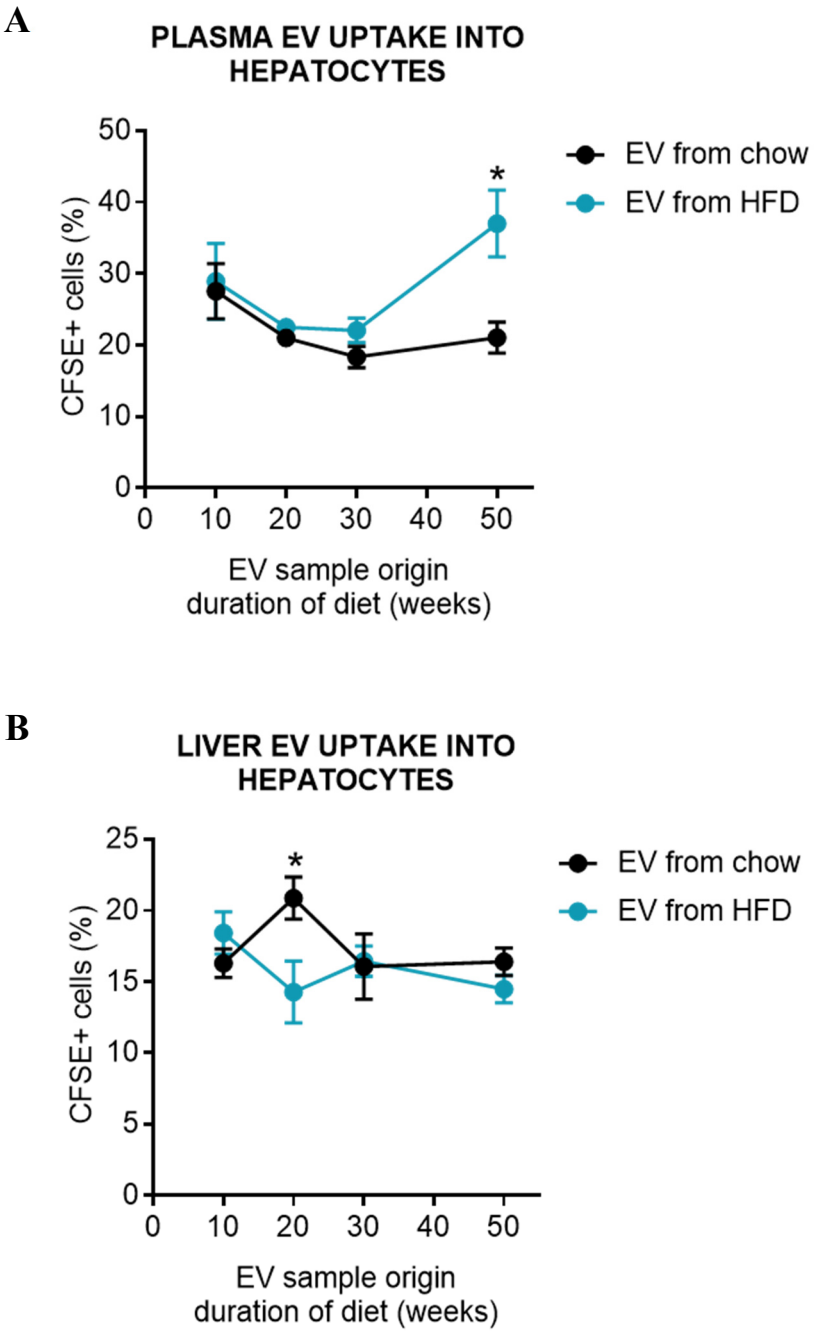

Figure 6.3. Quantification of EV uptake during NAFLD progression. CFSE-labelled EVs were incubated with a mouse hepatocyte cell line (AML12) to determine EV uptake, defined by percentage of CFSE-positive cells. Hepatocytes were exposed to plasma-derived (**A**) or liver-derived EVs (**B**) for 24 hr. Data is mean ± SEM for n=3-6 samples per group, with significant difference from chow accepted at $p<0.05$ (*) by 2-way ANOVA with Bonferroni's test for multiple comparisons. Abbreviations: CFSE, carboxyfluorescein succinimidyl ester.

6.2.2.2. EV uptake for lifestyle intervention study

Given the substantial decline in the number of liver-derived EVs following either exercise regimen, both independently of diet (see Chapter 5.3), functional analyses were performed only on plasma EVs. Henceforth, EV uptake and hepatocyte phenotype data will refer to plasma-derived EVs for the lifestyle intervention study. Intriguingly, despite a significant increase in the abundance of EVs during END training for both HFD and standard chow diet, exposing hepatocytes to a uniform number of vesicles (1,000/μL as above) did not impact on their responsiveness (Figure 6.4). That is, neither diet nor exercise status of the sample source had a significant effect on the uptake of plasma EVs into hepatocytes.

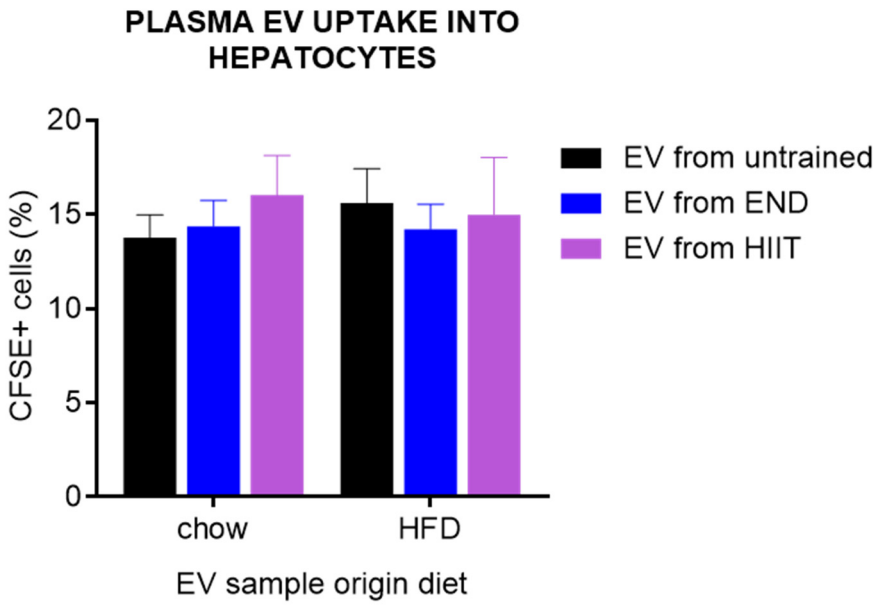

Figure 6.4. Quantification of EV uptake during exercise intervention for NAFLD. CFSE-labelled EVs were incubated with a mouse hepatocyte cell line (AML12) to determine EV uptake, defined by percentage of CFSE-positive cells. Hepatocytes were exposed to plasma-derived EVs for 24 hr. Data is mean ± SEM for n=4 samples per group, with significant difference from chow or untrained accepted at $p<0.05$ by 2-way ANOVA with Bonferroni's test or Dunnett's test for multiple comparisons, respectively. Abbreviations: CFSE, carboxy-fluorescein succinimidyl ester.

6.3. Effects on Hepatocyte Phenotype

In line with the data from previous Chapters, we first assessed whether heterologous EV uptake would affect the transcription of molecules involved in ECM remodelling and inflammation in hepatocytes (Calabro et al., 2014). Drawing on the data obtained from the characterisation of liver EVs by mass spectrometry, we then analysed how these EVs can modulate the hepatocyte gene expression of molecules associated with lipid metabolism (detailed in section 6.1).

6.3.1. Effect of donor EVs from a context of NAFLD progression

For this investigation, hepatocytes were stimulated with either plasma-derived EVs from mice spanning the entire progression study (10-50 weeks HFD or chow; see Chapter 4) or liver-derived EVs from either the young (10 weeks) or old (50 weeks) treatment groups. Two unstimulated hepatocyte samples acted as controls. Table 6.1 summarises the contribution of diet and age of the EV donors as a source of variation in the hepatocyte gene expression.

As a general rule, there was a significant effect of aging on expression of all markers when the mouse hepatocytes were exposed to plasma EVs (Table 6.1). Where aging accounted for a lower percentage of the total variation (less than 40%), there was an additional significant effect of diet on the mRNA trends (TNF: 13.8%, MMP9: 8.54%, others less than 2% and $p>0.05$). In terms of liver-derived EVs, the outcomes were more heterogeneous. Among the inflammation and ECM remodelling markers, only TNF expression was significantly affected by donor EV diet but not their age. This time, MMP9 was unaffected by the diet of EV donors whereas their age was almost exclusively responsible for any changes observed. In contrast, the expression of collagen I and TIMP1 were regulated by both factors. Perhaps the most profound finding, on the other hand, was that – with the exception of PLIN2 – there was no effect of donor HFD (and by extension, their NAFLD status) on the expression of lipid metabolism markers in recipient hepatocytes. As before, aging was a significant driver of gene expression changes across most samples, whereas interestingly, SREBP-1c was not significantly affected by either factor, despite a relatively higher percentage for diet as a source of variation (14.6%, $p=0.192$).

Table 6.1. Effect of diet and age of donor EVs on variation in the recipient hepatocyte phenotype.

Gene of interest	*Plasma EVs*				*Liver EVs*			
	Diet effect		*Age effect*		*Diet effect*		*Age effect*	
	%	*p value*	*%*	*p value*	*%*	*p value*	*%*	*p value*
Inflammation and ECM:								
TNF	13.8	**0.010**	16.3	**0.048**	33.3	**0.035**	2.60	0.515
Col1	0.02	0.907	42.7	**0.000**	5.95	**0.014**	86.3	**0.000**
MMP9	8.54	**0.014**	26.3	**0.001**	0.31	0.545	90.3	**0.000**
TIMP1	0.00	0.970	73.8	**0.000**	21.3	**0.040**	33.0	**0.014**
CTGF	0.08	0.805	47.4	**0.000**	-	-	-	-
TGFβ	1.05	0.347	47.7	**0.000**	-	-	-	-
Lipid metabolism:								
SREBP-1c	-	-	-	-	14.6	0.192	0.22	0.867
GCK	-	-	-	-	0.14	0.709	89.1	**0.000**
PLIN2	-	-	-	-	28.0	**0.043**	10.3	0.194
PPARγ	-	-	-	-	2.33	0.468	52.1	**0.005**
PPARα	-	-	-	-	7.54	0.232	37.1	**0.017**
FABP1	-	-	-	-	0.52	0.378	93.1	**0.000**

Data analysis for plasma EVs from whole cohort (10-50 weeks; n=43) or liver EVs from young versus old animals (10 and 50 weeks; n=15). Two-way ANOVA was used to determine the individual effect of either diet or age (of EV source) on the cell expression of each gene, as a percentage of the total variation in that gene (%). The associated p values are also shown; a significant contribution to total variation ($p<0.05$) is highlighted in bold. Abbreviations: ECM, extracellular matrix; TNF, tumour necrosis factor; Col1, collagen I; MMP9, matrix metalloproteinase 9; TIMP1, tissue inhibitor of metalloproteinase 1; CTGF, connective tissue growth factor; TGFβ, transforming growth factor beta; SREBP-1c, sterol regulatory element-binding protein 1c; GCK, glucokinase; PLIN2, perilipin 2; PPARγ or α, peroxisome proliferator activated receptor gamma or alpha; FABP1, fatty acid binding protein 1.

6.3.1.1. Inflammation, ECM and growth factors

To assess the capacity of EVs to stimulate a NAFLD-like inflammatory stress in hepatocytes, the gene expression of cellular TNF was quantified. When exposed to plasma-derived EVs from a standard chow background, TNF tended to decrease with the 20 and 30 week EVs when compared to unstimulated cells ($p<0.003$; one sample t test), however, there was no statistically significant deviation over time (Figure 6.5A). In contrast, hepatocytes were highly responsive to EVs from a NASH background (50 weeks HFD), which resulted in a significantly increased TNF expression when compared to either 10 weeks HFD ($p=0.019$) or age-matched chow ($p=0.004$). In contrast , an opposite pattern was seen for markers of ECM remodelling; collagen I (Figure 6.5B) was decreased with increasing age for both diets albeit to a greater extent for HFD (chow: $p=0.045$, HFD: $p<0.001$; 10 versus 50 weeks), whereas TIMP1 (Figure 6.5C) was also decreased relative to unstimulated cells ($p<0.001$ for all groups except 10 week chow). A similar pattern was observed for MMP9 expression (Figure 6.5D), although a transient peak from exposure to 20 week chow EVs meant that the aging trends for either diet were rendered not significant. Both of the studied hepatocyte growth factors – CTGF (Figure 6.5E) and TGFβ (Figure 6.5F) – declined with the donor EV age, however this effect was more prominent for chow-derived samples ($p<0.001$ both markers; 10 versus 50 weeks) than for HFD samples (CTGF: $p=0.035$, TGFβ: $p=0.095$). Due to the relatively small impact of EVs from HFD mice, growth factors were not studied for liver-derived EV stimulation.

A

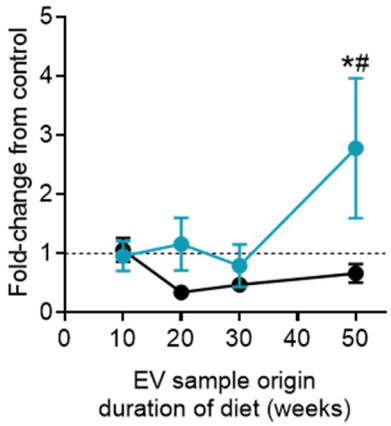
TNF hepatocyte mRNA
Fold-change from control
*#
EV sample origin
duration of diet (weeks)

B

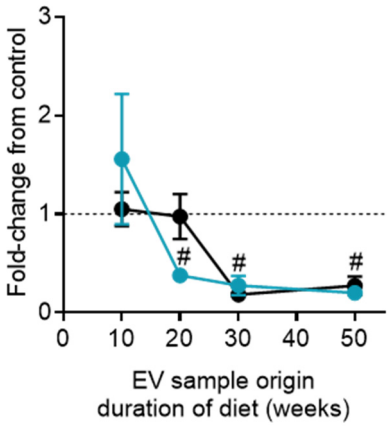
Col1 hepatocyte mRNA
Fold-change from control
#
#
#
EV sample origin
duration of diet (weeks)

C

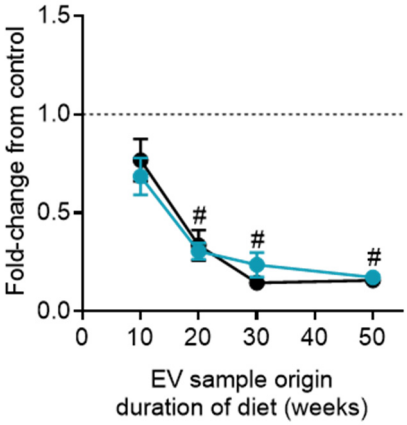
TIMP1 hepatocyte mRNA
Fold-change from control
#
#
#
EV sample origin
duration of diet (weeks)

D

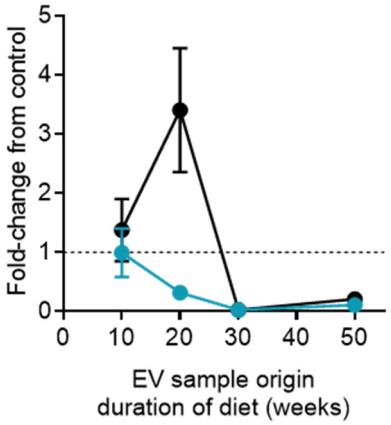
MMP9 hepatocyte mRNA
Fold-change from control
EV sample origin
duration of diet (weeks)

E

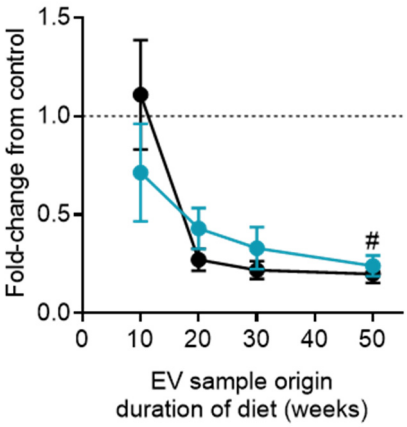
CTGF hepatocyte mRNA
Fold-change from control
#
EV sample origin
duration of diet (weeks)

F

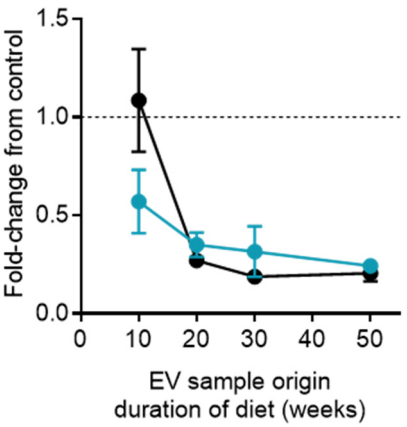
TGFβ hepatocyte mRNA
Fold-change from control
EV sample origin
duration of diet (weeks)

Figure 6.5. Gene expression of ECM markers following plasma EV uptake. Data shows mean ± SEM as fold-change from control (unstimulated hepatocytes) for n=4-6 animals/ group for chow (black line) and HFD (blue line). Analyses for HFD groups that were significantly different from age-matched chow (*) or 10 week HFD ($^{\#}$) by 2-way ANOVA with Bonferroni's test (diet) or Dunnett's test (age) for multiple comparisons. Abbreviations: TNF, tumour necrosis factor; Col1, collagen I; TIMP1, tissue inhibitor of metalloproteinase 1; MMP9, matrix metalloproteinase 9; CTGF, connective tissue growth factor; TGFβ, transforming growth factor beta.

To observe the changes in hepatocyte phenotype when stimulated with liver-derived EVs, cells were exposed to EVs from mice on either diet at 10 or 50 weeks. Interestingly, cellular TNF expression (Figure 6.6A) increased by over 5-fold following stimulation with EVs from any treatment group, when compared to the unstimulated control. This reached statistical significance for all but the 50 week HFD group ($p=0.128$), whereas neither the age nor diet related changes were significant, despite an apparent decrease with HFD at both timepoints. Consistent with the findings in Figure 6.5 using plasma-derived EVs, hepatocyte expression of ECM markers were more profoundly influenced by the age of the liver EV source rather than by its diet. For collagen I (Figure 6.6B) this is highlighted by an increase over time ($p<0.001$ both diets) whereas HFD also produced a further increase at 50 weeks ($p=0.027$ versus age-matched chow diet). While HFD did not affect the expression of either TIMP1 (Figure 6.6C) or MMP9 (Figure 6.6D) at either timepoint, MMP9 levels were significantly elevated by over 15-fold at 50 weeks, irrespective of diet (both $p<0.001$).

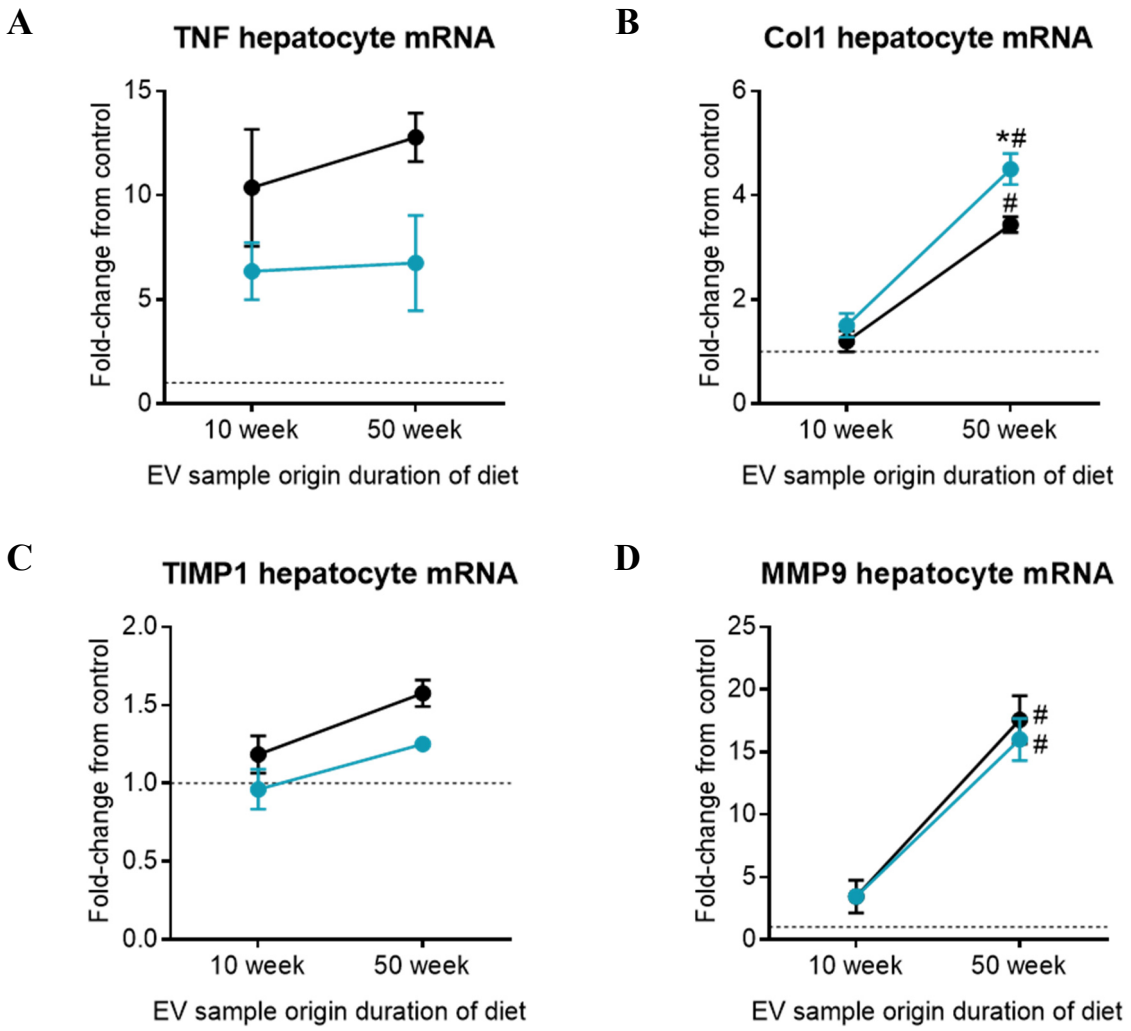

Figure 6.6. Gene expression of inflammation and ECM markers following liver EV uptake. Data shows mean ± SEM as fold-change from control (unstimulated hepatocytes) for n=3-5 animals/group for standard chow (black line) and high-fat diet (blue line). Significantly different from age-matched chow (*) or 10 week diet ($^{\#}$) by 2-way ANOVA with Bonferroni's test for multiple comparisons. Abbreviations: TNF, tumour necrosis factor; Col1, collagen I; MMP9, matrix metalloproteinase 9; TIMP1, tissue inhibitor of metalloproteinase 1.

6.3.1.2. Lipid metabolism

To complement the findings in Chapter 4 (section 4.4.2), which identified some treatment-enriched and shared EV proteins involved in lipid metabolism, the hepatocyte transcripts of markers involved in lipogenesis, lipid droplet formation and beta oxidation were analysed after stimulation with liver-derived EVs. There was no change by either diet or age of EV source for the master regulator of *de novo* lipogenesis, SREBP-1c (Figure 6.7A). On the other hand, hepatocyte GCK was significantly elevated following exposure to EVs from 50 weeks of either diet ($p<0.001$), however, there was no difference between the diets (Figure 6.7B). The development of lipid droplets was assessed by determining the hepatocyte expression of the transporter protein PLIN2 as well as the lipogenic regulator PPARγ. Interestingly, PPARγ expression was unaffected by diet, although stimulation with EVs from 50 weeks HFD was statistically elevated ($p=0.030$) when compared to the effect of EVs from livers at 10 weeks HFD (Figure 6.7C). Gene expression of PLIN2 was not changed when stimulated with EVs from different treatment groups (Figure 6.7D), and the same was observed for PPARα expression (Figure 6.7E). Finally, in a manner similar to GCK, the lipid transporter protein FABP1 was increased by the age of the EV source ($p<0.001$ both HFD and chow), independently of any dietary changes (Figure 6.7F).

***De novo* lipogenesis**

A

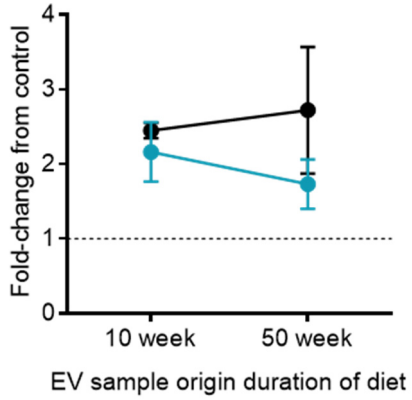

B

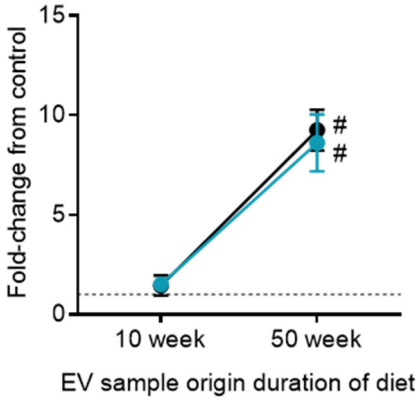

Lipid droplet

C

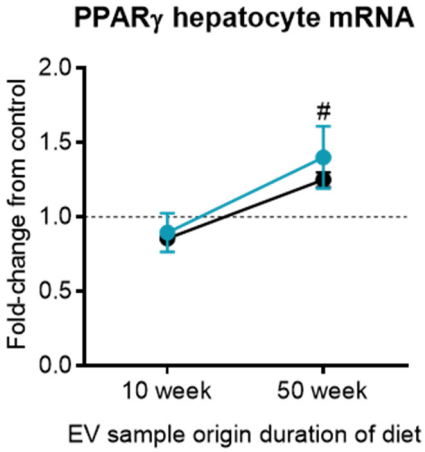

D

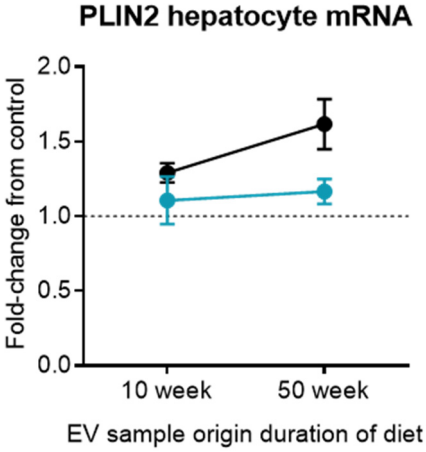

Beta oxidation

E

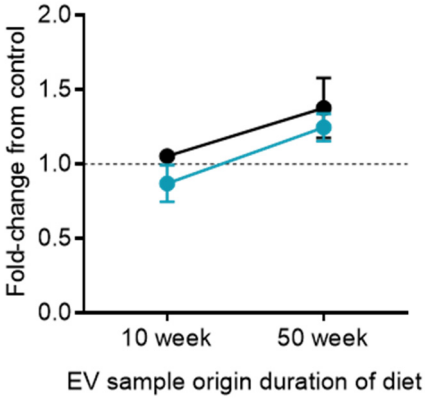

F

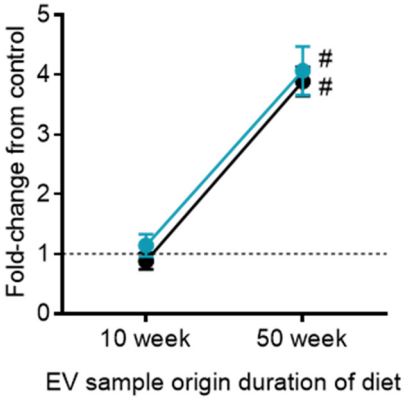

Figure 6.7. Gene expression of lipid metabolism markers following liver EV uptake. Data shows mean ± SEM as fold-change from control (unstimulated hepatocytes) for n=3-5 animals/group for standard chow (black line) and high-fat diet (blue line). Significantly different from 10 week diet ($^{\#}$) by 2-way ANOVA with Bonferroni's test for multiple comparisons. Abbreviations: SREBP-1c, sterol regulatory element-binding protein 1c; GCK, glucokinase; PPARγ or α, peroxisome proliferator activated receptor gamma or alpha; PLIN2, perilipin 2; FABP1, fatty acid binding protein 1.

6.3.2. Donor EVs from a context of exercise intervention

While it was predicted that EVs from a NAFLD progression context may promote a NAFLD-like change in hepatocyte gene expression, on the other hand, it was hypothesised that EVs from exercised animals would have a protective effect. The overall contribution of each independent variable – that is, diet and exercise – to the changes in gene expression imparted by EVs is outlined in Table 6.2. For genes of interest that were significantly affected by either variable, further statistical analyses were performed to highlight the changes between specific treatment groups (see Figure 6.8). With reference to the source of variation, there was a significant effect of donor EV diet but not exercise status for TNF and TIMP1 hepatocyte expression, whereas the opposite was true for collagen I and MMP9 (Table 6.2). When markers of lipid metabolism were considered, only PLIN2 expression was affected by both diet and exercise status of EV donors, while PPARγ and SREBP-1c were significantly affected by exercise only. Although GCK expression was weakly influenced by exercise status, this trend was not significant ($p=0.094$), whereas neither variable affected the expression of PPARα and FABP1. Since the latter two genes are involved in beta oxidation, it was assumed that the plasma EVs from this study do not regulate this process, and so no further analysis was performed for these genes.

Table 6.2. Effect of diet and exercise status of donor EVs on variation in the recipient hepatocyte phenotype.

Gene of interest	*Plasma EVs*			
	Diet effect		*Exercise effect*	
	%	*p value*	*%*	*p value*
Inflammation and ECM:				
TNF	21.4	**0.021**	11.7	0.204
Col1	0.43	0.731	30.2	**0.030**
MMP9	6.98	0.137	35.0	**0.010**
TIMP1	23.3	**0.014**	16.5	0.099
Lipid metabolism:				
SREBP-1c	0.18	0.812	37.9	**0.009**
GCK	0.06	0.898	20.3	0.094
PLIN2	17.5	**0.024**	27.9	**0.021**
PPARγ	8.86	0.103	35.8	**0.010**
PPARα	3.73	0.336	17.9	0.129
FABP1	4.60	0.265	1.65	0.791

Data analysis for plasma EVs, excluding outliers (n=4 per treatment group, n=24 total). Two-way ANOVA was used to determine the individual effect of either diet or exercise status (of EV source) on the cell expression of each gene, as a percentage of the total variation in that gene (%). The associated p values are also shown; a significant contribution to total variation ($p<0.05$) is highlighted in bold. Abbreviations: ECM, extracellular matrix; TNF, tumour necrosis factor; Col1, collagen I; MMP9, matrix metalloproteinase 9; TIMP1, tissue inhibitor of metalloproteinase 1; SREBP-1c, sterol regulatory element-binding protein 1c; GCK, glucokinase; PLIN2, perilipin 2; PPARγ or α, peroxisome proliferator activated receptor gamma or alpha; FABP1, fatty acid binding protein 1.

When analysing the changes between individual groups, no significant trends were observed among the standard chow cohort (data not shown), except for a decrease in collagen I expression ($p=0.034$) following exposure to HIIT-derived EVs versus the untrained group. There were also no significant changes between the two diets in the absence of exercise, therefore, the data presented in Figure 6.8 only shows the effect of EVs from the HFD cohort on hepatocyte gene expression. Overall, the fluctuations in gene expression were quite small (less than 2-fold). Due to the high intragroup variation within one or more treatment groups, no significant differences were recorded for EV-induced hepatocyte expression of TNF (Figure 6.8A), collagen I (Figure 6.8B) or TIMP1 (Figure 6.3C). In contrast, MMP9 was decreased following stimulation with EVs from donors undergoing either of the exercise regimens (END: $p=0.015$, HIIT: $p=0.013$) compared to untrained HFD (Figure 6.8D). While a similar pattern was observed for GCK expression (Figure 6.8E), the changes were not significant (END: $p=0.114$, HIIT: $p=0.065$). Finally, plasma EVs from the HIIT but not END regimen were able to reduce the gene expression of SREBP-1c (Figure 6.8F), PPARγ (Figure 6.8G) and PLIN2 (Figure 6.8H).

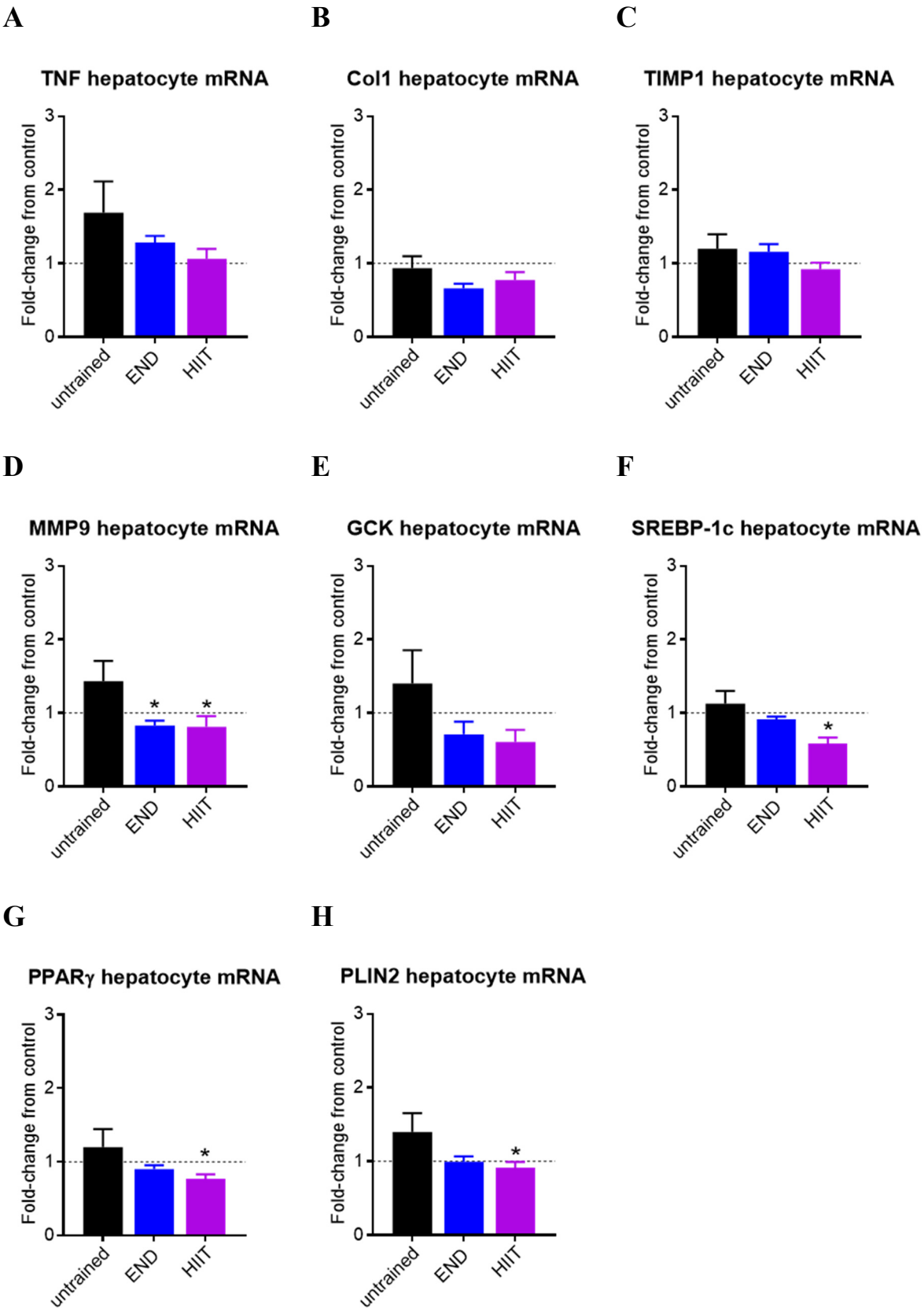
A
TNF hepatocyte mRNA
Fold-change from control
0
1
2
3
untrained
END
HIIT
B
Col1 hepatocyte mRNA
Fold-change from control
0
1
2
3
untrained
END
HIIT
C
TIMP1 hepatocyte mRNA
Fold-change from control
0
1
2
3
untrained
END
HIIT
D
MMP9 hepatocyte mRNA
Fold-change from control
0
1
2
3
*
*
untrained
END
HIIT
E
GCK hepatocyte mRNA
Fold-change from control
0
1
2
3
untrained
END
HIIT
F
SREBP-1c hepatocyte mRNA
Fold-change from control
0
1
2
3
*
untrained
END
HIIT
G
PPARγ hepatocyte mRNA
Fold-change from control
0
1
2
3
*
untrained
END
HIIT
H
PLIN2 hepatocyte mRNA
Fold-change from control
0
1
2
3
*
untrained
END
HIIT

Figure 6.8. Gene expression following HFD and exercised plasma EV uptake. Data shows mean ± SEM as fold-change from control (untrained standard chow diet) for n=4 animals/group for HFD cohort only. Significant difference from untrained HFD (*) by 2-way ANOVA with Dunnett's test for multiple comparisons (analysis of chow cohort not shown). Abbreviations: TNF, tumour necrosis factor; Col1, collagen I; TIMP1, tissue inhibitor of metalloproteinase 1; MMP9, matrix metalloproteinase 9; SREBP-1c, sterol regulatory element-binding protein 1c; GCK, glucokinase; PPARγ, peroxisome proliferator activated receptor gamma; PLIN2, perilipin 2.

6.4. Interpretation

Ultimately, the aim of the investigations in this Chapter were to observe whether EVs from a NAFLD context may recapitulate this phenotype by transferring their molecular information to a hepatocyte cell line. Cells were exposed to a uniform number of vesicles to control for any variations in EV abundance across samples; in this way, any effects of EV stimulation were dependent only on the hepatocyte responsiveness to EVs from a given treatment group. While exercise status had a negligible effect on plasma EV uptake, in contrast, vesicles from a NASH background (50 weeks HFD) were more likely to be endocytosed by hepatocytes (by almost two-fold), which corresponded with an increase in the gene expression of TNF. On the other hand, uptake of liver-derived EVs tended to be stable over time, with the exception of a statistically significant decrease (around 30%) in the uptake of vesicles from the 20 week HFD group. However, in order to align with the EV characterisation studies in Chapter 4, only 10 and 50 week EV samples – representing NAFL and NASH timepoints, respectively – were considered for the hepatocyte phenotype study.

While EV uptake in an *in vitro* NAFLD system has been previously documented, although not necessarily quantified (Koeck et al., 2014, Povero et al., 2013, Povero et al., 2015), hepatocyte stimulation with heterologous EVs from plasma or liver has not yet been reported. Rather, most models that examine EVs in the context of hepatic lipotoxicity are conducted entirely *in vitro*, whereby the vesicles are isolated from the hepatocyte conditioned media following incubation with palmitate; the EVs are then used to stimulate other cell lines, such as hepatic stellate cells (Lee et al., 2017, Povero et al., 2015), macrophages (Hirsova et al., 2016) or endothelial cells (Povero et al., 2013). These studies effectively highlight the paracrine or endocrine influence of steatotic hepatocytes via EVs, however, the reverse interactions are seldom explored and may provide some useful insight into the pathogenesis of NAFLD.

There have been two studies to date that have examined the phenotypic alterations in hepatocytes (HepG2 line) following EV exposure, both having sourced the vesicles from adipose tissue explants (Koeck et al., 2014, Kranendonk et al., 2014b). Interestingly, adipose EVs tended to impair insulin signalling in hepatocytes (Kranendonk et al., 2014b), whereas the gene expression of TIMP1 was reportedly elevated by EV stimulation, irrespective of the donor's obesity status (Koeck et al., 2014). While the latter study was arguably of small scale (n=5), it did highlight a dose-independent effect of EVs on hepatocyte phenotype, although intriguingly, uptake of EVs was significantly more pronounced when sourced from obese donors (Koeck et al., 2014).

These findings were in line with our observations following plasma EV treatment of AML12 hepatocytes, but this pattern was not reflected upon stimulation of the hepatocytes with liver EVs. This may suggest an important discrepancy between systemic or endocrine signalling from complex tissue sources and paracrine signalling from the liver. In fact, when taken collectively, the age of the plasma EV donor was significantly more likely to modulate the gene expression of growth factors and markers of ECM turnover than obesity status (Table 6.1). This in turn manifested as a gradual decline over time (Figure 6.5), whereas the opposite trend – significant or otherwise – was shown for liver EV stimulation of hepatocytes (Figure 6.6). Interestingly, a greater dietary influence was also reported for the latter (Table 6.1).

On the other hand, when markers of lipid metabolism were considered (Figure 6.7), the most pronounced changes were noted in discordant biological processes; that is, there was a significant positive effect of donor age on the expression of GCK (involved in lipogenesis) as well as the lipid transporter FABP1 (involved in beta oxidation). While the mechanisms behind these changes remain unclear, studies in rats have shown an age-related decline in liver FABP1 (Singer et al., 1996) and an impaired efficiency of GCK restoration in the absorptive state (Adelman and Freeman, 1972), which seems to imply a compensatory role for liver EVs in this context. However, it was suggested in the latter study that a decrease in circulating insulin may be responsible for the changes in GCK activity (Adelman and Freeman, 1972), whereas this finding was not seen in our EV donor cohort.

Hepatocytes were also amenable to plasma EVs from exercised donors, although changes in gene expression remained within a modest 2-fold range. While this may be explained by the low uptake of plasma EVs (approximately 15% cells), there were statistically significant changes across treatment groups within the HFD cohort (Figure 6.8). Firstly, there was a tendency for "exercise EVs" to decrease the expression of TNF and markers of ECM remodelling; however, only MMP9 was significantly affected when compared to EVs from untrained HFD, which was independent of the exercise protocol. A similar pattern was noted for GCK, although the higher intragroup variation meant the changes did not reach significance. Intriguingly, the hepatocyte expression of lipogenic markers were all suppressed by plasma EVs from HIIT-exercised HFD animals, but unaffected by END. Unlike the compensatory effects of liver EVs from the NAFLD progression study, these findings seemed to indicate an endocrine-mediated protective role, since HIIT itself has been shown to regulate both SREBP-1c (Kalaki-Jouybari et al., 2018) and PPARγ (Motta et al., 2016) in obese rodent livers, while PLIN2 depletion impairs hepatic lipid storage (Chang et al., 2006). A schematic of our findings for lipid metabolism genes is shown in Figure 6.9.

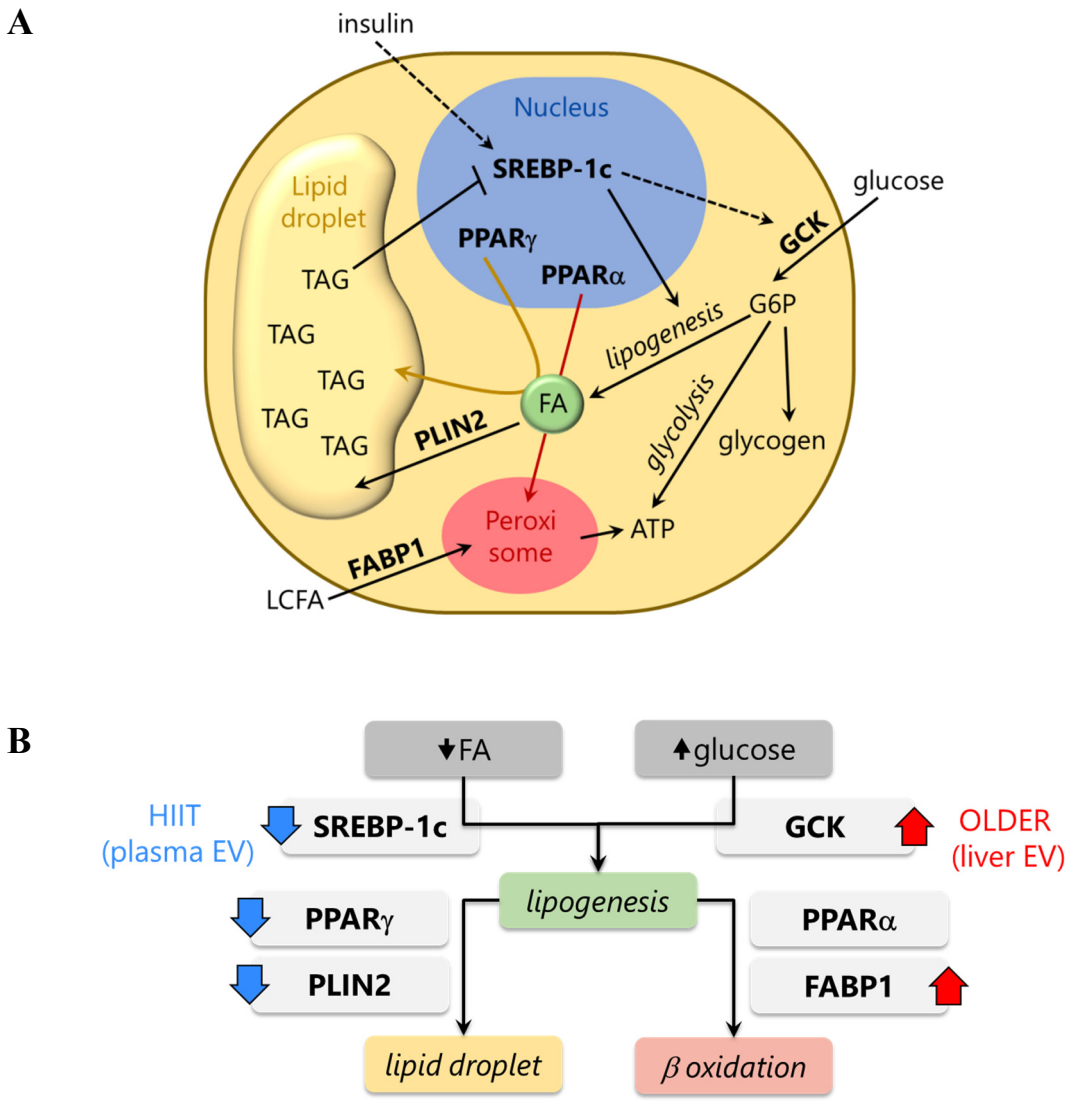

Figure 6.9. Hepatocyte markers of lipid metabolism and effect of EV exposure. (**A**) Cellular context of markers used in our study. Unbroken lines represent consequence (lipid transport or outcome of cellular process) and broken lines represent activation. (**B**) Summary of the markers assigned to their cellular process or context of activity. Red up arrows show increased gene expression following stimulation with liver EVs (paracrine) from older mice, blue down arrows show decreased gene expression when stimulated with plasma EVs (endocrine) from obese HIIT-exercised mice. To generalise the EV effect on hepatocyte phenotype, aging tends to promote beta oxidation while exercise suppresses lipid droplet formation. Abbreviations: FA, fatty acid; LCFA, long-chain fatty acid; TAG, triacylglycerol; ATP, adenosine triphosphate; G6P, glucose 6 phosphate; GCK, glucokinase; SREBP-1c, sterol regulatory element-binding protein 1c; PPARγ or α, peroxisome proliferator activated receptor gamma or alpha; PLIN2, perilipin 2; FABP1, fatty acid binding protein 1.

Chapter 7.

Conclusions & Future Studies

Chapter 7. Table of contents

7.1. Conclusions

To reflect on the purpose of this thesis, we aimed to investigate the hypotheses (presented in detail in Chapter 1) that EVs isolated from an *in vivo* model of diet-induced NAFLD may be reliably enumerated and characterised, such that they would provide a useful biomarker for the assessment of NAFLD progression. Expanding on this, we investigated the effects of intrinsic and extrinsic factors – age, lifestyle intervention and genetic manipulation – on EV number or phenotype, how this correlated with physical and metabolic parameters, and whether the EVs communicated with hepatocytes functionally *in vitro*.

7.1.1. Major findings

In the context of our studies mentioned above, the technique optimisation phase provided some insight into the general characteristics of our isolated vesicles. Firstly, both plasma and liver-derived EVs were similarly around 100μm in diameter, however, they appear to have differed in their biogenesis as plasma EVs were enriched in CD63 (suggesting an endosome origin) while the EVs from liver explants did not express this marker. Due to their small size, it was difficult to evaluate these populations by conventional flow cytometry, and so mass spectrometry was used as an alternative for EV characterisation, despite its own limitations (see section 7.1.3). During our preliminary investigations in the *in vivo* NAFLD model, there were distinct trends for an age-related increase in plasma EVs and a decrease in liver-derived EVs, independently of diet. The two populations were inversely correlated in terms of abundance, whereas both were strongly associated with (absolute) hepatic lipid burden. However, these trends were not replicated in the larger scale study of NAFLD progression, where plasma EVs only increased in abundance following 20 weeks of HFD and otherwise remained stable. Conversely, liver EVs increased with age in the absence of a diet related effect, although this population was still reflective of hepatic lipid in terms of TAG levels. Since there was little correlation with other parameters of disease severity, it was concluded that enumeration of EVs in isolation may not be a reliable biomarker for NAFLD progression. On the other hand, the plasma EV spike at 20 weeks was an indication of other subclinical events in NAFLD development, such as an increase in the gene expression of some fibrogenic markers as well as collagen staining on histology.

Using genetically modified mice, we modelled the effect of severe acute lipogenesis in the absence of the pleiotropic cytokine TNF. Remarkably, despite the predisposition to obesity and steatosis in the TNF-ablated animals on a HFD, there were no changes in either plasma or (relative) liver EV numbers. This supported the developing sentiment in our previous findings that obesity has a less crucial impact on EV secretion when compared to other biological factors, such as age. Importantly, however, the relationship between liver lipid and the absolute number of liver-derived EVs was maintained; that is, the number of EVs adjusted for liver weight (total secreted per liver) was strongly correlated with hepatic TAG.

The next step was to investigate whether a lifestyle intervention would effectively augment this response. By comparing two exercise training regimens in their ability to reverse the burden of NAFLD, it was not only demonstrated that END and HIIT impart differential benefits on the liver, but that they also modulate the plasma and liver EV populations differentially. For s start, only END was capable of increasing plasma EV abundance whereas there was no effect of diet (as expected). This was reflected in the liver gene expression profile, where END was superior to HIIT in terms of normalising some of the pathological changes (for example, an increase in collagen I). In contrast, liver EVs were significantly decreased by 10-fold for animals undergoing either exercise regimen irrespective of diets. Interestingly, since hepatic TAG was increased by HFD for both exercise groups, it was correlated negatively with the number of liver-derived EVs, although the same trend was not observed in lean animals. Therefore, it is unlikely that EVs could predict absolute liver lipid in this context.

To clarify the potential mechanistic influence of EVs, we first used proteomics to determine the molecular cargo of liver-derived vesicles, as a candidate for paracrine signalling. When all samples were examined collectively, it was shown (not unexpectedly) that liver-derived EVs are primarily involved in hepatocellular homeostasis, including carbohydrate and fatty acid metabolism. However, individual samples did not cluster according to treatment groups when their enriched proteins were considered, implying that EV phenotype tends to be susceptible to biological variation, even if they are derived from the same tissue and microenvironment. On the other hand, both diet and aging showed an upregulation of molecular pathways involved in anabolic processes, most of which are understood to play a protective role in liver homeostasis or in NAFLD pathogenesis.

This was further investigated using *in vitro* functional studies, whereby hepatocytes were exposed to plasma or liver EVs derived from our various mouse models. Indeed, the liver EVs from older mice seemed to compensate for some typical features of metabolic decline seen in aging, such as the impairment of hepatic beta oxidation. In contrast, plasma EVs were able to suppress the gene expression of fibrogenic markers, which also occurred independently of diet, whereas NASH-derived vesicles imparted an inflammatory effect by increasing the TNF levels in hepatocytes. Finally, when hepatocytes were stimulated with plasma EVs from HIIT-exercised HFD animals – but not END exercised animals from the same diet group – we found a modest but statistically significant decrease (by at least 2 fold) in the markers associated with hepatic lipogenesis. This was particularly interesting in that total hepatic lipid (by ORO staining) was also substantially decreased in HFD mice undergoing HIIT, but not in their END-trained counterparts. A summary of the major findings pertaining to the EV profile in animals fed a HFD in the presence of absence of exercise is shown in Figure 7.1 below.

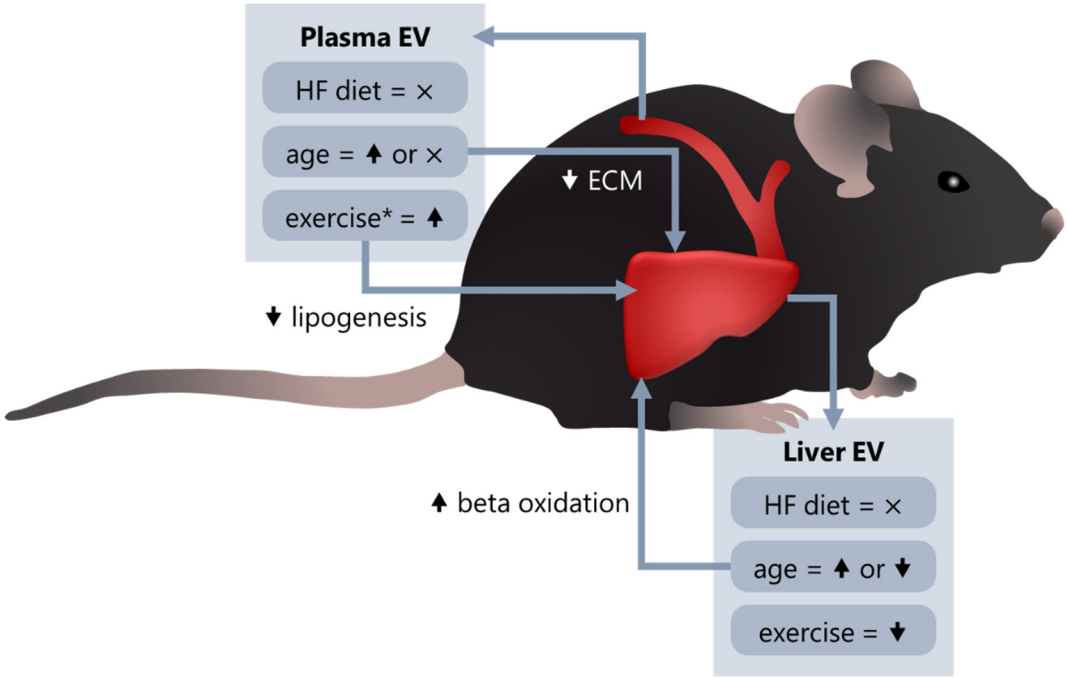

Figure 7.1. Summary of findings for EVs in NAFLD. Within boxes: cross (x) represents no change in EV number, arrows represent increase or decrease, depending on the study. Asterix (*) implies specific exercise: END increased EV number, HIIT affected hepatocyte phenotype. Abbreviations: HF, high fat; ECM, extracellular matrix (remodelling).

7.1.2. Clinical significance

While the underlying purpose of the studies in this thesis were to elaborate on the potential of utilising EVs as a novel biomarker candidate for NAFLD, other clinical implications were also highlighted. Notably, in the context of diet-induced obesity and the progression of NAFLD to NASH, it was demonstrated that fibrogenesis is actually a much earlier event than traditionally thought; fibrotic changes start becoming apparent by 20 weeks of HFD, as previously observed in our laboratory (Lo et al., 2011), whereas NASH fibrosis was ubiquitously evident following 50 weeks of HFD. Therefore, it can be extrapolated that a chronically poor diet – in the absence of further atherogenic stimuli, fructose, or genetic changes – is sufficient to cause irreversible liver damage. Furthermore, it was found that aerobic exercise is universally beneficial to treat NAFLD, however, that the training modality may differentially affect the liver. For example, HIIT was more successful at reducing steatosis burden (excluding TAG), while END tended to outperform HIIT on most other parameters. Interestingly, the opposite was true for other insulin-sensitive tissues such as adipose and skeletal muscle (Martinez-Huenchullan et al., unpublished manuscript). Another clinically relevant outcome was the discrepancy in EV abundance between studies, which was influenced by slight variations in the isolation methodology. This finding highlights the impact of sample processing and storage, and that technique standardisation is vitally important if EVs were to eventually be used as diagnostic markers for NAFLD in the clinic (Lener et al., 2015).

In the context of EV enumeration, it was shown that – within the scope of our investigations – the easily accessible plasma-derived population may not be a reliable tool for monitoring the progression of NAFLD severity overall. Furthermore, liver EVs may not be contributing to the circulating EV pool in the presence of liver disease, especially in the case of NAFLD where the systemic metabolic disturbances of obesity are likely to be masking the endocrine presence of tissue-specific disorders. It was repeatedly demonstrated, nonetheless, that EVs from either source were in some way correlated with hepatic lipid. This suggests that steatosis burden may be estimated by circulating EV abundance, although whether this option is practical given the currently available tools for the assessment of hepatic lipid (Table 1.2 and (Stern and Castera, 2017)) – not to mention the timeline for developing an efficient isolation procedure for EVs – remains to be seen.

On a more positive note, the fundamental role for EVs as "intercellular messengers" in NAFLD was supported in our findings, as well as previously by others (Cannito et al., 2017, Hirsova et al., 2016, Lee et al., 2017, Povero et al., 2013, Povero et al., 2015). Here we showed the effect that both plasma and liver-derived EVs had on hepatocyte phenotype, particularly in their ability to regulate lipogenesis and fatty acid beta oxidation at the transcriptional level, which shows promise for the therapeutic application of EVs in NAFLD (Ban et al., 2016) and in other disorders (Lener et al., 2015).

7.1.3. Limitations

Given the lack of experimental standardisation in the field of EV research, it is often inevitable that findings may not be supported in the literature or recapitulate previous research. Even within this thesis, some findings across our studies remain inconclusive due to adjustments in the methodology. For instance, the timing of EV storage relative to ultracentrifugation was significantly impactful on EV enumeration (see Figure 4.14) and was a major confounding factor in the interpretation of this finding. While the optimisation of EV isolation has been previously discussed (Jeyaram and Jay, 2017, Yuana et al., 2015), there is no single approach that is accepted in the ISEV community (Witwer et al., 2013).

To maintain the validity of EV research findings, however, ISEV has developed guidelines for the minimal requirements for the definition of EV structure and function (Lotvall et al., 2014, Witwer et al., 2017). This includes the ultracentrifugation-based isolation of EVs, used by over 80% of researchers (Gardiner et al., 2016) and also within this thesis, despite being considered as a "crude" sample fraction in the absence of further purification. Whether this is actually the case remains to be resolved. Studies that report on EV structure and downstream applications show inconsistent findings in terms of the reliability of ultracentrifugation when compared to other methods of isolation, including commercially available kits (Helwa et al., 2017, Rekker et al., 2014, Yamashita et al., 2016). Importantly, however, further purification steps are recommended prior to assessing the EV proteome to avoid any contamination with protein aggregates (Abramowicz et al., 2016). This was not performed during our studies, whereas TEM and cytometry showed minimal contaminating particles in our EV samples.

Other limitations that were derived from the biophysical properties of EVs were more difficult to avoid. The most widely understood example is the use of flow cytometry to characterise the EV markers of origin or biogenesis, given that most EV populations are below the size limit of detection. While it is possible that some conventional cytometers may be calibrated to resolve particles down to <200nm (van der Vlist et al., 2012), this is both laborious and requires a high level of technical expertise. Furthermore, this challenge is compounded by the fact that EVs have a relatively low, as yet undefined refractive index (Gardiner et al., 2013) that is difficult to confirm due to the inherent complexity and heterogeneity of these samples. On the other hand, there is an urgency to develop flow cytometry for the continued study of EV phenotype, given the low-throughput nature of many of its competitors (Momen-Heravi et al., 2012).

Finally, a more comprehensive elaboration of the study could have yielded more integrative results. Changes in hepatic lipid (especially TAG), for instance, may have been better informed by physiological data such as caloric intake and cardiac output, and hence related to EV abundance, particularly in the exercise intervention study. From the perspective of liver-derived vesicles, it can be anticipated that the culture of different cell types independently – isolated by collagenase digestion of the liver – may have delineated the contribution of the different cell populations. In contrast, the intact architecture has the advantage of more accurately reflecting the *in vivo* microenvironment in which liver EVs are secreted, and for the incubation period used in this study, it is expected that tissue viability would be largely preserved (Li et al., 2010). Since previous studies have dealt with surrogate markers to probe for liver-derived EVs in the plasma population (Csak et al., 2015, Povero et al., 2014, Povero et al., 2013), it may also be useful to compare this indirect method with the enumeration of EVs obtained directly from liver-conditioned media. This would help to determine the utility of the traditional approach, since "liver-specific" markers are a misnomer: most of the studied markers are enriched in, but not exclusive to, hepatocytes (Ban et al., 2016).

It is worth noting, however, that these logistical caveats arise as a function of practicality: although useful, the additional information is beyond the scope of the objectives of this thesis. Further integrative approaches to the study of EVs in NAFLD will be discussed in the following section, where the contributions of future studies are likely to provide a more holistic picture of this system of intercellular communication.

7.2. Future Directions

The study of EVs as biomarkers and mediators of disease is a very much established concept, however, its application to metabolic disorders (especially NAFLD) is still an emerging field. EV research will continue to face an uphill battle in terms of adequately characterising these structures until universal standards for their isolation and phenotyping have been realised. It is anticipated that in the future, EVs may be utilised for a variety of diagnostic, prognostic, and therapeutic applications (reviewed extensively in (Wauben, 2016)); for example, vaccine trials are already underway.

7.2.1. NAFLD models and translation

There is a wealth of research on obesity and related pathologies that utilise rodent models, both dietary and genetic, as described in Chapter 1 (section 1.2.4). While this thesis investigated the traditional HFD modified to include a sub-atherogenic level of cholesterol, to reflect a more physiological progression of NAFLD, previous studies have used a choline-deficient model to isolate and accelerate the liver-specific injury (Povero et al., 2014). It may also be valuable to examine EVs in a diabetic context – a phenotype that is known to exacerbate NAFLD (Lo et al., 2011) – by adding a streptozotocin insult to the diet-induced metabolic syndrome. Once characterised, these EVs would later be useful in distinguishing subsets of patients that may be susceptible to obesity-related complications or comorbidities.

However, it is worth considering the fact that obesity as a multisystemic condition would pose inherent challenges in terms of using EVs as biomarkers in a "liquid biopsy". For a start, the vesicles that have been mobilised into the circulation are heterogeneous; even under homeostatic conditions, the population is a cocktail of signals from multiple organs, many of which are simultaneously dysregulated in obesity. Therefore, exploiting EVs to give cues on tissue-specific changes will likely be unreliable – as was observed in our studies – especially if those specific populations are decreased or perhaps considered to be "rare events". On the other hand, it is possible to use an arbitrary population of EVs as a surrogate marker of changes; for example, one clinical study found that vesicles from a particular leukocyte subset were strongly associated with the histological severity of NAFLD (Kornek et al., 2012).

Nevertheless, until a reliable procedure is validated for the automation of EV detection and phenotyping, the translational utility of EVs as a NAFLD biomarker remains dubious. There is, however, a strongly recognised potential for a functional (that is, therapeutic) application. The "marker versus mediator" paradigm that was introduced in Chapter 1 is now increasingly relevant: EVs have an undisputed role in paracrine and endocrine communication in NAFLD, as shown in previous studies (Ban et al., 2016) and substantiated in this thesis, as well as other diseases ranging from infection to cancer (Wauben, 2016). In contrast, their biomarker utility is context (disease) dependent, affected by lifestyle factors and even aging, which dispels the idea that plasma EV abundance and disease severity are inextricably linked.

7.2.2. Experimental considerations

This section will deal with novel or understudied ideas that have the potential to advance our knowledge of the functional role of EVs in NAFLD. Some of these concepts have been raised previously in the context of homeostatic signalling (Wauben, 2016) and will be expanded upon. One such idea is the *in vitro* modelling of complex biological systems and interactions, using either 3D cell culture (organoids), or a transwell apparatus to monitor EV uptake and diffusion across a cellular barrier. The latter system would be especially useful to confirm our hypothesis in Chapter 3, regarding reduced permeability across liver sinusoidal endothelia as a result of age- or diet-induced defenestration (Figure 7.2). It may also be worth examining epithelial permeability, beyond the EV uptake capacity of hepatocytes. For instance, since the gut microbiome is known to be altered with NAFLD (recently reviewed in (Sharpton et al., 2018)) and interacts with the human host via EVs (Shen et al., 2012b), it is possible that enterocytes or enteric immunity may be affected (Figure 7.2).

Another often disregarded approach is the examination of the typical EV lifespan, not just their functional role. For example, interfering with exosome release by inhibiting the production of vesicular ceramide (Kosaka et al., 2010, Trajkovic et al., 2008) may provide a snapshot of the cellular phenotype at a static point, and of the longevity of EVs in a given biofluid or medium. Blocking EV fusion or endocytosis – both mechanisms of uptake – is another option, although these processes are highly versatile (Mulcahy et al., 2014); therefore, interfering with a single pathway is likely to be redundant, while blocking multiple pathways may affect viability.

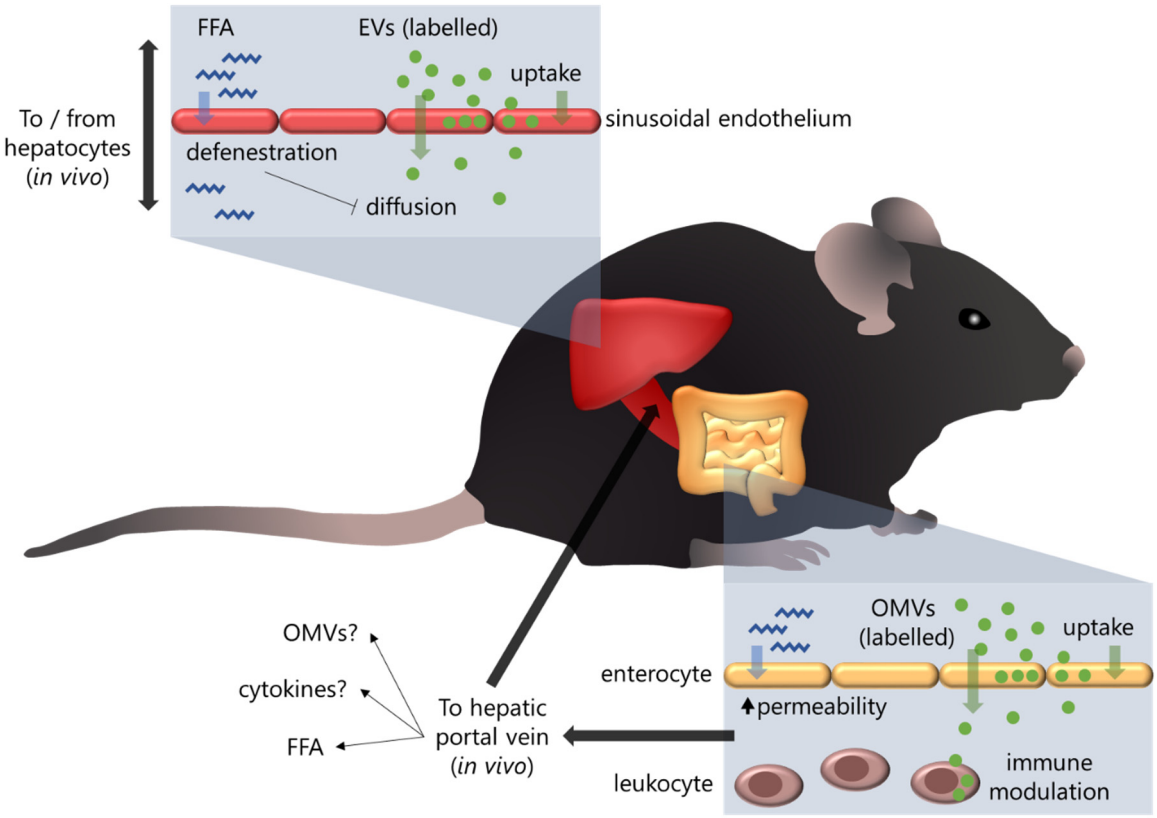

Figure 7.2. Future studies of EVs in NAFLD. Blue boxes represent potential scenarios for *in vitro* transwell experiments and how these are linked to the *in vivo* context (not anatomically correct on mouse). **Bottom panel:** Luminal EVs from the gut microbiome, known as outer membrane vesicles (OMVs) from the Gram negative bacteria that are typical of this micro-environment, may be taken into enterocytes and change epithelial permeability, or diffuse across to the leukocytes (representing Peyer's patches) to modulate their immune activity. In the *in vivo* setting, diffused OMVs – along with the cytokines they have elicited from the leukocytes and dietary free fatty acids (FFA) – may enter the portal circulation and establish an inflammatory niche in the liver, promoting the development of NAFLD. **Top panel:** Stimulation of (sinusoidal) endothelial cells with FFA to induce defenestration (Cogger et al., 2016) may change the dynamic of EV uptake into and diffusion across this cell monolayer, which in turn affects the availability of circulating EVs to hepatocytes and vice versa. For both models, sampling of fluorescently-labelled EVs on either side of the transwell chambers or within the cells might give a clue as to the dynamic of EV transport in a particular scenario, while molecular profiling of cells and diffused EVs before and after coculture would elucidate the functional role of these EVs.

Fluorescence microscopy may also be used to determine the uptake of specific EVs. This relies on the concept that, for example, fluorescently-labelled hepatocytes or hepatic cells stimulated with FFA will secrete fluorescent EVs with an altered cargo. While this type of study is not novel, there is potential to expand the design to answer novel questions: for instance, cells that have been differentially labelled depending on their treatment will have "colour-coded" EVs, hence, the stimulation of recipient cells with a combination of these EV populations can be used to monitor the preferential uptake of certain EV phenotypes. Whether cells are more receptive to the uptake of lipotoxic EVs derived from FFA-stimulated hepatocytes, versus EVs from untreated cells, is not known. However, this concept is supported by our studies in Chapter 6 which showed that plasma EVs from obese mice with NASH were more likely to be taken up by recipient hepatocytes than EVs from mice with simple steatosis or normal livers.

Differential labelling of EVs in this manner could also be exploited for *in vivo* tracking studies: it is possible that the microenvironment of cells, rather than their tissue origin, determines the downstream role of their EVs and therefore, which cells they will interact with. Of course, complex systems also pose several limitations, such as the increased potential for vesicle degradation and the phenotypic altering of EVs following the capture of soluble molecules that are present in the biofluid. This challenges the conventional idea of the "regulated release" of EVs and further complicates their characterisation by increasing the heterogeneity of the population. Nevertheless, it could be that molecular capture is yet another function of EVs that facilitates their role as intercellular messengers; this may in turn be analysed by incubating EVs in a complex medium (*in vitro*) and monitoring their phenotypic changes over time. In theory, injecting fluorescent EVs into the mouse circulation would be a more physiological alternative, however, difficulties with sample retrieval are an inevitable limitation.

7.2.3. Final remarks

In a recent invited presentation by Marca Wauben (secretary general of ISEV) at the University of Sydney, the audience was reminded of the complexities associated with EV research, not least of which was the inherent heterogeneity that serves as the greatest pitfall for the utility of this 'holy grail'. The functional redundancy of this method of intercellular communication was also discussed, which is important for maintaining and regulating a stable system, in concert with other pathways. However, it is interesting to note that, despite the fact that EV secretion and signalling is supposedly highly regulated, the diversity in the EV phenotypes and selection for uptake may all contribute to the ultimate feedback outcome.

In this thesis, we explored the role of EVs in the context of NAFLD, including their potential as circulating biomarkers and their treatment-dependent modulatory effect on hepatocytes. In summary, EV release into the circulation or specifically from the liver was regulated by both intrinsic and extrinsic factors and, interestingly, this process was least responsive to the HFD. However, correlations between EV number and hepatic lipid were evident, while liver-derived EVs had a dynamic proteome signature that seemed to be affected by experimental treatment as well as biological variation. In this regard, to propose that EVs may be of diagnostic value (at least in NAFLD) should be approached with caution. Nevertheless, there was certainly a demonstrable effect of EV stimulation on hepatocyte gene expression – be it compensatory or protective – which suggests that EVs are indeed a vital aspect of physiological and pathological signalling. This is reassuring; our findings show that while disease diagnosis or prognosis may not be the key utility of EVs in the context of obesity and its complications, their therapeutic potential does deserve further consideration.

References

ABRAMOWICZ, A., WIDLAK, P. & PIETROWSKA, M. 2016. Proteomic analysis of exosomal cargo: the challenge of high purity vesicle isolation. *Mol Biosyst,* 12**,** 1407-19.

ADELI, K., TAGHIBIGLOU, C., VAN IDERSTINE, S. C. & LEWIS, G. F. 2001. Mechanisms of hepatic very low-density lipoprotein overproduction in insulin resistance. *Trends Cardiovasc Med,* 11**,** 170-6.

ADELMAN, R. C. & FREEMAN, C. 1972. Age-dependent regulation of glucokinase and tyrosine aminotransferase activities of rat liver in vivo by adrenal, pancreatic and pituitary hormones. *Endocrinology,* 90**,** 1551-60.

AJAMIEH, H., FARRELL, G. C., MCCUSKEY, R. S., YU, J., CHU, E., WONG, H. J., LAM, W. & TEOH, N. C. 2015. Acute atorvastatin is hepatoprotective against ischaemia-reperfusion injury in mice by modulating eNOS and microparticle formation. *Liver Int,* 35**,** 2174-2186.

AKERS, J. C., GONDA, D., KIM, R., CARTER, B. S. & CHEN, C. C. 2013. Biogenesis of extracellular vesicles (EV): exosomes, microvesicles, retrovirus-like vesicles, and apoptotic bodies. *J Neurooncol,* 113**,** 1-11.

ALEX, S., BOSS, A., HEERSCHAP, A. & KERSTEN, S. 2015. Exercise training improves liver steatosis in mice. *Nutr Metab (Lond),* 12**,** 29.

ALEXANDER, M., LOOMIS, A. K., FAIRBURN-BEECH, J., VAN DER LEI, J., DUARTE-SALLES, T., PRIETO-ALHAMBRA, D., ANSELL, D., PASQUA, A., LAPI, F., RIJNBEEK, P., MOSSEVELD, M., AVILLACH, P., EGGER, P., KENDRICK, S., WATERWORTH, D. M., SATTAR, N. & ALAZAWI, W. 2018. Real-world data reveal a diagnostic gap in non-alcoholic fatty liver disease. *BMC Med,* 16**,** 130.

ALMEDA-VALDES, P., AGUILAR-SALINAS, C. A., URIBE, M., CANIZALES-QUINTEROS, S. & MENDEZ-SANCHEZ, N. 2016. Impact of anthropometric cut-off values in determining the prevalence of metabolic alterations. *Eur J Clin Invest,* 46**,** 940-946.

ANDERMANN, A., BLANCQUAERT, I., BEAUCHAMP, S. & DERY, V. 2008. Revisiting Wilson and Jungner in the genomic age: a review of screening criteria over the past 40 years. *Bull World Health Organ,* 86**,** 317-9.

ANGULO, P., KLEINER, D. E., DAM-LARSEN, S., ADAMS, L. A., BJORNSSON, E. S., CHARATCHAROENWITTHAYA, P., MILLS, P. R., KEACH, J. C., LAFFERTY, H. D., STAHLER, A., HAFLIDADOTTIR, S. & BENDTSEN, F. 2015. Liver Fibrosis, but No Other Histologic Features, Is Associated With Long-term Outcomes of Patients With Nonalcoholic Fatty Liver Disease. *Gastroenterology,* 149**,** 389-97 e10.

ARMSTRONG, M. J., ADAMS, L. A., CANBAY, A. & SYN, W. K. 2014. Extrahepatic complications of nonalcoholic fatty liver disease. *Hepatology,* 59**,** 1174-97.

ARRAUD, N., GOUNOU, C., LINARES, R. & BRISSON, A. R. 2015. A simple flow cytometry method improves the detection of phosphatidylserine-exposing extracellular vesicles. *J Thromb Haemost,* 13**,** 237-47.

ATSHAVES, B. P., MARTIN, G. G., HOSTETLER, H. A., MCINTOSH, A. L., KIER, A. B. & SCHROEDER, F. 2010. Liver fatty acid-binding protein and obesity. *J Nutr Biochem,* 21**,** 1015-32.

BAEK, R., VARMING, K. & JORGENSEN, M. M. 2016. Does smoking, age or gender affect the protein phenotype of extracellular vesicles in plasma? *Transfus Apher Sci,* 55**,** 44-52.

BAN, L. A., SHACKEL, N. A. & MCLENNAN, S. V. 2016. Extracellular Vesicles: A New Frontier in Biomarker Discovery for Non-Alcoholic Fatty Liver Disease. *Int J Mol Sci,* 17**,** 376.

BARAD, O., MEIRI, E., AVNIEL, A., AHARONOV, R., BARZILAI, A., BENTWICH, I., EINAV, U., GILAD, S., HURBAN, P., KAROV, Y., LOBENHOFER, E. K., SHARON, E., SHIBOLETH, Y. M., SHTUTMAN, M., BENTWICH, Z. & EINAT, P. 2004. MicroRNA expression detected by oligonucleotide microarrays: system establishment and expression profiling in human tissues. *Genome Res,* 14**,** 2486-94.

BARON, M., LEROYER, A. S., MAJD, Z., LALLOYER, F., VALLEZ, E., BANTUBUNGI, K., CHINETTI-GBAGUIDI, G., DELERIVE, P., BOULANGER, C. M., STAELS, B. & TAILLEUX, A. 2011. PPARalpha activation differently affects microparticle content in atherosclerotic lesions and liver of a mouse model of atherosclerosis and NASH. *Atherosclerosis,* 218**,** 69-76.

BATALLER, R. & BRENNER, D. A. 2005. Liver fibrosis. *J Clin Invest,* 115**,** 209-18.

BEDOGNI, G., BELLENTANI, S., MIGLIOLI, L., MASUTTI, F., PASSALACQUA, M., CASTIGLIONE, A. & TIRIBELLI, C. 2006. The Fatty Liver Index: a simple and accurate predictor of hepatic steatosis in the general population. *BMC Gastroenterol,* 6**,** 33.

BEDOGNI, G., KAHN, H. S., BELLENTANI, S. & TIRIBELLI, C. 2010. A simple index of lipid overaccumulation is a good marker of liver steatosis. *BMC Gastroenterol,* 10**,** 98.

BERGSMEDH, A., SZELES, A., HENRIKSSON, M., BRATT, A., FOLKMAN, M. J., SPETZ, A. L. & HOLMGREN, L. 2001. Horizontal transfer of oncogenes by uptake of apoptotic bodies. *Proc Natl Acad Sci U S A,* 98**,** 6407-11.

BERNIMOULIN, M., WATERS, E. K., FOY, M., STEELE, B. M., SULLIVAN, M., FALET, H., WALSH, M. T., BARTENEVA, N., GENG, J. G., HARTWIG, J. H., MAGUIRE, P. B. & WAGNER, D. D. 2009. Differential stimulation of monocytic cells results in distinct populations of microparticles. *J Thromb Haemost,* 7**,** 1019-28.

BERTOLOTTI, M., LONARDO, A., MUSSI, C., BALDELLI, E., PELLEGRINI, E., BALLESTRI, S., ROMAGNOLI, D. & LORIA, P. 2014. Nonalcoholic fatty liver disease and aging: epidemiology to management. *World J Gastroenterol,* 20**,** 14185-204.

BIDDINGER, S. B., ALMIND, K., MIYAZAKI, M., KOKKOTOU, E., NTAMBI, J. M. & KAHN, C. R. 2005. Effects of diet and genetic background on sterol regulatory element-binding protein-1c, stearoyl-CoA desaturase 1, and the development of the metabolic syndrome. *Diabetes,* 54**,** 1314-23.

BIERNACKA, A., DOBACZEWSKI, M. & FRANGOGIANNIS, N. G. 2011. TGF-beta signaling in fibrosis. *Growth Factors,* 29**,** 196-202.

BINAS, B. & EROL, E. 2007. FABPs as determinants of myocellular and hepatic fuel metabolism. *Mol Cell Biochem,* 299**,** 75-84.

BINNS, D., DIMMER, E., HUNTLEY, R., BARRELL, D., O'DONOVAN, C. & APWEILER, R. 2009. QuickGO: a web-based tool for Gene Ontology searching. *Bioinformatics,* 25**,** 3045-6.

BODEN, G., SHE, P., MOZZOLI, M., CHEUNG, P., GUMIREDDY, K., REDDY, P., XIANG, X., LUO, Z. & RUDERMAN, N. 2005. Free fatty acids produce insulin resistance and activate the proinflammatory nuclear factor-kappaB pathway in rat liver. *Diabetes,* 54**,** 3458-65.

BOTROS, M. & SIKARIS, K. A. 2013. The de ritis ratio: the test of time. *Clin Biochem Rev,* 34**,** 117-30.

BRAUNERSREUTHER, V., VIVIANI, G. L., MACH, F. & MONTECUCCO, F. 2012. Role of cytokines and chemokines in non-alcoholic fatty liver disease. *World J Gastroenterol,* 18**,** 727-35.

BRODSKY, S. V., FACCIUTO, M. E., HEYDT, D., CHEN, J., ISLAM, H. K., KAJSTURA, M., RAMASWAMY, G. & AGUERO-ROSENFELD, M. 2008. Dynamics of

circulating microparticles in liver transplant patients. *J Gastrointestin Liver Dis,* 17**,** 261-8.

BYRNE, C. D., OLUFADI, R., BRUCE, K. D., CAGAMPANG, F. R. & AHMED, M. H. 2009. Metabolic disturbances in non-alcoholic fatty liver disease. *Clin Sci (Lond),* 116**,** 539-64.

BYRNE, C. D. & TARGHER, G. 2015. NAFLD: a multisystem disease. *J Hepatol,* 62**,** S47-64.

CALABRO, S. R., MACZUREK, A. E., MORGAN, A. J., TU, T., WEN, V. W., YEE, C., MRIDHA, A., LEE, M., D'AVIGDOR, W., LOCARNINI, S. A., MCCAUGHAN, G. W., WARNER, F. J., MCLENNAN, S. V. & SHACKEL, N. A. 2014. Hepatocyte produced matrix metalloproteinases are regulated by CD147 in liver fibrogenesis. *PLoS One,* 9**,** e90571.

CANNITO, S., MORELLO, E., BOCCA, C., FOGLIA, B., BENETTI, E., NOVO, E., CHIAZZA, F., ROGAZZO, M., FANTOZZI, R., POVERO, D., SUTTI, S., BUGIANESI, E., FELDSTEIN, A. E., ALBANO, E., COLLINO, M. & PAROLA, M. 2017. Microvesicles released from fat-laden cells promote activation of hepatocellular NLRP3 inflammasome: A pro-inflammatory link between lipotoxicity and non-alcoholic steatohepatitis. *PLoS One,* 12**,** e0172575.

CASTERA, L., FOUCHER, J., BERNARD, P. H., CARVALHO, F., ALLAIX, D., MERROUCHE, W., COUZIGOU, P. & DE LEDINGHEN, V. 2010. Pitfalls of liver stiffness measurement: a 5-year prospective study of 13,369 examinations. *Hepatology,* 51**,** 828-35.

CAWTHORN, W. P. & SETHI, J. K. 2008. TNF-alpha and adipocyte biology. *FEBS Lett,* 582**,** 117-31.

CHALASANI, N., YOUNOSSI, Z., LAVINE, J. E., CHARLTON, M., CUSI, K., RINELLA, M., HARRISON, S. A., BRUNT, E. M. & SANYAL, A. J. 2018. The diagnosis and management of nonalcoholic fatty liver disease: Practice guidance from the American Association for the Study of Liver Diseases. *Hepatology,* 67**,** 328-357.

CHAN, W. K., NIK MUSTAPHA, N. R. & MAHADEVA, S. 2014. Controlled attenuation parameter for the detection and quantification of hepatic steatosis in nonalcoholic fatty liver disease. *J Gastroenterol Hepatol,* 29**,** 1470-6.

CHAN, W. K., NIK MUSTAPHA, N. R., WONG, G. L., WONG, V. W. & MAHADEVA, S. 2017. Controlled attenuation parameter using the FibroScan(R) XL probe for quantification of hepatic steatosis for non-alcoholic fatty liver disease in an Asian population. *United European Gastroenterol J,* 5**,** 76-85.

CHANG, B. H., LI, L., PAUL, A., TANIGUCHI, S., NANNEGARI, V., HEIRD, W. C. & CHAN, L. 2006. Protection against fatty liver but normal adipogenesis in mice lacking adipose differentiation-related protein. *Mol Cell Biol,* 26**,** 1063-76.

CHARRIER, A., CHEN, R., CHEN, L., KEMPER, S., HATTORI, T., TAKIGAWA, M. & BRIGSTOCK, D. R. 2014. Exosomes mediate intercellular transfer of pro-fibrogenic connective tissue growth factor (CCN2) between hepatic stellate cells, the principal fibrotic cells in the liver. *Surgery,* 156**,** 548-55.

CHAVEZ-TAPIA, N. C., ROSSO, N. & TIRIBELLI, C. 2011. In vitro models for the study of non-alcoholic fatty liver disease. *Curr Med Chem,* 18**,** 1079-84.

CHEN, L., CHARRIER, A., ZHOU, Y., CHEN, R., YU, B., AGARWAL, K., TSUKAMOTO, H., LEE, L. J., PAULAITIS, M. E. & BRIGSTOCK, D. R. 2014. Epigenetic regulation of connective tissue growth factor by MicroRNA-214 delivery in exosomes from mouse or human hepatic stellate cells. *Hepatology,* 59**,** 1118-29.

CHEN, X., GONG, Q., WANG, C. Y., ZHANG, K., JI, X., CHEN, Y. X. & YU, X. J. 2016. High-Fat Diet Induces Distinct Metabolic Response in Interleukin-6 and Tumor Necrosis Factor-alpha Knockout Mice. *J Interferon Cytokine Res,* 36**,** 580-588.

CHO, J., KIM, S., LEE, S. & KANG, H. 2015. Effect of Training Intensity on Nonalcoholic Fatty Liver Disease. *Med Sci Sports Exerc,* 47**,** 1624-34.

CHO, J., LEE, I., KIM, D., KOH, Y., KONG, J., LEE, S. & KANG, H. 2014. Effect of aerobic exercise training on non-alcoholic fatty liver disease induced by a high fat diet in C57BL/6 mice. *J Exerc Nutrition Biochem,* 18**,** 339-46.

CHOLANKERIL, G., WONG, R. J., HU, M., PERUMPAIL, R. B., YOO, E. R., PURI, P., YOUNOSSI, Z. M., HARRISON, S. A. & AHMED, A. 2017. Liver Transplantation for Nonalcoholic Steatohepatitis in the US: Temporal Trends and Outcomes. *Dig Dis Sci,* 62**,** 2915-2922.

CIAPAITE, J., VAN DEN BROEK, N. M., TE BRINKE, H., NICOLAY, K., JENESON, J. A., HOUTEN, S. M. & PROMPERS, J. J. 2011. Differential effects of short- and long-term high-fat diet feeding on hepatic fatty acid metabolism in rats. *Biochim Biophys Acta,* 1811**,** 441-51.

COGGER, V. C., MOHAMAD, M., SOLON-BIET, S. M., SENIOR, A. M., WARREN, A., O'REILLY, J. N., TUNG, B. T., SVISTOUNOV, D., MCMAHON, A. C., FRASER, R., RAUBENHEIMER, D., HOLMES, A. J., SIMPSON, S. J. & LE COUTEUR, D. G. 2016. Dietary macronutrients and the aging liver sinusoidal endothelial cell. *Am J Physiol Heart Circ Physiol,* 310**,** H1064-70.

CONDE-VANCELLS, J., RODRIGUEZ-SUAREZ, E., EMBADE, N., GIL, D., MATTHIESEN, R., VALLE, M., ELORTZA, F., LU, S. C., MATO, J. M. & FALCON-PEREZ, J. M. 2008. Characterization and comprehensive proteome profiling of exosomes secreted by hepatocytes. *J Proteome Res,* 7**,** 5157-66.

COSGROVE, B. D., CHENG, C., PRITCHARD, J. R., STOLZ, D. B., LAUFFENBURGER, D. A. & GRIFFITH, L. G. 2008. An inducible autocrine cascade regulates rat hepatocyte proliferation and apoptosis responses to tumor necrosis factor-alpha. *Hepatology,* 48**,** 276-88.

COSTA-SILVA, B., AIELLO, N. M., OCEAN, A. J., SINGH, S., ZHANG, H., THAKUR, B. K., BECKER, A., HOSHINO, A., MARK, M. T., MOLINA, H., XIANG, J., ZHANG, T., THEILEN, T. M., GARCIA-SANTOS, G., WILLIAMS, C., ARARSO, Y., HUANG, Y., RODRIGUES, G., SHEN, T. L., LABORI, K. J., LOTHE, I. M., KURE, E. H., HERNANDEZ, J., DOUSSOT, A., EBBESEN, S. H., GRANDGENETT, P. M., HOLLINGSWORTH, M. A., JAIN, M., MALLYA, K., BATRA, S. K., JARNAGIN, W. R., SCHWARTZ, R. E., MATEI, I., PEINADO, H., STANGER, B. Z., BROMBERG, J. & LYDEN, D. 2015. Pancreatic cancer exosomes initiate pre-metastatic niche formation in the liver. *Nat Cell Biol,* 17**,** 816-26.

COSTA VERDERA, H., GITZ-FRANCOIS, J. J., SCHIFFELERS, R. M. & VADER, P. 2017. Cellular uptake of extracellular vesicles is mediated by clathrin-independent endocytosis and macropinocytosis. *J Control Release,* 266**,** 100-108.

CSAK, T., BALA, S., LIPPAI, D., SATISHCHANDRAN, A., CATALANO, D., KODYS, K. & SZABO, G. 2015. microRNA-122 regulates hypoxia-inducible factor-1 and vimentin in hepatocytes and correlates with fibrosis in diet-induced steatohepatitis. *Liver Int,* 35**,** 532-41.

CUSI, K., CHANG, Z., HARRISON, S., LOMONACO, R., BRIL, F., ORSAK, B., ORTIZ-LOPEZ, C., HECHT, J., FELDSTEIN, A. E., WEBB, A., LOUDEN, C., GOROS, M. & TIO, F. 2014. Limited value of plasma cytokeratin-18 as a biomarker for NASH and fibrosis in patients with non-alcoholic fatty liver disease. *J Hepatol,* 60**,** 167-74.

DELOITTE ACCESS ECONOMICS. 2013. *The economic cost and health burden of liver diseases in Australia* [Online]. The Gastroenterological Society of Australia. Available: http://www.gesa.org.au/resources/economic-cost-and-health-burden-of-liver-disease-in-australia/ [Accessed May 2017.

DENG, Z. B., LIU, Y., LIU, C., XIANG, X., WANG, J., CHENG, Z., SHAH, S. V., ZHANG, S., ZHANG, L., ZHUANG, X., MICHALEK, S., GRIZZLE, W. E. & ZHANG, H. G. 2009a. Immature myeloid cells induced by a high-fat diet contribute to liver inflammation. *Hepatology,* 50**,** 1412-20.

DENG, Z. B., POLIAKOV, A., HARDY, R. W., CLEMENTS, R., LIU, C., LIU, Y., WANG, J., XIANG, X., ZHANG, S., ZHUANG, X., SHAH, S. V., SUN, D., MICHALEK, S., GRIZZLE, W. E., GARVEY, T., MOBLEY, J. & ZHANG, H. G. 2009b. Adipose tissue exosome-like vesicles mediate activation of macrophage-induced insulin resistance. *Diabetes,* 58**,** 2498-505.

DESHMANE, S. L., KREMLEV, S., AMINI, S. & SAWAYA, B. E. 2009. Monocyte chemoattractant protein-1 (MCP-1): an overview. *J Interferon Cytokine Res,* 29**,** 313-26.

DOHERTY, D. G. 2016. Immunity, tolerance and autoimmunity in the liver: A comprehensive review. *J Autoimmun,* 66**,** 60-75.

DURHAM, H. A. & TRUETT, G. E. 2006. Development of insulin resistance and hyperphagia in Zucker fatty rats. *Am J Physiol Regul Integr Comp Physiol,* 290**,** R652-8.

DURRER, C., ROBINSON, E., WAN, Z., MARTINEZ, N., HUMMEL, M. L., JENKINS, N. T., KILPATRICK, M. W. & LITTLE, J. P. 2015. Differential impact of acute high-intensity exercise on circulating endothelial microparticles and insulin resistance between overweight/obese males and females. *PLoS One,* 10**,** e0115860.

EKSTEDT, M., FRANZEN, L. E., MATHIESEN, U. L., THORELIUS, L., HOLMQVIST, M., BODEMAR, G. & KECHAGIAS, S. 2006. Long-term follow-up of patients with NAFLD and elevated liver enzymes. *Hepatology,* 44**,** 865-73.

ELDH, M., OLOFSSON BAGGE, R., LASSER, C., SVANVIK, J., SJOSTRAND, M., MATTSSON, J., LINDNER, P., CHOI, D. S., GHO, Y. S. & LOTVALL, J. 2014. MicroRNA in exosomes isolated directly from the liver circulation in patients with metastatic uveal melanoma. *BMC Cancer,* 14**,** 962.

EUROPEAN ASSOCIATION FOR THE STUDY OF THE LIVER, EUROPEAN ASSOCIATION FOR THE STUDY OF DIABETES & OBESITY, E. A. F. T. S. O. 2016. EASL-EASD-EASO Clinical Practice Guidelines for the management of non-alcoholic fatty liver disease. *J Hepatol,* 64**,** 1388-402.

EUROPEAN ASSOCIATION FOR THE STUDY OF THE LIVER (EASL), EUROPEAN ASSOCIATION FOR THE STUDY OF DIABETES (EASD) & EUROPEAN ASSOCIATION FOR THE STUDY OF OBESITY (EASO) 2016. EASL-EASD-EASO Clinical Practice Guidelines for the management of non-alcoholic fatty liver disease. *Journal of Hepatology,* 64**,** 1388-1402.

FARAZUDDIN, M., DUA, B., ZIA, Q., KHAN, A. A., JOSHI, B. & OWAIS, M. 2014. Chemotherapeutic potential of curcumin-bearing microcells against hepatocellular carcinoma in model animals. *Int J Nanomedicine,* 9**,** 1139-52.

FARRELL, G. C., MRIDHA, A. R., YEH, M. M., ARSOV, T., VAN ROOYEN, D. M., BROOLING, J., NGUYEN, T., HEYDET, D., DELGHINGARO-AUGUSTO, V., NOLAN, C. J., SHACKEL, N. A., MCLENNAN, S. V., TEOH, N. C. & LARTER, C. Z. 2014. Strain dependence of diet-induced NASH and liver fibrosis in obese mice is linked to diabetes and inflammatory phenotype. *Liver Int,* 34**,** 1084-93.

FEDCHUK, L., NASCIMBENI, F., PAIS, R., CHARLOTTE, F., HOUSSET, C., RATZIU, V. & GROUP, L. S. 2014. Performance and limitations of steatosis biomarkers in patients with nonalcoholic fatty liver disease. *Aliment Pharmacol Ther,* 40**,** 1209-22.

FEINSTEIN, R., KANETY, H., PAPA, M. Z., LUNENFELD, B. & KARASIK, A. 1993. Tumor necrosis factor-alpha suppresses insulin-induced tyrosine phosphorylation of insulin receptor and its substrates. *J Biol Chem,* 268**,** 26055-8.

FILINGERI, V., SFORZA, D. & TISONE, G. 2015. Complications and risk factors of a large series of percutaneous liver biopsies in patients with liver transplantation or liver disease. *Eur Rev Med Pharmacol Sci,* 19**,** 1621-9.

FINK, R. I., KOLTERMAN, O. G., GRIFFIN, J. & OLEFSKY, J. M. 1983. Mechanisms of insulin resistance in aging. *J Clin Invest,* 71**,** 1523-35.

FONSATO, V., COLLINO, F., HERRERA, M. B., CAVALLARI, C., DEREGIBUS, M. C., CISTERNA, B., BRUNO, S., ROMAGNOLI, R., SALIZZONI, M., TETTA, C. & CAMUSSI, G. 2012. Human liver stem cell-derived microvesicles inhibit hepatoma growth in SCID mice by delivering antitumor microRNAs. *Stem Cells,* 30**,** 1985-98.

FONTANA, L., ZHAO, E., AMIR, M., DONG, H., TANAKA, K. & CZAJA, M. J. 2013. Aging promotes the development of diet-induced murine steatohepatitis but not steatosis. *Hepatology,* 57**,** 995-1004.

FORETZ, M., GUICHARD, C., FERRE, P. & FOUFELLE, F. 1999. Sterol regulatory element binding protein-1c is a major mediator of insulin action on the hepatic expression of glucokinase and lipogenesis-related genes. *Proc Natl Acad Sci U S A,* 96**,** 12737-42.

FREEMAN, C. M., QUILLIN, R. C., 3RD, WILSON, G. C., NOJIMA, H., JOHNSON, B. L., 3RD, SUTTON, J. M., SCHUSTER, R. M., BLANCHARD, J., EDWARDS, M. J., CALDWELL, C. C. & LENTSCH, A. B. 2014. Characterization of microparticles after hepatic ischemia-reperfusion injury. *PLoS One,* 9**,** e97945.

FRITH, J., DAY, C. P., HENDERSON, E., BURT, A. D. & NEWTON, J. L. 2009. Non-alcoholic fatty liver disease in older people. *Gerontology,* 55**,** 607-13.

GAN, L., CHITTURI, S. & FARRELL, G. C. 2011. Mechanisms and implications of age-related changes in the liver: nonalcoholic Fatty liver disease in the elderly. *Curr Gerontol Geriatr Res,* 2011**,** 831536.

GAO, S., HE, L., DING, Y. & LIU, G. 2010. Mechanisms underlying different responses of plasma triglyceride to high-fat diets in hamsters and mice: roles of hepatic MTP and triglyceride secretion. *Biochem Biophys Res Commun,* 398**,** 619-26.

GARDINER, C., DI VIZIO, D., SAHOO, S., THERY, C., WITWER, K. W., WAUBEN, M. & HILL, A. F. 2016. Techniques used for the isolation and characterization of extracellular vesicles: results of a worldwide survey. *J Extracell Vesicles,* 5**,** 32945.

GARDINER, C., FERREIRA, Y. J., DRAGOVIC, R. A., REDMAN, C. W. & SARGENT, I. L. 2013. Extracellular vesicle sizing and enumeration by nanoparticle tracking analysis. *J Extracell Vesicles,* 2.

GORDEN, D. L., IVANOVA, P. T., MYERS, D. S., MCINTYRE, J. O., VANSAUN, M. N., WRIGHT, J. K., MATRISIAN, L. M. & BROWN, H. A. 2011. Increased diacylglycerols characterize hepatic lipid changes in progression of human nonalcoholic fatty liver disease; comparison to a murine model. *PLoS One,* 6**,** e22775.

GORSKI, J., NOWACKA, M., NAMIOT, Z. & PUCH, U. 1988. Effect of prolonged exercise on the level of triglycerides in the rat liver. *Eur J Appl Physiol Occup Physiol,* 57**,** 554-7.

GOULD, S. J. & RAPOSO, G. 2013. As we wait: coping with an imperfect nomenclature for extracellular vesicles. *J Extracell Vesicles,* 2.

GUGLIELMI, A., RUZZENENTE, A., CONCI, S., VALDEGAMBERI, A. & IACONO, C. 2012. How much remnant is enough in liver resection? *Dig Surg,* 29**,** 6-17.

GUO, J., JOU, W., GAVRILOVA, O. & HALL, K. D. 2009. Persistent diet-induced obesity in male C57BL/6 mice resulting from temporary obesigenic diets. *PLoS One,* 4**,** e5370.
GUTIERREZ-GROBE, Y., PONCIANO-RODRIGUEZ, G., RAMOS, M. H., URIBE, M. & MENDEZ-SANCHEZ, N. 2010. Prevalence of non alcoholic fatty liver disease in premenopausal, posmenopausal and polycystic ovary syndrome women. The role of estrogens. *Ann Hepatol,* 9**,** 402-9.
HAGAN, C. 2017. *When are mice considered old?* [Online]. The Jackson Laboratory. Available: https://www.jax.org/news-and-insights/jax-blog/2017/november/when-are-mice-considered-old [Accessed September 2018.
HALLSWORTH, K., THOMA, C., HOLLINGSWORTH, K. G., CASSIDY, S., ANSTEE, Q. M., DAY, C. P. & TRENELL, M. I. 2015. Modified high-intensity interval training reduces liver fat and improves cardiac function in non-alcoholic fatty liver disease: a randomized controlled trial. *Clin Sci (Lond),* 129**,** 1097-105.
HARIRI, N. & THIBAULT, L. 2010. High-fat diet-induced obesity in animal models. *Nutr Res Rev,* 23**,** 270-99.
HASHIDA, R., KAWAGUCHI, T., BEKKI, M., OMOTO, M., MATSUSE, H., NAGO, T., TAKANO, Y., UENO, T., KOGA, H., GEORGE, J., SHIBA, N. & TORIMURA, T. 2017. Aerobic vs. resistance exercise in non-alcoholic fatty liver disease: A systematic review. *J Hepatol,* 66**,** 142-152.
HE, M., QIN, H., POON, T. C., SZE, S. C., DING, X., CO, N. N., NGAI, S. M., CHAN, T. F. & WONG, N. 2015. Hepatocellular carcinoma-derived exosomes promote motility of immortalized hepatocyte through transfer of oncogenic proteins and RNAs. *Carcinogenesis,* 36**,** 1008-1018.
HEBERLE, H., MEIRELLES, G. V., DA SILVA, F. R., TELLES, G. P. & MINGHIM, R. 2015. InteractiVenn: a web-based tool for the analysis of sets through Venn diagrams. *BMC Bioinformatics,* 16**,** 169.
HELWA, I., CAI, J., DREWRY, M. D., ZIMMERMAN, A., DINKINS, M. B., KHALED, M. L., SEREMWE, M., DISMUKE, W. M., BIEBERICH, E., STAMER, W. D., HAMRICK, M. W. & LIU, Y. 2017. A Comparative Study of Serum Exosome Isolation Using Differential Ultracentrifugation and Three Commercial Reagents. *PLoS One,* 12**,** e0170628.
HERNANDEZ-GEA, V. & FRIEDMAN, S. L. 2011. Pathogenesis of liver fibrosis. *Annu Rev Pathol,* 6**,** 425-56.
HESSVIK, N. P. & LLORENTE, A. 2018. Current knowledge on exosome biogenesis and release. *Cell Mol Life Sci,* 75**,** 193-208.
HEYDET, D., CHEN, L. X., LARTER, C. Z., INGLIS, C., SILVERMAN, M. A., FARRELL, G. C. & LEROUX, M. R. 2013. A truncating mutation of Alms1 reduces the number of hypothalamic neuronal cilia in obese mice. *Dev Neurobiol,* 73**,** 1-13.
HIRSOVA, P., IBRAHIM, S. H., KRISHNAN, A., VERMA, V. K., BRONK, S. F., WERNEBURG, N. W., CHARLTON, M. R., SHAH, V. H., MALHI, H. & GORES, G. J. 2016. Lipid-Induced Signaling Causes Release of Inflammatory Extracellular Vesicles From Hepatocytes. *Gastroenterology,* 150**,** 956-67.
HLA, T. & KOLESNICK, R. 2014. C16:0-ceramide signals insulin resistance. *Cell Metab,* 20**,** 703-705.
HORTON, J. D., SHIMANO, H., HAMILTON, R. L., BROWN, M. S. & GOLDSTEIN, J. L. 1999. Disruption of LDL receptor gene in transgenic SREBP-1a mice unmasks hyperlipidemia resulting from production of lipid-rich VLDL. *J Clin Invest,* 103**,** 1067-76.
HORVATH, S., ERHART, W., BROSCH, M., AMMERPOHL, O., VON SCHONFELS, W., AHRENS, M., HEITS, N., BELL, J. T., TSAI, P. C., SPECTOR, T. D., DELOUKAS,

P., SIEBERT, R., SIPOS, B., BECKER, T., ROCKEN, C., SCHAFMAYER, C. & HAMPE, J. 2014. Obesity accelerates epigenetic aging of human liver. *Proc Natl Acad Sci U S A,* 111**,** 15538-43.

HOTAMISLIGIL, G. S., MURRAY, D. L., CHOY, L. N. & SPIEGELMAN, B. M. 1994. Tumor necrosis factor alpha inhibits signaling from the insulin receptor. *Proc Natl Acad Sci U S A,* 91**,** 4854-8.

HOUTKOOPER, R. H., ARGMANN, C., HOUTEN, S. M., CANTO, C., JENINGA, E. H., ANDREUX, P. A., THOMAS, C., DOENLEN, R., SCHOONJANS, K. & AUWERX, J. 2011. The metabolic footprint of aging in mice. *Sci Rep,* 1**,** 134.

HOWELL, J., BALDERSON, G., HELLARD, M., GOW, P., STRASSER, S., STUART, K., WIGG, A., JEFFREY, G., GANE, E. & ANGUS, P. W. 2016. The increasing burden of potentially preventable liver disease among adult liver transplant recipients: A comparative analysis of liver transplant indication by era in Australia and New Zealand. *J Gastroenterol Hepatol,* 31**,** 434-41.

HUANG DA, W., SHERMAN, B. T. & LEMPICKI, R. A. 2009. Systematic and integrative analysis of large gene lists using DAVID bioinformatics resources. *Nat Protoc,* 4**,** 44-57.

HUGEL, B., MARTINEZ, M. C., KUNZELMANN, C. & FREYSSINET, J. M. 2005. Membrane microparticles: two sides of the coin. *Physiology (Bethesda),* 20**,** 22-7.

IBRAHIM, S. H., HIRSOVA, P., TOMITA, K., BRONK, S. F., WERNEBURG, N. W., HARRISON, S. A., GOODFELLOW, V. S., MALHI, H. & GORES, G. J. 2016. Mixed lineage kinase 3 mediates release of C-X-C motif ligand 10-bearing chemotactic extracellular vesicles from lipotoxic hepatocytes. *Hepatology,* 63**,** 731-44.

INGLIS, H., NORRIS, P. & DANESH, A. 2015. Techniques for the analysis of extracellular vesicles using flow cytometry. *J Vis Exp*.

ISMAIL, I., KEATING, S. E., BAKER, M. K. & JOHNSON, N. A. 2012. A systematic review and meta-analysis of the effect of aerobic vs. resistance exercise training on visceral fat. *Obes Rev,* 13**,** 68-91.

ITO, M., SUZUKI, J., TSUJIOKA, S., SASAKI, M., GOMORI, A., SHIRAKURA, T., HIROSE, H., ITO, M., ISHIHARA, A., IWAASA, H. & KANATANI, A. 2007. Longitudinal analysis of murine steatohepatitis model induced by chronic exposure to high-fat diet. *Hepatol Res,* 37**,** 50-7.

JACOBS, A., WARDA, A. S., VERBEEK, J., CASSIMAN, D. & SPINCEMAILLE, P. 2016. An Overview of Mouse Models of Nonalcoholic Steatohepatitis: From Past to Present. *Curr Protoc Mouse Biol,* 6**,** 185-200.

JAIRAM, V., UCHIDA, K. & NARAYANASWAMI, V. 2012. Pathophysiology of Lipoprotein Oxidation. *In:* FRANK, S. & KOSTNER, G. (eds.) *Lipoproteins - Role in Health and Diseases.* Rijeka: InTech.

JENJAROENPUN, P., KREMENSKA, Y., NAIR, V. M., KREMENSKOY, M., JOSEPH, B. & KUROCHKIN, I. V. 2013. Characterization of RNA in exosomes secreted by human breast cancer cell lines using next-generation sequencing. *PeerJ,* 1**,** e201.

JENSEN, M. D. 2008. Role of body fat distribution and the metabolic complications of obesity. *J Clin Endocrinol Metab,* 93**,** S57-63.

JEYARAM, A. & JAY, S. M. 2017. Preservation and Storage Stability of Extracellular Vesicles for Therapeutic Applications. *AAPS J,* 20**,** 1.

JOHNSON, N. A., SACHINWALLA, T., WALTON, D. W., SMITH, K., ARMSTRONG, A., THOMPSON, M. W. & GEORGE, J. 2009. Aerobic exercise training reduces hepatic and visceral lipids in obese individuals without weight loss. *Hepatology,* 50**,** 1105-12.

JORNAYVAZ, F. R. & SHULMAN, G. I. 2012. Diacylglycerol activation of protein kinase Cepsilon and hepatic insulin resistance. *Cell Metab,* 15**,** 574-84.

KADOTA, T., FUJITA, Y., YOSHIOKA, Y., ARAYA, J., KUWANO, K. & OCHIYA, T. 2018. Emerging role of extracellular vesicles as a senescence-associated secretory phenotype: Insights into the pathophysiology of lung diseases. *Mol Aspects Med,* 60**,** 92-103.

KAKAZU, E., MAUER, A. S., YIN, M. & MALHI, H. 2016. Hepatocytes release ceramide-enriched pro-inflammatory extracellular vesicles in an IRE1alpha-dependent manner. *J Lipid Res,* 57**,** 233-45.

KAKINO, S., OHKI, T., NAKAYAMA, H., YUAN, X., OTABE, S., HASHINAGA, T., WADA, N., KURITA, Y., TANAKA, K., HARA, K., SOEJIMA, E., TAJIRI, Y. & YAMADA, K. 2018. Pivotal Role of TNF-alpha in the Development and Progression of Nonalcoholic Fatty Liver Disease in a Murine Model. *Horm Metab Res,* 50**,** 80-87.

KALAKI-JOUYBARI, F., SHANAKI, M., DELFAN, M., GORGANI-FIROUZJAE, S. & KHAKDAN, S. 2018. High-intensity interval training (HIIT) alleviated NAFLD feature via miR-122 induction in liver of high-fat high-fructose diet induced diabetic rats. *Arch Physiol Biochem***,** 1-8.

KALRA, H., ADDA, C. G., LIEM, M., ANG, C. S., MECHLER, A., SIMPSON, R. J., HULETT, M. D. & MATHIVANAN, S. 2013. Comparative proteomics evaluation of plasma exosome isolation techniques and assessment of the stability of exosomes in normal human blood plasma. *Proteomics,* 13**,** 3354-64.

KALRA, H., SIMPSON, R. J., JI, H., AIKAWA, E., ALTEVOGT, P., ASKENASE, P., BOND, V. C., BORRAS, F. E., BREAKEFIELD, X., BUDNIK, V., BUZAS, E., CAMUSSI, G., CLAYTON, A., COCUCCI, E., FALCON-PEREZ, J. M., GABRIELSSON, S., GHO, Y. S., GUPTA, D., HARSHA, H. C., HENDRIX, A., HILL, A. F., INAL, J. M., JENSTER, G., KRAMER-ALBERS, E. M., LIM, S. K., LLORENTE, A., LOTVALL, J., MARCILLA, A., MINCHEVA-NILSSON, L., NAZARENKO, I., NIEUWLAND, R., NOLTE-'T HOEN, E. N., PANDEY, A., PATEL, T., PIPER, M. G., PLUCHINO, S., PRASAD, T. S., RAJENDRAN, L., RAPOSO, G., RECORD, M., REID, G. E., SANCHEZ-MADRID, F., SCHIFFELERS, R. M., SILJANDER, P., STENSBALLE, A., STOORVOGEL, W., TAYLOR, D., THERY, C., VALADI, H., VAN BALKOM, B. W., VAZQUEZ, J., VIDAL, M., WAUBEN, M. H., YANEZ-MO, M., ZOELLER, M. & MATHIVANAN, S. 2012. Vesiclepedia: a compendium for extracellular vesicles with continuous community annotation. *PLoS Biol,* 10**,** e1001450.

KARLAS, T., PETROFF, D., GARNOV, N., BOHM, S., TENCKHOFF, H., WITTEKIND, C., WIESE, M., SCHIEFKE, I., LINDER, N., SCHAUDINN, A., BUSSE, H., KAHN, T., MOSSNER, J., BERG, T., TROLTZSCH, M., KEIM, V. & WIEGAND, J. 2014. Non-invasive assessment of hepatic steatosis in patients with NAFLD using controlled attenuation parameter and 1H-MR spectroscopy. *PLoS One,* 9**,** e91987.

KAWANISHI, N., YANO, H., MIZOKAMI, T., TAKAHASHI, M., OYANAGI, E. & SUZUKI, K. 2012. Exercise training attenuates hepatic inflammation, fibrosis and macrophage infiltration during diet induced-obesity in mice. *Brain Behav Immun,* 26**,** 931-41.

KEATING, S. E., HACKETT, D. A., GEORGE, J. & JOHNSON, N. A. 2012. Exercise and non-alcoholic fatty liver disease: a systematic review and meta-analysis. *J Hepatol,* 57**,** 157-66.

KEATING, S. E., HACKETT, D. A., PARKER, H. M., O'CONNOR, H. T., GEROFI, J. A., SAINSBURY, A., BAKER, M. K., CHUTER, V. H., CATERSON, I. D., GEORGE, J. & JOHNSON, N. A. 2015. Effect of aerobic exercise training dose on liver fat and visceral adiposity. *J Hepatol,* 63**,** 174-82.

KEERTHIKUMAR, S., CHISANGA, D., ARIYARATNE, D., AL SAFFAR, H., ANAND, S., ZHAO, K., SAMUEL, M., PATHAN, M., JOIS, M., CHILAMKURTI, N., GANGODA, L. & MATHIVANAN, S. 2016. ExoCarta: A Web-Based Compendium of Exosomal Cargo. *J Mol Biol,* 428**,** 688-692.

KERSTEN, S., SEYDOUX, J., PETERS, J. M., GONZALEZ, F. J., DESVERGNE, B. & WAHLI, W. 1999. Peroxisome proliferator-activated receptor alpha mediates the adaptive response to fasting. *J Clin Invest,* 103**,** 1489-98.

KICHIAN, K., MCLEAN, R., GRAMLICH, L. M., BAILEY, R. J. & BAIN, V. G. 2003. Nonalcoholic fatty liver disease in patients investigated for elevated liver enzymes. *Can J Gastroenterol,* 17**,** 38-42.

KIRK, E. A., MOE, G. L., CALDWELL, M. T., LERNMARK, J. A., WILSON, D. L. & LEBOEUF, R. C. 1995. Hyper- and hypo-responsiveness to dietary fat and cholesterol among inbred mice: searching for level and variability genes. *J Lipid Res,* 36**,** 1522-32.

KLEINER, D. E., BRUNT, E. M., VAN NATTA, M., BEHLING, C., CONTOS, M. J., CUMMINGS, O. W., FERRELL, L. D., LIU, Y. C., TORBENSON, M. S., UNALP-ARIDA, A., YEH, M., MCCULLOUGH, A. J., SANYAL, A. J. & NONALCOHOLIC STEATOHEPATITIS CLINICAL RESEARCH, N. 2005. Design and validation of a histological scoring system for nonalcoholic fatty liver disease. *Hepatology,* 41**,** 1313-21.

KMIEĆ, Z. 2001. *Cooperation of liver cells in health and disease,* Berlin ; New York, Springer.

KNITTEL, T., MEHDE, M., KOBOLD, D., SAILE, B., DINTER, C. & RAMADORI, G. 1999. Expression patterns of matrix metalloproteinases and their inhibitors in parenchymal and non-parenchymal cells of rat liver: regulation by TNF-alpha and TGF-beta1. *J Hepatol,* 30**,** 48-60.

KO, S. F., YIP, H. K., ZHEN, Y. Y., LEE, C. C., LEE, C. C., HUANG, C. C., NG, S. H. & LIN, J. W. 2015. Adipose-Derived Mesenchymal Stem Cell Exosomes Suppress Hepatocellular Carcinoma Growth in a Rat Model: Apparent Diffusion Coefficient, Natural Killer T-Cell Responses, and Histopathological Features. *Stem Cells Int,* 2015**,** 853506.

KOECK, E. S., IORDANSKAIA, T., SEVILLA, S., FERRANTE, S. C., HUBAL, M. J., FREISHTAT, R. J. & NADLER, E. P. 2014. Adipocyte exosomes induce transforming growth factor beta pathway dysregulation in hepatocytes: a novel paradigm for obesity-related liver disease. *J Surg Res,* 192**,** 268-75.

KOGURE, T., LIN, W. L., YAN, I. K., BRACONI, C. & PATEL, T. 2011. Intercellular nanovesicle-mediated microRNA transfer: a mechanism of environmental modulation of hepatocellular cancer cell growth. *Hepatology,* 54**,** 1237-48.

KOGURE, T., YAN, I. K., LIN, W. L. & PATEL, T. 2013. Extracellular Vesicle-Mediated Transfer of a Novel Long Noncoding RNA TUC339: A Mechanism of Intercellular Signaling in Human Hepatocellular Cancer. *Genes Cancer,* 4**,** 261-72.

KOHJIMA, M., ENJOJI, M., HIGUCHI, N., KATO, M., KOTOH, K., YOSHIMOTO, T., FUJINO, T., YADA, M., YADA, R., HARADA, N., TAKAYANAGI, R. & NAKAMUTA, M. 2007. Re-evaluation of fatty acid metabolism-related gene expression in nonalcoholic fatty liver disease. *Int J Mol Med,* 20**,** 351-8.

KOHLI, R., KIRBY, M., XANTHAKOS, S. A., SOFTIC, S., FELDSTEIN, A. E., SAXENA, V., TANG, P. H., MILES, L., MILES, M. V., BALISTRERI, W. F., WOODS, S. C. & SEELEY, R. J. 2010. High-fructose, medium chain trans fat diet induces liver fibrosis and elevates plasma coenzyme Q9 in a novel murine model of obesity and nonalcoholic steatohepatitis. *Hepatology,* 52**,** 934-44.

KOOIJMANS, S. A., VADER, P., VAN DOMMELEN, S. M., VAN SOLINGE, W. W. & SCHIFFELERS, R. M. 2012. Exosome mimetics: a novel class of drug delivery systems. *Int J Nanomedicine,* 7**,** 1525-41.

KORNBERG, H. 2000. Krebs and his trinity of cycles. *Nat Rev Mol Cell Biol,* 1**,** 225-8.

KORNEK, M., LYNCH, M., MEHTA, S. H., LAI, M., EXLEY, M., AFDHAL, N. H. & SCHUPPAN, D. 2012. Circulating microparticles as disease-specific biomarkers of severity of inflammation in patients with hepatitis C or nonalcoholic steatohepatitis. *Gastroenterology,* 143**,** 448-58.

KORNEK, M., POPOV, Y., LIBERMANN, T. A., AFDHAL, N. H. & SCHUPPAN, D. 2011. Human T cell microparticles circulate in blood of hepatitis patients and induce fibrolytic activation of hepatic stellate cells. *Hepatology,* 53**,** 230-42.

KORNER, H., COOK, M., RIMINTON, D. S., LEMCKERT, F. A., HOEK, R. M., LEDERMANN, B., KONTGEN, F., FAZEKAS DE ST GROTH, B. & SEDGWICK, J. D. 1997. Distinct roles for lymphotoxin-alpha and tumor necrosis factor in organogenesis and spatial organization of lymphoid tissue. *Eur J Immunol,* 27**,** 2600-9.

KOSAKA, N., IGUCHI, H., YOSHIOKA, Y., TAKESHITA, F., MATSUKI, Y. & OCHIYA, T. 2010. Secretory mechanisms and intercellular transfer of microRNAs in living cells. *J Biol Chem,* 285**,** 17442-52.

KOTRONEN, A., PELTONEN, M., HAKKARAINEN, A., SEVASTIANOVA, K., BERGHOLM, R., JOHANSSON, L. M., LUNDBOM, N., RISSANEN, A., RIDDERSTRALE, M., GROOP, L., ORHO-MELANDER, M. & YKI-JARVINEN, H. 2009. Prediction of non-alcoholic fatty liver disease and liver fat using metabolic and genetic factors. *Gastroenterology,* 137**,** 865-72.

KRANENDONK, M. E., DE KLEIJN, D. P., KALKHOVEN, E., KANHAI, D. A., UITERWAAL, C. S., VAN DER GRAAF, Y., PASTERKAMP, G., VISSEREN, F. L. & GROUP, S. S. 2014a. Extracellular vesicle markers in relation to obesity and metabolic complications in patients with manifest cardiovascular disease. *Cardiovasc Diabetol,* 13**,** 37.

KRANENDONK, M. E., VISSEREN, F. L., VAN HERWAARDEN, J. A., NOLTE-'T HOEN, E. N., DE JAGER, W., WAUBEN, M. H. & KALKHOVEN, E. 2014b. Effect of extracellular vesicles of human adipose tissue on insulin signaling in liver and muscle cells. *Obesity (Silver Spring),* 22**,** 2216-23.

KUCERA, O. & CERVINKOVA, Z. 2014. Experimental models of non-alcoholic fatty liver disease in rats. *World J Gastroenterol,* 20**,** 8364-76.

LAAKSO, T., EDMAN, P. & BRUNK, U. 1988. Biodegradable microspheres. VII: Alterations in mouse liver morphology after intravenous administration of polyacryl starch microparticles with different biodegradability. *J Pharm Sci,* 77**,** 138-44.

LABRECQUE, D. R., ABBAS, Z., ANANIA, F., FERENCI, P., KHAN, A. G., GOH, K. L., HAMID, S. S., ISAKOV, V., LIZARZABAL, M., PENARANDA, M. M., RAMOS, J. F., SARIN, S., STIMAC, D., THOMSON, A. B., UMAR, M., KRABSHUIS, J., LEMAIR, A. & WORLD GASTROENTEROLOGY, O. 2014. World Gastroenterology Organisation global guidelines: Nonalcoholic fatty liver disease and nonalcoholic steatohepatitis. *J Clin Gastroenterol,* 48**,** 467-73.

LACKNER, C. 2011. Hepatocellular ballooning in nonalcoholic steatohepatitis: the pathologist's perspective. *Expert Rev Gastroenterol Hepatol,* 5**,** 223-31.

LAGOS-QUINTANA, M., RAUHUT, R., YALCIN, A., MEYER, J., LENDECKEL, W. & TUSCHL, T. 2002. Identification of tissue-specific microRNAs from mouse. *Curr Biol,* 12**,** 735-9.

LEE, A., RODE, A., NICOLL, A., MACZUREK, A. E., LIM, L., LIM, S., ANGUS, P., KRONBORG, I., ARACHCHI, N., GORELIK, A., LIEW, D., WARNER, F. J.,

MCCAUGHAN, G. W., MCLENNAN, S. V. & SHACKEL, N. A. 2016. Circulating CD147 predicts mortality in advanced hepatocellular carcinoma. *J Gastroenterol Hepatol,* 31**,** 459-66.

LEE, J. H., KIM, D., KIM, H. J., LEE, C. H., YANG, J. I., KIM, W., KIM, Y. J., YOON, J. H., CHO, S. H., SUNG, M. W. & LEE, H. S. 2010a. Hepatic steatosis index: a simple screening tool reflecting nonalcoholic fatty liver disease. *Dig Liver Dis,* 42**,** 503-8.

LEE, S. S., PARK, S. H., KIM, H. J., KIM, S. Y., KIM, M. Y., KIM, D. Y., SUH, D. J., KIM, K. M., BAE, M. H., LEE, J. Y., LEE, S. G. & YU, E. S. 2010b. Non-invasive assessment of hepatic steatosis: prospective comparison of the accuracy of imaging examinations. *J Hepatol,* 52**,** 579-85.

LEE, Y. S., KIM, S. Y., KO, E., LEE, J. H., YI, H. S., YOO, Y. J., JE, J., SUH, S. J., JUNG, Y. K., KIM, J. H., SEO, Y. S., YIM, H. J., JEONG, W. I., YEON, J. E., UM, S. H. & BYUN, K. S. 2017. Exosomes derived from palmitic acid-treated hepatocytes induce fibrotic activation of hepatic stellate cells. *Sci Rep,* 7**,** 3710.

LENER, T., GIMONA, M., AIGNER, L., BORGER, V., BUZAS, E., CAMUSSI, G., CHAPUT, N., CHATTERJEE, D., COURT, F. A., DEL PORTILLO, H. A., O'DRISCOLL, L., FAIS, S., FALCON-PEREZ, J. M., FELDERHOFF-MUESER, U., FRAILE, L., GHO, Y. S., GORGENS, A., GUPTA, R. C., HENDRIX, A., HERMANN, D. M., HILL, A. F., HOCHBERG, F., HORN, P. A., DE KLEIJN, D., KORDELAS, L., KRAMER, B. W., KRAMER-ALBERS, E. M., LANER-PLAMBERGER, S., LAITINEN, S., LEONARDI, T., LORENOWICZ, M. J., LIM, S. K., LOTVALL, J., MAGUIRE, C. A., MARCILLA, A., NAZARENKO, I., OCHIYA, T., PATEL, T., PEDERSEN, S., POCSFALVI, G., PLUCHINO, S., QUESENBERRY, P., REISCHL, I. G., RIVERA, F. J., SANZENBACHER, R., SCHALLMOSER, K., SLAPER-CORTENBACH, I., STRUNK, D., TONN, T., VADER, P., VAN BALKOM, B. W., WAUBEN, M., ANDALOUSSI, S. E., THERY, C., ROHDE, E. & GIEBEL, B. 2015. Applying extracellular vesicles based therapeutics in clinical trials - an ISEV position paper. *J Extracell Vesicles,* 4**,** 30087.

LEONE, T. C., WEINHEIMER, C. J. & KELLY, D. P. 1999. A critical role for the peroxisome proliferator-activated receptor alpha (PPARalpha) in the cellular fasting response: the PPARalpha-null mouse as a model of fatty acid oxidation disorders. *Proc Natl Acad Sci U S A,* 96**,** 7473-8.

LEWIS, G. F. & STEINER, G. 1996. Acute effects of insulin in the control of VLDL production in humans. Implications for the insulin-resistant state. *Diabetes Care,* 19**,** 390-3.

LI, W. C., RALPHS, K. L. & TOSH, D. 2010. Isolation and culture of adult mouse hepatocytes. *Methods Mol Biol,* 633**,** 185-96.

LI, Y., ZHANG, L., LIU, F., XIANG, G., JIANG, D. & PU, X. 2015. Identification of endogenous controls for analyzing serum exosomal miRNA in patients with hepatitis B or hepatocellular carcinoma. *Dis Markers,* 2015**,** 893594.

LIANG, W., MENKE, A. L., DRIESSEN, A., KOEK, G. H., LINDEMAN, J. H., STOOP, R., HAVEKES, L. M., KLEEMANN, R. & VAN DEN HOEK, A. M. 2014. Establishment of a general NAFLD scoring system for rodent models and comparison to human liver pathology. *PLoS One,* 9**,** e115922.

LILLIE, R. D. & ASHBURN, L. L. 1943. Supersaturated solutions of fat stains in dilute isopropanol for demonstration of acute fatty degeneration not shown by Herxheimer's technique. *Archives of Pathology,* 36**,** 432-440.

LO, L., MCLENNAN, S. V., WILLIAMS, P. F., BONNER, J., CHOWDHURY, S., MCCAUGHAN, G. W., GORRELL, M. D., YUE, D. K. & TWIGG, S. M. 2011.

Diabetes is a progression factor for hepatic fibrosis in a high fat fed mouse obesity model of non-alcoholic steatohepatitis. *J Hepatol,* 55**,** 435-44.

LOOMBA, R. & SANYAL, A. J. 2013. The global NAFLD epidemic. *Nat Rev Gastroenterol Hepatol,* 10**,** 686-90.

LOTVALL, J., HILL, A. F., HOCHBERG, F., BUZAS, E. I., DI VIZIO, D., GARDINER, C., GHO, Y. S., KUROCHKIN, I. V., MATHIVANAN, S., QUESENBERRY, P., SAHOO, S., TAHARA, H., WAUBEN, M. H., WITWER, K. W. & THERY, C. 2014. Minimal experimental requirements for definition of extracellular vesicles and their functions: a position statement from the International Society for Extracellular Vesicles. *J Extracell Vesicles,* 3**,** 26913.

LV, L. H., WAN, Y. L., LIN, Y., ZHANG, W., YANG, M., LI, G. L., LIN, H. M., SHANG, C. Z., CHEN, Y. J. & MIN, J. 2012. Anticancer drugs cause release of exosomes with heat shock proteins from human hepatocellular carcinoma cells that elicit effective natural killer cell antitumor responses in vitro. *J Biol Chem,* 287**,** 15874-85.

LYNCH, S. F. & LUDLAM, C. A. 2007. Plasma microparticles and vascular disorders. *Br J Haematol,* 137**,** 36-48.

MACHADO, M. V., MICHELOTTI, G. A., XIE, G., ALMEIDA PEREIRA, T., BOURSIER, J., BOHNIC, B., GUY, C. D. & DIEHL, A. M. 2015. Mouse models of diet-induced nonalcoholic steatohepatitis reproduce the heterogeneity of the human disease. *PLoS One,* 10**,** e0127991.

MARCINKO, K., SIKKEMA, S. R., SAMAAN, M. C., KEMP, B. E., FULLERTON, M. D. & STEINBERG, G. R. 2015. High intensity interval training improves liver and adipose tissue insulin sensitivity. *Mol Metab,* 4**,** 903-15.

MATSUZAWA, N., TAKAMURA, T., KURITA, S., MISU, H., OTA, T., ANDO, H., YOKOYAMA, M., HONDA, M., ZEN, Y., NAKANUMA, Y., MIYAMOTO, K. & KANEKO, S. 2007. Lipid-induced oxidative stress causes steatohepatitis in mice fed an atherogenic diet. *Hepatology,* 46**,** 1392-403.

MCPHERSON, S., HARDY, T., DUFOUR, J. F., PETTA, S., ROMERO-GOMEZ, M., ALLISON, M., OLIVEIRA, C. P., FRANCQUE, S., VAN GAAL, L., SCHATTENBERG, J. M., TINIAKOS, D., BURT, A., BUGIANESI, E., RATZIU, V., DAY, C. P. & ANSTEE, Q. M. 2017. Age as a Confounding Factor for the Accurate Non-Invasive Diagnosis of Advanced NAFLD Fibrosis. *Am J Gastroenterol,* 112**,** 740-751.

MCPHERSON, S., JONSSON, J. R., COWIN, G. J., O'ROURKE, P., CLOUSTON, A. D., VOLP, A., HORSFALL, L., JOTHIMANI, D., FAWCETT, J., GALLOWAY, G. J., BENSON, M. & POWELL, E. E. 2009. Magnetic resonance imaging and spectroscopy accurately estimate the severity of steatosis provided the stage of fibrosis is considered. *J Hepatol,* 51**,** 389-97.

MEMON, R. A., BASS, N. M., MOSER, A. H., FULLER, J., APPEL, R., GRUNFELD, C. & FEINGOLD, K. R. 1999. Down-regulation of liver and heart specific fatty acid binding proteins by endotoxin and cytokines in vivo. *Biochim Biophys Acta,* 1440**,** 118-26.

MEMON, R. A., FEINGOLD, K. R., MOSER, A. H., FULLER, J. & GRUNFELD, C. 1998. Regulation of fatty acid transport protein and fatty acid translocase mRNA levels by endotoxin and cytokines. *Am J Physiol,* 274**,** E210-7.

MEMON, R. A. & GILANI, A. H. 1995. An update on hyperlipidemia and its management. *J Pak Med Assoc,* 45**,** 275-82.

MICHELOTTI, G. A., MACHADO, M. V. & DIEHL, A. M. 2013. NAFLD, NASH and liver cancer. *Nat Rev Gastroenterol Hepatol,* 10**,** 656-65.

MILLIMAGGI, D., MARI, M., D'ASCENZO, S., CAROSA, E., JANNINI, E. A., ZUCKER, S., CARTA, G., PAVAN, A. & DOLO, V. 2007. Tumor vesicle-associated CD147 modulates the angiogenic capability of endothelial cells. *Neoplasia,* 9**,** 349-57.

MOFRAD, P., CONTOS, M. J., HAQUE, M., SARGEANT, C., FISHER, R. A., LUKETIC, V. A., STERLING, R. K., SHIFFMAN, M. L., STRAVITZ, R. T. & SANYAL, A. J. 2003. Clinical and histologic spectrum of nonalcoholic fatty liver disease associated with normal ALT values. *Hepatology,* 37**,** 1286-92.

MOMEN-HERAVI, F., BALA, S., KODYS, K. & SZABO, G. 2015. Exosomes derived from alcohol-treated hepatocytes horizontally transfer liver specific miRNA-122 and sensitize monocytes to LPS. *Sci Rep,* 5**,** 9991.

MOMEN-HERAVI, F., BALAJ, L., ALIAN, S., TIGGES, J., TOXAVIDIS, V., ERICSSON, M., DISTEL, R. J., IVANOV, A. R., SKOG, J. & KUO, W. P. 2012. Alternative methods for characterization of extracellular vesicles. *Front Physiol,* 3**,** 354.

MOTTA, V. F., AGUILA, M. B. & MANDARIM, D. E. L. C. A. 2016. High-intensity interval training (swimming) significantly improves the adverse metabolism and comorbidities in diet-induced obese mice. *J Sports Med Phys Fitness,* 56**,** 655-63.

MOTTIN, C. C., MORETTO, M., PADOIN, A. V., SWAROWSKY, A. M., TONETO, M. G., GLOCK, L. & REPETTO, G. 2004. The role of ultrasound in the diagnosis of hepatic steatosis in morbidly obese patients. *Obes Surg,* 14**,** 635-7.

MULCAHY, L. A., PINK, R. C. & CARTER, D. R. 2014. Routes and mechanisms of extracellular vesicle uptake. *J Extracell Vesicles,* 3.

MURAKAMI, Y., TOYODA, H., TANAHASHI, T., TANAKA, J., KUMADA, T., YOSHIOKA, Y., KOSAKA, N., OCHIYA, T. & TAGUCHI, Y. H. 2012. Comprehensive miRNA expression analysis in peripheral blood can diagnose liver disease. *PLoS One,* 7**,** e48366.

MUSSO, G., GAMBINO, R., CASSADER, M. & PAGANO, G. 2011. Meta-analysis: natural history of non-alcoholic fatty liver disease (NAFLD) and diagnostic accuracy of non-invasive tests for liver disease severity. *Ann Med,* 43**,** 617-49.

NALBANTOGLU, I. L. & BRUNT, E. M. 2014. Role of liver biopsy in nonalcoholic fatty liver disease. *World J Gastroenterol,* 20**,** 9026-37.

O'REILLY, J. N., COGGER, V. C. & LE COUTEUR, D. G. 2010. Old age is associated with ultrastructural changes in isolated rat liver sinusoidal endothelial cells. *J Electron Microsc (Tokyo),* 59**,** 65-9.

OGASAWARA, F., FUSEGAWA, H., HARUKI, Y., SHIRAISHI, K., WATANABE, N. & MATSUZAKI, S. 2005. Platelet activation in patients with alcoholic liver disease. *Tokai J Exp Clin Med,* 30**,** 41-8.

OKUMURA, T. 2011. Role of lipid droplet proteins in liver steatosis. *J Physiol Biochem,* 67**,** 629-36.

OTGONSUREN, M., ESTEP, M. J., HOSSAIN, N., YOUNOSSI, E., FROST, S., HENRY, L., HUNT, S., FANG, Y., GOODMAN, Z. & YOUNOSSI, Z. M. 2014. Single non-invasive model to diagnose non-alcoholic fatty liver disease (NAFLD) and non-alcoholic steatohepatitis (NASH). *J Gastroenterol Hepatol,* 29**,** 2006-13.

PAMIR, N., MCMILLEN, T. S., KAIYALA, K. J., SCHWARTZ, M. W. & LEBOEUF, R. C. 2009. Receptors for tumor necrosis factor-alpha play a protective role against obesity and alter adipose tissue macrophage status. *Endocrinology,* 150**,** 4124-34.

PARK, S. H., KIM, P. N., KIM, K. W., LEE, S. W., YOON, S. E., PARK, S. W., HA, H. K., LEE, M. G., HWANG, S., LEE, S. G., YU, E. S. & CHO, E. Y. 2006. Macrovesicular hepatic steatosis in living liver donors: use of CT for quantitative and qualitative assessment. *Radiology,* 239**,** 105-12.

PATSOURIS, D., REDDY, J. K., MULLER, M. & KERSTEN, S. 2006. Peroxisome proliferator-activated receptor alpha mediates the effects of high-fat diet on hepatic gene expression. *Endocrinology,* 147**,** 1508-16.

PERAZZO, H. & DUFOUR, J. F. 2017. The therapeutic landscape of non-alcoholic steatohepatitis. *Liver Int,* 37**,** 634-647.

PERRY, R. J., SAMUEL, V. T., PETERSEN, K. F. & SHULMAN, G. I. 2014. The role of hepatic lipids in hepatic insulin resistance and type 2 diabetes. *Nature,* 510**,** 84-91.

PETER, A., STEFAN, N., CEGAN, A., WALENTA, M., WAGNER, S., KONIGSRAINER, A., KONIGSRAINER, I., MACHICAO, F., SCHICK, F., HARING, H. U. & SCHLEICHER, E. 2011. Hepatic glucokinase expression is associated with lipogenesis and fatty liver in humans. *J Clin Endocrinol Metab,* 96**,** E1126-30.

PETERSEN, M. C., VATNER, D. F. & SHULMAN, G. I. 2017. Regulation of hepatic glucose metabolism in health and disease. *Nat Rev Endocrinol,* 13**,** 572-587.

PETIT, J. M., MASSON, D., GUIU, B., ROLLOT, F., DUVILLARD, L., BOUILLET, B., BRINDISI, M. C., BUFFIER, P., HILLON, P., CERCUEIL, J. P. & VERGES, B. 2016. GCKR polymorphism influences liver fat content in patients with type 2 diabetes. *Acta Diabetol,* 53**,** 237-42.

PHILLIPS, M. S., LIU, Q., HAMMOND, H. A., DUGAN, V., HEY, P. J., CASKEY, C. J. & HESS, J. F. 1996. Leptin receptor missense mutation in the fatty Zucker rat. *Nat Genet,* 13**,** 18-9.

POCOCK, G., RICHARDS, C. D. & RICHARDS, D. A. 2013. The Gastrointestinal System. *Human Physiology.* 4th ed.: OUP Oxford.

POSPICHALOVA, V., SVOBODA, J., DAVE, Z., KOTRBOVA, A., KAISER, K., KLEMOVA, D., ILKOVICS, L., HAMPL, A., CRHA, I., JANDAKOVA, E., MINAR, L., WEINBERGER, V. & BRYJA, V. 2015. Simplified protocol for flow cytometry analysis of fluorescently labeled exosomes and microvesicles using dedicated flow cytometer. *J Extracell Vesicles,* 4**,** 25530.

POSTIC, C. & GIRARD, J. 2008. Contribution of de novo fatty acid synthesis to hepatic steatosis and insulin resistance: lessons from genetically engineered mice. *J Clin Invest,* 118**,** 829-38.

POSTIC, C., SHIOTA, M. & MAGNUSON, M. A. 2001. Cell-specific roles of glucokinase in glucose homeostasis. *Recent Prog Horm Res,* 56**,** 195-217.

POVERO, D., EGUCHI, A., LI, H., JOHNSON, C. D., PAPOUCHADO, B. G., WREE, A., MESSER, K. & FELDSTEIN, A. E. 2014. Circulating extracellular vesicles with specific proteome and liver microRNAs are potential biomarkers for liver injury in experimental fatty liver disease. *PLoS One,* 9**,** e113651.

POVERO, D., EGUCHI, A., NIESMAN, I. R., ANDRONIKOU, N., DE MOLLERAT DU JEU, X., MULYA, A., BERK, M., LAZIC, M., THAPALIYA, S., PAROLA, M., PATEL, H. H. & FELDSTEIN, A. E. 2013. Lipid-induced toxicity stimulates hepatocytes to release angiogenic microparticles that require Vanin-1 for uptake by endothelial cells. *Sci Signal,* 6**,** ra88.

POVERO, D., PANERA, N., EGUCHI, A., JOHNSON, C. D., PAPOUCHADO, B. G., DE ARAUJO HORCEL, L., PINATEL, E. M., ALISI, A., NOBILI, V. & FELDSTEIN, A. E. 2015. Lipid-induced hepatocyte-derived extracellular vesicles regulate hepatic stellate cell via microRNAs targeting PPAR-gamma. *Cell Mol Gastroenterol Hepatol,* 1**,** 646-663 e4.

POYNARD, T., RATZIU, V., CHARLOTTE, F., MESSOUS, D., MUNTEANU, M., IMBERT-BISMUT, F., MASSARD, J., BONYHAY, L., TAHIRI, M., THABUT, D., CADRANEL, J. F., LE BAIL, B., DE LEDINGHEN, V., GROUP, L. S. & GROUP, C. S. 2006. Diagnostic value of biochemical markers (NashTest) for the prediction of

non alcoholo steato hepatitis in patients with non-alcoholic fatty liver disease. *BMC Gastroenterol,* 6**,** 34.

POYNARD, T., RATZIU, V., NAVEAU, S., THABUT, D., CHARLOTTE, F., MESSOUS, D., CAPRON, D., ABELLA, A., MASSARD, J., NGO, Y., MUNTEANU, M., MERCADIER, A., MANNS, M. & ALBRECHT, J. 2005. The diagnostic value of biomarkers (SteatoTest) for the prediction of liver steatosis. *Comp Hepatol,* 4**,** 10.

PRADERE, J. P., KLUWE, J., DE MINICIS, S., JIAO, J. J., GWAK, G. Y., DAPITO, D. H., JANG, M. K., GUENTHER, N. D., MEDERACKE, I., FRIEDMAN, R., DRAGOMIR, A. C., ALOMAN, C. & SCHWABE, R. F. 2013. Hepatic macrophages but not dendritic cells contribute to liver fibrosis by promoting the survival of activated hepatic stellate cells in mice. *Hepatology,* 58**,** 1461-73.

PURI, P., BAILLIE, R. A., WIEST, M. M., MIRSHAHI, F., CHOUDHURY, J., CHEUNG, O., SARGEANT, C., CONTOS, M. J. & SANYAL, A. J. 2007. A lipidomic analysis of nonalcoholic fatty liver disease. *Hepatology,* 46**,** 1081-90.

PURI, P., WIEST, M. M., CHEUNG, O., MIRSHAHI, F., SARGEANT, C., MIN, H. K., CONTOS, M. J., STERLING, R. K., FUCHS, M., ZHOU, H., WATKINS, S. M. & SANYAL, A. J. 2009. The plasma lipidomic signature of nonalcoholic steatohepatitis. *Hepatology,* 50**,** 1827-38.

RAMLO-HALSTED, B. A. & EDELMAN, S. V. 1999. The natural history of type 2 diabetes. Implications for clinical practice. *Prim Care,* 26**,** 771-89.

RAND, M. L., WANG, H., PLUTHERO, F. G., STAFFORD, A. R., NI, R., VAEZZADEH, N., ALLISON, A. C., KAHR, W. H., WEITZ, J. I. & GROSS, P. L. 2012. Diannexin, an annexin A5 homodimer, binds phosphatidylserine with high affinity and is a potent inhibitor of platelet-mediated events during thrombus formation. *J Thromb Haemost,* 10**,** 1109-19.

RATZIU, V., CADRANEL, J. F., SERFATY, L., DENIS, J., RENOU, C., DELASSALLE, P., BERNHARDT, C. & PERLEMUTER, G. 2012. A survey of patterns of practice and perception of NAFLD in a large sample of practicing gastroenterologists in France. *J Hepatol,* 57**,** 376-83.

RATZIU, V., CHARLOTTE, F., HEURTIER, A., GOMBERT, S., GIRAL, P., BRUCKERT, E., GRIMALDI, A., CAPRON, F., POYNARD, T. & GROUP, L. S. 2005. Sampling variability of liver biopsy in nonalcoholic fatty liver disease. *Gastroenterology,* 128**,** 1898-906.

RAUBENHEIMER, P. J., NYIRENDA, M. J. & WALKER, B. R. 2006. A choline-deficient diet exacerbates fatty liver but attenuates insulin resistance and glucose intolerance in mice fed a high-fat diet. *Diabetes,* 55**,** 2015-20.

REDONNET, A., GROUBET, R., NOEL-SUBERVILLE, C., BONILLA, S., MARTINEZ, A. & HIGUERET, P. 2001. Exposure to an obesity-inducing diet early affects the pattern of expression of peroxisome proliferator, retinoic acid, and triiodothyronine nuclear receptors in the rat. *Metabolism,* 50**,** 1161-7.

REDZIC, J. S., KENDRICK, A. A., BAHMED, K., DAHL, K. D., PEARSON, C. G., ROBINSON, W. A., ROBINSON, S. E., GRANER, M. W. & EISENMESSER, E. Z. 2013. Extracellular vesicles secreted from cancer cell lines stimulate secretion of MMP-9, IL-6, TGF-beta1 and EMMPRIN. *PLoS One,* 8**,** e71225.

REEDER, S. B., CRUITE, I., HAMILTON, G. & SIRLIN, C. B. 2011. Quantitative assessment of liver fat with magnetic resonance imaging and spectroscopy. *J Magn Reson Imaging,* 34**,** 729-49.

REKKER, K., SAARE, M., ROOST, A. M., KUBO, A. L., ZAROVNI, N., CHIESI, A., SALUMETS, A. & PETERS, M. 2014. Comparison of serum exosome isolation methods for microRNA profiling. *Clin Biochem,* 47**,** 135-8.

RINELLA, M. E. & GREEN, R. M. 2004. The methionine-choline deficient dietary model of steatohepatitis does not exhibit insulin resistance. *J Hepatol,* 40**,** 47-51.
ROBBINS, P. D. 2017. Extracellular vesicles and aging. *Stem Cell Investig,* 4**,** 98.
ROWE, J. W., MINAKER, K. L., PALLOTTA, J. A. & FLIER, J. S. 1983. Characterization of the insulin resistance of aging. *J Clin Invest,* 71**,** 1581-7.
RULL, A., CAMPS, J., ALONSO-VILLAVERDE, C. & JOVEN, J. 2010. Insulin resistance, inflammation, and obesity: role of monocyte chemoattractant protein-1 (or CCL2) in the regulation of metabolism. *Mediators Inflamm,* 2010**,** 326580.
RYAN, C. K., JOHNSON, L. A., GERMIN, B. I. & MARCOS, A. 2002. One hundred consecutive hepatic biopsies in the workup of living donors for right lobe liver transplantation. *Liver Transpl,* 8**,** 1114-22.
SAFDAR, A., SALEEM, A. & TARNOPOLSKY, M. A. 2016. The potential of endurance exercise-derived exosomes to treat metabolic diseases. *Nat Rev Endocrinol,* 12**,** 504-17.
SAILE, B., MATTHES, N., KNITTEL, T. & RAMADORI, G. 1999. Transforming growth factor beta and tumor necrosis factor alpha inhibit both apoptosis and proliferation of activated rat hepatic stellate cells. *Hepatology,* 30**,** 196-202.
SALLES, J., TARDIF, N., LANDRIER, J. F., MOTHE-SATNEY, I., GUILLET, C., BOUE-VAYSSE, C., COMBARET, L., GIRAUDET, C., PATRAC, V., BERTRAND-MICHEL, J., DENIS, P., CHARDIGNY, J. M., BOIRIE, Y. & WALRAND, S. 2012. TNFalpha gene knockout differentially affects lipid deposition in liver and skeletal muscle of high-fat-diet mice. *J Nutr Biochem,* 23**,** 1685-93.
SARTIPY, P. & LOSKUTOFF, D. J. 2003. Monocyte chemoattractant protein 1 in obesity and insulin resistance. *Proc Natl Acad Sci U S A,* 100**,** 7265-70.
SASSO, M., BEAUGRAND, M., DE LEDINGHEN, V., DOUVIN, C., MARCELLIN, P., POUPON, R., SANDRIN, L. & MIETTE, V. 2010. Controlled attenuation parameter (CAP): a novel VCTE guided ultrasonic attenuation measurement for the evaluation of hepatic steatosis: preliminary study and validation in a cohort of patients with chronic liver disease from various causes. *Ultrasound Med Biol,* 36**,** 1825-35.
SHARPTON, S. R., AJMERA, V. & LOOMBA, R. 2018. Emerging Role of the Gut Microbiome in Nonalcoholic Fatty Liver Disease: From Composition to Function. *Clin Gastroenterol Hepatol,* 17**,** 296-306.
SHEN, F., ZHENG, R. D., MI, Y. Q., WANG, X. Y., PAN, Q., CHEN, G. Y., CAO, H. X., CHEN, M. L., XU, L., CHEN, J. N., CAO, Y., ZHANG, R. N., XU, L. M. & FAN, J. G. 2014. Controlled attenuation parameter for non-invasive assessment of hepatic steatosis in Chinese patients. *World J Gastroenterol,* 20**,** 4702-11.
SHEN, J., CHAN, H. L., WONG, G. L., CHOI, P. C., CHAN, A. W., CHAN, H. Y., CHIM, A. M., YEUNG, D. K., CHAN, F. K., WOO, J., YU, J., CHU, W. C. & WONG, V. W. 2012a. Non-invasive diagnosis of non-alcoholic steatohepatitis by combined serum biomarkers. *J Hepatol,* 56**,** 1363-70.
SHEN, Y., GIARDINO TORCHIA, M. L., LAWSON, G. W., KARP, C. L., ASHWELL, J. D. & MAZMANIAN, S. K. 2012b. Outer membrane vesicles of a human commensal mediate immune regulation and disease protection. *Cell Host Microbe,* 12**,** 509-20.
SHIMANO, H., YAHAGI, N., AMEMIYA-KUDO, M., HASTY, A. H., OSUGA, J., TAMURA, Y., SHIONOIRI, F., IIZUKA, Y., OHASHI, K., HARADA, K., GOTODA, T., ISHIBASHI, S. & YAMADA, N. 1999. Sterol regulatory element-binding protein-1 as a key transcription factor for nutritional induction of lipogenic enzyme genes. *J Biol Chem,* 274**,** 35832-9.
SHOJAEE-MORADIE, F., CUTHBERTSON, D. J., BARRETT, M., JACKSON, N. C., HERRING, R., THOMAS, E. L., BELL, J., KEMP, G. J., WRIGHT, J. & UMPLEBY,

A. M. 2016. Exercise Training Reduces Liver Fat and Increases Rates of VLDL Clearance But Not VLDL Production in NAFLD. *J Clin Endocrinol Metab,* 101**,** 4219-4228.

SIDHU, S. S., MENGISTAB, A. T., TAUSCHER, A. N., LAVAIL, J. & BASBAUM, C. 2004. The microvesicle as a vehicle for EMMPRIN in tumor-stromal interactions. *Oncogene,* 23**,** 956-63.

SIMONS, M. & RAPOSO, G. 2009. Exosomes--vesicular carriers for intercellular communication. *Curr Opin Cell Biol,* 21**,** 575-81.

SINGER, S. S., HENKELS, K., DEUCHER, A., BARKER, M., SINGER, J. & TRULZSCH, D. V. 1996. Growth hormone and aging change rat liver fatty acid binding protein levels. *J Am Coll Nutr,* 15**,** 169-74.

SINGH, S., ALLEN, A. M., WANG, Z., PROKOP, L. J., MURAD, M. H. & LOOMBA, R. 2015. Fibrosis progression in nonalcoholic fatty liver vs nonalcoholic steatohepatitis: a systematic review and meta-analysis of paired-biopsy studies. *Clin Gastroenterol Hepatol,* 13**,** 643-54 e1-9; quiz e39-40.

SODAR, B. W., KITTEL, A., PALOCZI, K., VUKMAN, K. V., OSTEIKOETXEA, X., SZABO-TAYLOR, K., NEMETH, A., SPERLAGH, B., BARANYAI, T., GIRICZ, Z., WIENER, Z., TURIAK, L., DRAHOS, L., PALLINGER, E., VEKEY, K., FERDINANDY, P., FALUS, A. & BUZAS, E. I. 2016. Low-density lipoprotein mimics blood plasma-derived exosomes and microvesicles during isolation and detection. *Sci Rep,* 6**,** 24316.

SORBI, D., BOYNTON, J. & LINDOR, K. D. 1999. The ratio of aspartate aminotransferase to alanine aminotransferase: potential value in differentiating nonalcoholic steatohepatitis from alcoholic liver disease. *Am J Gastroenterol,* 94**,** 1018-22.

SOSSDORF, M., OTTO, G. P., CLAUS, R. A., GABRIEL, H. H. & LOSCHE, W. 2011. Cell-derived microparticles promote coagulation after moderate exercise. *Med Sci Sports Exerc,* 43**,** 1169-76.

STERN, C. & CASTERA, L. 2017. Non-invasive diagnosis of hepatic steatosis. *Hepatol Int,* 11**,** 70-78.

STINCONE, A., PRIGIONE, A., CRAMER, T., WAMELINK, M. M., CAMPBELL, K., CHEUNG, E., OLIN-SANDOVAL, V., GRUNING, N. M., KRUGER, A., TAUQEER ALAM, M., KELLER, M. A., BREITENBACH, M., BRINDLE, K. M., RABINOWITZ, J. D. & RALSER, M. 2015. The return of metabolism: biochemistry and physiology of the pentose phosphate pathway. *Biol Rev Camb Philos Soc,* 90**,** 927-63.

STRAVITZ, R. T., BOWLING, R., BRADFORD, R. L., KEY, N. S., GLOVER, S., THACKER, L. R. & GABRIEL, D. A. 2013. Role of procoagulant microparticles in mediating complications and outcome of acute liver injury/acute liver failure. *Hepatology,* 58**,** 304-13.

SUGIMACHI, K., MATSUMURA, T., HIRATA, H., UCHI, R., UEDA, M., UEO, H., SHINDEN, Y., IGUCHI, T., EGUCHI, H., SHIRABE, K., OCHIYA, T., MAEHARA, Y. & MIMORI, K. 2015. Identification of a bona fide microRNA biomarker in serum exosomes that predicts hepatocellular carcinoma recurrence after liver transplantation. *Br J Cancer,* 112**,** 532-8.

SULLIVAN, S., KIRK, E. P., MITTENDORFER, B., PATTERSON, B. W. & KLEIN, S. 2012. Randomized trial of exercise effect on intrahepatic triglyceride content and lipid kinetics in nonalcoholic fatty liver disease. *Hepatology,* 55**,** 1738-45.

SUN, L., HU, J., XIONG, W., CHEN, X., LI, H. & JIE, S. 2013. MicroRNA expression profiles of circulating microvesicles in hepatocellular carcinoma. *Acta Gastroenterol Belg,* 76**,** 386-92.

TAKAHASHI, K., YAN, I. K., KOGURE, T., HAGA, H. & PATEL, T. 2014. Extracellular vesicle-mediated transfer of long non-coding RNA ROR modulates chemosensitivity in human hepatocellular cancer. *FEBS Open Bio,* 4**,** 458-67.

TAKASUGI, M., OKADA, R., TAKAHASHI, A., VIRYA CHEN, D., WATANABE, S. & HARA, E. 2017. Small extracellular vesicles secreted from senescent cells promote cancer cell proliferation through EphA2. *Nat Commun,* 8**,** 15729.

TAYLOR, D. D. & SHAH, S. 2015. Methods of isolating extracellular vesicles impact down-stream analyses of their cargoes. *Methods,* 87**,** 3-10.

TEUFEL, A., ITZEL, T., ERHART, W., BROSCH, M., WANG, X. Y., KIM, Y. O., VON SCHONFELS, W., HERRMANN, A., BRUCKNER, S., STICKEL, F., DUFOUR, J. F., CHAVAKIS, T., HELLERBRAND, C., SPANG, R., MAASS, T., BECKER, T., SCHREIBER, S., SCHAFMAYER, C., SCHUPPAN, D. & HAMPE, J. 2016. Comparison of Gene Expression Patterns Between Mouse Models of Nonalcoholic Fatty Liver Disease and Liver Tissues From Patients. *Gastroenterology,* 151**,** 513-525 e0.

THERY, C., AMIGORENA, S., RAPOSO, G. & CLAYTON, A. 2006. Isolation and characterization of exosomes from cell culture supernatants and biological fluids. *Curr Protoc Cell Biol,* Chapter 3**,** Unit 3 22.

THRIFT, R. N., FORTE, T. M., CAHOON, B. E. & SHORE, V. G. 1986. Characterization of lipoproteins produced by the human liver cell line, Hep G2, under defined conditions. *J Lipid Res,* 27**,** 236-50.

TILG, H. & MOSCHEN, A. R. 2008. Insulin resistance, inflammation, and non-alcoholic fatty liver disease. *Trends Endocrinol Metab,* 19**,** 371-9.

TOMITA, K., TAMIYA, G., ANDO, S., OHSUMI, K., CHIYO, T., MIZUTANI, A., KITAMURA, N., TODA, K., KANEKO, T., HORIE, Y., HAN, J. Y., KATO, S., SHIMODA, M., OIKE, Y., TOMIZAWA, M., MAKINO, S., OHKURA, T., SAITO, H., KUMAGAI, N., NAGATA, H., ISHII, H. & HIBI, T. 2006. Tumour necrosis factor alpha signalling through activation of Kupffer cells plays an essential role in liver fibrosis of non-alcoholic steatohepatitis in mice. *Gut,* 55**,** 415-24.

TRAJKOVIC, K., HSU, C., CHIANTIA, S., RAJENDRAN, L., WENZEL, D., WIELAND, F., SCHWILLE, P., BRUGGER, B. & SIMONS, M. 2008. Ceramide triggers budding of exosome vesicles into multivesicular endosomes. *Science,* 319**,** 1244-7.

TRAK-SMAYRA, V., PARADIS, V., MASSART, J., NASSER, S., JEBARA, V. & FROMENTY, B. 2011. Pathology of the liver in obese and diabetic ob/ob and db/db mice fed a standard or high-calorie diet. *Int J Exp Pathol,* 92**,** 413-21.

TURNER, N., KOWALSKI, G. M., LESLIE, S. J., RISIS, S., YANG, C., LEE-YOUNG, R. S., BABB, J. R., MEIKLE, P. J., LANCASTER, G. I., HENSTRIDGE, D. C., WHITE, P. J., KRAEGEN, E. W., MARETTE, A., COONEY, G. J., FEBBRAIO, M. A. & BRUCE, C. R. 2013. Distinct patterns of tissue-specific lipid accumulation during the induction of insulin resistance in mice by high-fat feeding. *Diabetologia,* 56**,** 1638-48.

UYSAL, K. T., WIESBROCK, S. M. & HOTAMISLIGIL, G. S. 1998. Functional analysis of tumor necrosis factor (TNF) receptors in TNF-alpha-mediated insulin resistance in genetic obesity. *Endocrinology,* 139**,** 4832-8.

UYSAL, K. T., WIESBROCK, S. M., MARINO, M. W. & HOTAMISLIGIL, G. S. 1997. Protection from obesity-induced insulin resistance in mice lacking TNF-alpha function. *Nature,* 389**,** 610-4.

VALADI, H., EKSTROM, K., BOSSIOS, A., SJOSTRAND, M., LEE, J. J. & LOTVALL, J. O. 2007. Exosome-mediated transfer of mRNAs and microRNAs is a novel mechanism of genetic exchange between cells. *Nat Cell Biol,* 9**,** 654-9.

VAN DER POL, E., BOING, A. N., HARRISON, P., STURK, A. & NIEUWLAND, R. 2012. Classification, functions, and clinical relevance of extracellular vesicles. *Pharmacol Rev,* 64**,** 676-705.

VAN DER VLIST, E. J., NOLTE-'T HOEN, E. N., STOORVOGEL, W., ARKESTEIJN, G. J. & WAUBEN, M. H. 2012. Fluorescent labeling of nano-sized vesicles released by cells and subsequent quantitative and qualitative analysis by high-resolution flow cytometry. *Nat Protoc,* 7**,** 1311-26.

VANPUTTE, C. L., REGAN, J. L., RUSSO, A. F. & SEELEY, R. R. 2010. *Seeley's essentials of anatomy and physiology,* Dubuque, McGraw-Hill.

VILAR-GOMEZ, E., MARTINEZ-PEREZ, Y., CALZADILLA-BERTOT, L., TORRES-GONZALEZ, A., GRA-ORAMAS, B., GONZALEZ-FABIAN, L., FRIEDMAN, S. L., DIAGO, M. & ROMERO-GOMEZ, M. 2015. Weight Loss Through Lifestyle Modification Significantly Reduces Features of Nonalcoholic Steatohepatitis. *Gastroenterology,* 149**,** 367-78 e5; quiz e14-5.

VUPPALANCHI, R., UNALP, A., VAN NATTA, M. L., CUMMINGS, O. W., SANDRASEGARAN, K. E., HAMEED, T., TONASCIA, J. & CHALASANI, N. 2009. Effects of liver biopsy sample length and number of readings on sampling variability in nonalcoholic Fatty liver disease. *Clin Gastroenterol Hepatol,* 7**,** 481-6.

WAHL, P., JANSEN, F., ACHTZEHN, S., SCHMITZ, T., BLOCH, W., MESTER, J. & WERNER, N. 2014. Effects of high intensity training and high volume training on endothelial microparticles and angiogenic growth factors. *PLoS One,* 9**,** e96024.

WANG, H., HOU, L., LI, A., DUAN, Y., GAO, H. & SONG, X. 2014. Expression of serum exosomal microRNA-21 in human hepatocellular carcinoma. *Biomed Res Int,* 2014**,** 864894.

WANG, X., DING, X., NAN, L., WANG, Y., WANG, J., YAN, Z., ZHANG, W., SUN, J., ZHU, W., NI, B., DONG, S. & YU, L. 2015. Investigation of the roles of exosomes in colorectal cancer liver metastasis. *Oncol Rep,* 33**,** 2445-53.

WARNE, J. P. 2003. Tumour necrosis factor alpha: a key regulator of adipose tissue mass. *J Endocrinol,* 177**,** 351-5.

WAUBEN, M. H. M. 2016. Extracellular Vesicles. *In:* BRADSHAW, R. A. & STAHL, P. D. (eds.) *Encyclopedia of Cell Biology.* Waltham: Academic Press.

WELSH, J. A., SCORLETTI, E., CLOUGH, G. F., ENGLYST, N. A. & BYRNE, C. D. 2018. Leukocyte extracellular vesicle concentration is inversely associated with liver fibrosis severity in NAFLD. *J Leukoc Biol,* 104**,** 631-639.

WENG, Y., SUI, Z., SHAN, Y., HU, Y., CHEN, Y., ZHANG, L. & ZHANG, Y. 2016. Effective isolation of exosomes with polyethylene glycol from cell culture supernatant for in-depth proteome profiling. *Analyst,* 141**,** 4640-6.

WHITHAM, M., PARKER, B. L., FRIEDRICHSEN, M., HINGST, J. R., HJORTH, M., HUGHES, W. E., EGAN, C. L., CRON, L., WATT, K. I., KUCHEL, R. P., JAYASOORIAH, N., ESTEVEZ, E., PETZOLD, T., SUTER, C. M., GREGOREVIC, P., KIENS, B., RICHTER, E. A., JAMES, D. E., WOJTASZEWSKI, J. F. P. & FEBBRAIO, M. A. 2018. Extracellular Vesicles Provide a Means for Tissue Crosstalk during Exercise. *Cell Metab,* 27**,** 237-251 e4.

WILHELM, E. N., GONZALEZ-ALONSO, J., PARRIS, C. & RAKOBOWCHUK, M. 2016. Exercise intensity modulates the appearance of circulating microvesicles with proangiogenic potential upon endothelial cells. *Am J Physiol Heart Circ Physiol,* 311**,** H1297-H1310.

WITWER, K. W., BUZAS, E. I., BEMIS, L. T., BORA, A., LASSER, C., LOTVALL, J., NOLTE-'T HOEN, E. N., PIPER, M. G., SIVARAMAN, S., SKOG, J., THERY, C.,

WAUBEN, M. H. & HOCHBERG, F. 2013. Standardization of sample collection, isolation and analysis methods in extracellular vesicle research. *J Extracell Vesicles,* 2.
WITWER, K. W., SOEKMADJI, C., HILL, A. F., WAUBEN, M. H., BUZAS, E. I., DI VIZIO, D., FALCON-PEREZ, J. M., GARDINER, C., HOCHBERG, F., KUROCHKIN, I. V., LOTVALL, J., MATHIVANAN, S., NIEUWLAND, R., SAHOO, S., TAHARA, H., TORRECILHAS, A. C., WEAVER, A. M., YIN, H., ZHENG, L., GHO, Y. S., QUESENBERRY, P. & THERY, C. 2017. Updating the MISEV minimal requirements for extracellular vesicle studies: building bridges to reproducibility. *J Extracell Vesicles,* 6**,** 1396823.
WOOD, T. 1986. Physiological functions of the pentose phosphate pathway. *Cell Biochem Funct,* 4**,** 241-7.
WORLD HEALTH ORGANIZATION. 2017. Global Hepatitis Report 2017. Available: http://www.who.int/iris/handle/10665/255016 [Accessed Jan 2017].
WYNNE, H. A., COPE, L. H., MUTCH, E., RAWLINS, M. D., WOODHOUSE, K. W. & JAMES, O. F. 1989. The effect of age upon liver volume and apparent liver blood flow in healthy man. *Hepatology,* 9**,** 297-301.
WYNNE, H. A. & JAMES, O. F. 1990. The ageing liver. *Age Ageing,* 19**,** 1-3.
XIAO, W., DONG, W., ZHANG, C., SAREN, G., GENG, P., ZHAO, H., LI, Q., ZHU, J., LI, G., ZHANG, S. & YE, M. 2013. Effects of the epigenetic drug MS-275 on the release and function of exosome-related immune molecules in hepatocellular carcinoma cells. *Eur J Med Res,* 18**,** 61.
XIONG, X., WANG, X., LU, Y., WANG, E., ZHANG, Z., YANG, J., ZHANG, H. & LI, X. 2014. Hepatic steatosis exacerbated by endoplasmic reticulum stress-mediated downregulation of FXR in aging mice. *J Hepatol,* 60**,** 847-54.
XU, J., TERAN-GARCIA, M., PARK, J. H., NAKAMURA, M. T. & CLARKE, S. D. 2001. Polyunsaturated fatty acids suppress hepatic sterol regulatory element-binding protein-1 expression by accelerating transcript decay. *J Biol Chem,* 276**,** 9800-7.
XU, Y., BIALIK, S., JONES, B. E., IIMURO, Y., KITSIS, R. N., SRINIVASAN, A., BRENNER, D. A. & CZAJA, M. J. 1998. NF-kappaB inactivation converts a hepatocyte cell line TNF-alpha response from proliferation to apoptosis. *Am J Physiol,* 275**,** C1058-66.
YAHAGI, N., SHIMANO, H., HASTY, A. H., MATSUZAKA, T., IDE, T., YOSHIKAWA, T., AMEMIYA-KUDO, M., TOMITA, S., OKAZAKI, H., TAMURA, Y., IIZUKA, Y., OHASHI, K., OSUGA, J., HARADA, K., GOTODA, T., NAGAI, R., ISHIBASHI, S. & YAMADA, N. 2002. Absence of sterol regulatory element-binding protein-1 (SREBP-1) ameliorates fatty livers but not obesity or insulin resistance in Lep(ob)/Lep(ob) mice. *J Biol Chem,* 277**,** 19353-7.
YAMADA, H., OHASHI, K., SUZUKI, K., MUNETSUNA, E., ANDO, Y., YAMAZAKI, M., ISHIKAWA, H., ICHINO, N., TERADAIRA, R. & HASHIMOTO, S. 2015. Longitudinal study of circulating miR-122 in a rat model of non-alcoholic fatty liver disease. *Clin Chim Acta,* 446**,** 267-71.
YAMASHITA, T., TAKAHASHI, Y., NISHIKAWA, M. & TAKAKURA, Y. 2016. Effect of exosome isolation methods on physicochemical properties of exosomes and clearance of exosomes from the blood circulation. *Eur J Pharm Biopharm,* 98**,** 1-8.
YANEZ-MO, M., SILJANDER, P. R., ANDREU, Z., ZAVEC, A. B., BORRAS, F. E., BUZAS, E. I., BUZAS, K., CASAL, E., CAPPELLO, F., CARVALHO, J., COLAS, E., CORDEIRO-DA SILVA, A., FAIS, S., FALCON-PEREZ, J. M., GHOBRIAL, I. M., GIEBEL, B., GIMONA, M., GRANER, M., GURSEL, I., GURSEL, M., HEEGAARD, N. H., HENDRIX, A., KIERULF, P., KOKUBUN, K., KOSANOVIC, M., KRALJ-IGLIC, V., KRAMER-ALBERS, E. M., LAITINEN, S., LASSER, C.,

LENER, T., LIGETI, E., LINE, A., LIPPS, G., LLORENTE, A., LOTVALL, J., MANCEK-KEBER, M., MARCILLA, A., MITTELBRUNN, M., NAZARENKO, I., NOLTE-'T HOEN, E. N., NYMAN, T. A., O'DRISCOLL, L., OLIVAN, M., OLIVEIRA, C., PALLINGER, E., DEL PORTILLO, H. A., REVENTOS, J., RIGAU, M., ROHDE, E., SAMMAR, M., SANCHEZ-MADRID, F., SANTAREM, N., SCHALLMOSER, K., OSTENFELD, M. S., STOORVOGEL, W., STUKELJ, R., VAN DER GREIN, S. G., VASCONCELOS, M. H., WAUBEN, M. H. & DE WEVER, O. 2015. Biological properties of extracellular vesicles and their physiological functions. *J Extracell Vesicles,* 4**,** 27066.

YANG, L., ROH, Y. S., SONG, J., ZHANG, B., LIU, C., LOOMBA, R. & SEKI, E. 2014. Transforming growth factor beta signaling in hepatocytes participates in steatohepatitis through regulation of cell death and lipid metabolism in mice. *Hepatology,* 59**,** 483-95.

YOUNOSSI, Z. M., KOENIG, A. B., ABDELATIF, D., FAZEL, Y., HENRY, L. & WYMER, M. 2016. Global epidemiology of nonalcoholic fatty liver disease-Meta-analytic assessment of prevalence, incidence, and outcomes. *Hepatology,* 64**,** 73-84.

YUANA, Y., BOING, A. N., GROOTEMAAT, A. E., VAN DER POL, E., HAU, C. M., CIZMAR, P., BUHR, E., STURK, A. & NIEUWLAND, R. 2015. Handling and storage of human body fluids for analysis of extracellular vesicles. *J Extracell Vesicles,* 4**,** 29260.

ZELBER-SAGI, S., RATZIU, V. & OREN, R. 2011. Nutrition and physical activity in NAFLD: an overview of the epidemiological evidence. *World J Gastroenterol,* 17**,** 3377-89.

ZHANG, F., HAO, G., SHAO, M., NHAM, K., AN, Y., WANG, Q., ZHU, Y., KUSMINSKI, C. M., HASSAN, G., GUPTA, R. K., ZHAI, Q., SUN, X., SCHERER, P. E. & OZ, O. K. 2018. An Adipose Tissue Atlas: An Image-Guided Identification of Human-like BAT and Beige Depots in Rodents. *Cell Metab,* 27**,** 252-262 e3.

ZHANG, J., SHAN, W. F., JIN, T. T., WU, G. Q., XIONG, X. X., JIN, H. Y. & ZHU, S. M. 2014. Propofol exerts anti-hepatocellular carcinoma by microvesicle-mediated transfer of miR-142-3p from macrophage to cancer cells. *J Transl Med,* 12**,** 279.

ZHANG, W., KUDO, H., KAWAI, K., FUJISAKA, S., USUI, I., SUGIYAMA, T., TSUKADA, K., CHEN, N. & TAKAHARA, T. 2010. Tumor necrosis factor-alpha accelerates apoptosis of steatotic hepatocytes from a murine model of non-alcoholic fatty liver disease. *Biochem Biophys Res Commun,* 391**,** 1731-6.

ZHANG, W., ZHAO, P., XU, X. L., CAI, L., SONG, Z. S., CAO, D. Y., TAO, K. S., ZHOU, W. P., CHEN, Z. N. & DOU, K. F. 2013. Annexin A2 promotes the migration and invasion of human hepatocellular carcinoma cells in vitro by regulating the shedding of CD147-harboring microvesicles from tumor cells. *PLoS One,* 8**,** e67268.

ZHAO, H., SHANG, Q., PAN, Z., BAI, Y., LI, Z., ZHANG, H., ZHANG, Q., GUO, C., ZHANG, L. & WANG, Q. 2018. Exosomes From Adipose-Derived Stem Cells Attenuate Adipose Inflammation and Obesity Through Polarizing M2 Macrophages and Beiging in White Adipose Tissue. *Diabetes,* 67**,** 235-247.

Appendix

Table A1. Unique proteins from liver EV dataset recognised in other studies*.

Symbol	*Protein name*
ACADL	Long-chain specific acyl-CoA dehydrogenase, mitochondrial
ACADM	Medium-chain specific acyl-CoA dehydrogenase, mitochondrial
ACLY	ATP-citrate synthase
ACOT1	Acyl-coenzyme A thioesterase 1
ACOT2	Acyl-coenzyme A thioesterase 2, mitochondrial
ACOX1	Peroxisomal acyl-coenzyme A oxidase 1
ACTB	Actin, cytoplasmic 1
ACTN1	Alpha-actinin-1
ACTN4	Alpha-actinin-4
ACYP1	Acylphosphatase-1
ADK	Adenosine kinase
AHSA1	Activator of 90 kDa heat shock protein ATPase homolog 1
AIFM1	Apoptosis-inducing factor 1, mitochondrial
ALDH2	Aldehyde dehydrogenase, mitochondrial
ALDOA	Fructose-bisphosphate aldolase A
ALDOB	Fructose-bisphosphate aldolase B
AMACR	Alpha-methylacyl-CoA racemase
ANXA2	Annexin A2
ANXA4	Annexin A4
ANXA5	Annexin A5
ANXA6	Annexin A6
APEH	Acylamino-acid-releasing enzyme
APOA1	Apolipoprotein A-I
APOB	Apolipoprotein B-100
ARPC2	Actin-related protein 2/3 complex subunit 2
ARPC3	Actin-related protein 2/3 complex subunit 3
ARPC4	Actin-related protein 2/3 complex subunit 4
ARPC5	Actin-related protein 2/3 complex subunit 5
ATOX1	Copper transport protein ATOX1

BLMH	Bleomycin hydrolase
BLVRB	Flavin reductase (NADPH)
BPHL	Valacyclovir hydrolase
BPNT1	3'(2'),5'-bisphosphate nucleotidase 1
BTF3	Transcription factor BTF3
CALM1	Calmodulin-1
CAND1	Cullin-associated NEDD8-dissociated protein 1
CAP1	Adenylyl cyclase-associated protein 1
CAPZB	F-actin-capping protein subunit beta
CDV3	Protein CDV3
CISD3	CDGSH iron-sulfur domain-containing protein 3, mitochondrial
CLYBL	Citrate lyase subunit beta-like protein, mitochondrial
CNDP2	Cytosolic non-specific dipeptidase
COMT	Catechol O-methyltransferase
COPB2	Coatomer subunit beta'
COQ9	Ubiquinone biosynthesis protein COQ9, mitochondrial
COTL1	Coactosin-like protein
CREG1	Protein CREG1
CYB5	Cytochrome b5
DCPS	m7GpppX diphosphatase
DCXR	L-xylulose reductase
DDAH1	N(G),N(G)-dimethylarginine dimethylaminohydrolase 1
DDB1	DNA damage-binding protein 1
DNPEP	Aspartyl aminopeptidase
DPP3	Dipeptidyl peptidase 3
DPP4	Dipeptidyl peptidase 4
ECH1	Delta(3,5)-Delta(2,4)-dienoyl-CoA isomerase, mitochondrial
ECI1	Enoyl-CoA delta isomerase 1, mitochondrial
ERH	Enhancer of rudimentary homolog
ETFA	Electron transfer flavoprotein subunit alpha, mitochondrial
ETFB	Electron transfer flavoprotein subunit beta
FABP4	Fatty acid-binding protein, adipocyte

FABP5	Fatty acid-binding protein, epidermal
FAHD1	Acylpyruvase FAHD1, mitochondrial
FAS	Fatty acid synthase
FIS1	Mitochondrial fission 1 protein
FKBP3	Peptidyl-prolyl cis-trans isomerase FKBP3
FLNB	Filamin-B
GALM	Aldose 1-epimerase
GCDH	Glutaryl-CoA dehydrogenase, mitochondrial
GCSH	Glycine cleavage system H protein, mitochondrial
GLOD4	Glyoxalase domain-containing protein 4
GMPPA	Mannose-1-phosphate guanyltransferase alpha
GMPPB	Mannose-1-phosphate guanyltransferase beta
GPX1	Glutathione peroxidase 1
GPX3	Glutathione peroxidase 3
GRHPR	Glyoxylate reductase/hydroxypyruvate reductase
GSTA1	Glutathione S-transferase A1
GSTA4	Glutathione S-transferase A4
GSTM1	Glutathione S-transferase Mu 1
GSTM2	Glutathione S-transferase Mu 2
GSTM3	Glutathione S-transferase Mu 3
GSTM6	Glutathione S-transferase Mu 6
GSTM7	Glutathione S-transferase Mu 7
GSTO1	Glutathione S-transferase omega-1
GSTP1	Glutathione S-transferase P 1
GSTP2	Glutathione S-transferase P 2
GSTT3	Glutathione S-transferase theta-3
HACL1	2-hydroxyacyl-CoA lyase 1
HDHD2	Haloacid dehalogenase-like hydrolase domain-containing protein 2
HGD	Homogentisate 1,2-dioxygenase
HINT1	Histidine triad nucleotide-binding protein 1
HMGB1	High mobility group protein B1
HMGCL	Hydroxymethylglutaryl-CoA lyase, mitochondrial

HPRT	Hypoxanthine-guanine phosphoribosyltransferase
IAH1	Isoamyl acetate-hydrolyzing esterase 1 homolog
IDE	Insulin-degrading enzyme
IIGP1	Interferon-inducible GTPase 1
IMPA1	Inositol monophosphatase 1
IPO5	Importin-5
ITIH2	Inter-alpha-trypsin inhibitor heavy chain H2
ITIH4	Inter alpha-trypsin inhibitor, heavy chain 4
ITPA	Inosine triphosphate pyrophosphatase
IVD	Isovaleryl-CoA dehydrogenase, mitochondrial
KNG1	Kininogen-1
LAMP1	Lysosome-associated membrane glycoprotein 1
LAMP2	Lysosome-associated membrane glycoprotein 2
LASP1	LIM and SH3 domain protein 1
LDHA	L-lactate dehydrogenase A chain
LDHB	L-lactate dehydrogenase B chain
LMNA	Prelamin-A/C
LUM	Lumican
LYZ1	Lysozyme C-1
MCEE	Methylmalonyl-CoA epimerase, mitochondrial
MEMO1	Protein MEMO1
MIF	Macrophage migration inhibitory factor
MRC1	Macrophage mannose receptor 1
MTAP	S-methyl-5'-thioadenosine phosphorylase
MUG1	Murinoglobulin-1
MVP	Major vault protein
NAMPT	Nicotinamide phosphoribosyltransferase
NIT1	Deaminated glutathione amidase
NIT2	Omega-amidase NIT2
NPC2	Epididymal secretory protein E1
NQO2	Ribosyldihydronicotinamide dehydrogenase [quinone]
NUDC	Nuclear migration protein nudC

NUDT7	Peroxisomal coenzyme A diphosphatase NUDT7
OAT	Ornithine aminotransferase, mitochondrial
OLA1	Obg-like ATPase 1
OPA1	Dynamin-like 120 kDa protein, mitochondrial
OTUB1	Ubiquitin thioesterase OTUB1
PAK2	Serine/threonine-protein kinase PAK 2
PARK7	Protein/nucleic acid deglycase DJ-1
PCBP1	Poly(rC)-binding protein 1
PCCA	Propionyl-CoA carboxylase alpha chain, mitochondrial
PCCB	Propionyl-CoA carboxylase beta chain, mitochondrial
PDIA3	Protein disulfide-isomerase A3
PDIA4	Protein disulfide-isomerase A4
PDXK	Pyridoxal kinase
PEBP1	Phosphatidylethanolamine-binding protein 1
PECR	Peroxisomal trans-2-enoyl-CoA reductase
PEPD	Xaa-Pro dipeptidase
PGAM1	Phosphoglycerate mutase 1
PGK1	Phosphoglycerate kinase 1
PGM1	Phosphoglucomutase-1
PGM2	Phosphoglucomutase-2
PGP	Glycerol-3-phosphate phosphatase
PPIA	Peptidyl-prolyl cis-trans isomerase A
PPIB	Peptidyl-prolyl cis-trans isomerase B
PPIF	Peptidyl-prolyl cis-trans isomerase F, mitochondrial
PRDX1	Peroxiredoxin-1
PRDX2	Peroxiredoxin-2
PRDX3	Thioredoxin-dependent peroxide reductase, mitochondrial
PRDX4	Peroxiredoxin-4
PRDX5	Peroxiredoxin-5, mitochondrial
PRDX6	Peroxiredoxin-6
PREP	Presequence protease, mitochondrial
PRPS1	Ribose-phosphate pyrophosphokinase 1

PSMD9	26S proteasome non-ATPase regulatory subunit 9
PSME1	Proteasome activator complex subunit 1
PSME2	Proteasome activator complex subunit 2
PSME3	Proteasome activator complex subunit 3
PURA	Transcriptional activator protein Pur-alpha
PYGB	Glycogen phosphorylase, brain form
PYGL	Glycogen phosphorylase, liver form
PZP	Pregnancy zone protein
RAB18	Ras-related protein Rab-18
RBX1	E3 ubiquitin-protein ligase RBX1
REEP6	Receptor expression-enhancing protein 6
RGN	Regucalcin
RPE	Ribulose-phosphate 3-epimerase
RRBP1	Ribosome-binding protein 1
RSU1	Ras suppressor protein 1
SARDH	Sarcosine dehydrogenase, mitochondrial
SCLY	Selenocysteine lyase
SDHA	Succinate dehydrogenase [ubiquinone] flavoprotein subunit, mitochondrial
SEC13	Protein SEC13 homolog
SET	Protein SET
SRSF2	Serine/arginine-rich splicing factor 2
STIP1	Stress-induced-phosphoprotein 1
SYK	Lysine--tRNA ligase
TBCA	Tubulin-specific chaperone A
TGM2	Protein-glutamine gamma-glutamyltransferase 2
THOP1	Thimet oligopeptidase
TKT	Transketolase
TLN1	Talin-1
TPM3	Tropomyosin alpha-3 chain
TPP2	Tripeptidyl-peptidase 2
TSN	Translin
TSNAX	Translin-associated protein X

TWF1	Twinfilin-1
TXNL1	Thioredoxin-like protein 1
UBA1	Ubiquitin-like modifier-activating enzyme 1
UFC1	Ubiquitin-fold modifier-conjugating enzyme 1
UGDH	UDP-glucose 6-dehydrogenase
WDR1	WD repeat-containing protein 1
XDH	Xanthine dehydrogenase/oxidase

*Compared to a large pooled dataset (n=4845 unique proteins) in Vesiclepedia (Kalra et al., 2012). Screening of *Mus musculus* proteins was available from 77 individual studies, using a range of techniques including mass spectrometry, western blotting, flow cytometry, protein assay, immunoelectron microscopy, or a combination of any two.

Table A2. Unique proteins from liver EV dataset novel to study*.

Symbol	*Protein name*
1433B	14-3-3 protein beta/alpha
1433E	14-3-3 protein epsilon
1433F	14-3-3 protein eta
1433G	14-3-3 protein gamma
1433T	14-3-3 protein theta
1433Z	14-3-3 protein zeta/delta
3HAO	3-hydroxyanthranilate 3,4-dioxygenase
3HIDH	3-hydroxyisobutyrate dehydrogenase, mitochondrial
6PGD	6-phosphogluconate dehydrogenase, decarboxylating
6PGL	6-phosphogluconolactonase
A16A1	Aldehyde dehydrogenase family 16 member A1
A1AG1	Alpha-1-acid glycoprotein 1
A1AT2	Alpha-1-antitrypsin 1-2
A1AT3	Alpha-1-antitrypsin 1-3
A1AT4	Alpha-1-antitrypsin 1-4
A1AT5	Alpha-1-antitrypsin 1-5
AADAT	Kynurenine/alpha-aminoadipate aminotransferase, mitochondrial
AATC	Aspartate aminotransferase, cytoplasmic
AATM	Aspartate aminotransferase, mitochondrial
ABHEB	Protein ABHD14B
ACADV	Very long-chain specific acyl-CoA dehydrogenase, mitochondrial
ACBP	Acyl-CoA-binding protein
ACOC	Cytoplasmic aconitate hydratase
ACON	Aconitate hydratase, mitochondrial
ACOX2	Peroxisomal acyl-coenzyme A oxidase 2
ACSM1	Acyl-coenzyme A synthetase ACSM1, mitochondrial
ACTS	Actin, alpha skeletal muscle
ACTY	Beta-centractin
ACTZ	Alpha-centractin

ACY1	Aminoacylase-1
ACY3	N-acyl-aromatic-L-amino acid amidohydrolase (carboxylate-forming)
ADH1	Alcohol dehydrogenase 1
ADHX	Alcohol dehydrogenase class-3
ADX	Adrenodoxin, mitochondrial
AGM1	Phosphoacetylglucosamine mutase
AGT2	Alanine--glyoxylate aminotransferase 2, mitochondrial
AK1A1	Alcohol dehydrogenase [NADP(+)]
AK1CD	Aldo-keto reductase family 1 member C13
AKC1H	Aldo-keto reductase family 1 member C18
AL1A1	Retinal dehydrogenase 1
AL1A7	Aldehyde dehydrogenase, cytosolic 1
AL1B1	Aldehyde dehydrogenase X, mitochondrial
AL1L1	Cytosolic 10-formyltetrahydrofolate dehydrogenase
AL7A1	Alpha-aminoadipic semialdehyde dehydrogenase
AL8A1	Aldehyde dehydrogenase family 8 member A1
AL9A1	4-trimethylaminobutyraldehyde dehydrogenase
ALAT1	Alanine aminotransferase 1
ALAT2	Alanine aminotransferase 2
ALBU	Serum albumin
ALR	FAD-linked sulfhydryl oxidase ALR
AMPB	Aminopeptidase B
AMPD2	AMP deaminase 2
AMPL	Cytosol aminopeptidase
AN32A	Acidic leucine-rich nuclear phosphoprotein 32 family member A
ANT3	Antithrombin-III
AOXA	Aldehyde oxidase 1
AOXC	Aldehyde oxidase 3
AP1B1	AP-1 complex subunit beta-1
AP1M1	AP-1 complex subunit mu-1
AP2A1	AP-2 complex subunit alpha-1
AP2A2	AP-2 complex subunit alpha-2

AP2B1	AP-2 complex subunit beta
AP2M1	AP-2 complex subunit mu
AP4A	Bis(5'-nucleosyl)-tetraphosphatase [asymmetrical]
APOH	Beta-2-glycoprotein 1
ARC1A	Actin-related protein 2/3 complex subunit 1A
ARC1B	Actin-related protein 2/3 complex subunit 1B
ARGI1	Arginase-1
ARK72	Aflatoxin B1 aldehyde reductase member 2
ARLY	Argininosuccinate lyase
ARP2	Actin-related protein 2
ARP3	Actin-related protein 3
ARP5L	Actin-related protein 2/3 complex subunit 5-like protein
AS3MT	Arsenite methyltransferase
ASGL1	Isoaspartyl peptidase/L-asparaginase
ASPD	Putative L-aspartate dehydrogenase
ASSY	Argininosuccinate synthase
ATPA	ATP synthase subunit alpha, mitochondrial
ATPB	ATP synthase subunit beta, mitochondrial
AUHM	Methylglutaconyl-CoA hydratase, mitochondrial
B2L13	Bcl-2-like protein 13
BAAT	Bile acid-CoA:amino acid N-acyltransferase
BACH	Cytosolic acyl coenzyme A thioester hydrolase
BHMT1	Betaine--homocysteine S-methyltransferase 1
BHMT2	S-methylmethionine--homocysteine S-methyltransferase BHMT2
BODG	Gamma-butyrobetaine dioxygenase
BT3L4	Transcription factor BTF3 homolog 4
BUP1	Beta-ureidopropionase
CA050	Uncharacterized protein C1orf50 homolog
CAH1	Carbonic anhydrase 1
CAH2	Carbonic anhydrase 2
CAH3	Carbonic anhydrase 3
CAH5A	Carbonic anhydrase 5A, mitochondrial

CAN2	Calpain-2 catalytic subunit
CAPR1	Caprin-1
CATA	Catalase
CATC	Dipeptidyl peptidase 1
CATD	Cathepsin D
CATH	Pro-cathepsin H
CAZA1	F-actin-capping protein subunit alpha-1
CAZA2	F-actin-capping protein subunit alpha-2
CBR4	Carbonyl reductase family member 4
CBS	Cystathionine beta-synthase
CCS	Copper chaperone for superoxide dismutase
CDD	Cytidine deaminase
CE162	Centrosomal protein of 162 kDa
CERU	Ceruloplasmin
CES1D	Carboxylesterase 1D
CES1F	Carboxylesterase 1F
CFAH	Complement factor H
CGL	Cystathionine gamma-lyase
CH10	10 kDa heat shock protein, mitochondrial
CH60	60 kDa heat shock protein, mitochondrial
CHM2A	Charged multivesicular body protein 2a
CISY	Citrate synthase, mitochondrial
CK054	Ester hydrolase C11orf54 homolog
CMBL	Carboxymethylenebutenolidase homolog
CO3	Complement C3
COF1	Cofilin-1
COF2	Cofilin-2
COPD	Coatomer subunit delta
COR1C	Coronin-1C
CP2DQ	Cytochrome P450 2D26
CPPED	Serine/threonine-protein phosphatase CPPED1
CPSM	Carbamoyl-phosphate synthase [ammonia], mitochondrial

CRYL1	Lambda-crystallin homolog
CRYM	Ketimine reductase mu-crystallin
CSAD	Cysteine sulfinic acid decarboxylase
CSN4	COP9 signalosome complex subunit 4
CYBP	Calcyclin-binding protein
CYC	Cytochrome c, somatic
CYTB	Cystatin-B
DCA11	DDB1- and CUL4-associated factor 11
DDC	Aromatic-L-amino-acid decarboxylase
DECR	2,4-dienoyl-CoA reductase, mitochondrial
DEOC	Deoxyribose-phosphate aldolase
DESP	Desmoplakin
DEST	Destrin
DHB4	Peroxisomal multifunctional enzyme type 2
DHB5	Estradiol 17 beta-dehydrogenase 5
DHB8	Estradiol 17-beta-dehydrogenase 8
DHDH	Trans-1,2-dihydrobenzene-1,2-diol dehydrogenase
DHE3	Glutamate dehydrogenase 1, mitochondrial
DHPR	Dihydropteridine reductase
DHSO	Sorbitol dehydrogenase
DLDH	Dihydrolipoyl dehydrogenase, mitochondrial
DOPD	D-dopachrome decarboxylase
DPP2	Dipeptidyl peptidase 2
DPYD	Dihydropyrimidine dehydrogenase [NADP(+)]
DPYL2	Dihydropyrimidinase-related protein 2
DPYS	Dihydropyrimidinase
DTD2	Putative D-tyrosyl-tRNA(Tyr) deacylase 2
DX39B	Spliceosome RNA helicase Ddx39b
DYL2	Dynein light chain 2, cytoplasmic
ECHD1	Ethylmalonyl-CoA decarboxylase
ECHD3	Enoyl-CoA hydratase domain-containing protein 3, mitochondrial
ECHM	Enoyl-CoA hydratase, mitochondrial

EF1A1	Elongation factor 1-alpha 1
EF1B	Elongation factor 1-beta
EF1D	Elongation factor 1-delta
EF1G	Elongation factor 1-gamma
EF2	Elongation factor 2
EI3JA	Eukaryotic translation initiation factor 3 subunit J-A
EIF2A	Eukaryotic translation initiation factor 2A
EIF3A	Eukaryotic translation initiation factor 3 subunit A
EIF3H	Eukaryotic translation initiation factor 3 subunit H
EMAL2	Echinoderm microtubule-associated protein-like 2
ENOA	Alpha-enolase
EST1	Liver carboxylesterase 1
EST1C	Carboxylesterase 1C
EST2A	Pyrethroid hydrolase Ces2a
EST2C	Acylcarnitine hydrolase
EST2E	Pyrethroid hydrolase Ces2e
EST3A	Carboxylesterase 3A
EST3B	Carboxylesterase 3B
ESTD	S-formylglutathione hydrolase
ETHE1	Persulfide dioxygenase ETHE1, mitochondrial
F10A1	Hsc70-interacting protein
F13A	Coagulation factor XIII A chain
F16P1	Fructose-1,6-bisphosphatase 1
FAAA	Fumarylacetoacetase
FABPI	Fatty acid-binding protein, intestinal
FABPL	Fatty acid-binding protein, liver
FETUA	Alpha-2-HS-glycoprotein
FGGY	FGGY carbohydrate kinase domain-containing protein
FHIT	Bis(5'-adenosyl)-triphosphatase
FIBA	Fibrinogen alpha chain
FIBB	Fibrinogen beta chain
FIBG	Fibrinogen gamma chain

FINC	Fibronectin
FKB1A	Peptidyl-prolyl cis-trans isomerase FKBP1A
FPPS	Farnesyl pyrophosphate synthase
FRIH	Ferritin heavy chain
FRIL1	Ferritin light chain 1
FUMH	Fumarate hydratase, mitochondrial
G3P	Glyceraldehyde-3-phosphate dehydrogenase
G3PT	Glyceraldehyde-3-phosphate dehydrogenase, testis-specific
G6PI	Glucose-6-phosphate isomerase
GABT	4-aminobutyrate aminotransferase, mitochondrial
GALT	Galactose-1-phosphate uridylyltransferase
GAMT	Guanidinoacetate N-methyltransferase
GCAB	Ig gamma-2A chain C region secreted form
GCSP	Glycine dehydrogenase (decarboxylating), mitochondrial
GDIA	Rab GDP dissociation inhibitor alpha
GDIB	Rab GDP dissociation inhibitor beta
GDIR1	Rho GDP-dissociation inhibitor 1
GDIR2	Rho GDP-dissociation inhibitor 2
GEPH	Gephyrin
GFRP	GTP cyclohydrolase 1 feedback regulatory protein
GGACT	Gamma-glutamylaminecyclotransferase
GLNA	Glutamine synthetase
GLO2	Hydroxyacylglutathione hydrolase, mitochondrial
GLPK	Glycerol kinase
GLRX1	Glutaredoxin-1
GLUCM	D-glutamate cyclase, mitochondrial
GLYAL	Glycine N-acyltransferase-like protein
GLYAT	Glycine N-acyltransferase
GLYC	Serine hydroxymethyltransferase, cytosolic
GNMT	Glycine N-methyltransferase
GNPI1	Glucosamine-6-phosphate isomerase 1
GPDA	Glycerol-3-phosphate dehydrogenase [NAD(+)], cytoplasmic

GRP75	Stress-70 protein, mitochondrial
GRP78	78 kDa glucose-regulated protein
GRPE1	GrpE protein homolog 1, mitochondrial
GSH0	Glutamate--cysteine ligase regulatory subunit
GSH1	Glutamate--cysteine ligase catalytic subunit
GSHB	Glutathione synthetase
GSHR	Glutathione reductase, mitochondrial
GSTA2	Glutathione S-transferase A2
GSTA3	Glutathione S-transferase A3
GSTK1	Glutathione S-transferase kappa 1
GSTT1	Glutathione S-transferase theta-1
GSTT2	Glutathione S-transferase theta-2
GUAD	Guanine deaminase
H14	Histone H1.4
H2A2A	Histone H2A type 2-A
H2A2B	Histone H2A type 2-B
H2AV	Histone H2A.V
H2B1C	Histone H2B type 1-C/E/G
H32	Histone H3.2
H33	Histone H3.3
H4	Histone H4
HA10	H-2 class I histocompatibility antigen, Q10 alpha chain
HAOX1	Hydroxyacid oxidase 1
HBA	Hemoglobin subunit alpha
HBB1	Hemoglobin subunit beta-1
HCD2	3-hydroxyacyl-CoA dehydrogenase type-2
HCDH	Hydroxyacyl-coenzyme A dehydrogenase, mitochondrial
HDGF	Hepatoma-derived growth factor
HDHD3	Haloacid dehalogenase-like hydrolase domain-containing protein 3
HEM2	Delta-aminolevulinic acid dehydratase
HEM3	Porphobilinogen deaminase
HEM6	Oxygen-dependent coproporphyrinogen-III oxidase, mitochondrial

HEMO	Hemopexin
HIBCH	3-hydroxyisobutyryl-CoA hydrolase, mitochondrial
HIUH	5-hydroxyisourate hydrolase
HMCS2	Hydroxymethylglutaryl-CoA synthase, mitochondrial
HNMT	Histamine N-methyltransferase
HNRPF	Heterogeneous nuclear ribonucleoprotein F
HNRPK	Heterogeneous nuclear ribonucleoprotein K
HNRPQ	Heterogeneous nuclear ribonucleoprotein Q
HOGA1	4-hydroxy-2-oxoglutarate aldolase, mitochondrial
HOT	Hydroxyacid-oxoacid transhydrogenase, mitochondrial
HPPD	4-hydroxyphenylpyruvate dioxygenase
HPT	Haptoglobin
HS105	Heat shock protein 105 kDa
HS71A	Heat shock 70 kDa protein 1A
HS71L	Heat shock 70 kDa protein 1-like
HS90A	Heat shock protein HSP 90-alpha
HS90B	Heat shock protein HSP 90-beta
HSP74	Heat shock 70 kDa protein 4
HSP7C	Heat shock cognate 71 kDa protein
HUTH	Histidine ammonia-lyase
HUTI	Probable imidazolonepropionase
HUTU	Urocanate hydratase
HUWE1	E3 ubiquitin-protein ligase HUWE1
HVM51	Ig heavy chain V region AC38 205.12
HYES	Bifunctional epoxide hydrolase 2
HYKK	Hydroxylysine kinase
IDHC	Isocitrate dehydrogenase [NADP] cytoplasmic
IDHP	Isocitrate dehydrogenase [NADP], mitochondrial
IF2A	Eukaryotic translation initiation factor 2 subunit 1
IF2G	Eukaryotic translation initiation factor 2 subunit 3, X-linked
IF2H	Eukaryotic translation initiation factor 2 subunit 3, Y-linked
IF4A1	Eukaryotic initiation factor 4A-I

IF4A2	Eukaryotic initiation factor 4A-II
IF5A1	Eukaryotic translation initiation factor 5A-1
IF6	Eukaryotic translation initiation factor 6
IGG2B	Ig gamma-2B chain C region
IGH1M	Ig gamma-1 chain C region, membrane-bound form
IGHM	Ig mu chain C region
IGKC	Ig kappa chain C region
INMT	Indolethylamine N-methyltransferase
IPYR	Inorganic pyrophosphatase
IPYR2	Inorganic pyrophosphatase 2, mitochondrial
ISC2A	Isochorismatase domain-containing protein 2A
ISOC1	Isochorismatase domain-containing protein 1
KAD2	Adenylate kinase 2, mitochondrial
KAT1	Kynurenine--oxoglutarate transaminase 1
KAT3	Kynurenine--oxoglutarate transaminase 3
KBL	2-amino-3-ketobutyrate coenzyme A ligase, mitochondrial
KCY	UMP-CMP kinase
KHK	Ketohexokinase
KPRA	Phosphoribosyl pyrophosphate synthase-associated protein 1
KPYM	Pyruvate kinase PKM
KPYR	Pyruvate kinase PKLR
KV5AB	Ig kappa chain V-V region HP R16.7
KYNU	Kynureninase
LACB2	Endoribonuclease LACTB2
LDHD	Probable D-lactate dehydrogenase, mitochondrial
LEG1	Galectin-1
LEG9	Galectin-9
LGUL	Lactoylglutathione lyase
LHPP	Phospholysine phosphohistidine inorganic pyrophosphate phosphatase
LIS1	Platelet-activating factor acetylhydrolase IB subunit alpha
LKHA4	Leukotriene A-4 hydrolase
LPP60	60 kDa lysophospholipase

LYPA1	Acyl-protein thioesterase 1
LYPA2	Acyl-protein thioesterase 2
M2GD	Dimethylglycine dehydrogenase, mitochondrial
MAAI	Maleylacetoacetate isomerase
MAOX	NADP-dependent malic enzyme
MAP2	Methionine aminopeptidase 2
MCCB	Methylcrotonoyl-CoA carboxylase beta chain, mitochondrial
MDHC	Malate dehydrogenase, cytoplasmic
MDHM	Malate dehydrogenase, mitochondrial
METK1	S-adenosylmethionine synthase isoform type-1
MOES	Moesin
MSRA	Mitochondrial peptide methionine sulfoxide reductase
MTL26	Methyltransferase-like 26
MTNB	Methylthioribulose-1-phosphate dehydratase
MTND	1,2-dihydroxy-3-keto-5-methylthiopentene dioxygenase
MTP	Microsomal triglyceride transfer protein large subunit
MUTA	Methylmalonyl-CoA mutase, mitochondrial
MYDGF	Myeloid-derived growth factor
NACAM	Nascent polypeptide-associated complex subunit alpha, muscle-specific form
NADC	Nicotinate-nucleotide pyrophosphorylase [carboxylating]
NAKD2	NAD kinase 2, mitochondrial
NDK3	Nucleoside diphosphate kinase 3
NDKA	Nucleoside diphosphate kinase A
NDKB	Nucleoside diphosphate kinase B
NDRG2	Protein NDRG2
NEUL	Neurolysin, mitochondrial
NHRF1	Na(+)/H(+) exchange regulatory cofactor NHE-RF1
NHRF3	Na(+)/H(+) exchange regulatory cofactor NHE-RF3
NIF3L	NIF3-like protein 1
NIPS1	Protein NipSnap homolog 1
NLTP	Non-specific lipid-transfer protein
NNRD	ATP-dependent (S)-NAD(P)H-hydrate dehydratase

NNRE	NAD(P)H-hydrate epimerase
NPL	N-acetylneuraminate lyase
NPM	Nucleophosmin
NPS3B	Protein NipSnap homolog 3B
NTF2	Nuclear transport factor 2
NUCL	Nucleolin
NUD12	Peroxisomal NADH pyrophosphatase NUDT12
NUDC2	NudC domain-containing protein 2
OCTC	Peroxisomal carnitine O-octanoyltransferase
ODO1	2-oxoglutarate dehydrogenase, mitochondrial
ODO2	Dihydrolipoyllysine-residue succinyltransferase component of 2-oxoglutarate dehydrogenase complex, mitochondrial
ODP2	Dihydrolipoyllysine-residue acetyltransferase component of pyruvate dehydrogenase complex, mitochondrial
OPLA	5-oxoprolinase
ORN	Oligoribonuclease, mitochondrial
OTC	Ornithine carbamoyltransferase, mitochondrial
PABP1	Polyadenylate-binding protein 1
PAPS2	Bifunctional 3'-phosphoadenosine 5'-phosphosulfate synthase 2
PBLD1	Phenazine biosynthesis-like domain-containing protein 1
PBLD2	Phenazine biosynthesis-like domain-containing protein 2
PCKGC	Phosphoenolpyruvate carboxykinase, cytosolic [GTP]
PCY2	Ethanolamine-phosphate cytidylyltransferase
PDIA1	Protein disulfide-isomerase
PDXD1	Pyridoxal-dependent decarboxylase domain-containing protein 1
PEPL1	Probable aminopeptidase NPEPL1
PGBM	Basement membrane-specific heparan sulfate proteoglycan core protein
PH4H	Phenylalanine-4-hydroxylase
PHS	Pterin-4-alpha-carbinolamine dehydratase
PHS2	Pterin-4-alpha-carbinolamine dehydratase 2
PHYD1	Phytanoyl-CoA dioxygenase domain-containing protein 1
PICAL	Phosphatidylinositol-binding clathrin assembly protein

PIPNB	Phosphatidylinositol transfer protein beta isoform
PLAK	Junction plakoglobin
PLAP	Phospholipase A-2-activating protein
PLIN2	Perilipin-2
PLSL	Plastin-2
PLST	Plastin-3
PMGE	Bisphosphoglycerate mutase
PNCB	Nicotinate phosphoribosyltransferase
PNPH	Purine nucleoside phosphorylase
PNPO	Pyridoxine-5'-phosphate oxidase
PP1A	Serine/threonine-protein phosphatase PP1-alpha catalytic subunit
PP1R7	Protein phosphatase 1 regulatory subunit 7
PP2AA	Serine/threonine-protein phosphatase 2A catalytic subunit alpha isoform
PPA6	Lysophosphatidic acid phosphatase type 6
PPAC	Low molecular weight phosphotyrosine protein phosphatase
PPCS	Phosphopantothenate--cysteine ligase
PPCT	Phosphatidylcholine transfer protein
PPM1A	Protein phosphatase 1A
PPM1B	Protein phosphatase 1B
PPP5	Serine/threonine-protein phosphatase 5
PROF1	Profilin-1
PRRC1	Protein PRRC1
PSA	Puromycin-sensitive aminopeptidase
PSA1	Proteasome subunit alpha type-1
PSA2	Proteasome subunit alpha type-2
PSA3	Proteasome subunit alpha type-3
PSA4	Proteasome subunit alpha type-4
PSA5	Proteasome subunit alpha type-5
PSA6	Proteasome subunit alpha type-6
PSA7	Proteasome subunit alpha type-7
PSB1	Proteasome subunit beta type-1
PSB10	Proteasome subunit beta type-10

PSB2	Proteasome subunit beta type-2
PSB3	Proteasome subunit beta type-3
PSB4	Proteasome subunit beta type-4
PSB5	Proteasome subunit beta type-5
PSB6	Proteasome subunit beta type-6
PSB7	Proteasome subunit beta type-7
PSB8	Proteasome subunit beta type-8
PSB9	Proteasome subunit beta type-9
PSDE	26S proteasome non-ATPase regulatory subunit 14
PTER	Phosphotriesterase-related protein
PTGR2	Prostaglandin reductase 2
PTPS	6-pyruvoyl tetrahydrobiopterin synthase
PUR6	Multifunctional protein ADE2
PUR8	Adenylosuccinate lyase
PURA2	Adenylosuccinate synthetase isozyme 2
PYC	Pyruvate carboxylase, mitochondrial
QOR	Quinone oxidoreductase
RADI	Radixin
RBBP9	Putative hydrolase RBBP9
RD23B	UV excision repair protein RAD23 homolog B
RET1	Retinol-binding protein 1
RET4	Retinol-binding protein 4
RIDA	2-iminobutanoate/2-iminopropanoate deaminase
RINI	Ribonuclease inhibitor
RL10A	60S ribosomal protein L10a
RL12	60S ribosomal protein L12
RL14	60S ribosomal protein L14
RL8	60S ribosomal protein L8
RMD1	Regulator of microtubule dynamics protein 1
RS18	40S ribosomal protein S18
RS19	40S ribosomal protein S19
RS20	40S ribosomal protein S20

RS27A	Ubiquitin-40S ribosomal protein S27a
RSSA	40S ribosomal protein SA
S14L2	SEC14-like protein 2
SAHH	Adenosylhomocysteinase
SAMH1	Deoxynucleoside triphosphate triphosphohydrolase SAMHD1
SAP	Prosaposin
SAP3	Ganglioside GM2 activator
SBP1	Selenium-binding protein 1
SBP2	Selenium-binding protein 2
SC23A	Protein transport protein Sec23A
SC23B	Protein transport protein Sec23B
SC31A	Protein transport protein Sec31A
SCRN2	Secernin-2
SCRN3	Secernin-3
SH3L1	SH3 domain-binding glutamic acid-rich-like protein
SH3L3	SH3 domain-binding glutamic acid-rich-like protein 3
SHPK	Sedoheptulokinase
SIAS	Sialic acid synthase
SKP1	S-phase kinase-associated protein 1
SODC	Superoxide dismutase [Cu-Zn]
SODM	Superoxide dismutase [Mn], mitochondrial
SOX	Peroxisomal sarcosine oxidase
SPA3K	Serine protease inhibitor A3K
SPA3M	Serine protease inhibitor A3M
SPB6	Serpin B6
SPEB	Agmatinase, mitochondrial
SPEE	Spermidine synthase
SPRE	Sepiapterin reductase
SPS1	Selenide, water dikinase 1
SPS2	Selenide, water dikinase 2
SPTB2	Spectrin beta chain, non-erythrocytic 1
SPTN1	Spectrin alpha chain, non-erythrocytic 1

SPYA	Serine--pyruvate aminotransferase, mitochondrial
SSBP	Single-stranded DNA-binding protein, mitochondrial
SSDH	Succinate-semialdehyde dehydrogenase, mitochondrial
STA10	START domain-containing protein 10
SUOX	Sulfite oxidase, mitochondrial
SYCC	Cysteine--tRNA ligase, cytoplasmic
SYHC	Histidine--tRNA ligase, cytoplasmic
SYIM	Isoleucine--tRNA ligase, mitochondrial
SYTC	Threonine--tRNA ligase, cytoplasmic
SYWC	Tryptophan--tRNA ligase, cytoplasmic
SYYC	Tyrosine--tRNA ligase, cytoplasmic
T23O	Tryptophan 2,3-dioxygenase
T3HPD	Trans-L-3-hydroxyproline dehydratase
TAGL2	Transgelin-2
TALDO	Transaldolase
TCPG	T-complex protein 1 subunit gamma
TCTP	Translationally-controlled tumor protein
TEBP	Prostaglandin E synthase 3
TERA	Transitional endoplasmic reticulum ATPase
THIC	Acetyl-CoA acetyltransferase, cytosolic
THIKA	3-ketoacyl-CoA thiolase A, peroxisomal
THIKB	3-ketoacyl-CoA thiolase B, peroxisomal
THIL	Acetyl-CoA acetyltransferase, mitochondrial
THIM	3-ketoacyl-CoA thiolase, mitochondrial
THIO	Thioredoxin
THNS2	Threonine synthase-like 2
THTM	3-mercaptopyruvate sulfurtransferase
THTR	Thiosulfate sulfurtransferase
TIM13	Mitochondrial import inner membrane translocase subunit Tim13
TIM8A	Mitochondrial import inner membrane translocase subunit Tim8 A
TKFC	Triokinase/FMN cyclase
TPIS	Triosephosphate isomerase

TPMT	Thiopurine S-methyltransferase
TRFE	Serotransferrin
TRXR1	Thioredoxin reductase 1, cytoplasmic
TRXR2	Thioredoxin reductase 2, mitochondrial
TTC36	Tetratricopeptide repeat protein 36
TTC38	Tetratricopeptide repeat protein 38
TTHY	Transthyretin
TTPA	Alpha-tocopherol transfer protein
TXD17	Thioredoxin domain-containing protein 17
UB2D3	Ubiquitin-conjugating enzyme E2 D3
UB2L3	Ubiquitin-conjugating enzyme E2 L3
UB2V2	Ubiquitin-conjugating enzyme E2 variant 2
UBE2K	Ubiquitin-conjugating enzyme E2 K
UBE2N	Ubiquitin-conjugating enzyme E2 N
UCRI	Cytochrome b-c1 complex subunit Rieske, mitochondrial
UFD1	Ubiquitin recognition factor in ER-associated degradation protein 1
UGPA	UTP--glucose-1-phosphate uridylyltransferase
URIC	Uricase
USP9X	Probable ubiquitin carboxyl-terminal hydrolase FAF-X
VATA	V-type proton ATPase catalytic subunit A
VATB2	V-type proton ATPase subunit B, brain isoform
VATE1	V-type proton ATPase subunit E 1
VIME	Vimentin
VINC	Vinculin
VMA5A	von Willebrand factor A domain-containing protein 5A
VTDB	Vitamin D-binding protein
XYLB	Xylulose kinase
YBOX1	Nuclease-sensitive element-binding protein 1

*Excluding keratin proteins, likely introduced as contamination.

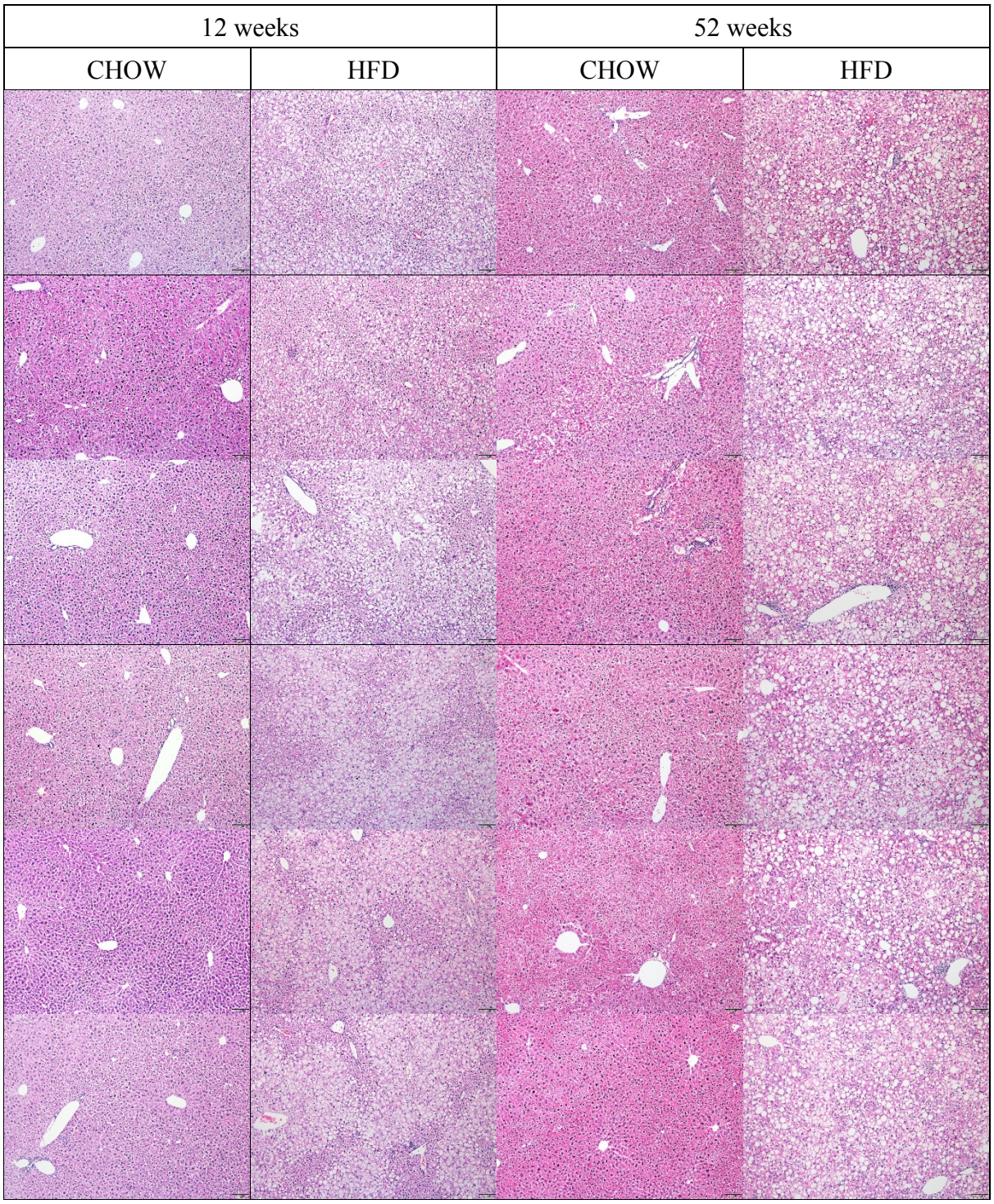

Figure A1. Liver histology for pilot study (Chapter 3). Sections include all samples that were processed (n=6/6 per group) and stained using haematoxylin and eosin (H&E). Magnification is 100× and scale bars represent 100µm.

Figure A2. Liver histology for pilot study (Chapter 3). Sections include all samples that were processed (n=6/6 per group) and stained using picro-sirius red (PSR). Magnification is 100× and scale bars represent 100μm.

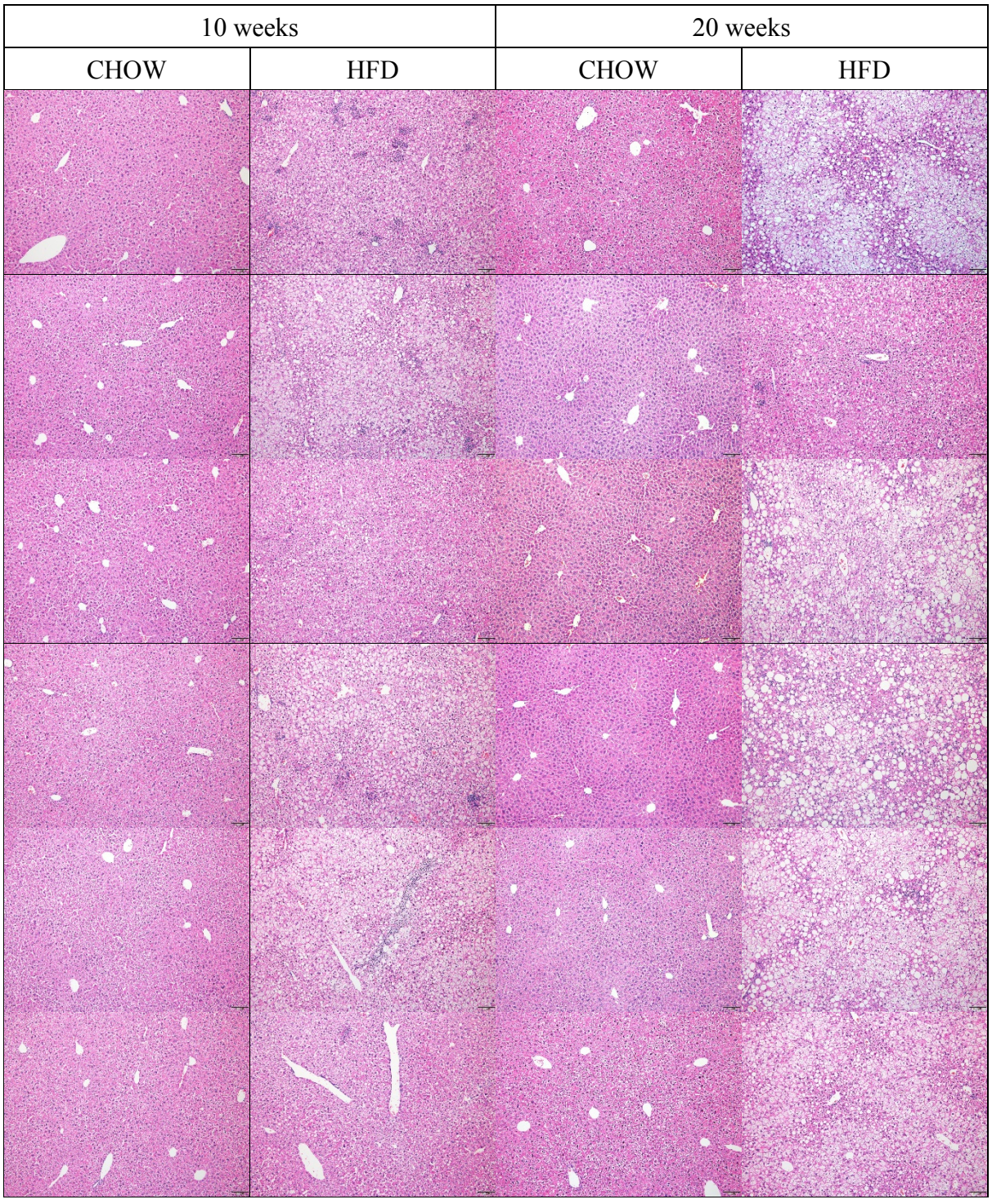

Figure A3. Liver histology for progression study (Chapter 4). Sections include all samples that were processed (n=6/12 per group) and stained using haematoxylin and eosin (H&E). Magnification is 100× and scale bars represent 100μm.

(continued over page)

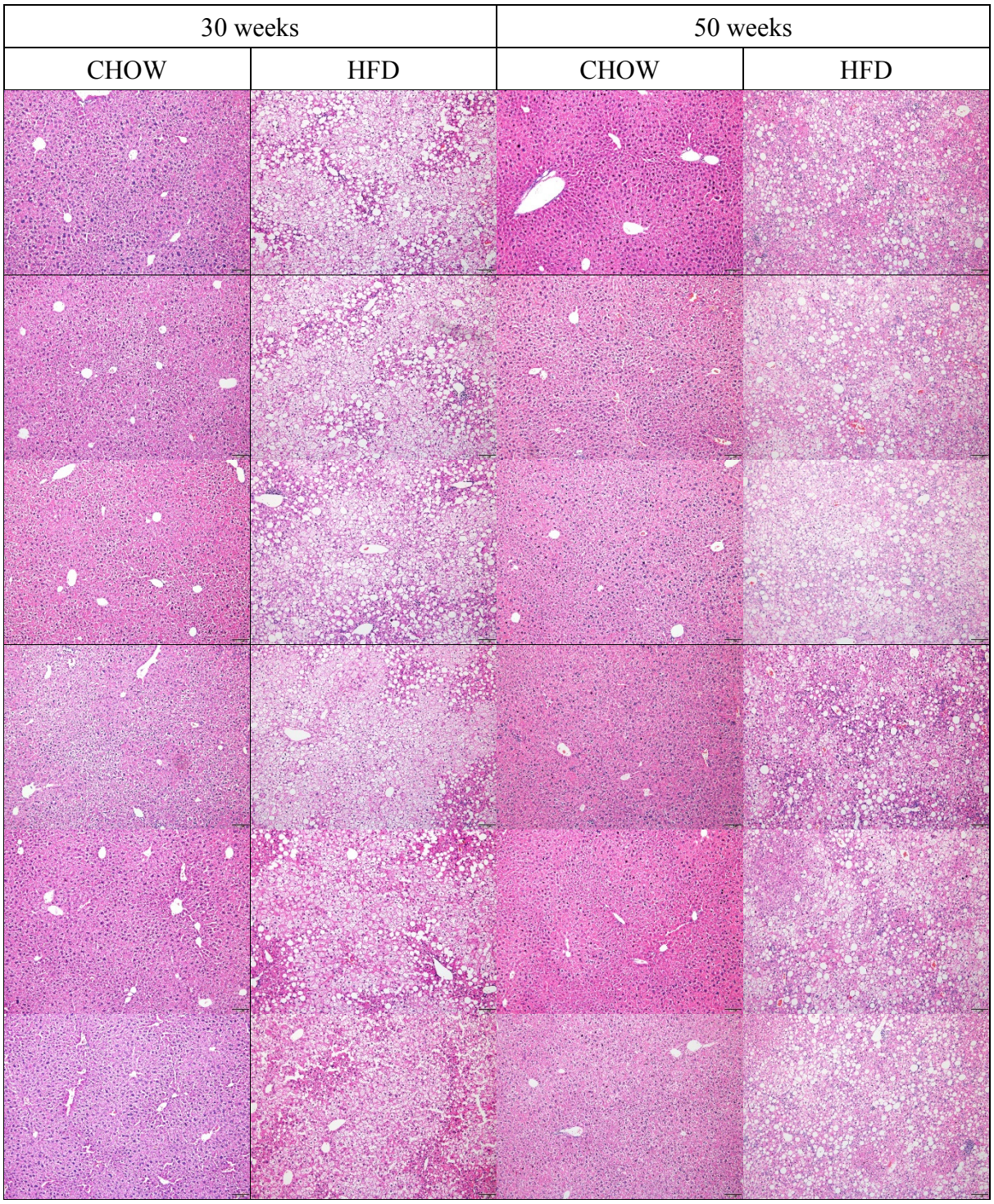

Figure A3. (continued)

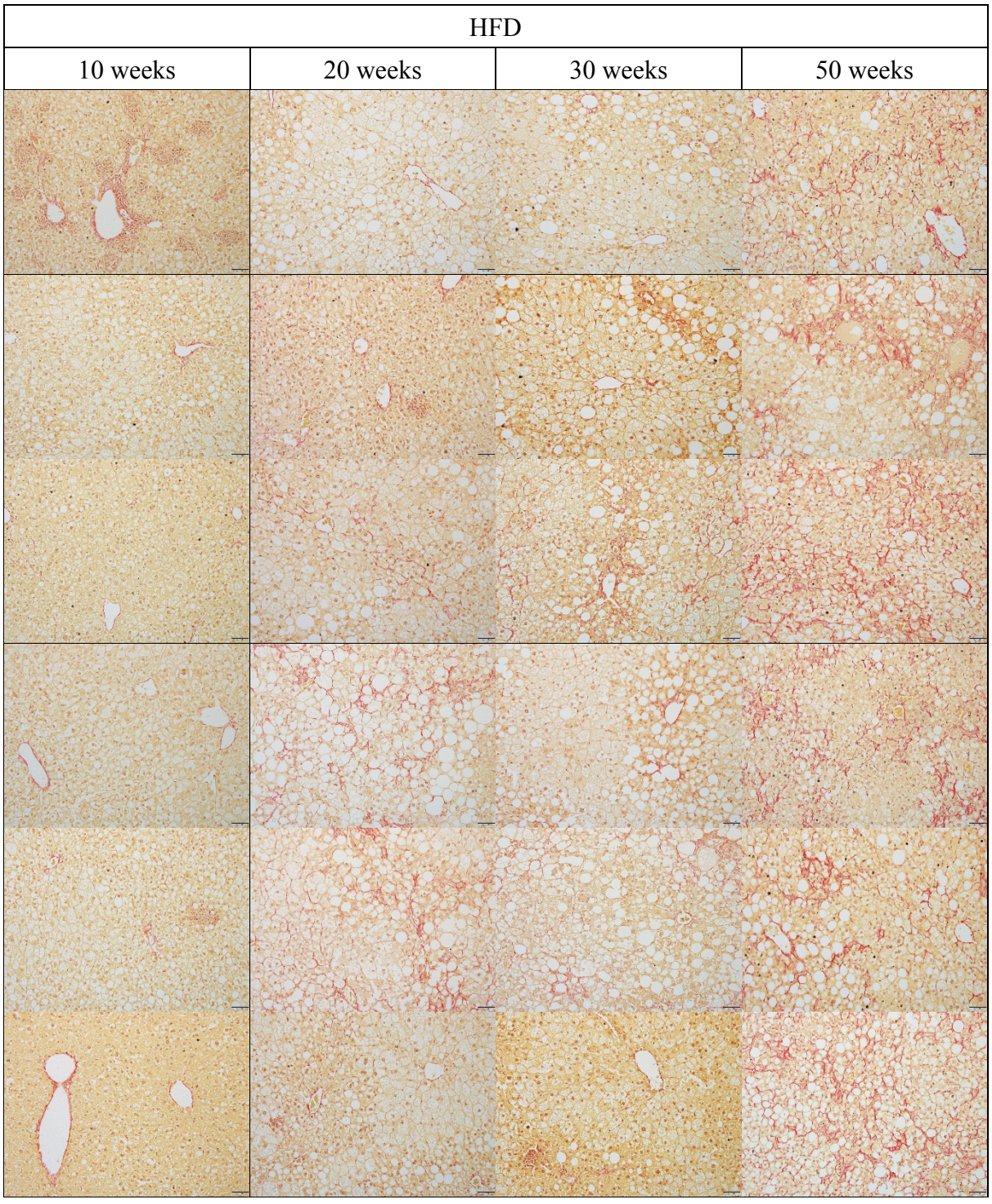

Figure A4. Liver histology for HFD animals in progression study (Chapter 4). Sections include all samples that were processed (n=6/12 per group) and stained using picro-sirius red (PSR). Magnification is 200× and scale bars represent 50μm.

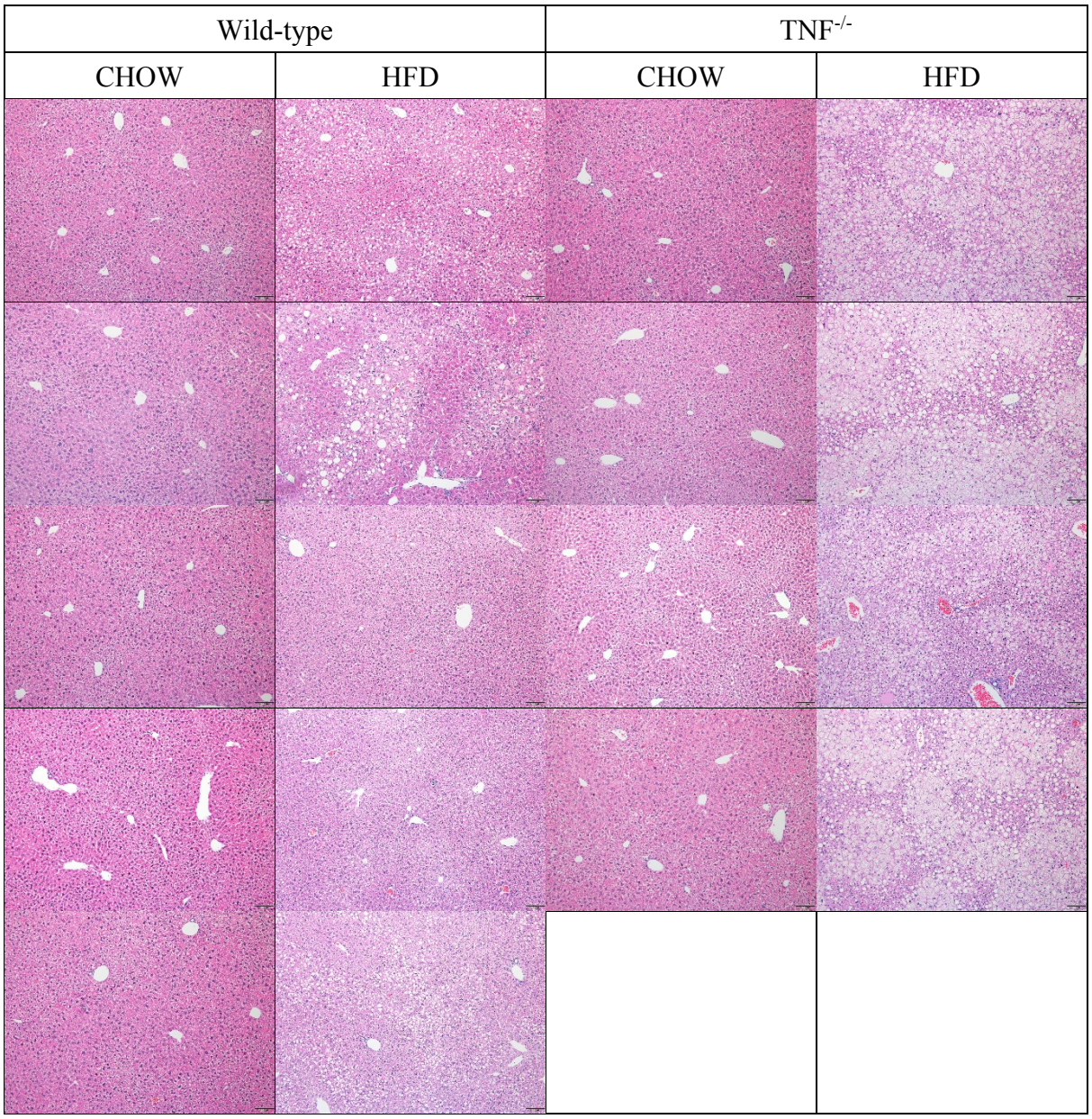

Figure A5. Liver histology for genetic intervention study (Chapter 5.2). Sections include all samples that were processed (n=5/5 for wild-type; n=4/8 for $TNF^{-/-}$) and stained using haematoxylin and eosin (H&E). Magnification is 100× and scale bars represent 100µm.

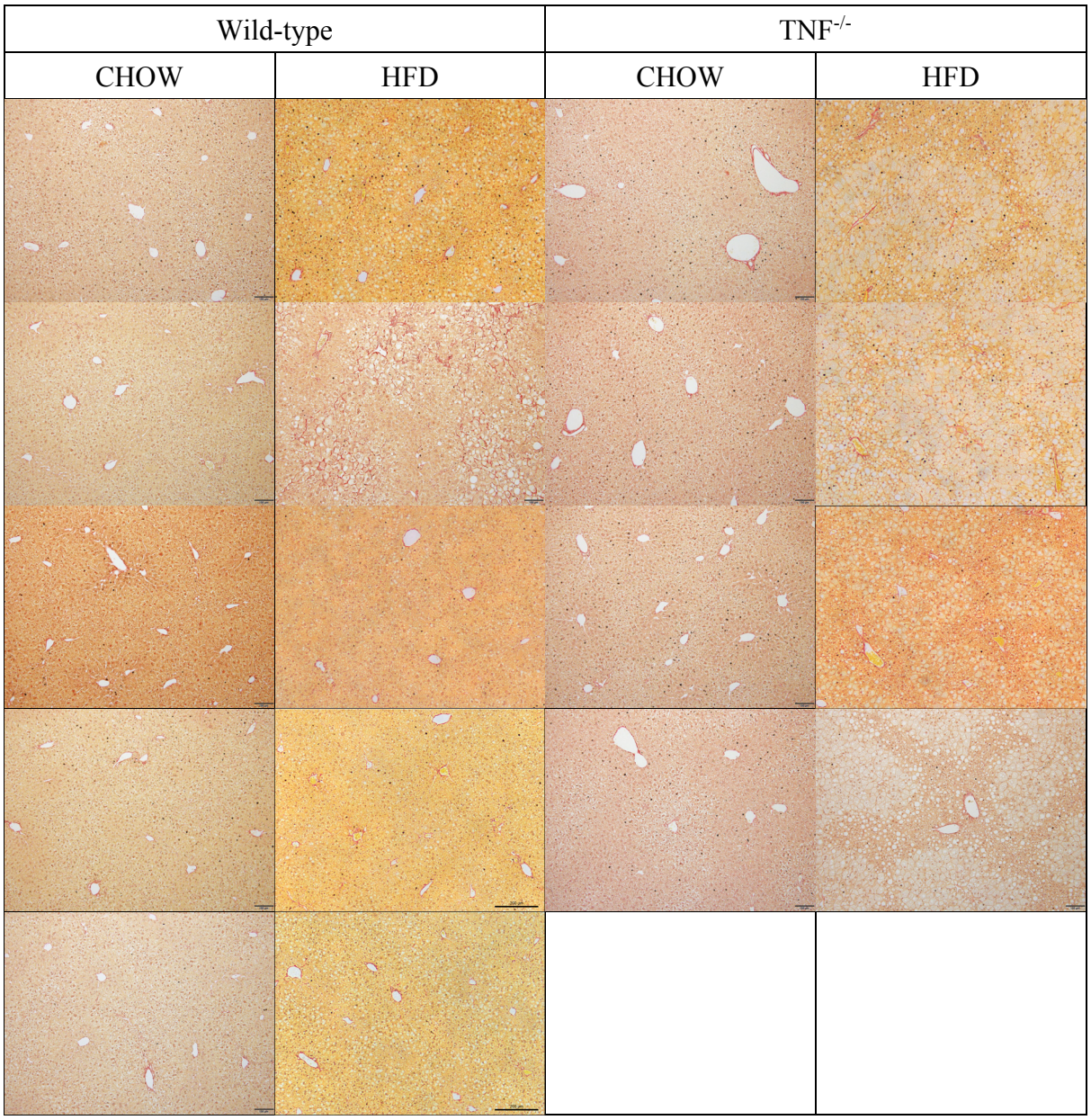

Figure A6. Liver histology for genetic intervention study (Chapter 5.2). Sections include all samples that were processed (n=5/5 for wild-type; n=4/8 for $TNF^{-/-}$) and stained using picro-sirius red (PSR). Magnification is 100×. *The author wishes to thank Ms Christine Yee for contributing in part to the acquisition of these images.*

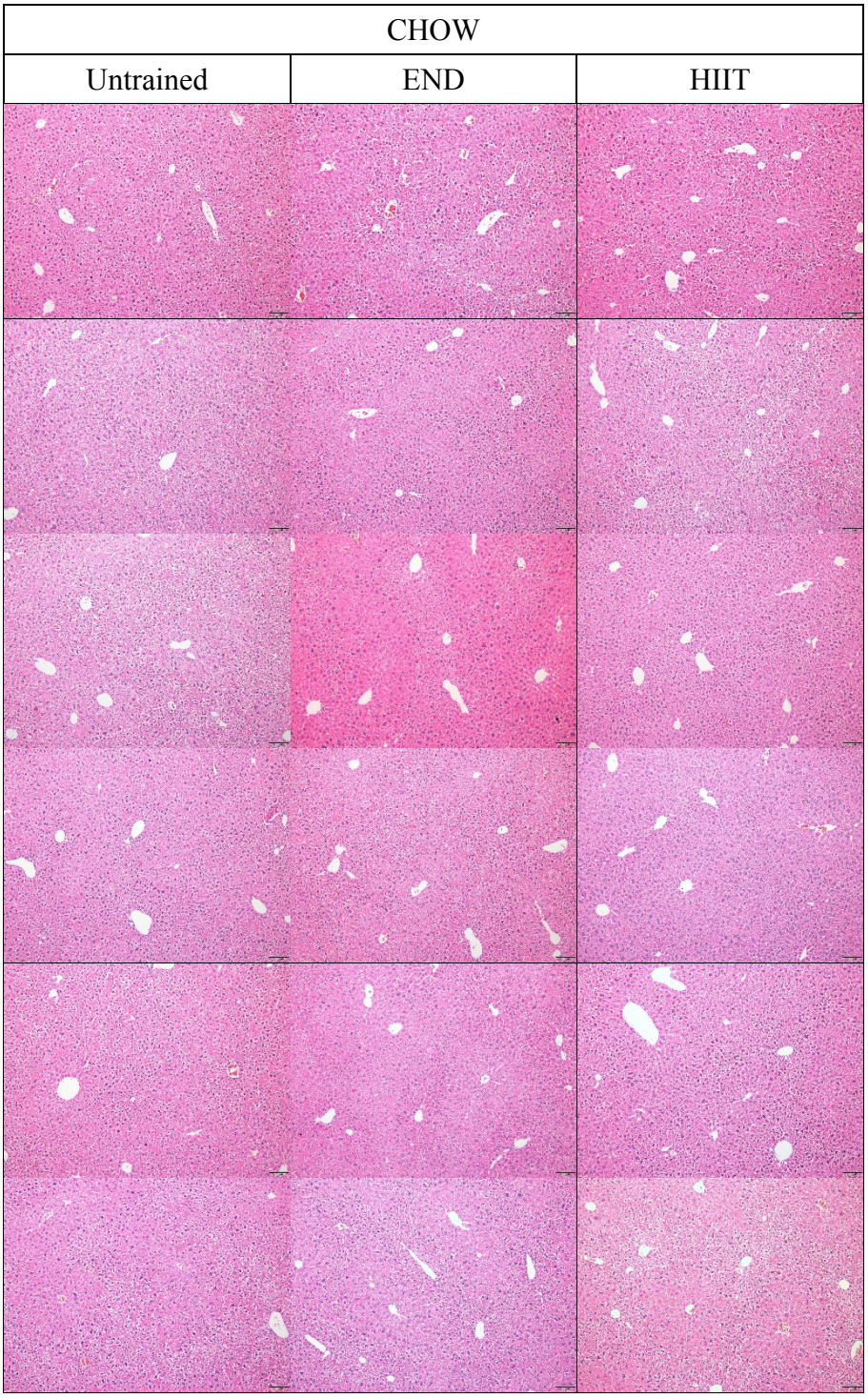

Figure A7. Liver histology for lifestyle intervention study (Chapter 5.3). Sections include all samples that were processed (n=6/10-12 per group) and stained using haematoxylin and eosin. Magnification is 100× and scale bars represent 100µm. Abbreviations: END, endurance training; HIIT, high-intensity interval training.

(continued over page)

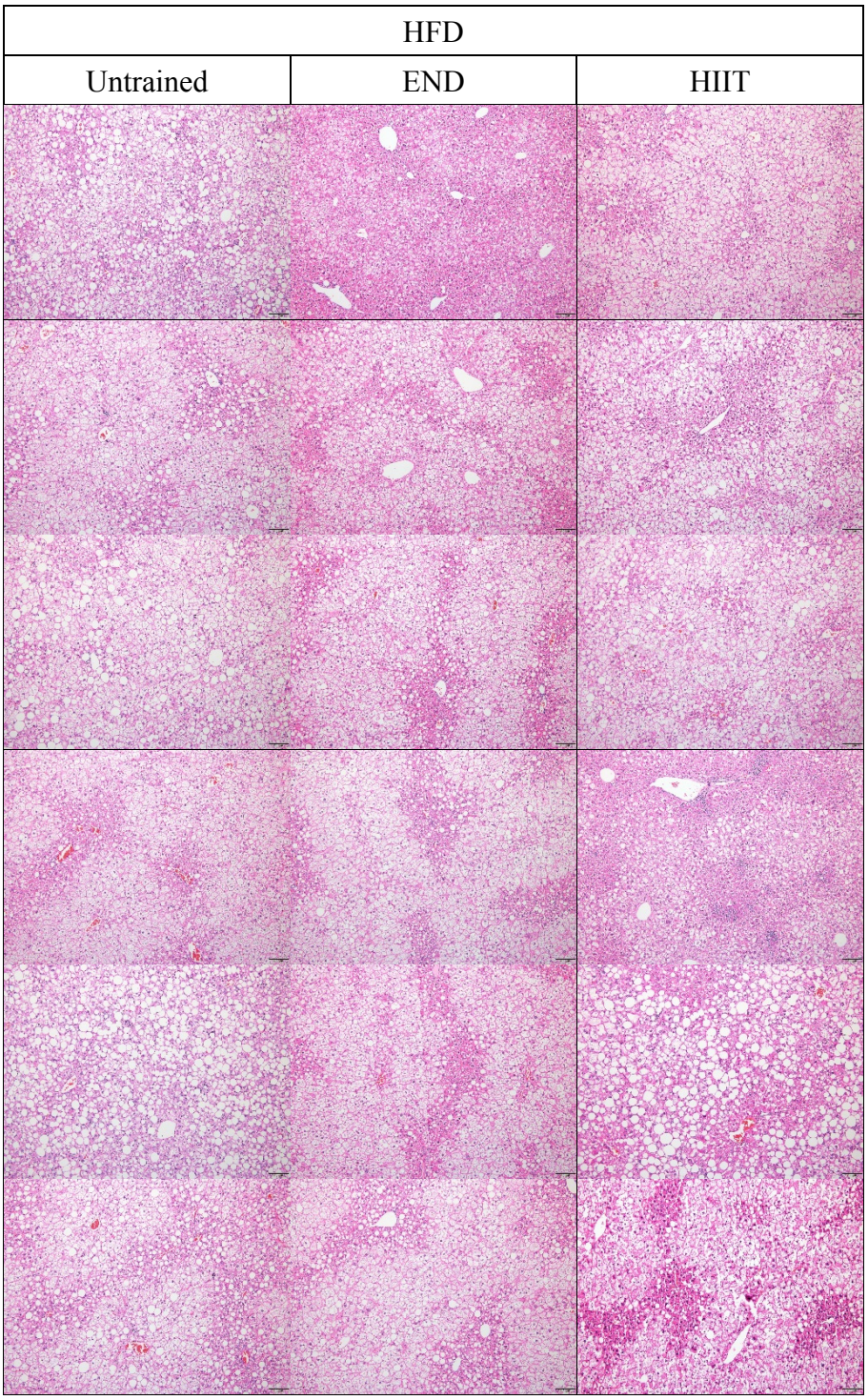

Figure A7. (continued)

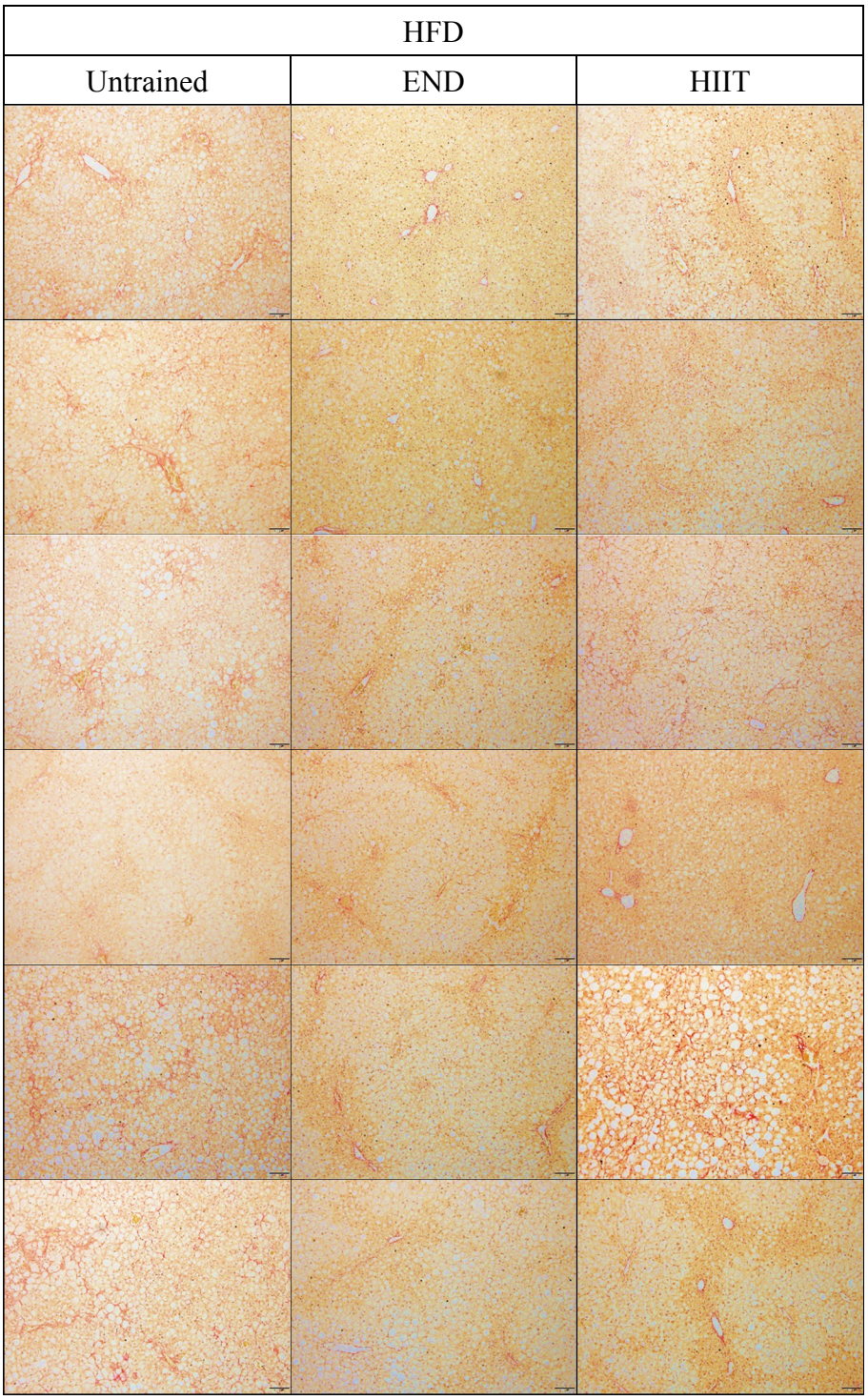

Figure A8. Liver histology for HFD animals in lifestyle intervention study (Chapter 5.3). Sections include all samples that were processed (n=6/10-12 per group) and stained using picro-sirius red. Magnification is 100× and scale bars represent 100µm. Abbreviations: END, endurance training; HIIT, high-intensity interval training.

NanoDrop™ RNA purity

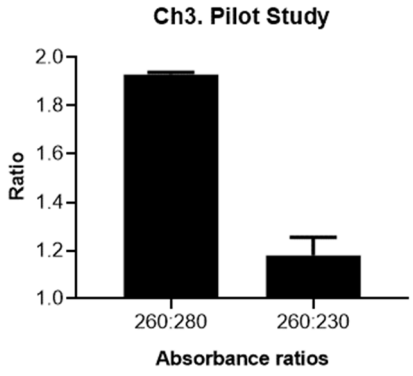

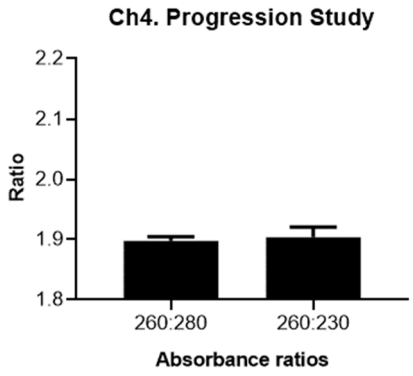

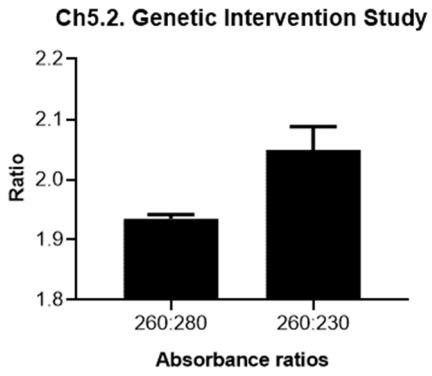

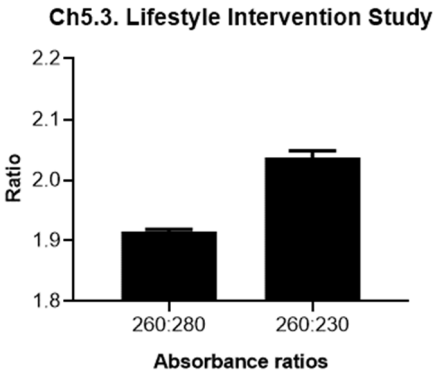

Reference Gene Amplification

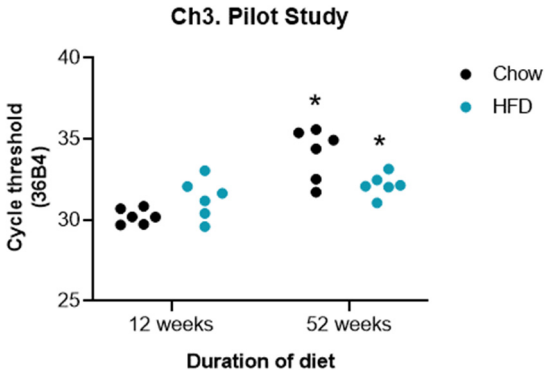

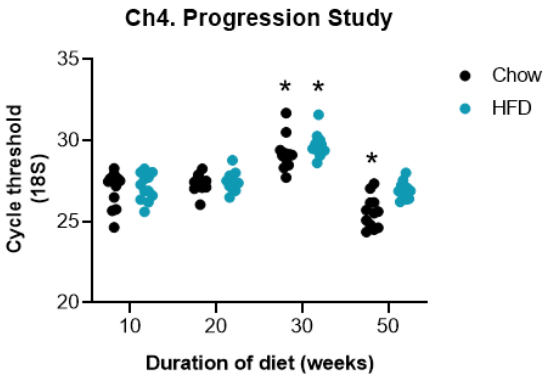

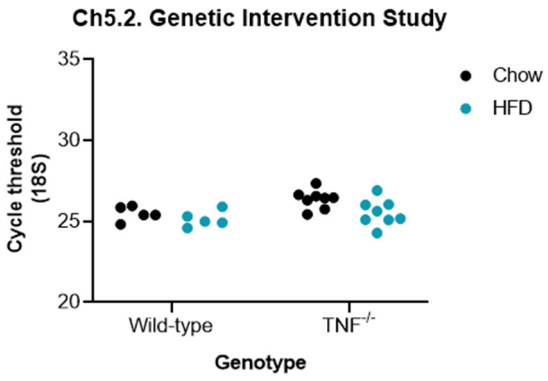

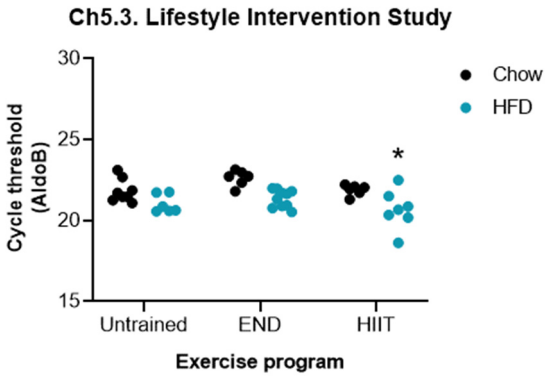

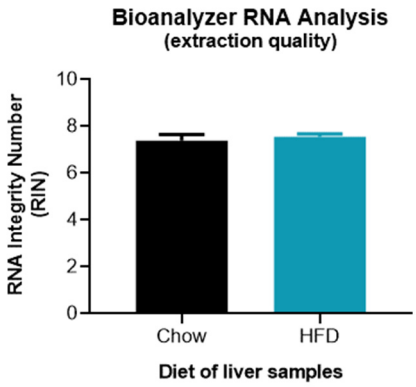

Figure A9. Analysis of sample quality for gene expression studies (starts on previous page). **Left panels:** A NanoDrop™ spectrophotometer was used to determine absorbance ratios as an indicator for RNA contamination. Acceptable values (as a rule of thumb) are approximately 1.8-2.0 for 260:280 and slightly higher, 2.0-2.2 for 260:230. A greater absorbance at 280 nm may imply protein or phenol contamination, while phenol also absorbs strongly at 230 nm. Each column represents pooled values for all samples within the study. **Right panels:** Cycle threshold for reference genes in respective studies, following cDNA synthesis and amplification. Data show all individual samples, excluding outliers determined by the ROUT method (Q=5.0%). Significant difference from control group (chow diet of earliest timepoint, wild-type or untrained animals) accepted at $p<0.05$ (*), determined by two-way ANOVA with Dunnett's test for multiple comparisons. **Current page:** RNA integrity was determined using an Agilent Bioanalyzer™ electrophoresis. Samples were taken at random from the progression study 10-week cohort (n=12). High values close to 10 for RNA integrity number (RIN) indicate less samples degradation, lower values indicate more degradation. RIN values greater than 7 are generally accepted as sufficient quality for down-stream analysis by RT-qPCR.